UMTRI-90-43

# DYNAMIC EFFECTS IN LOADING OF MATERIALS AND STRUCTURES: A LITERATURE REVIEW

Bruce M. Bowman

University of Michigan
Transportation Research Institute

October 16, 1990

**Technical Report Documentation Page**

| 1. Report No. | 2. Government Accession No. | 3. Recipient's Catalog No. |
|---|---|---|
| UMTRI-90-42 | | |

| 4. Title and Subtitle | 5. Report Date |
|---|---|
| DYNAMIC EFFECTS IN LOADING OF MATERIALS AND STRUCTURES: A LITERATURE REVIEW | October 16, 1990 |
| | 6. Performing Organization Code |
| 7. Author(s) | 8. Performing Organization Report No. |
| Bruce M. Bowman | UMTRI-90-42 |
| 9. Performing Organization Name and Address | 10. Work Unit No. (TRAIS) |
| University of Michigan<br>Transportation Research Institute<br>2901 Baxter Road, Ann Arbor, Michigan 48109 | 302364 |
| | 11. Contract or Grant No. |
| | 13. Type of Report and Period Covered |
| 12. Sponsoring Agency Name and Address | FINAL REPORT |
| Hyundai Motor Company, Ulsan, Korea<br>Hyundai America Technical Center, Inc.<br>5075 Venture Drive, Ann Arbor, Michigan 48108 | 14. Sponsoring Agency Code |

15. Supplementary Notes

16. Abstract

This report summarizes the findings of a modest literature search for information pertaining to the differences between quasi-static and dynamic loading properties of materials and structures. The primary purpose of the study is to find information that can help to establish, in relation to simulation work, whether it is important to modify load-deflection data obtained from static tests to account for dynamic effects. The impetus for the study is the need to have the best available data for use in occupant dynamics simulations, which require specifications for vehicle interior components such as the seat cushion, instrument panel, knee bolster, seat belts, etc. In addition to identifying the differences between static and dynamic loading, the report documents procedures that have been used by various researchers for adjusting the static test data where that has been found to be important.

| 17. Key Words | 18. Distribution Statement |
|---|---|
| Dynamic Loads, Structural Mechanics, Material Properties, Mechanical Impedance, Impact Absorption, Occupant Protection Components | Unlimited |

| 19. Security Classif. (of this report) | 20. Security Classif. (of this page) | 21. No. of Pages | 22. Price |
|---|---|---|---|
| Unclassified | Unclassified | 220 | |

TABLE OF CONTENTS

Acknowledgments

The author gratefully acknowledges the support provided by Hyundai Motor Company and Hyundai America Technical Center, Inc., toward the literature search and review reported here.

# DYNAMIC EFFECTS IN LOADING OF MATERIALS AND STRUCTURES: A LITERATURE REVIEW

## OBJECTIVES AND METHODOLOGY

This report summarizes the findings of a modest literature search for information pertaining to the differences between quasi-static and dynamic loading properties of materials and structures. The primary purpose of the study is to find information that can help to establish, in relation to simulation work, whether it is important to modify load-deflection data obtained from static tests to account for dynamic effects. The impetus for the study is the need to have the best available data for use in occupant dynamics simulations, which require specifications for vehicle interior components such as the seat cushion, instrument panel, knee bolster, seat belts, etc. In addition to identifying the differences between static and dynamic loading, it is also of interest to document the procedures that have been used by various researchers for adjusting the static test data where that has been found to be important.

The Structured Thesaurus in the UMTRI Research Information and Publications Center was examined for 20 different subjects, as listed below, that it was thought might include papers and reports of pertinence.

| | |
|---|---|
| NLSJ | Dynamic Loads |
| XQC | Dynamic Test Equipment |
| NCYQ | Damping Capacity |
| DGEOC | Components, Occupant Protection |
| XQ | Test Equipment, Mechanical |
| NB | Structural Mechanics |
| NC | Material/Mechanical Properties |
| NURI | Mechanical Impedance |
| NUM*NLSI | Impact Absorption |
| NCN | Impact Properties |
| CDQ | Impact Attenuators, Vehicle |
| DGED | Instrument Panels |
| DGEORBN | Belt Restraint Systems, Energy Absorbing |
| NUM | Energy Absorption, Mechanical |
| NLSI | Shock |
| not found | Strain Rate |
| not found | Component Testing |
| not found | Effective Mass |
| not found | Amplification Factor |
| not found | Energy Management |

For the 15 subjects for which there were entries in the Structured Thesaurus, all of the cards in the card catalog were examined. There were cards for approximately 1800 papers and reports. From reading the titles, 73 references were selected for further examination. Those 73 papers and reports were taken from the library shelves for review. Of the 73, only 14 were found that include information of some interest in relation to understanding dynamic effects in loading. Summaries of the pertinent content of those documents are given in this report, with references to page numbers, figure numbers, and table numbers in the respective documents. Copies of material from the 14 papers and reports are appended to this report. For some a copy of the entire document is included here, and for others copies of only selected pages are included.

## SUMMARY OF FINDINGS

This literature search seems to support a generally held opinion that very little research related to dynamic effects has been conducted and reported in the literature. However, this effort has documented enough information to support the general views that:

1) For impacted components that offer primarily a "material resistance" (for example, like a spring and damper, without mass), dynamic effects can be accounted for by increasing the static stiffness by a small percentage (usually 0 to 5 or 10 per cent). Foam paddings may be an exception, however, as one study (Orringer, et al.) reports dynamic effects of 35 to 80 per cent.

2) For components that offer significant inertial resistance because of their mass, dynamic effects are greater and they increase with an increase in initial impact velocity.

3) Yield, or breaking, strengths of materials and structures are almost always greater for larger loading rates. Values for strengths in high-rate loading are often approximately 5 to 30 per cent greater than in quasi-static loading. An exception is in belt system "joints," i.e., places where components of the system are fastened to each other. There, typically, breaking strengths are lower by 10 per cent or so for high-rate loading than for static loading.

## RECOMMENDATIONS FOR FUTURE RESEARCH

This study has made it clear that little pertinent research has been reported in the literature. Nonetheless,

the study was a small one, and certainly there is additional useful information regarding dynamic effects to be found at the UMTRI Research Information and Publications Center. A computer search will find references not examined in the current study, and there are references cited in some of the 14 papers and reports reviewed in this study that may well contain additional information of interest. It would be useful to supplement the results of this literature search with additional pertinent material from a computer search of the library database of the UMTRI Information Center. Additionally, a computer search should be conducted to find references of possible interest available from the University of Michigan Engineering Transportation Library.

# APPENDIX A

# REVIEW/SUMMARY OF SELECTED REFERENCES

DYNAMIC EFFECTS

- - -

REVIEW/SUMMARY OF SELECTED REFERENCES

Development of Energy-Absorbing Safety Belt Webbing. Juichiro Takada. 3rd International Conference on Occupant Protection, 1974. SAE-740581. UMTRI-30029.

> Slopes for belt load vs. strain curves were found to be slightly higher for high velocity sled impacts than for low velocity sled impacts. See curves on pg. 270. Sled velocities were 10, 20, and 30 mph. Strain rates are not given--and, of course, are not constant--but it may probably be deduced from the data that belt stiffness does not vary greatly (probably less than 5 per cent) for strain rates that are different by a factor of three.

Impact Strength of Joints in Seat Belts. M. Veysey and D.C. Herbert. Department of Motor Transport, New South Wales, 1977. UMTRI-40653.

> This study was focused on strength (i.e., force for breaking) of "joints" in belt systems. "Joints" are defined as the connections between webbing and other components, or those components themselves. Stiffnesses (i.e., force-deflection or force-strain curves) were not measured in this study. It was found that, for the various joints tested, strength under dynamic testing conditions was between 21 per cent lower and 8 per cent higher, and on average 11 per cent lower than strength under static testing conditions (pg. 6). That is, belt system joints were usually found to break under smaller loads dynamically than statically. Seat belt joints were found to be weaker than the webbing itself (pg. 5).

The Dynamic Properties of Seat Belt Webbings and End Fixings as Tested on the Pneumatic Accelerator. E.J. Brabin. MIRA Bulletin No. 4, July/August 1970. UMTRI-15375.

> Belt webbing was tested quasi-statically (less than 1 inch/min; pg. 6) and at strain rates of 0/sec (quasi-static), 2/sec, 6/sec, and 10/sec. The graphs on pages 8 and 9 show that stiffnesses are only slightly different over this wide range of strain rates. In the conclusions they note that "Webbing end fixings behave differently under dynamic load to static loading and alter considerably the overall characteristic of the seat belt."

Material and Design Interactions in Collision Energy Management. Bernard S. Levy. SAE International Congress and Exposition, Detroit, February 1981. SAE-810234. UMTRI-45537.

Many different modes of energy absorption are discussed in this paper. Experimental work was done with different kinds of steel. Tests were conducted at constant loading rates of 0.1, 0.5, 100, and 500 inches per minute. Estimates for 31,680 inches per minute (30 mph) are discussed on page 6 and shown in Table IX.

In the tables on pages 5, 7, and 8, YS is yield strength, K is the "strength coefficient" (see pg. 2), n is the "strain hardening exponent" (see pg. 2), and sigma-.08 is the tensile flow stress at 8% strain (see pg. 3). (Also, see equation 3 on page 2 regarding the definitions of K and n.) At the top of page 4 the authors mention that there is little data in the literature that describes the sensitivity of these quantities to strain rate. (The quantifies m and m' included in some of the tables are defined on page 5.) Values determined by the authors for YS, K, and n for 500 inches/min and 0.5 inches/min are shown in Table VI. Values at 0.1 inches/min and 31,680 inches/min (estimated) are shown in Table IX. The quantity n (strain hardening exponent) is probably the characteristic that relates most directly to stiffness. (YS and K relate to strength). Table VI shows that four the four steels tested, n is about 12 per cent larger on the average for the dynamic test as compared with the quasi-static test.

In their conclusions (page 9) the authors say that the data suggest that a lower bound for strain rate corrections for collision deformation energy is 9 to 16 per cent.

In contrast to the findings of Veysey and Herbert regarding belts in the paper Impact Strength of Joints in Seat Belts, yield strength of steel is found to increase with increased strain rate.

Metallic Energy Dissipating Systems. W. Johnson and S.R. Reid. Applied Mechanics Reviews, Vol.1, No.3, 1978. UMTRI-40452.

The authors say on page 285 that "When these devices [vehicle components] are used as impact energy absorbers where the loading is dynamic, a consideration which should always be kept in mind is the influence of strain-rate on the plastic yielding of the material, though its effects can indeed be exaggerated. Strain-rate is most important in its effects on initial yield or collapse load." At the top of page 286 they say "Broadly speaking, both strain-hardening and strain-rate increase the effective yield stress of the material."

Regarding the effect of strain rate on stiffness, they say on page 286 that "Nonlinearities in the load-deflection response of a device...have also been treated by defining equivalent mass-nonlinear spring-dashpot systems. They cite two references, both by K. Ohmata (and H. Fukuda for the second). The first of these is reviewed below.

Dynamic Analysis of Impact Attenuation Utilizing Plastic Deformations (Case in Which Effect of Strain-rate Sensitivity is Considered). K. Ohmata. Bulletin of the JSME, Vol.19, No.134, August 1976. UMTRI-37461.

The author develops a lumped-mass mathematical model which takes into account the elasticity, viscosity, plasticity, and strain-rate sensitivity of a structure. His model can be made dynamically equivalent to an impact attenuation system whose idealized static load-deflection curve consists of an elastic range and a range for unrestricted plastic flow. He analyzes the dynamic response of the modeled system to impact by a moving mass.

He illustrates his method by calculating the "equivalent viscous damping coefficient" for a simply supported beam that is impacted in the center by a freely falling mass. (The definition for "e.v.d.c." is given on page 886.) He finds that there is good agreement with experiment for fall heights ranging from 50 to 150 cm. These results are shown in Table 1 on page 887 and described on pages 886 through 890. Figure 15 on page 890 illustrates that there is approximate agreement between his model and experimental results for dynamic load as a function of deflection.

The model developed by Ohmata requires the determination of several empirical constants by conducting impact tests. These constants would be difficult, if not impossible, to obtain for components of a vehicle interior. Thus, even if a simulation model (e.g., MVMA 2-D) included such a representation of material and structure characteristics, it is not likely that the required input data could be obtained. The paper may nonetheless contain some useful information in the dependencies on strain rate, etc., that are assumed in the equations.

Impact: The Theory and Physical Behaviour of Colliding Solids. Werner Goldsmith. Edward Arnold (Publishers) Ltd., London, 1960. UMTRI-00129.

This reference is a book. Figure 123 on page 203 shows a hypothetical, or estimated, stress-strain loading curves for aluminium (aluminum?). It shows a quasi-

static loading curve (strain rate equal to zero) and loading curves for other strain rates from 100/sec to 400/sec. Note that Goldsmith estimates the loading stiffness (slope) to be independent of strain rate for strains less than some limit and that loading is plastic for larger strains at levels dependent on strain rate.

Table 20 on pages 324 and 325 shows that the ultimate strength (for breaking) for all metals tested is 5 to 30 per cent greater for dynamic loading than for static loading. This is in agreement with Levy's findings as described in the paper Material and Design Interactions in Collision Energy Management.

In Figure 268 on page 331, for temperature 68 degrees F, Goldsmith shows that there are only small differences between the loading curves for aluminum at strain rates of 0/sec, 4.38/sec, and 39.3/sec. Figure 269 on page 332 similarly shows that loading curves for copper are not greatly sensitive to strain rate.

AATD System Technical Characteristics, Design Concepts, and Trauma Assessment Criteria. J.W. Melvin, A.I. King, and N.M. Alem. Phase 1 Reports: Concept Definition, Advanced Anthropomorphic Test Device Development Program, 1988. UMTRI-76738.

This report includes an analysis of the dynamic loading properties of the human chest. Original data (from testing by C. Kroell) were obtained from chest impacts of human cadavers at different impact velocities. Melvin, et al., have characterized the Kroell data for frontal and side impacts as illustrated in Figures 16 and 17. These are force-deflection curves. The rates indicated are not loading rates, but rather the initial velocities of the impactor. It may be true that loading at constant rates would show similar dependence on loading rate, i.e., characterized by "plastic", plateau-like response for larger deflections. Such plastic response dependence on loading rate would be similar to that illustrated by Goldsmith for metals.

High and Low Rate Force-Deformation Characteristics of Motorcycle Helmets. H.B. Kingsbury, W.C. Herrick, and Dinesh Mohan. SAE Congress and Exposition, Detroit, February 1979. SAE-790324. UMTRI-41703.

Quasi-static and dynamic loading tests were conducted for trilaminar motorcycle helmets. The data obtained may be considered to be primarily for the properties of the middle shell material, which was expanded bead polystyrene, although the properties of the inner foam-backed cloth lining and the outer shell (polycarbonate polymer or fiberglass) also affect the results. Quasi-static loading was done at 0.065 cm/sec. Fixed rate

dynamic loadings were done at 0.8, 3, 3.5, 4, 5, and 5.5 m/sec. The authors found that the load-deflection curves were significantly affected by the rate of loading, as illustrated in Figures 11 through 16.

It may be observed, however, that the slopes of the curves are approximately the same for all loading rates except for the initial part of the loading. In Figure 11, for example, if we ignore the first 2 cm of the quasi-static loading curves (1 and 2), the first 0.5 cm of the 4 m/sec loading curve (15), and the first 1.1 cm of the 5 m/sec loading curve (17), the curves are all approximately linear and with the same slope. Interestingly (and confusingly), however, examination of all of the Figures 11 through 16 shows that the amount of initial deflection that must be ignored is not a uniform function of loading rate; i.e., it is sometimes more for higher loading rates and sometimes less.

Crash Padding Research. O. Orringer, K.T. Knadle, and J.F. Mandell. Transportation Systems Center, Cambridge, Massachusetts, 3 volumes, July 1986. DOT-TSC-NHTSA-85-4, 85-5, and 86-1. UMTRI-74436 to 74438.

The research described in this report pertained to experimental and theoretical work on Uniroyal Ensolite AAC, a recoverable closed-cell foam rubber material that is used in vehicle interior padding. Strain rates studied experimentally ranged from 0.8/sec to 2000/sec.

The numbers in Table 4-1 (pg. 23 of Vol. 1) show that maximum stresses for any value of maximum strain are dependent on strain rate; in particular, compressive stresses are from about 35 to 80 per cent larger at strain rates of 73/sec than at 1.2/sec. The amount of dependency on strain rate decreases as maximum strain is increased. Additional data for loading (LD) and unloading (UL) at different strain rates are shown in Table B-5 (pg. B-6 of Vol. 1). The data there can be used to reconstruct entire loading/unloading curves, but there are no figures in the report showing those curves.

Dynamic Test Criteria for Aircraft Seats. National Aviation Facilities Experimental Center (DOT), Report No. NA-69-5 (DS-69-10), Project No. 510-002-04X, October 1969. UMTRI-17120.

This report describes research done for the purpose of determining the relationship between static and dynamic loading characteristics of aircraft seats. On pages 2 through 9 the authors describe the definition of what they call a "sensitivity curve" for a specified response. Such a curve is illustrated in Figure 5, page 8. It plots velocity change against average

acceleration for an impact. That is, each impact test conducted results in one point to plot, and all points taken together constitute the "sensitivity curve." They use the sensitivity curve determined from a series of dynamic tests to establish an equivalency to static seat strength requirements. This is described on pages 18 through 48. The results described in this report do not have immediate application in understanding dynamic effects in terms of force-deflection loading specifications for simulation data sets, but the methodology used is an interesting way of studying dynamic effects in general.

Influence of Inertia in Structural Crashworthiness. S.R. Reid and C.D. Austin. International Conference on Vehicle Structures, Cranfield Institute of Technology, London, July 1984. UMTRI-72087.

This paper discusses the effect that the inertia, or mass, of structural elements has on impact loading. That is, while the author recognizes that velocity-dependent damping and other factors contribute to the overall dynamic effects on loading curves, he discusses specifically the effect of non-negligible mass in the impacted structural elements. He says on page 2 that "...it should be noted that treatments such as that described in (2) often use dynamic enhancement factors to scale the static non-linear spring characteristics attributed to the deformable elements. The source of these factors is sometimes unclear." [His reference "(2)" citation is the paper by Emmerson and Fowler discussed below.]

This paper does not contain any informative numerical data, but its discussion of one aspect of dynamic effects in impact loading is nonetheless interesting.

The Application of Computer Simulations in Vehicle Safety. W.C. Emmerson and J.E. Fowler. 5th International Technical Conference on Experimental Safety Vehicles, London, 1974. UMTRI-32385.

This paper examines dynamic effects in crash loadings of a vehicle. Thus, it does not examine any particular material or any particular component (of an occupant compartment), but rather it looks globally at the structure of a vehicle that is deformed by external crash loadings. General findings, nonetheless, should have pertinence to the effects of dynamic loading of occupant compartment components.

The approach taken by the authors in representing the relationship of dynamic impact force to static load-deflection forces is to determine a multiplier for the

static load, where, specifically, the multiplier is (1.0 + T) and T is equal to a "dynamic magnifier" multiplied by the rate of deformation and divided by the reference velocity at which the dynamic magnifier, called "lambda," is determined. (See page 713.) No detail is given in the paper about the experimental methods used for determining the dynamic magnifier; it is stated only that it "varies for different types of construction" and that "the actual values used are based on previous comparisons between theory and experiment." The "rate of deformation" used in the calculation is a time-dependent crush rate and not the "Initial Impact Velocity" used in somewhat similar calculations by Prasad and Padgaonkar in the paper discussed below. The initial impact velocity is used in a different manner by Emmerson and Fowler--apparently as the divisor quantity, the "reference velocity."

On page 713 the authors state that the method they use can be used for any type of vehicle impact simulation and is not restricted to frontal impacts. Further, they state explicitly that they use this method "for different parts of the structure"--i.e., for separate components. While their application has been for modeling dynamic vehicle crush, it would seem that it could also be applied in representing dynamic effects for loading of occupant compartment components.

Static-to-Dynamic Amplification Factors for Use in Lumped-Mass Vehicle Crash Models. P. Prasad and A.J. Padgaonkar. SAE International Congress and Exposition, Detroit, February 1981. SAE-810475. UMTRI-45586.

As in the paper by Emmerson and Fowler (discussed above) the analysis in this paper relates not to impact against component elements but, rather, to the dynamic effects in crash loadings of a full vehicle.

On pages 1 and 2, the authors say, "In order to be able to use the statically obtained crush data for dynamic simulation, a transformation is required to account for deformation rate effects. Therefore, the key to the use of the lumped-mass models is in obtaining (a) valid static force-deflection relationships and (b) the static-to-dynamic transformations for the various energy absorbers used in the models. The valid static force-deflection relationships are obtained by carefully matching the crush modes produced during the static crush tests with those observed during full-scale crash tests. However, considerable variations in approach exist in determining the static-to-dynamic transformation factors... The determination of these factors has been essentially an empirical process based on comparisons of model results with crash test

results." They further point out that the two main factors affecting behaviors of structures under impact loading are sensitivity of material properties to strain rate and the effect of wave propagation and inertial effects within the structure itself. On page 2 they note that Macaulay and Redwood have shown that material strain rate sensitivity alone cannot explain the increase in energy absorption observed in dynamic tests, and they conclude that inertial rate effects are important in structures in which the crush modes are not predetermined by design. (This is reiterated on page 3.)

On pages 3 through 12 the authors describe their development of a "dynamic amplification factor" for transforming their static data into dynamic-equivalent data for use in full vehicle crash simulations. They indicate on page 4 that they tried vaious definitions of a "dynamic amplification factor" and that the best results were obtained by using a factor for the "vehicle frame" that was linearly dependent on initial impact velocity (page 5, Figure 2) together with an inertia spike for the "aft frame" (Figure 3). [Note that the horizontal axis of Figures 2 and 23 are labeled "Crush Rate", but they <u>should</u> be labeled "Initial Impact Velocity."] In Table 2 on page 27 values are given for the "overall dynamic amplification factor" for four, C-section frame vehicles. The values range from 1.64 to 2.0. It may be seen by using other numbers given in Table 2 that the authors' definition of "dynamic amplification factor" is simply the ratio of the kinetic energy for an impact divided by the static loading energy that is required to produce the same amount of maximum crush. (This is discussed on page 13.) The amplification factor that they established for C-section frame vehicles is illustrated in Figure 23 on page 27. It should be noted that this result is different from their result for subcompact vehicle frames, which is shown in Figure 2 on page 5. Also, it should be mentioned again that the horizontal axis of Figures 2 and 23 should be labeled "Initial Impact Velocity" and not "Crush Rate", a quantity which varies with time and which was not measured in the authors' crash tests.

# APPENDIX B

# SELECTED REFERENCES

APPENDIX B

TABLE OF CONTENTS


| NO. | REFERENCE |
|---|---|
| 1 | Development of Energy-Absorbing Safety Belt Webbing. Juichiro Takada. 3rd International Conference on Occupant Protection, 1974. SAE-740581. UMTRI-30029. |
| 2 | Impact Strength of Joints in Seat Belts. M. Veysey and D.C. Herbert. Department of Motor Transport, New South Wales, 1977. UMTRI-40653. |
| 3 | The Dynamic Properties of Seat Belt Webbings and End Fixings as Tested on the Pneumatic Accelerator. E.J. Brabin. MIRA Bulletin No. 4, July/August 1970. UMTRI-15375. |
| 4 | Material and Design Interactions in Collision Energy Management. Bernard S. Levy. SAE International Congress and Exposition, Detroit, February 1981. SAE-810234. UMTRI-45537. |
| 5 | Metallic Energy Dissipating Systems. W. Johnson and S.R. Reid. Applied Mechanics Reviews, Vol.1, No.3, 1978. UMTRI-40452. |
| 6 | Dynamic Analysis of Impact Attenuation Utilizing Plastic Deformations (Case in Which Effect of Strain-rate Sensitivity is Considered). K. Ohmata. Bulletin of the JSME, Vol.19, No.134, August 1976. UMTRI-37461. |
| 7 | Impact: The Theory and Physical Behaviour of Colliding Solids. Werner Goldsmith. Edward Arnold (Publishers) Ltd., London, 1960. UMTRI-00129. |
| 8 | AATD System Technical Characteristics, Design Concepts, and Trauma Assessment Criteria. J.W. Melvin, A.I. King, and N.M. Alem. Phase 1 Reports: Concept Definition, Advanced Anthropomorphic Test Device Development Program, 1988. UMTRI-76738. |
| 9 | High and Low Rate Force-Deformation Characteristics of Motorcycle Helmets. H.B. Kingsbury, W.C. Herrick, and Dinesh Mohan. SAE Congress and Exposition, Detroit, February 1979. SAE-790324. UMTRI-41703. |
| 10 | Crash Padding Research. O. Orringer, K.T. Knadle, and J.F. Mandell. Transportation Systems Center, Cambridge, Massachusetts, 3 volumes, July 1986. DOT-TSC-NHTSA-85-4, 85-5, and 86-1. UMTRI-74436 to 74438. |

11 Dynamic Test Criteria for Aircraft Seats. National Aviation Facilities Experimental Center (DOT), Report No. NA-69-5 (DS-69-10), Project No. 510-002-04X, October 1969. UMTRI-17120.

12 Influence of Inertia in Structural Crashworthiness. S.R. Reid and C.D. Austin. International Conference on Vehicle Structures, Cranfield Institute of Technology, London, July 1984. UMTRI-72087.

13 The Application of Computer Simulations in Vehicle Safety. W.C. Emmerson and J.E. Fowler. 5th International Technical Conference on Experimental Safety Vehicles, London, 1974. UMTRI-32385.

14 Static-to-Dynamic Amplification Factors for Use in Lumped-Mass Vehicle Crash Models. P. Prasad and A.J. Padgaonkar. SAE International Congress and Exposition, Detroit, February 1981. SAE-810475. UMTRI-45586.

740581

# Development of Energy-Absorbing Safety Belt Webbing

**Juichiro Takada**
Takata Kojyo Co., Ltd.

ABSTRACT

Seat belt systems can be considered as the most convenient and practical system for occupant protection in automotive crash situations.

Takata Kojyo Co., Ltd. has been striving to design and create a seat belt system that would be both practical and effective in absorbing impact energy with no injury in high speed crashes.

In our search for more effective seat belt systems, we have conducted various comparison tests between conventional webbings and our newly developed webbing in regard to rheological property.

1. In regard to the dynamic performance of the webbing, the quantity of absorbed impact energy and the rate of absorbing energy were obtained and compared through tests at various impact speeds.
2. Dummy tests were conducted in our laboratories to compare the improved Takata energy-absorbing (EA) webbing with conventional webbing. The results showed the conspicuous superiority of the Takata webbing over the conventional types.
3. Using our improved webbing, two live human volunteers were able to successfully complete tests at impact speeds of 30.3 and 30.4 mph without injury or pain.
4. In the future, to enhance safety, seat belts, as well as other restraint systems, should be evaluated with the use of dynamic tests with living human volunteer subjects rather than with anthropomorphic dummies.

Development of a three-point seat belt system comprised of webbing with controllable dynamic performance characteristics is important as the most cost-effective means of providing occupant protection in automotive crashes.

Analysis of data and various information obtained from both actual and simulated crashes is important in order to improve system technology. Analysis of our seat belt system characteristics was conducted using the spring dash-pot system as indicated in Figure 1. We established dynamic performance targets for the webbing based on the data derived from our analysis and produced webbing to meet those targets.

To compare the controlled performance of Takata webbing versus conventional webbing under both dynamic and static tests, dummy tests were first conducted. The test results showed that the new webbing was superior to conventional webbing in absorbing impact energy. Static tests indicated that there were many problems which could not be confirmed or evaluated. Dynamic tests, on the other hand, showed us that although some answers were available, there were still some uncertain areas which needed additional testing.

## DYNAMIC PERFORMANCE TEST OF WEBBING

The evaluation of webbing performance can be divided into static and dynamic characteristics. There have been numerous discussions on both phenomena. As far as automotive safety seat belts are concerned, the use of static test phenomena may be standard practice but we doubt its real values.

Because there has been no standardized testing method for evaluating dynamic

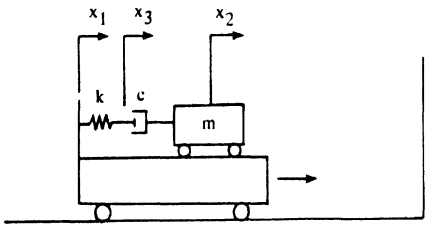


m MASS OF OCCUPANTS
k SPRING CONSTANT
c DASH POT DAMPING CONSTANT
$x_1$ VEHICLE DISPLACEMENT
$x_2$ OCCUPANT POSTURE DISPLACEMENT

Fig. 1 - Simple crash model

conditions, we created our own test equipment,. an impact test sled, as shown in Figures 2, 3 and 4. Webbing pieces to be tested were placed on the impact sled. One end of the webbing was attached to the sled and a weight was attached to the opposite end of the webbing. The weight was free to move horizontally on the sled during impact. The sled was accelerated and impacted against a barrier. At impact, the weight loaded the webbing causing dynamic elongation which was determined by analysis of high speed films of photographic targets or marks attached to the webbing.

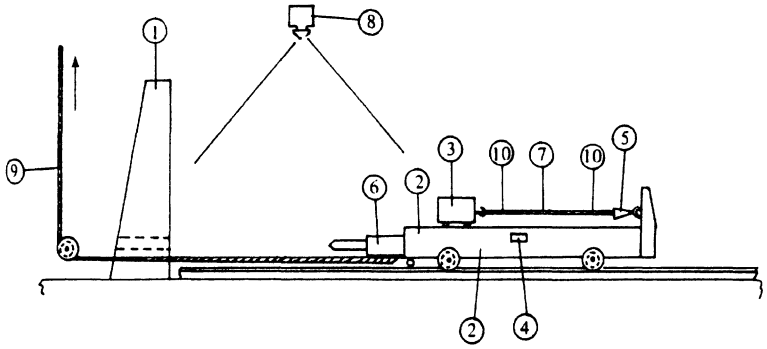


1 FIXED BARRIER
2 SLED
3 WEIGHT
4 ACCELEROMETER
5 TENSIOMETER
6 LEAD PIPE
7 WEBBING
8 HIGH SPEED CAMERA
9 WIRE ROPE
10 TARGET POINT

Fig. 2 - Dynamic test configuration of webbing utilizing sled impact test equipment

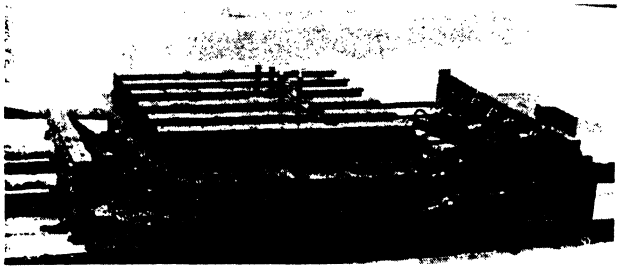

Fig. 3 - Sled for dynamic test of webbing

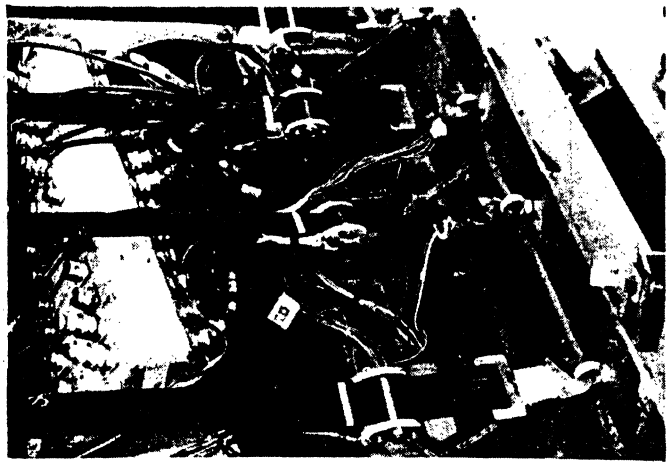

Fig. 4 - Sled for dynamic test of webbing

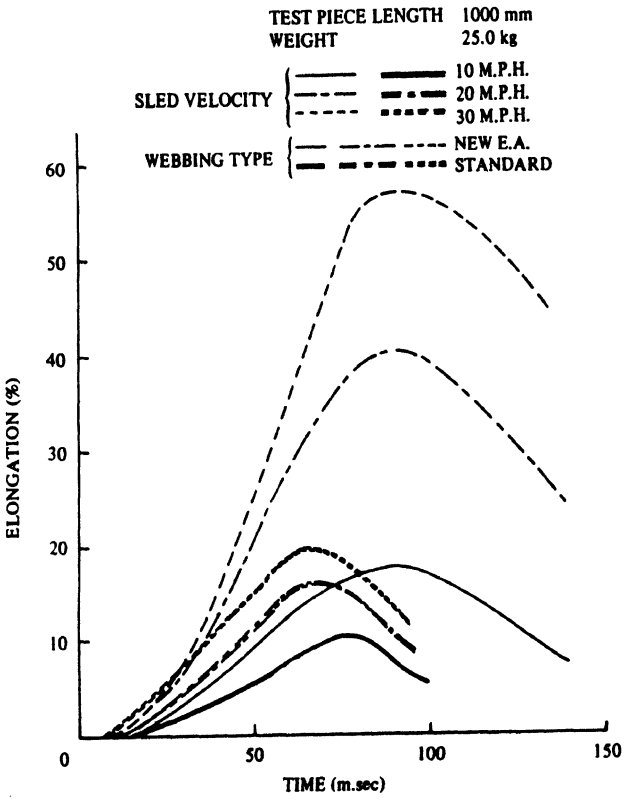


Fig. 5 - Dynamic test length versus time (webbing)

Using the time data (T) from the high speed cameras, strain vs. time curves were drawn. Examples are shown on Figures 5 and 6.

The strain rate curves show the time at which the maximum strain rates occur

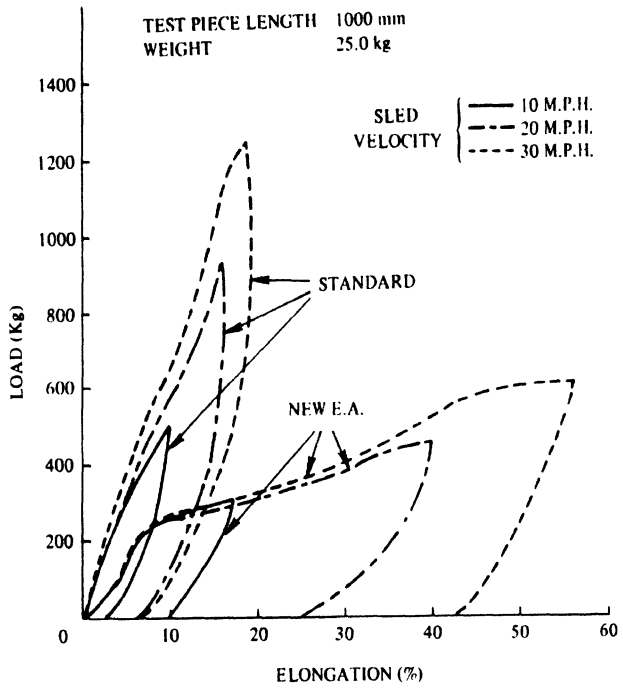


Fig. 7 - Dynamic test webbing elongation versus load

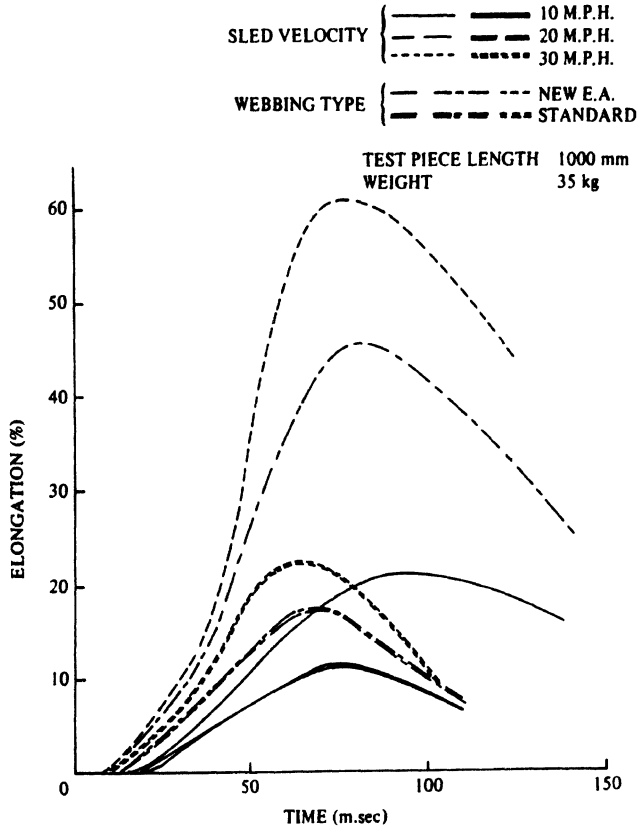


Fig. 6 - Dynamic test webbing elongation versus time

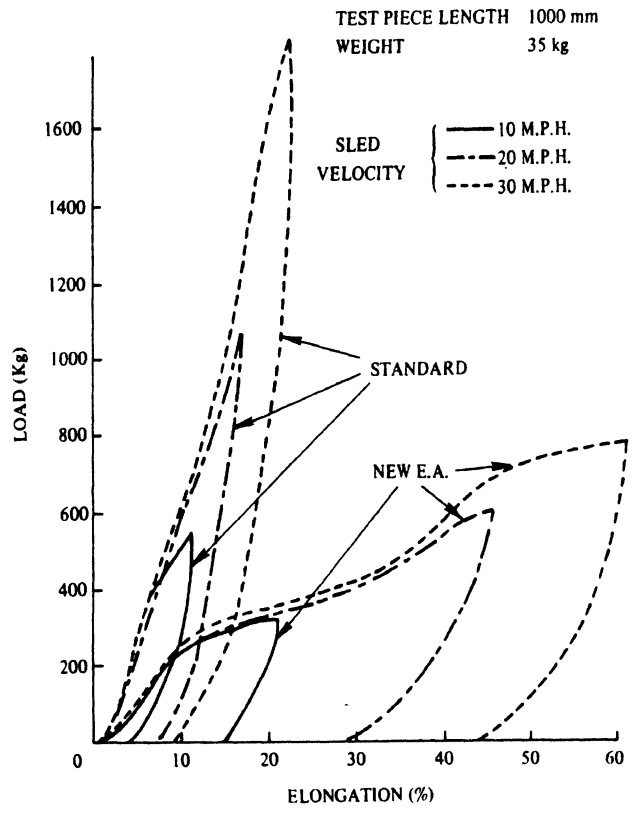


Fig. 8 - Dynamic test webbing elongation versus load

as well as the time when the strain rates become zero. However, the rate of onset of load as applied by the impact sled was not constant.

Oscillographic records of the impact sled tests, and the strain vs. time curves were used to create the load vs. strain curve. The results of the measurements are shown at Figures 7 and 8.

In Figure 9, the area O A B represent energy absorbed by the webbing per unit length in the impact sled tests. The area under the curve designated by O A C is equivalent to the work done on webbing per unit length. The energy absorbed divided by the work can be described as the energy absorption ratio.

According to our results, type F121 among the newly developed energy absorbing webbing was found to be the best as shown in Figure 10. That webbing, therefore, was expected to provide the most favorable results in dummy as well as in the live human testing at Naval Air Development Center, Philadelphia.

The Type F121 Takata webbing was

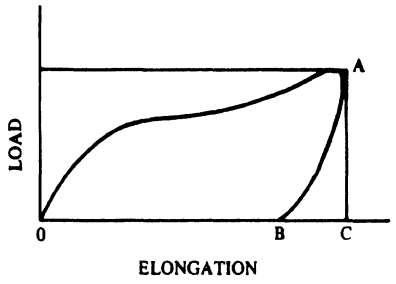


Fig. 9 - Load versus elongation curve

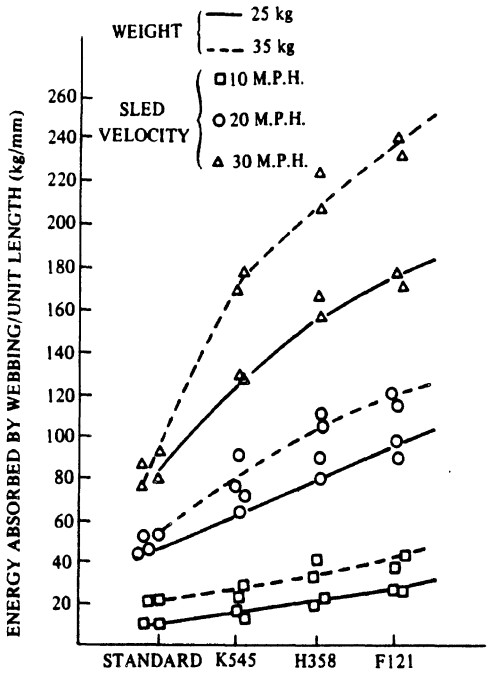


Fig. 10 - Dynamic test energy absorbed by webbing

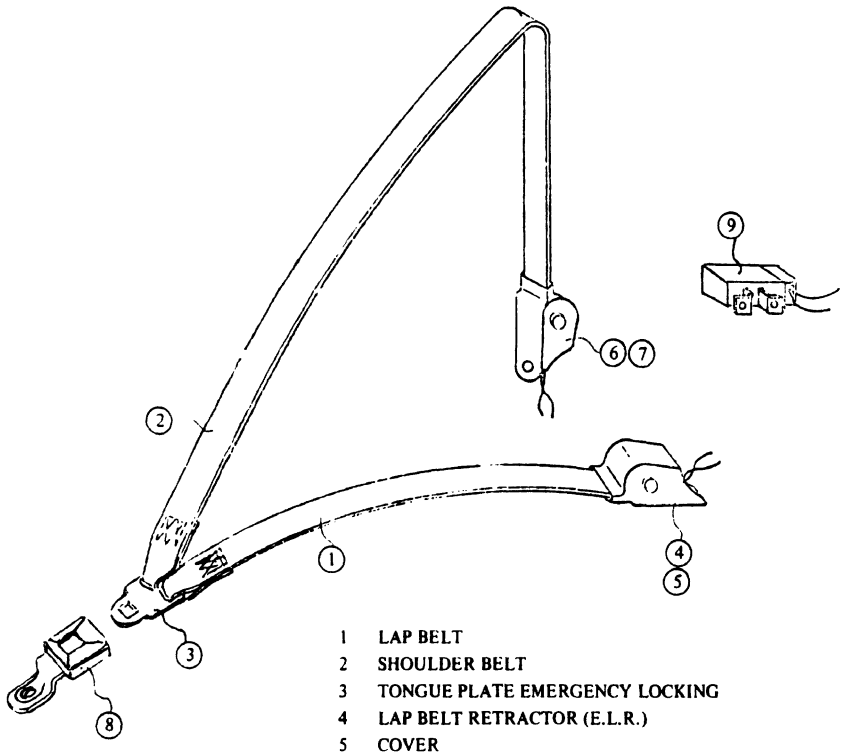


Fig. 11 - Seat belt assembly

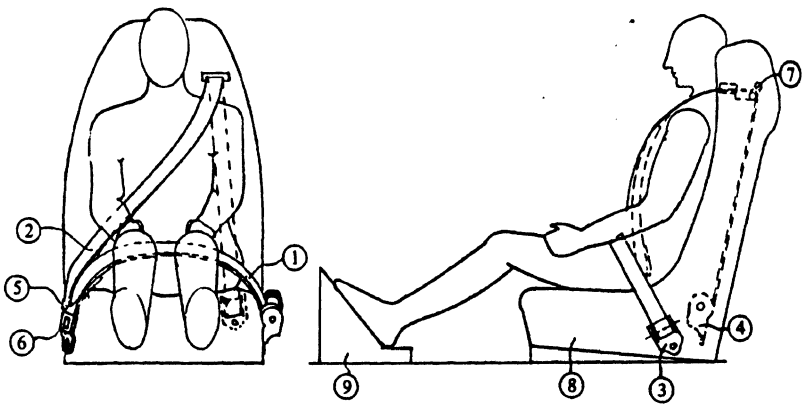

1 LAP BELT
2 SHOULDER BELT
3 LAP E.L.R.
4 SHOULDER E.L.R.
5 TONGUE PLATE
6 BUCKLE
7 SHOULDER BELT GUIDE RING
8 SEAT
9 FOOT CELL

Fig. 12 - Seat belt seat occupant system

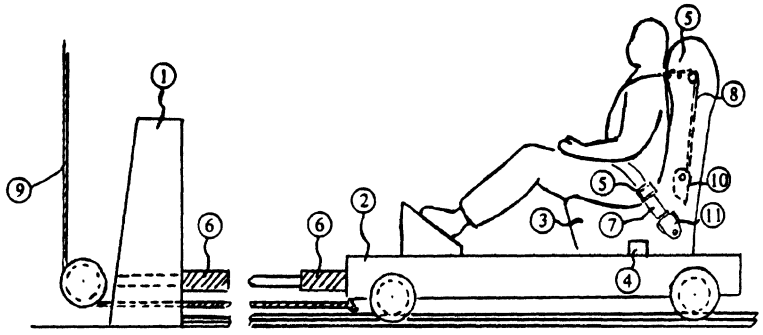

1 FIXED BARRIER
2 SLED
3 SEAT
4 ACCELEROMETER
4 ACCELEROMETER
5 TENSIOMETER
6 LEAD PIPE
7 LAP BELT
8 SHOULDER BELT
9 WIRE ROPE
10 SHOULDER E.L.R.
11 LAP E.L.R.

Fig. 13 - Dummy test configuration at Takata Kojyo

developed specifically for use as the shoulder belt in restraint belt systems. The system components are shown in Figures 11 and 12.

ANTHROPOMORPHIC DUMMY TESTS

We conducted a series of dynamic dummy tests on our sled with three-point belt systems as shown in Figures 13 and 14. One system included the newly developed webbing (F121) while the other used conventional webbing. The dummy used for the tests was the Alderson VIP 50A. The sled tests

Fig. 14 - Sled for dynamic test of seat belt assembly

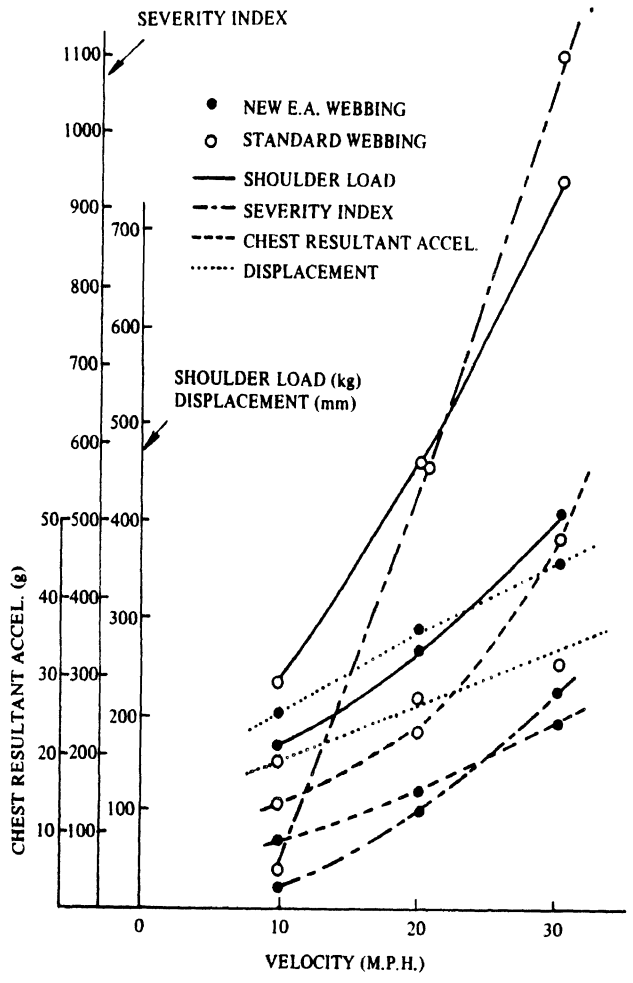


Fig. 15 - Results of dummy tests

were run at 10, 20 and 30 mph. As shown in Figure 15, the distinctive effectiveness of the seat belt system with the newly developed F121 webbing is seen by the reduction of the Severity Index as well as other performance data. The effectiveness of our new webbing was shown through our basic tests and also through dummy tests for advanced/passive belt restraint systems run by Department of Transportation's National Highway and Traffic Safety Administration at the Philadelphia Naval Base. The dummy used in those tests was the Hybrid 2. The maximum test speed was approximately 30 mph.

## HUMAN VOLUNTEER TEST

In order to determine the most effective energy absorbing belt system used in NHTSA's test program involving advanced/passive belt restraint systems, a series of tests with live human volunteers were run. Five human volunteers using three-point seat belt systems developed by Takata Kojyo participated in a series of tests starting at 5 mph and ending at 30.4 mph. Test speeds were increased in increments of 2.5 mph. The final results show that the live human volunteers were able to successfully complete a simulated car crash test of slightly more than 30 mph at slightly over 21G without injury or pain.

## SUMMARY

1. The dynamic performance of the various energy absorbing webbings developed by Takata Kojyo Co., Ltd. has been proven.
2. The results of live human tests with a three-point belt system including the new energy absorbing webbing has shown that the volunteers can endure impacts of more than 30 mph without injury.
3. Although conventional seat belt performance can be tested statically, the real performance of belts can only be shown by dynamic crash tests. Our experience shows that effective evaluation of performance lies in dynamic tests.

## ACKNOWLEDGEMENT

The author gratefully acknowledges NHTSA's contribution through its series of dummy and live human tests and the contribution made by all the people at Naval Air Development Center, Philadelphia concerned with the tests.

## REFERENCE

Juichiro Takada, "Seat Belt Type Passive Restraint System," Paper 720689X0 presented at SAE 2nd International Conference on Passive Restraints, Detroit, May 1972.

# IMPACT STRENGTH OF JOINTS IN SEAT BELTS

M. VEYSEY, B.E.
Project Engineer

D.C. HERBERT, B.Sc. (Eng.), M.I.E. (Aust.)
Assistant Director, Traffic Accident Research Unit



TRAFFIC ACCIDENT RESEARCH UNIT,
DEPARTMENT OF MOTOR TRANSPORT,
NEW SOUTH WALES.

AUGUST, 1977

ISSN 0313-2854

# ABSTRACT

The strength of seat belt joints was determined under conditions of high strain rate similar to those experienced in traffic crashes. For these tests a dynamic test rig was designed, manufactured and operated in a shock testing machine. The results of these dynamic tests were compared with the results of tests of similar joints under conditions of conventional slow strain rate (so called static) testing.

It was found that, for the various joints tested, joint strength under dynamic testing conditions was between 21 per cent lower and 8 per cent higher, and on average 11 per cent lower than that under static testing conditions.

# INTRODUCTION

The strength of a seat belt is limited by the strength of its weakest part. The weakest parts of a seat belt are the joints between webbing and other components, or those components themselves. Seat belt webbing breakage is rarely located away from such joints which explains why a minimum webbing strength is not specified in the Australian Standard[1] for seat belts (AS E35).

Although a seat belt is required to perform satisfactorily under conditions of very high strain rate and,in Australia and some other countries, to pass a dynamic test[2], the strength of seat belt webbing is usually determined by means of conventional slow strain rate (so-called "static" tension testing[3]). In addition AS E35 requires that the static strength of webbing connections be evaluated as part of a program of tests required for the purpose of examining the detrimental effects of sunlight and heat on the strength of webbing, thread and webbing connections. Results of any such tests that may have been performed have not previously been reported.

Dynamic testing of seat belt webbing has been undertaken previously[4,5,6] and the results have indicated that the breaking force of webbing is greater in the dynamic case[5,6]. Seat belt joints are known to behave differently under dynamic and static testing and it was intended to investigate this phenomenon during this study.

The direct determination of the dynamic strength of webbing is a difficult matter chiefly because of the problem of gripping the webbing without inducing fracture of the test specimen in the grips. Even under conditions of static testing, very elaborate grips are required and even then some 5 to 10 per cent of test results have to be discarded because fracture occurs outside the middle third of the between-grip length, within which valid test fractures must occur. (See AS 1753[3]).

---

[1]. Numerals refer to References.

Webbing connections do not present this problem of dynamic testing because, as already stated, they are weaker than webbing. This permits comparative tests to be conducted, in which a specially made reference joint is used to connect the test specimen, including the joint to be tested, to the testing machine.

## THE TESTING MACHINE

The determination of dynamic strength naturally requires the availability of a suitable testing machine. The main characteristics of such a machine are as follows:-

(a) The machine must be able to reproduce the strain rates encountered in real crashes in which complete belts are involved.

(b) The machine stiffness and mass must be enough to ensure that they do not unduly influence the test results

(c) An accurate record of webbing tension against time is required.

(d) The machine stroke should exceed 100 mm in order that specimens of adequate length can be broken.

In selecting a suitable testing machine for the work reported here it was decided that the machine should be adjustable over a wide range of seat belt testing pulses, be capable of much higher velocity changes than the 50 km/h upper limit of the Department's Monterey crash sled, and be capable of carrying out dynamic compression and shear tests on other crushable materials and structures, intended to be investigated in later studies.

No machine could be found that would meet these requirements, especially the 100 mm stroke figure. Accordingly it was decided to purchase a shock testing machine and to design and manufacture the necessary test rigs and instrumentation. The machine selected was the IMPAC model 1212 HVA shock testing machine supplied by MTS Systems Corporation. Details of the tension testing rig, developed for seat belt component tests, are given in the Appendix. The rig was designed and finely tuned to reproduce approximately the webbing force pulses recorded during full-scale dynamic tests performed at a velocity change of 50 km/h on the Monterey Sled.

## TEST SPECIMENS

The test specimens were selected following a survey of seat belts commercially available for use in motor vehicles. For our purposes it was not intended to test the inertia reel mechanism used in emergency locking retractor seat belts and so it was decided to test non-retractable seat belts. The joints used in both the retractable and non-retractable belts were in any case found to be similar, the webbing for example being normally identical, and the anchorage joints usually the same.

It was found that the commercially available brands of non-retractable belts were all very similar in appearance. Two brands of seat belt were chosen as being representative of those available.

Six lap/sash belts designated brand A* and six lap belts designated brand B** were purchased for test in a pilot series of static tests. Two prototype joints were designed and five samples of each were produced using brand B webbing, as shown in Figures 1 to 4.

---

* Manufactured by Cooldrive Consolidated Industries

** Manufactured by TRW Australia Ltd.

In the full series of static tests it was considered more valuable to test the lap/sash type of belt of each brand, rather than the lap/sash belts of brand A and the lap belts of brand B, in order that two types of each of the joints used in lap/sash belts could be tested. To this end 20 lap/sash seat belts of brand A and 20 of brand B were purchased. Samples of the webbing used in each brand of seat belt were also obtained; from this extra webbing, 30 lengths suitable for static testing were cut for each brand and also 20 test specimens with D-rings at one end were made for each webbing type. For the dynamic testing, half of the belt samples were sewn one end with the D-ring joint with the joint to be tested at the other end, and 30 lengths of webbing of each type were sewn both ends with D-ring joints.

## TEST PROGRAM

The pilot series of static tests was undertaken using an Avery Universal Testing Machine of 50 kN capacity. Following consideration of these results, the number and type of test specimens and the test program for the full series of static and dynamic tests were finalised.

The full series of static tests used the Avery Universal Testing Machine utilised for the pilot series. The dynamic test series was undertaken using the Impac model 1212 HVA shock testing machine and the tension testing rig as described in Appendix 1.

# DISCUSSION OF RESULTS

The results of the tests are shown in the Tables as follows:

TABLE 1:- Summary of Results of Pilot Static Tests

The results obtained in the pilot static tests confirmed that the seat belt joints were weaker than the webbing itself. In order to describe the strength of the various joints in terms of the strength of the webbing, joint efficiency was defined in the following relationship:

$$\text{Joint efficiency (per cent)} = \frac{\text{breaking force of joint}}{\text{breaking force of webbing}} \times 100$$

In the pilot study, mean joint efficiencies ranged from 44 to 77 per cent for different types of joints.

TABLE 2:- Summary of Results of Static Tests

In the full series of static tests, joint efficiencies ranged from 47 to 74 per cent.

TABLE 3:- Summary of Static Test Results. Results Divided According to the Particular Part of Joint Broken

In order to identify the particular part of the seat belt joint broken, the concept of part-of-joint efficiency was developed. By "part-of-joint" is meant the stitching, webbing or metal component part of a complete joint.

Part-of-joint efficiency was defined in the following relationship:

$$\text{Part-of-joint efficiency (per cent)} = \frac{\text{breaking force of part-of-joint}}{\text{breaking force of webbing}} \times 100$$

For the full series of static tests, part-of-joing efficiencies ranged from 44 to 74 per cent as shown in Table 3 and Figures 5 to 9 .

TABLE 4:- Summary of Results of Dynamic Tests

The mean breaking forces required to break parts of particular joints are listed in Table 4. A limitation of the dynamic test results was that no testing could be carried out on webbing alone because of the problems previously outlined, involving the design of a non-slip webbing attachment for impact accelerations of up to 30 times gravity.

TABLE 5:- Summary of Dynamic Test Results. Results Divided According to the Particular Part-of-Joint Broken

Part-of-joint mean strengths were determined by grouping the test results according to the particular part of the joint broken (stitching, webbing or metal).

TABLE 6:- Comparison Between Static and Dynamic Part-of-Joint Strength

As shown in Table 6 and Figures 10 to 14, the difference in the mean strength of the various joints in the dynamic as compared with the static case ranged from 21 per cent lower to 8 per cent higher. The dynamic test results displayed,on average, an 11 per cent lower part-of-joint breaking force than recorded in the static test.

TABLE 7:- Comparison Between the Prototype D-Ring Joint and Other Joint Strengths

In the absence of dynamic test results for webbing alone, the D-ring joint was used as a basis for comparison of the strengths of the other joints under static and dynamic testing conditions respectively.

A comparison between the force pulses recorded in test specimens and that produced in seat belt webbing during sled runs using seat belted dummies, is described in the Appendix. This comparison indicates that the force pulses recorded in the test specimens were representative of sled crashes (and therefore real life crashes), except in so far as misalignment problems were not reproduced.

## CONCLUSIONS

The joint efficiency of seat belt joints in two commercially available seat belts under conventional static testing ranged from 44 to 58 per cent. Joint strength under dynamic testing conditions was between 21 per cent lower and 8 per cent higher, and on average 11 per cent lower than that under static testing conditions.

It was found to be possible to design a joint which had an efficiency under static test conditions of over 73 per cent for each brand of webbing tested. This joint used readily available seat belt components and a typical stitching technique and appears suitable for use as an anchorage joint.

The difference between the static and dynamic test results indicated that the static testing of seat belt joints was probably both an unreliable and (usually) an optimistic technique.

For a better understanding of the strength of seat belt joints it would be necessary to dynamically test webbing concurrently with tests of seat belt joints. This would permit the determination of joint efficiency in the dynamic case.

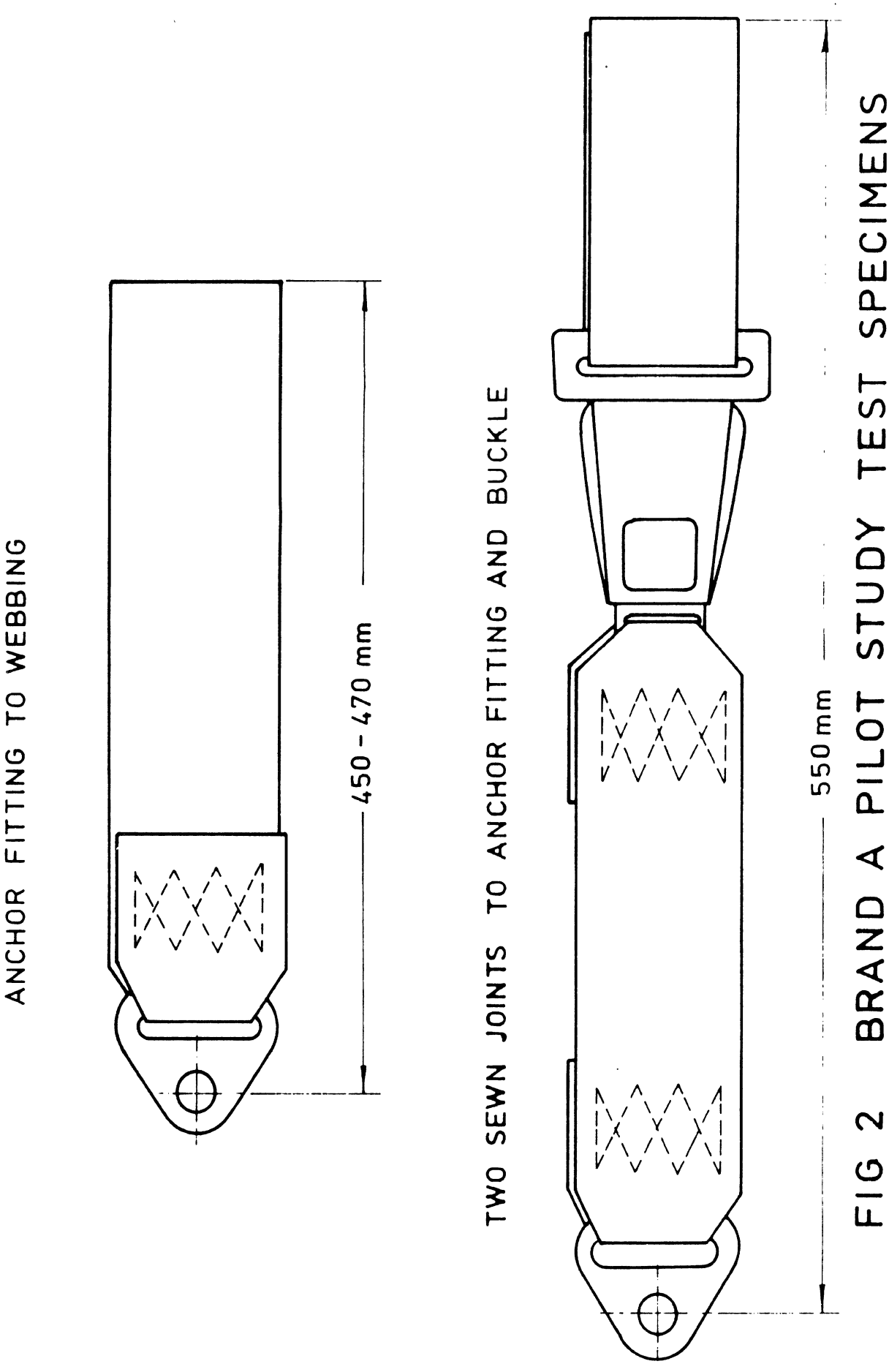


FIG 2 BRAND A PILOT STUDY TEST SPECIMENS

# APPENDIX 1

## THE DYNAMIC TEST RIG

(a) Design

The dynamic test rig was designed, manufactured and mounted in the IMPAC 1212 HVA shock testing machine as shown in the photographs of Figures 15 to 17. The test rig was designed using a computer simulation of a mass spring system as shown in Figure 18. The theoretical webbing force curve approximates the actual webbing force curve for the first 15 milliseconds or so and then deviates. This can be explained by the fact that the computer simulation assumed a length of webbing only was being testing i.e. no stitching or hardware joints - after the initial webbing stretch, breakage and stretching of the stitching (in the particular D-ring case used in Figure 18) changed the dynamic behaviour of the specimen.

The performance of the rig and machine was finely tuned to produce the required testing conditions. The requirements of the sled deceleration in seat belted dummy runs for Australian Design Rule 4C compliance testing were taken as a guide to the deceleration pulse for the IMPAC machine table deceleration. These requirements were:-

1. Velocity change > 49 km/h
2. (a) Acceleration 24 < peak G's < 34
   (b) Acceleration of the table to achieve 24g within 30 milliseconds (of impact) and to be maintained at this level for not less than 20 milliseconds
3. 30 ms < pulse duration < 80 ms

The most important requirement of these was considered to be that of 'peak G' in requirement 2(a). Variations in the parameters of drop height and programmer pressure were made and it was possible to achieve between 24 and 30G's consistently for the properties of

the different types of test sample. The pulse duration complied with requirements 2(b) and 3 and the velocity change then ranged between 35 and 42 km/h which was considered unlikely to significantly affect the results, since the breakages occurred before even this full velocity change.

These parameters produced an "acceptable" force pulse in the tested specimen as has been demonstrated in Figure 19. "Acceptable" here refers to the force pulse recorded in the tested specimen approximating that produced in seat belt webbing during sled runs using seat belted dummies. The two pulses are comparable for the first 15 milliseconds or so, and then the IMPAC curves break away from the sled curves because loading was heavier and designed to break every sample in the IMPAC case.

The typical loading rate for the specimen under dynamic test is approximately 300 kN/sec or about 10 kN/30 msec compared with the static loading rate of conventional seat belt webbing testing of about 0.37 kN/sec (22kN (Specified minimum dry breaking load) achieved in 60 seconds as specified in Appendix A of Australian Standard 1753-1975).

(b) Accuracy of measurement

One particular problem when designing the test rig was to ensure that the force maintained accurately represented the real force applied to the webbing under test. The error in the webbing force measurement due to the strain gauge transducer monitoring the force produced by the mass of the top anchorage fitting as well as the webbing force was calculated to be less than 1 per cent in a typical dynamic test. The relevant calculations follow:-

1. STATIC CONDITIONS

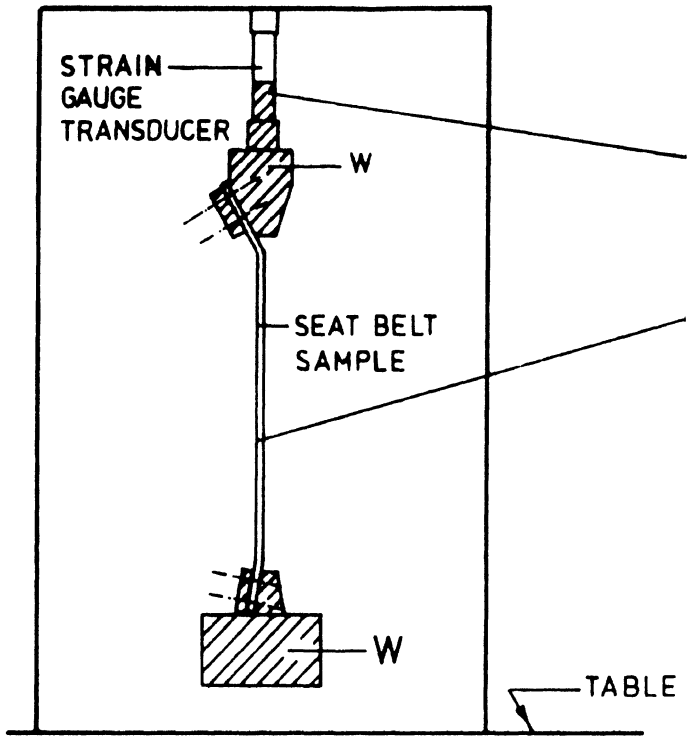


Measured in static case,

$F = W + w$

Actual Force in Seat Belt Sample,

$F_o = W$

2. DYNAMIC CONDITIONS

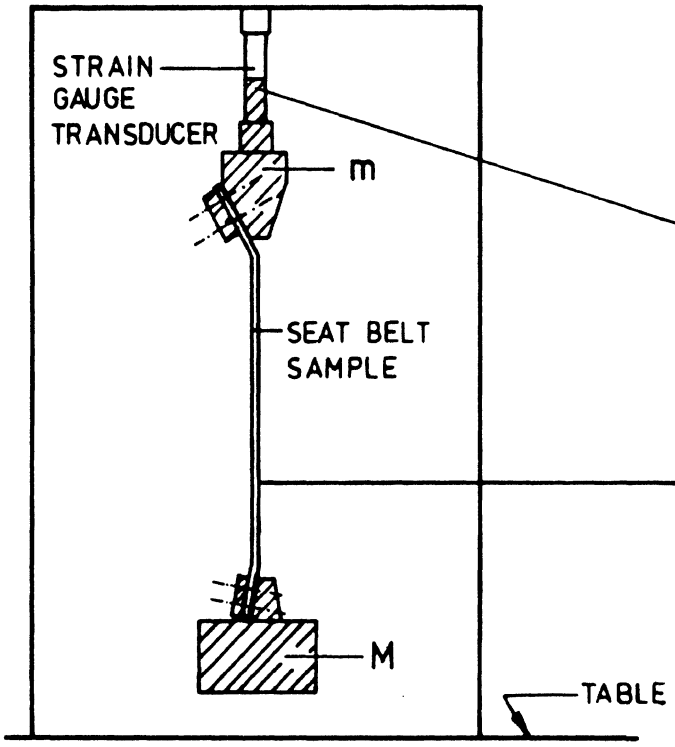


Measured in dynamic case,

$F_m = W + w + a_t.M + a_M.M$

($a_t$ = acc. of IMPAC's Aluminium Table)

Actual Force in dynamic case in Seat Belt Sample,

$F_1 = W + a_M.M$

Hence required Force, $F_{max} = F_1(max) = W + a_M(max).M$

In the dynamic case, measured force is reduced by the static value (W + w) to ensure zero offset at zero acceleration.

Hence $F_{monitored} = W + w + a_t.m + a_M.M - W - w$

$= a_t.m + a_M.M$

Now, Required Force $= F_1 = W + a_M.M$

$= F_{monitored} + W - a_t.m$

And at $F_1 = F_{max}$ (10 - 18kN), $a_t = a_t(max) = 26g$

and W = const. = (51 x 9.8)N and m = const. = 1.7kg,

Thus $F_{max} = F_{monitored} + 0.4998kN - 0.43316\ kN$

Say: $F_{max} \quad F_{monitored}$

(at $F_{max}$(min.expected) = 10kN, error = 0.06664kN

= 0.66%

< 1%).

3

# The Dynamic Properties of Seat Belt Webbings and End Fixings as Tested on the Pneumatic Accelerator

by E. J. Brabin

Mr. Brabin graduated from the University of Technology, Loughborough, with a degree in Automobile Engineering. Prior to joining MIRA in 1967, he was employed by Standard-Triumph Motor Co. Ltd. and by Lotus Developments Ltd.



## 1. Introduction

AN investigation of the properties of seat belt webbing is necessary for a general examination of how effective present webbing materials are and in particular for use in mathematical models of restraint systems in occupant dynamics work. In spite of there being static and dynamic British Standard tests of seat belt assemblies (Ref. 1) there seems to have been little published work on this subject. Dynamic tests are necessary as the properties of the belt tested statically are not necessarily those of a belt under dynamic conditions, many materials behaving differently under high rates of strain. Also for occupant dynamics work it is useful to isolate rate of strain and determine load/extension curves for constant strain rates, previous attempts at obtaining dynamic properties of webbing have generally contained a mixture of strain rates from very high rates to zero as the energy of the impacting body is absorbed. In a seat belt assembly the end clamps of the belt could also have a large effect on the performance on the belt itself so an examination of these fixings was also carried out.

There are two common materials in use to-day for seat belts, terylene and nylon. In this investigation four webbings were chosen all in current use by vehicle and accessory manufacturers, two of terylene and two of nylon. The webbing materials tested were: Pebble Weave terylene, Standard 316/9 terylene, 270 Teleflex nylon and Dynasafe nylon (Fig. 1). All these belts conformed to B.S.I. and the manufacturer's specifications which set a maximum elongation for a given load. One further belt material was used as a standard for all the clamp tests, this was a WR1021A nylon webbing having abrasion resistant properties, again

Fig. 1. Seat Belt Webbings
*Top left:* Dynasafe Nylon. *Top right:* W.R.1021A Nylon
*Centre:* Pebble Weave Terylene
*Bottom left:* Teleflex Nylon. *Bottom right:* Standard 316/9 Terylene

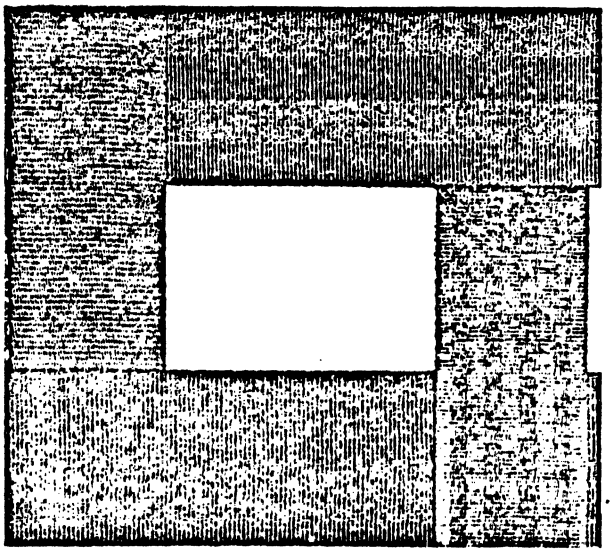

Fig. 2. Seat Belt End Fixings
*Top left:* Double Slot Clamps *Top right:* Slot and Ring Clamps
*Bottom left:* A.I.D. Clamps. *Bottom right:* Slab Clamps

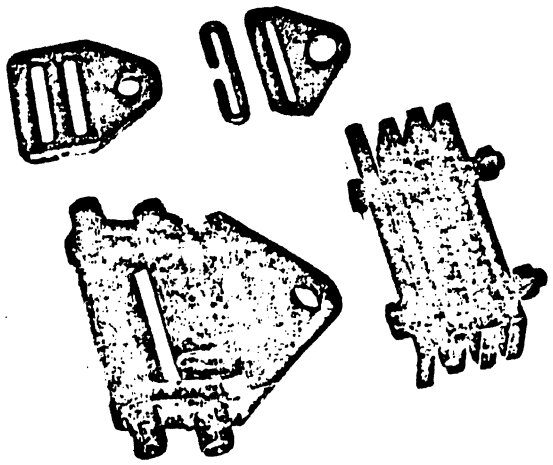

currently used by a large vehicle manufacturer. The four pairs of end clamps tested consisted of two types used for laboratory testing and two types in current vehicle use. (Fig. 2.) The first type of clamp considered was the webbing bollard used by the Aeronautical Inspection Directorate for laboratory tests, the second laboratory clamp was a simple slab design holding the belt in a zig-zag pattern. The two vehicle clamps tested were firstly a slot and ring type in which the webbing passes through the slot round the ring and back out of the slot, a variation on this type was also tested which had anti rubbing caps either side of the slot and secondly a double slot type of clamp threaded the same way as the A.I.D. clamps. These clamps were in fact manufactured at MIRA in a heavier gauge material but in all other respects were identical to standard clamps.

## 2. Air Gun and Instrumentation

All the dynamic webbing tests were carried out on a pneumatic linear accelerator housed in the impact laboratory. The principle of the "air gun" is based on a smaller device in use at Birmingham University, the intention being to build a dynamic tensile and compressive testing machine which could impact materials and small structures at rates up to 75 ft./sec. with readings of load and extension being readily obtainable. A pneumatic device was chosen as being simple, reliable and cheap to build and run. Speed control is fairly accurate (within 5%) though not of course as accurate as its lab. mate the linear induction motor. Fig. 3 shows a diagram of the Air Gun and Control System. The air gun is operated by charging cylinder C via orifice A with air to the required pressure. The same pressure is then imparted to the back of the piston via orifice B, this releases the piston off its seal and with the piston surrounded by compressed air it is driven through its working stroke. The inertia at the end of the stroke is absorbed by a ring spring D and the whole air gun body moving forwards through plain bearings E controlled by a damper F. The energy of the piston is imparted to a trolley which can either be used for crushing a material against a small steel faced concrete block or for stretching a material by attaching one end to the trolley and the other to the air gun bed. (Fig. 4.)

As can be seen from Fig. 3 the compressed air can be obtained from a 100 p.s.i. supply and its pressure raised to 1,500 p.s.i. by use of an air booster or the reservoir can be replaced by one or two compressed air cylinders containing air at 2,000 p.s.i. This high pressure air is then bled into the cylinder via a control valve and pressure gauge. Also on this line is a control valve to atmosphere to allow the gun to be de-pressurised if for example it is found to be necessary to adjust the test sample, and this valve is also kept open when working in the gun test area to remove any possibility of an accidental firing. During this process a 3-way solenoid valve vents orifice B to atmosphere to

Fig. 3. Diagrammatic View of Pneumatic Accelerator and Control System.

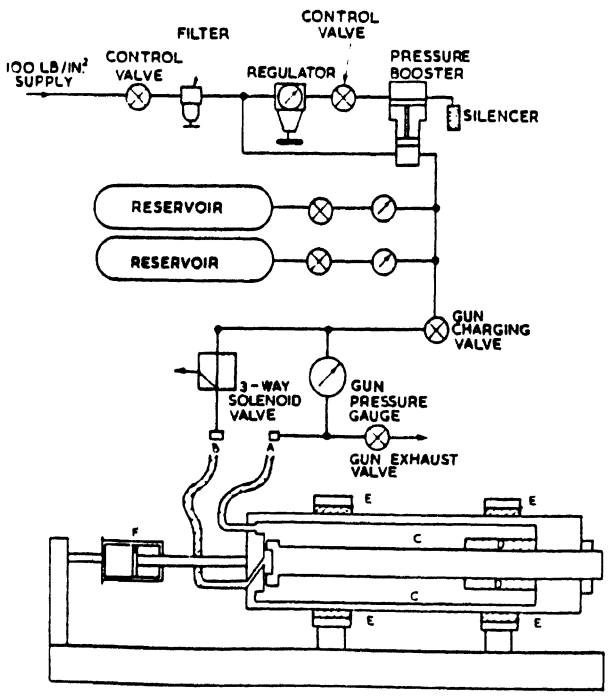


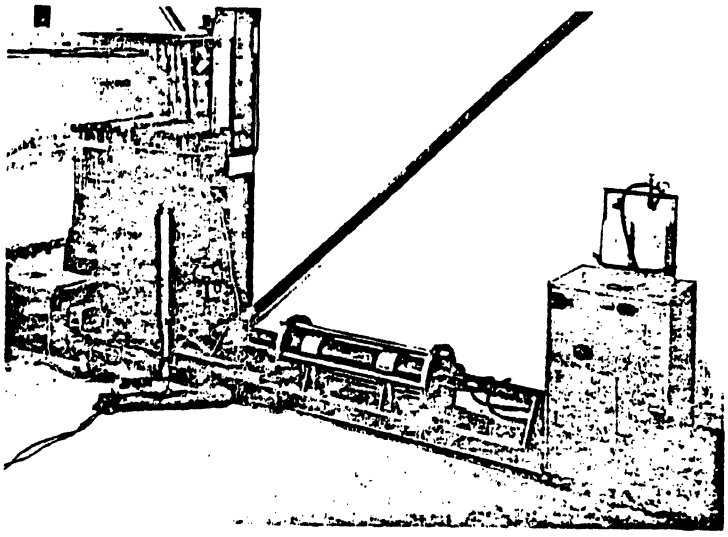

*Above:* Fig. 4. Air Gun and Control Console

*Below:* Fig. 5. Air Gun Trolley showing webbing in test position with the camera mounted directly above it. The grid of the displacement sensor is attached to the side of the trolley and the accelerometer can be seen mounted on the back plate of the trolley

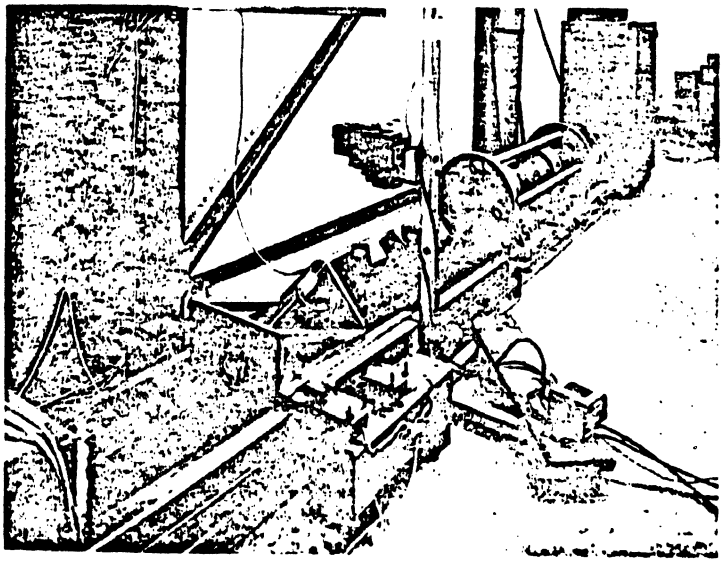

prevent any pressure build up behind the piston which again may cause accidental firing. This solenoid valve is operated by an ignition key and when the desired pressure is registered on the gauge the key is turned which closes the valve and allows cylinder pressure to reach the back of the piston, thus firing the gun. The ignition switch operates the solenoid valve via relays which also switch on and off the U.V. recorder at the correct moments.

The U.V. recorder gives readouts from the accelerometer mounted on the trolley, displacement sensor, timing lights, and velocity. Thus for any moment of impact, strain rate, displacement and load may be immediately obtained. Load is obtained directly from the accelerometer reading as the trolley weight is constant throughout impact and in cases where the sample is attached to the trolley the sample weight is assumed to be negligible compared with the weight of the trolley. Displacement is obtained by means of a copper etched grid attached to the trolley passing through a sensing device consisting of a pair of lights and photocells. (Fig. 5.) This gives a square pulse on the trace for every 0·1″ movement on the fine scale and every 1″ displacement on the coarse scale, thus displacement at any point after impact is obtainable by counting the number of pulses from the start of the impact. These displacement pulses are also electronically summed over time to give a direct velocity readout for the entire impact and rebound. Finally the trolley passes through a pair of timing lights just before impact to give impact speed and calibrate the velocity trace. There is also a numerical readout from a racal counter of the time taken between these lights.

## 3a. Dynamic Tests

For the webbing tests a 70 lb. trolley was used, as there are three attachments in a lap and diagonal seat belt assembly for which the webbing was intended, this approximates to a 210 lb. wearer. (The 95 percentile weight of an American male is 217 lbs.) One end of the belt was clamped to the air gun bed, the other to the trolley, and enough slack was allowed in the system to ensure the trolley was rolling free and not energised by the piston at impact. A sample length of 30″ was chosen to both be economical on webbing and reduce clamp effects, the clamp effects being noted by photographing a marked gauge length in the centre of the belt alongside a fixed graduation. A photosonics camera was used at first but due to the high cost of film and delay in processing a Cossor scope camera is under development for this purpose. This camera works on the principal of a length of film travelling normally to the direction of belt strain continuously recording graduation lines and two marker dots on the belt, the shutter being permanently open. The camera has also been fitted with a timing light to enable it to be synchronised with the U.V. Recorder. Thus from the enlarged film negative the strain can be directly measured for a given load, and if this is then subtracted from the overall extension obtained from the U.V. trace, the clamp effects may be determined.

Fig. 6. Damaged Clamps.
*Left:* Slot and Ring Type with anti-abrasion inserts
*Right:* Double Slot Type

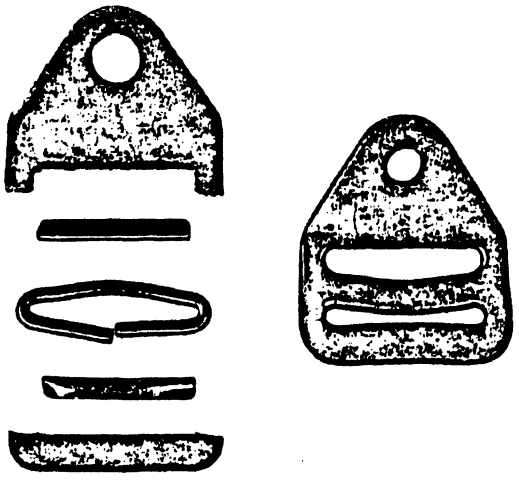

From each impact a load/extension curve is obtained showing the energy absorbed by the belt and its elasticity, and also the load and extensions were noted at particular velocities. The four webbing materials were subjected to several impacts at increasing velocities up to breakage, thus load/extension curves were obtained for these particular velocities. Also at one low and one high speed the belt was given a second impact to determine any change in property after the initial impact.

The dynamic clamp tests were conducted in a similar manner to the above using four pairs of clamps and the standard anti-abrasive nylon belt, each test being photographed, and the effect of the clamp determined.

## 3b. Static Tests

The webbings were tested statically (i.e., at a speed where dynamic effects are minimised, usually less than 1 in./min.) on the Dennison tensile testing machine. To avoid any errors due to end clamp effects, lengths of the webbing were held in the serrated jaws of the Dennison and a marked gauge length in the centre of the belt was photographed alongside a ruler at given increments of load. Finally the four webbings were taken to their failure load with various end clamps and the load and extension at failure was noted.

Static clamp tests were also carried out on the Dennison machine. Using the standard webbing four pairs of clamps were individually mounted in the jaws of the tensile machine and readings of load and extension were taken together with a measurement of the amount of belt that had slipped through the clamps. Also a note was made, for each pair of clamps, of the load and extension of the standard belt at breakage.

## 4. Results of Clamp Tests

The tests on seat belt clamps were carried out both to find a suitable clamp for the webbing tests and to discover what effect the clamp had on the webbing. Hence only clamps in which it is easy to load the belt and require no special method of attachment, such as stitching, were tested.

The clamp effect was determined in both static and dynamic tests by subtracting the actual webbing characteristic from the belt characteristic when held by a pair of the clamps under test. This gave the clamp effect for a pair of similar clamps, which was then halved to obtain the total slip for one clamp It was difficult to measure accurately the actual slip through the clamp as determining the strain of the belt at the clamp edge is complex. The clamping action interferes with the volumetric strain of the belt so alters the strain in the direction of the load. Thus the belt slipping through the clamp not only takes up the strain of the rest of the webbing under load and the strain due to clamp

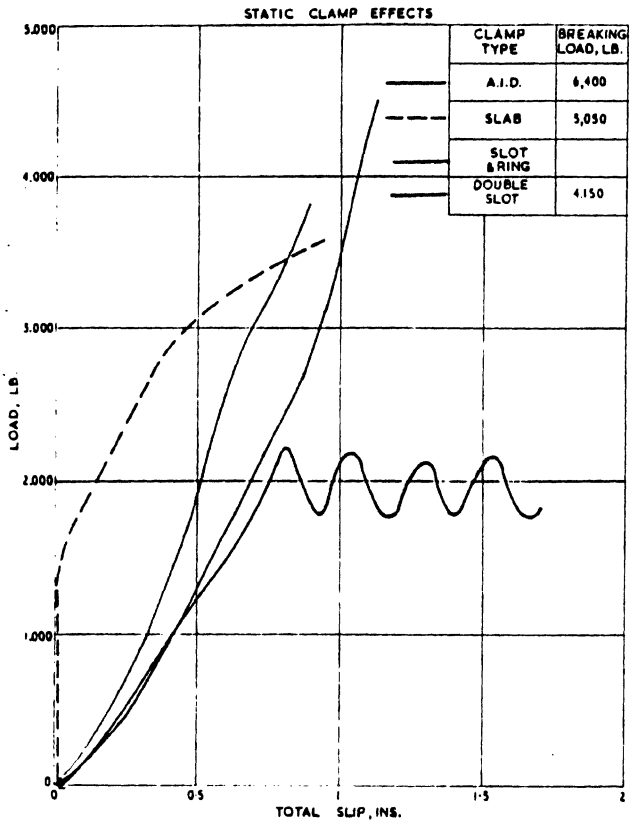


Fig. 7

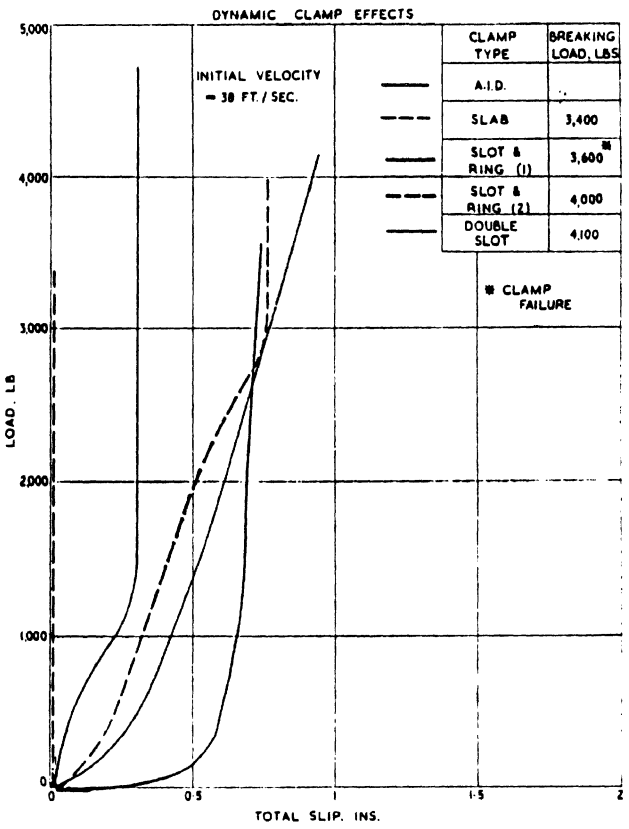


Fig. 8

interference but has possibly been prestrained by its passage through the clamp as well. Total slip is the sum of all these effects and to obtain actual extension for a belt at a given load would have to be added to the figure obtained from the load extension curve for each clamp.

Figs. 7 and 8 show load plotted against Total Slip for static and dynamic tests using the standard WR.1021A nylon belt. It is immediately noticeable that clamps behave differently under impact loading and allow much less slip with dynamic loading. Most noticeable is the slot and ring type of clamp which under static loading slipped continuously over 2,000 lb. and was unable to take the belt to its failure load. At an impact loading at 38 ft./sec. the same clamp allowed about ¾ in. slip and then held the webbing firmly. This clamp was fitted with anti-abrasion caps either side of the slot and failed under a load of 3,600 lb. (Fig. 6) so another pair of clamps were tested similar to this type but without the caps (slot and ring (2) ) and these took the belt to its dynamic failure load. The only other damage that occurred to clamps was to the double slot type which were slightly bent (Fig. 6). These clamps were of thicker gauge steel than those used in vehicles so it is likely that this damage would also occur to the standard clamp.

From Figs. 7 and 8 it can be seen that the method of clamping can alter both the breaking load and total extension of the same belt quite considerably. For the tests on webbing properties the slab clamps were chosen as they allowed no belt slip at all under high rate of strain but they suffered from the disadvantage of giving a low belt breakage load. To overcome this the A.I.D. clamps were used as well which allowed about ¼ in. slip and then held the belt firmly; possibly due in part to this small amount of slip, the belt had a far higher failure load when held in this clamp, these being the only clamps in which the belt did not fail when impacted at 38 ft./sec. by the 70 lb. trolley.

## 5. Results of Webbing Tests

Figs. 11 to 14 show the characteristics obtained by testing the four webbing materials at three different constant speeds and statically. The two nylons are fairly similar, giving high failure loads at their maximum strain of 20–25%. Also the shape of the Pebble Weave terylene curve is similar to the nylons, but giving lower loads before breakage again at a strain of 20–25%. The Standard 316/9 terylene webbing however has a somewhat differently shaped characteristic in that failure does not occur until 35% strain and at lower load than the failure load of nylon belts. The failure loads of the webbing are less under impact loading than those obtained statically, but generally the static failure gives some indication of the dynamic failure load.

The difference in the characteristics for varying speeds seem very small and the dynamic curves can be considered similar within the scatter due to webbing irregularities. Also the curve obtained by static testing again gives a reasonable indication of the shape of the dynamically tested webbings at speeds up to 40 ft./sec. Curves were not plotted for higher speeds than 25 ft./sec. as belt breakage prevented enough points being taken. However all the data collected on dynamic tests were used to obtain the following equations for the dynamic characteristics and the static characteristic equations were also obtained.

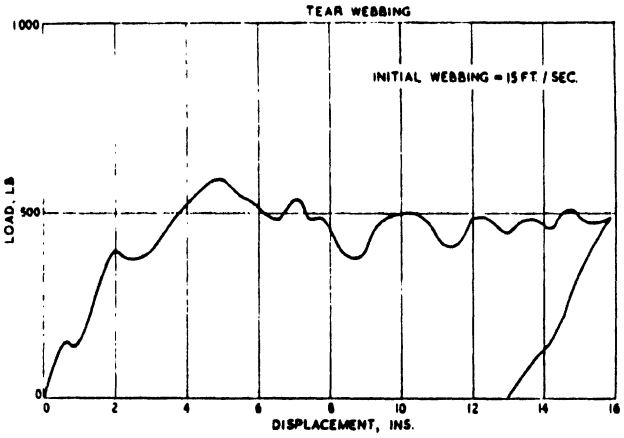


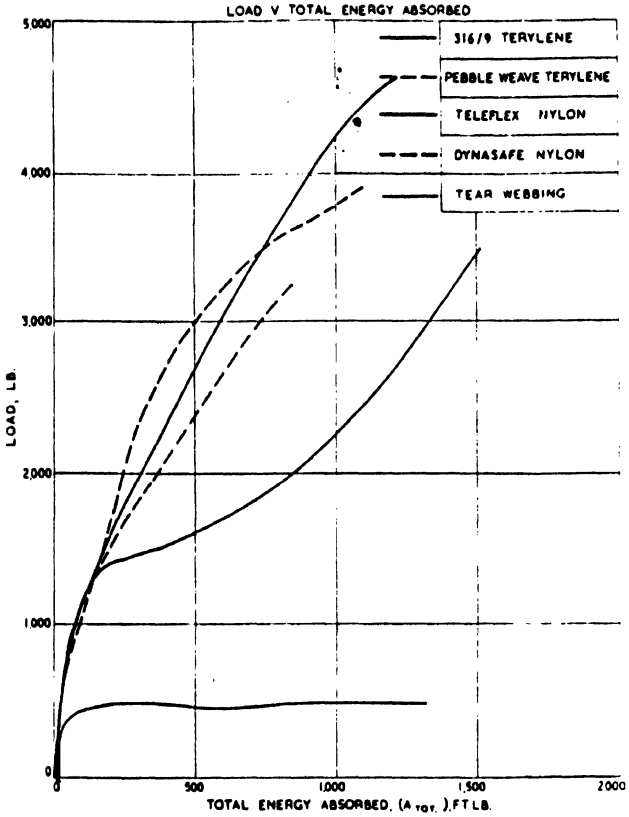


*Above:* Fig. 9

*Right:* Fig. 10

*Below left:* Fig. 11

*Below right:* Fig. 12

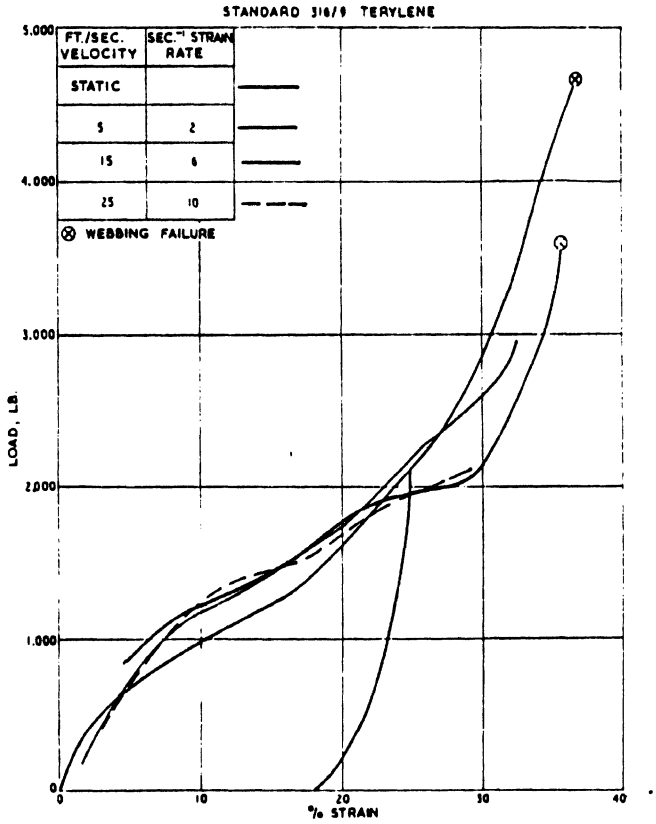


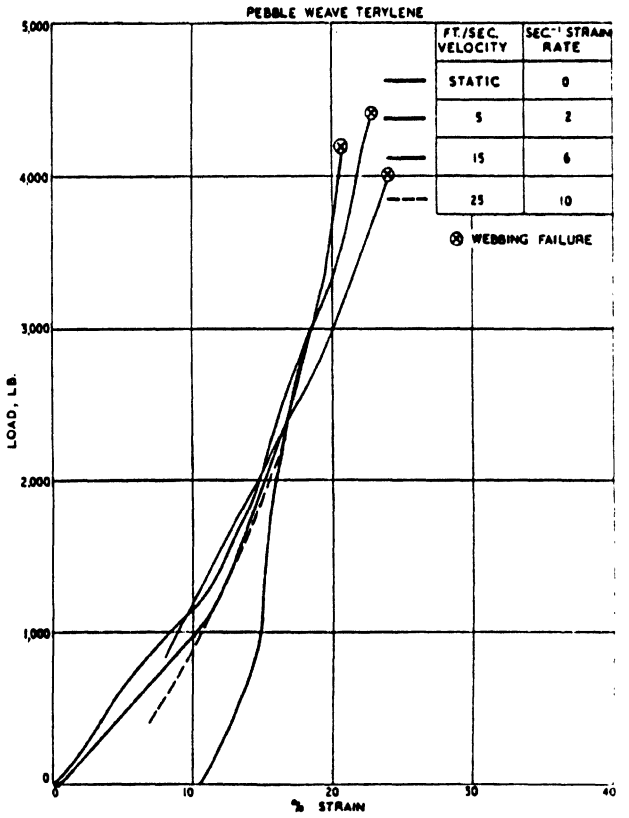

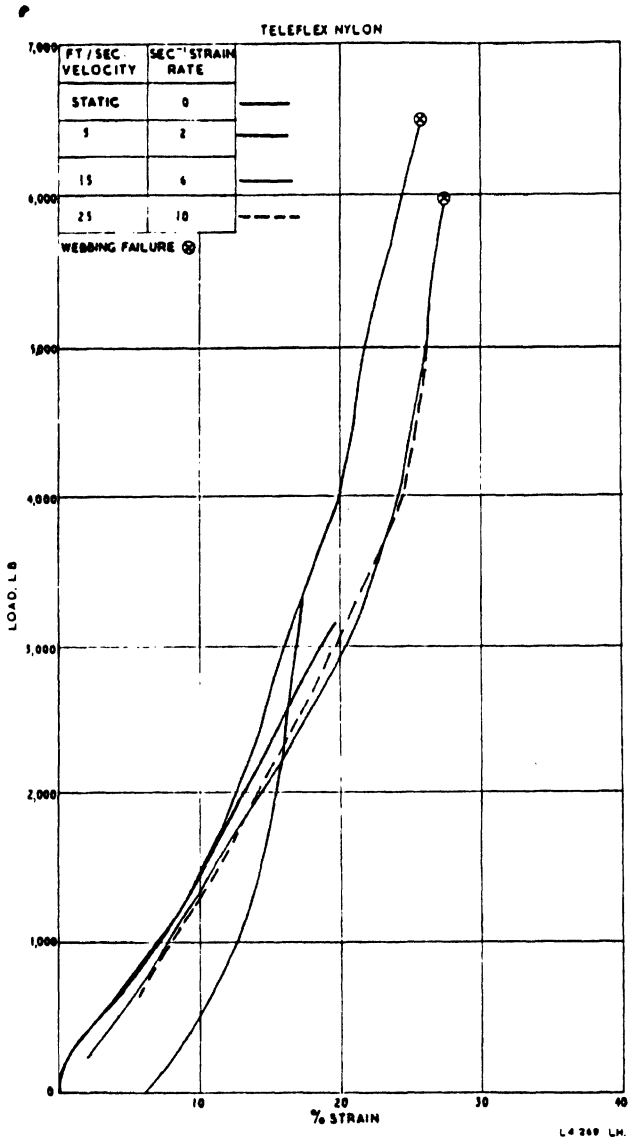


Fig. 13

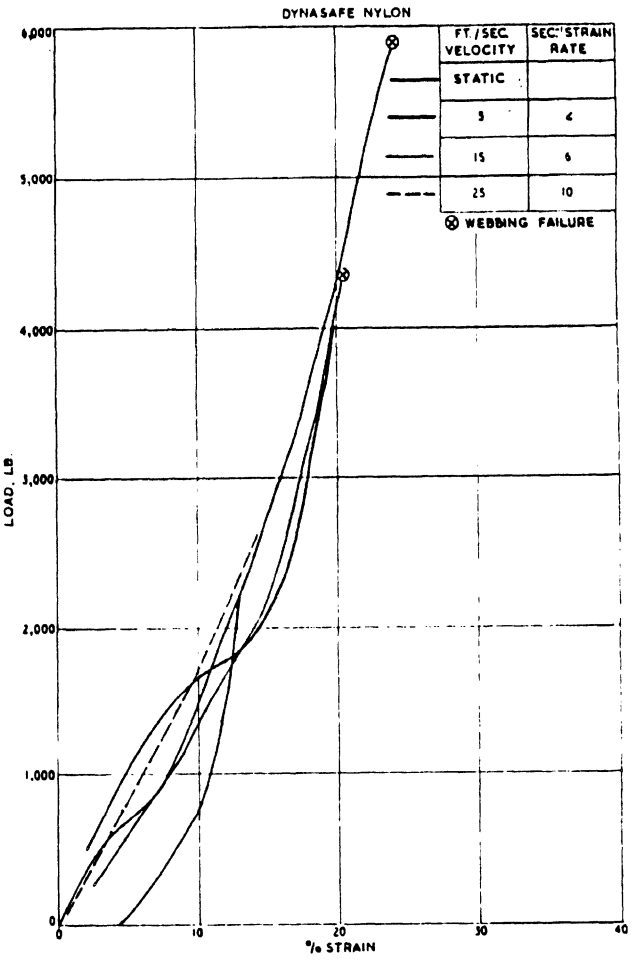


Fig. 14

*Standard* 316/9 *Terylene*

Static $P = 165x - 7{\cdot}96x^2 + 0{\cdot}191x^3$
Dynamic $P = 210x - 9{\cdot}95x^2 + 0{\cdot}186x^3$

*Pebble Weave Terylene*

Static $P = 124x + 0{\cdot}70x^2$
Dynamic $P = 80x + 4{\cdot}94x^2$

*Teleflex Nylon*

Static $P = 78{\cdot}7x + 6{\cdot}75x^2$
Dynamic $P = 100x + 3{\cdot}30x^2$

*Dynasafe Nylon*

Static $P = 110x + 5{\cdot}49x^2$
Dynamic $P = 128x + 2{\cdot}51x^2$

Where $P$ = Load in lb.
and $x$ = % strain

The dynamic characteristic equations were integrated to find the total energy absorbed ($A_{TOT}$). This is the sum of the reversible ($A_R$) and the irreversible ($A_I$) energies absorbed. Total energy absorbed was plotted against load for the four webbing materials and is shown in Fig. 10. Also in this figure is shown the curve obtained from a material used for energy absorption purposes called tear webbing (Ref. 2). The load/displacement curve for tear webbing is shown in Fig. 9; it can be seen that it is a good constant yield energy absorber with only a small amount of elasticity.

Figs. 15–18 show graphs plotted of load against percentage strain for two different initial impact velocities, 28·5 ft./sec. and 15 ft./sec. These graphs show the reversible and irreversible energies absorbed at these two speeds for the four materials, although of course the speed varies down to zero at maximum strain. Also on these graphs is shown the result of a second impact at the same speed. The two nylon webbing properties are not altered very much by the first impact. However the Standard terylene gives high loads for less strain under the second high speed impact and the Pebble Weave terylene failed when impacted twice at its normal failure load. Also the tables in these figures show the percentage irreversible energy absorbed of the total energy to be absorbed. The Standard terylene was by far the highest in this respect and thus is a better energy absorber than the Pebble Weave terylene and the two nylon webbings.

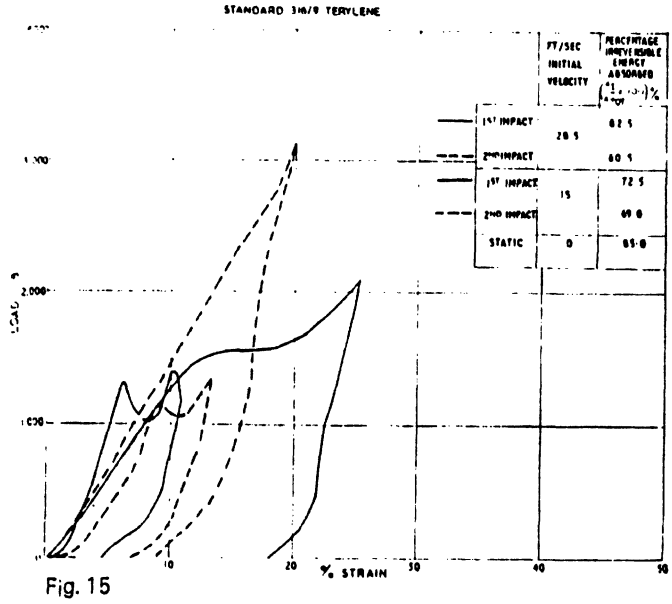


Fig. 15

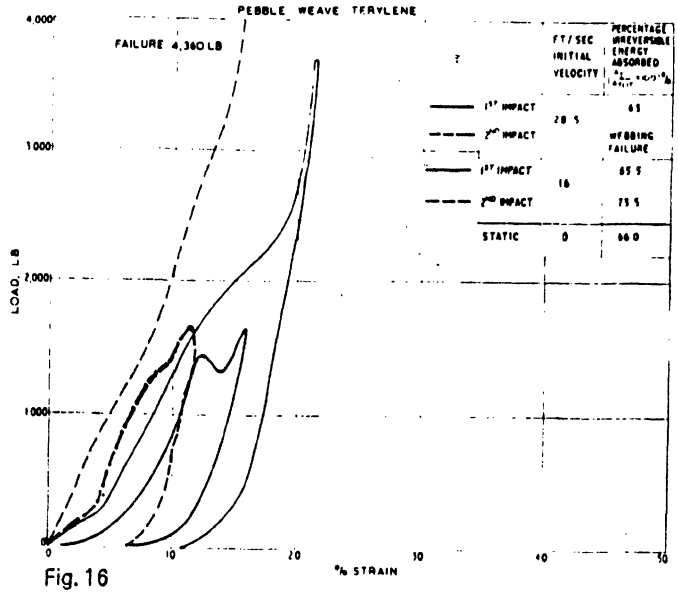


Fig. 16

Fig. 17

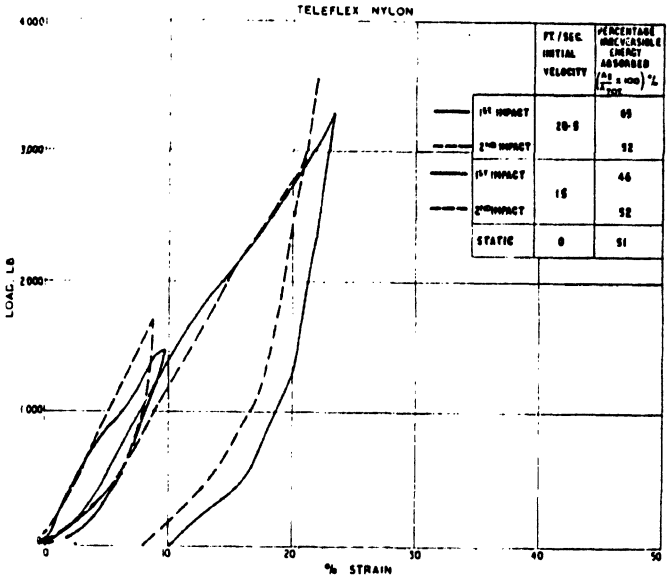


Fig. 18

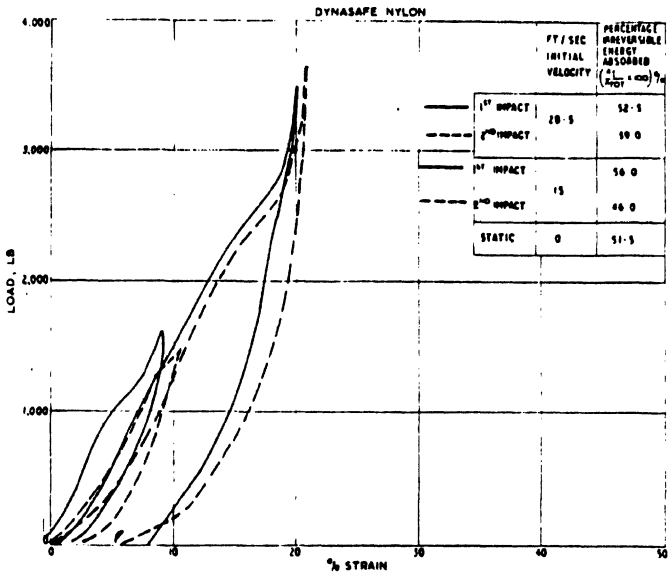


## Discussion of Results

The ideal webbing property is probably a constant yield device. According to Searle (Ref. 3) the replacement of a linear spring device by a constant yield device will reduce by approximately 50% the peak deceleration of the occupant. A low hysteresis seat belt should tend to give the occupant a high rebound velocity after restraint. However this is possibly a minor effect as Lister and Nielson (Ref. 4) concluded that there is no significant difference in the rebound velocity of dummies in crash situations between terylene and nylon webbings. The major effects of low hysteresis, high elasticity type of seat belts are the small amounts of energy absorbed and the high belt loadings under small strain; this may be clearly seen in Figs. 9–18. For example, in Fig. 10, to absorb 1,000 ft. lb. of energy, Teleflex nylon would be loaded to a maximum of 4,250 lb., Standard terylene to a maximum load of 2,250 lb. and the efficient energy absorber would be operating at only 500 lb. to absorb this energy. Obviously there is also the stroke of the absorbing device to consider. Grime (Ref. 5) states that out of a sample of injuries to belt wearers in vehicle accidents, two-thirds were caused by striking some part of the car and the remaining one-third were caused by the forces imposed by the safety belt. Thus at present the shorter stroke, higher load belt would seem to be slightly better in practice but this is far from the ideal. Belts at present could be selected to suit the space available in front of the wearer and ultimately this space could be increased to allow lower belt loadings.

The energy of the occupant in an actual frontal impact however is not only absorbed by the belt hysteresis. Energy is also absorbed by the compression of the occupant's body, belt slip through the clamps and by transmission of the energy to the vehicle body increasing the vehicle deformation.

To obtain a realistic figure for belt loadings a number of 30 m.p.h. vehicle crash tests carried out at MIRA were examined. These crashes were all frontal into the flat faced

block and the dummies used in the vehicles were the Royal Aircraft Establishment Mk. VB.

Table I gives the results of this investigation. Ten vehicles were crashed with nylon and terylene belts fitted, all being of the lap and diagonal type. This gave a total of thirteen seat belts tested out of which there were two clamp failures and one belt failure. The highest load seen was 2,400 lb. at the floor mounting of the lap and diagonal belts. This is probably rather high and by averaging out the maximum loads for the three attachment points, Table I shows that the highest is again the floor mounting of the lap and diagonal at 1,600 lb. This may still be slightly high due to the high rate of the dummies used compared with human occupants. Of interest are the very much lower shoulder attachment point loads when inertia reel belts are used; this would agree with the results obtained by Grime (Ref. 5) from actual vehicle accidents. The belt and clamp failure loads encountered in the webbing investigation were well above these two maxima and so possibly are of no concern, although there were belt and clamp breakages in the vehicle crash tests.

| *Test No.* | *Shoulder Mount* | *Floor Lap Mount* | *Floor Lap and Diagonal Mount* |
|---|---|---|---|
| 1 | 1,511 | 869 | 1,803 |
| 2 | 1,898 | 2,055 | 2,395 |
| 3 | 1,747 | 1,726 | 1,823 |
| 4 | 1,806 | 896 | 1,565 |
| 5 | 1,750 | 1,134 | 940 |
| 6 | 1,380 | 1,010 | 1,620 |
| 7 | 1,390 | Failed at 1,000 | — |
| 8 | 1,235 | 305 | 1,067 |
| Average | 1,590 | 1,140 | 1,600 |
| | *Shoulder Mount with Inertia reel* | | |
| 9(*a*) | 1,087 | | |
| (*b*) | 894 | | |
| 10 | 1,050 | | |
| Average | 1,010 | | |

**Table I**

Maximum Belt Loads of Lap and Diagonal Safety Belts in vehicles crashed at 30 m.p.h. (Loads in lb.)

## Conclusions

1. Present webbing material is adequately strong for occupant restraint.
2. Static testing of webbing material gives a good indication of the dynamic properties up to strain rates of 40 ft./sec. (16 $sec^{-1}$).
3. Webbing End fixings behave differently under dynamic load to static loading and alter considerably the overall characteristic of the seat belt.
4. Compared with an energy absorbing material, the Standard 316/9 Terylene webbing is reasonable and the Pebble Weave Terylene, Teleflex Nylon and Dynasafe Nylon webbings are poor energy absorbers.
5. Belt loads could be lessened considerably and the occupant striking the interior of the vehicle in frontal impacts could be avoided by fitting belts of good energy absorption properties with their working lengths and loads adjusted to suit the space available in front of the occupant.
6. To calculate the total displacement of the belt at a particular load, the strain is determined from the webbing characteristic equation or curve and to this is added the total slip at the clamp for each fixing.

## References


1. British Standard 3254:1960.
2. BRABIN, E. J. Energy Absorbing Devices Used in Crash Testing. *MIRA Bulletin* No. 2, 1968.
3. SEARLE, J. A. The Optimisation of Occupant Restraint for Frontal Impact. *MIRA Report* No. 1969/11.
4. LISTER, R. D., and NEILSON, I. D. Materials for Seat Belt Assembly Webbing Observations of Rebound of Dummies for terylene and nylon. Road Research Laboratory Note No. LN/206/RDL.IDN.
5. GRIME, G. Accidents and Injuries to Car Occupants Wearing Safety Belts.


## Acknowledgements


The Author thanks Mr. E. Thompson, Technical Director of Alberton Ltd., for his co-operation and for supplying the majority of the webbings tested in this article.

The Author also wishes to acknowledge Mr. M. G. Tarratt for his work on the instrumentation of the Air Gun and Miss A. M. Wilson for her help in the analysis of the results.

SAE Technical Paper Series

810234

# Material and Design Interactions in Collision Energy Management

**Bernard S. Levy**
Inland Steel Co.

**International Congress and Exposition**
**Cobo Hall, Detroit, Michigan**
**February 23-27, 1981**



FREEDOM THROUGH MOBILITY 1905 1980 75th anniversary

SOCIETY OF AUTOMOTIVE ENGINEERS, INC.
400 COMMONWEALTH DRIVE
WARRENDALE, PENNSYLVANIA 15096

# Material and Design Interactions in Collision Energy Management

**Bernard S. Levy**
Inland Steel Co.

ABSTRACT

Conventional analysis of energy management works with force, velocity, vehicle mass, and time. The purpose of this paper is to view energy management by analyzing how the material in the structure absorbs energy. To supplement the analysis, strain rate sensitivity data on a variety of mild and high-strength cold-rolled steels are presented and the implications of the results analyzed. Other results from the literature are also discussed.

A SERIES OF EXISTING and contemplated passenger car regulations for occupant protection in 30 mph collisions have focused considerable attention on collision energy management. As these requirements are met, more attention will focus on meeting them with more cost effectiveness. To date, the basic engineering approach for collision energy management has been through experimental and analytical structural mechanics. Some of the topics covered in the structural mechanics approach include measurement and prediction of force-distance and velocity-time relationships during simulated collisions and empirical or analytical studies on the effect of structural geometry. With this and related work, much is being accomplished. However, use of a metallurgical approach to supplement the structural mechanics approach can provide additional insights.

In a metallurgical approach, attention is focused on the behavior of the yield strength and the ability of the metal to absorb elastic and plastic energy. Thus, in a metallurgical view, the kinetic energy of a collision is absorbed by elastic and plastic deformation if friction from tire motion and body panels sliding against other objects are neglected. It is the purpose of this paper to describe the equations governing the work from elastic and plastic deformation, define the metallurgical properties that are required for use of these equations, and present strain rate data on these properties for a range of high strength cold rolled steels. These data will also be used to discuss some of the implications of this approach. Other relevant data from the literature will also be presented.

## DEFORMATION WORK

The work of deformation for a vehicle involved in a collision can be described by Equation

$$E_D = \iiint_{\forall} \int_0^{(\varepsilon_D)} \sigma d\varepsilon_D \, dxdydz \qquad (1)$$

where $E_D$ is the deformation energy
$\forall$ is the volume of the car
$\sigma$ is true stress
$\varepsilon_D$ is true strain of collision deformation
x,y,z are a coordinate system

While Equation 1 is difficult to utilize, its basic concept is simple. The first integral sign is a volume integral which sums the collision deformation work for each unit

0148-7191/81/0223-0234$02.50

element of the car. Even with the biggest currently available computers, attempting such an integration over an entire vehicle is probably impractical. However, this type of analysis could in some cases be usefully applied to specific components or parts of components. That is, for instance, summing the collision deformation work of each unit element of a rail-like part could be a useful complement to current approaches of analytically modeling buckling and crippling or empirically analyzing data. The additional insight from this approach is the focus on how much material is deformed rather than how many folds are formed. In a sense, the collapse process can be treated as a formability problem.

The second integral defines the area under the stress strain curve. If Hookes Law is assumed for elastic behavior, parabolic work hardening is assumed for plastic behavior, and anelastic behavior is neglected, then the evaluation of the integral is straightforward. This, definition of deformation behavior describes a material that is ideally elastic to the yield point then parabolicly work hardening thereafter. For most steels, this is a reasonable engineering approximation. Thus, the elastic deformation work for steel can be described by Equation 2.

$$(E_D)_e = 1/2\ E\varepsilon^2_{max};\varepsilon_{max} < \varepsilon_{E.L.} \qquad (2)$$

where $(E_D)_e$ is elastic deformation energy per unit volume

E is Young's modulus

$\varepsilon_{max}$ is the maximum elastic strain

$\varepsilon_{E.L.}$ is the elastic limit i.e., the yield strength divided by Young's Modulus

Figure 1 describes the elastic deformation energy per unit volume as a function of elastic strain. Also included as an insert to Figure 1 is a plot of elastic limit strain as a function of yield strength. From Figure 1, it can be seen that even for high strength steels, the maximum elastic energy per cubic inch is relatively low.

For the more important case of plastic deformation energy, this quantity can be determined from Equation 3.

$$(E_D)_p = K\varepsilon_D^{1+n}/(1+n) \qquad (3)$$

where $(E_D)_p$ is plastic deformation energy per unit volume

K & n are the strength coefficient and strain hardening exponent and must be evaluated for the formed and paint-baked aged condition

$\varepsilon_D$ is the total strain from the collision deformation as the elastic strain component can usually be neglected.

In analyzing Equation 3, it can be seen that the plastic deformation energy per unit volume is directly proportional to the strength coefficient, K, and depends in a more complex way on the strain hardening exponent, n, and the collision deformation strain. These interactions are depicted graphically in Figure 2 which relates the plastic deformation energy per unit volume divided by the strength coefficient, K, to the collision deformation strain. The effect of strain hardening is illustrated by lines for varying n-values.

From Figure 2, it can be seen that the plastic deformation energy increases as the deformation strain increases but that at any given strain, an increasing value of n decreases the plastic deformation energy. This somewhat surprising result is a consequence of the definition of K. K is defined as the flow stress at a strain of one. Thus, for no work hardening, i.e., n equals zero, the stress strain curve is horizontal and the deformation energy is a maximum. In contrast, a steel with the same K value that exhibits significant work hardening, say n equals 0.25, yields at a very much lower stress and then work hardens rapidly, reaching the same stress as the non work hardening steel at a strain of one. While as produced steels with low work hardening exponents exhibit limited formability, steels in formed parts sometimes are strained sufficiently so that if a new stress-strain curve is determined, its n-value might approach zero. This topic is discussed more completely in another paper.(1)*

Since Figure 2 does not describe plastic deformation energy directly, further analysis is warranted. In order to describe this phenomena more clearly, the plastic deformation energy is related to the kinetic energy of a 2500 lb. car at 30 mph. Specifically, the measure that will be used is the weight of steel necessary to absorb the total kinetic energy of a 2500 lb. car at 30 mph. The derivation of this relationship is straightforward.

The kinetic energy can be described by Equation 4.

$$E_K = 0.275\ W_C\ S^2 \qquad (4)$$

where $E_K$ is the kinetic energy in in-lbs.

$W_C$ is the weight of the car in pounds

S is the speed of the car in miles per hour.

*Numbers in parentheses designate References at end of paper.

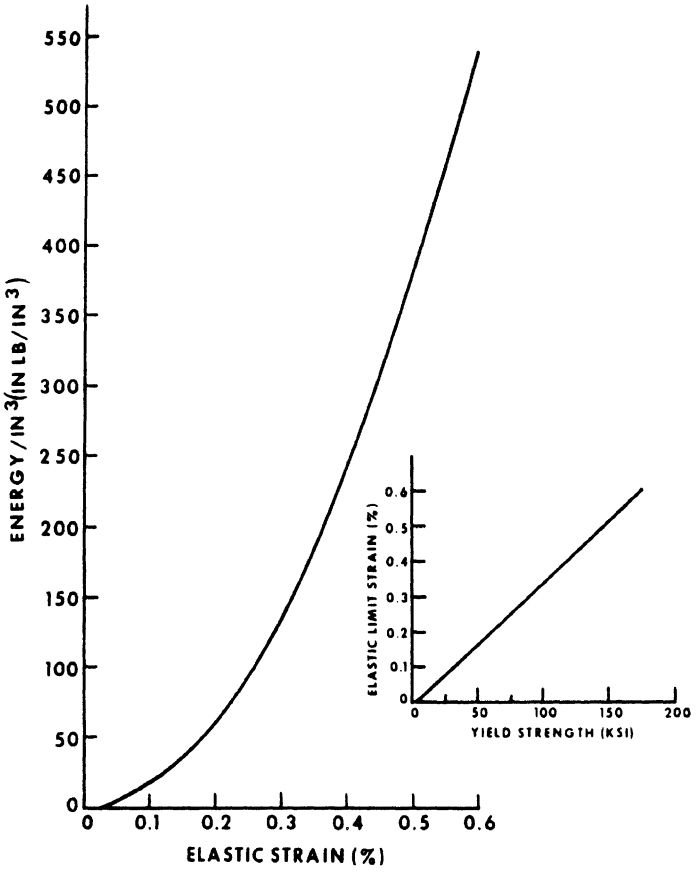


Fig. 1

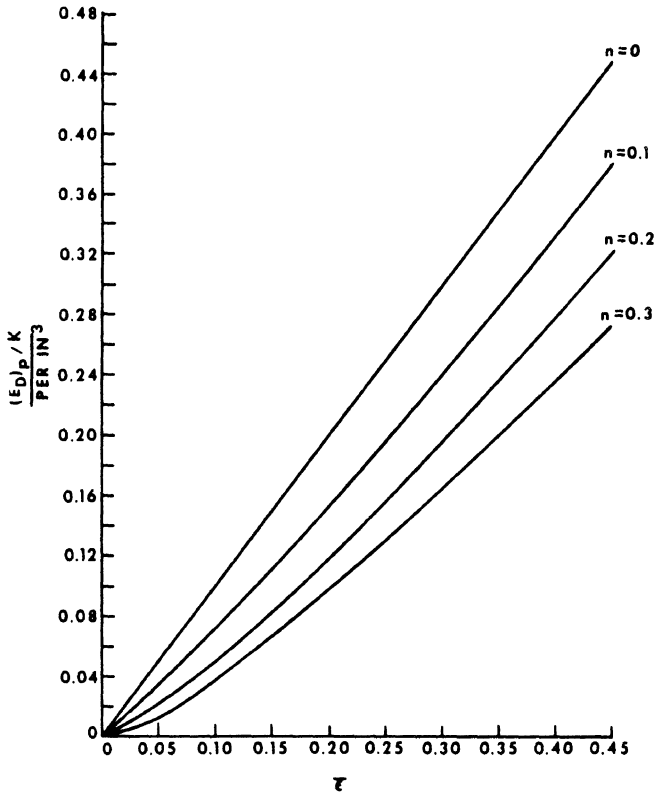


Fig. 2

By equating, the kinetic energy to the total plastic deformation energy and by relating the volume of steel that must be deformed to its comparable weight by using the density of steel, the following equation can be developed.

$$W_D/W_C = 0.0779(1+n)S^2/K\varepsilon_D^{1+n} \qquad (5)$$

where $W_D$ is the weight of steel in lbs. that is deformed to some strain.

$\varepsilon_D$ is the deformation strain

$W_C$ is the weight of the car in lbs.

S is the speed of the car in miles per hour

K,n have their usual meaning & K is in psi

It should be noted that Equation 5 assumes a single deformation strain for the vehicle which is unrealistic for design purposes but is useful to illustrate the potential of plastic work for absorbing kinetic energy. Figure 3 shows the weight of steel that must be deformed at various deformation strains to absorb the kinetic energy of a 2500 lb. car at 30 mph. These results are shown for two actual steel samples, a cold-rolled AISI 1006 aluminum-killed, drawing quality steel and a galvanized SAE 960X steel. The n and K values shown in this figure are the actual values for those samples and were used to calculate the two lines.

The results of Figure 3 dramatically demonstrate the importance of increasing plastic strain on the amount of steel that is required to absorb the kinetic energy of a 2500 lb. car at 30 mph. Specifically, for the drawing quality steel at a deformation strain of 0.025, about 250 lbs. of steel are required while at strains of 0.1 and 0.2 only 46 and 20 lbs. are required, respectively. In order to illustrate the effect of high strength steels more clearly, data are shown in Table I giving specific values of the required weight to absorb the kinetic energy of a 2500 lb. car at 30 mph. In addition to the two steels shown in Figure 3, data are included for a water-quenched, cold-rolled dual-phase 80 steel and for a hot-rolled pickled and oiled, SAE 980X steel. The dramatic benefits of the various high-strength steels are evident from Table I.

From the preceding discussion, it has been shown that yield strength, K and n are important to a metallurgical understanding of collision energy management. In addition, the tensile flow stress at 8% strain, $\sigma_{.08}$, is often a useful indication of the deformation characteristics of steel. In order to use these properties in the analysis

of high speed collisions, it is generally desirable to attempt to account for strain rate effects, because deformation rates in high speed collisions are greater than in conventional tensile tests. However, the metallurgical characteristic that is important is the strain rate not the deformation rate. Thus, data on the strain rate sensitivity of the yield strength, K, n, and $\sigma.08$ are necessary. Since little data of this nature are available in the literature for the cold-rolled steels of interest, the balance of the report provides such data. Data where available from the literature are also included.

## EXPERIMENTAL PROCEDURE

MATERIALS - All the steels used in this study were produced on production scale equipment and with the exception of the dual-phase steel represent commercial products. However, it must be emphasized that these results are only for single samples. The steels used in this study are tabulated below:

1. cold-rolled AISI 1006 aluminum-killed steel (batch annealed)

2. cold-rolled SAE 950X steel (phosphorus-columbium strengthened, batch-annealed)

3. cold-rolled SAE 960X steel (phosphorus-titanium strengthened, continuous heat-treated)

4. galvanized SAE 960X steel (phosphorus-columbium strengthened)

5. experimental, cold-rolled, lean-alloy dual-phase 60 steel

6. experimental, cold-rolled, lean-alloy dual-phase 80 steel

7. hot-rolled, pickled and oiled SAE 980X steel

TEST METHODS - Conventional ASTM tensile samples were prepared and tested at constant crosshead speeds of 0.1 and 100 in/min in a hydraulic tensile tester. The 0.1 in/min tests were recorded with a conventional X-Y recorder while the 100 in/min data were recorded with a Nicholet recorder. No other adjustments were made in test practice as it was believed 100 in/min is below the threshold where difficulties in high strain rate testing are encountered. This practice is described as the companion specimen method. Other tests were pulled at 0.1 in/min to a strain of about 8% where the crosshead rate was essentially instantaneously increased to 100 in/min. This latter practice is described as the jump method.

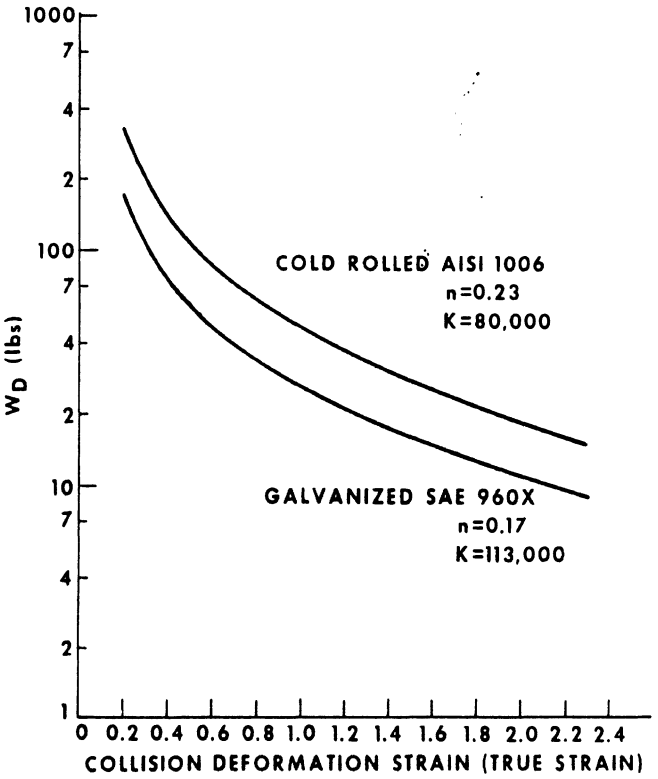


Fig. 3

Table I - Weight of Steel Required to Absorb the Kinetic Energy of a 2500 lb Car Moving at 30 mph at Various Collision Deformation Strains

| Steel | True Strain | | | |
|---|---|---|---|---|
| Cold Rolled | 0.025 | 0.05 | 0.10 | 0.20 |
| AISI 1006 Cold Rolled<br>YS = 23.5, TS = 45.1**<br>n = 0.23; K = 80.0 | 252.5 | 107.5 | 46.0 | 19.6 |
| SAE 960X Galvanized<br>YS = 62, TS = 73<br>n = 0.17; K = 118.0 | 130.2<br>(48.4%)* | 57.8<br>(46.2%) | 25.8<br>(43.9%) | 11.4<br>(41.8%) |
| DPL-80 Cold Rolled<br>YS = 61.6, TS = 86.0<br>n = 0.15; K = 132.0 | 106.2<br>(57.9%) | 47.8<br>(55.5%) | 21.6<br>(53.0%) | 9.72<br>(50.5%) |
| SAE 980X Hot Rolled<br>YS = 88.9, TS = 102<br>n = 0.13; K = 151.0 | 84.8<br>(66.4%) | 38.7<br>(64.0%) | 17.7<br>(61.5%) | 8.1<br>(58.7%) |

* % weight saving compared to the AISI 1006 Cold rolled steel.
** YS = Yield Strength (ksi), TS = Tensile Strength (ksi), n = Strain Hardening Exponent, K = Strength Coefficient (ksi).

In analyzing the data from the jump method, it is necessary to account for the upper yield strength type phenomena which is observed as a consequence of the up jump. This was done by extending the smooth portion of the upjumped curve back to 8% strain and comparing this result with the stress at the same strain for the 0.1 in/min curve. In all cases, samples were tested in triplicate and good reproducibility was obtained.

ANALYSIS METHODS - Strain rate sensitivity data are usually described by a

Table II - Strain Rate Sensitivity Data by the Companion Specimen Method

| | 100"/min | 0.1"/min | 100-0.1 (ksi) | 100/0.1 | m´ (ksi) | m |
|---|---|---|---|---|---|---|
| **Cold Rolled AISI 1006 AK** | | | | | | |
| YS | 34.2 | 23.5 | 10.7 | 1.46 | 3.6 | 0.054 |
| $\sigma_{.08}$ | 52.5 | 44.1 | 8.4 | 1.19 | 2.8 | 0.025 |
| K | 86.6 | 79.8 | 6.8 | 1.09 | 2.3 | 0.012 |
| n | 0.190 | 0.230 | -- | -- | -- | -- |
| **Cold Rolled SAE 950X (P-Cb)** | | | | | | |
| YS | 57.6 | 52.2 | 5.4 | 1.10 | 1.8 | 0.014 |
| $\sigma_{.08}$ | 78.8 | 71.2 | 7.6 | 1.11 | 2.5 | 0.015 |
| K | 113.2 | 103.1 | 10.1 | 1.10 | 3.4 | 0.014 |
| n | 0.137 | 0.137 | -- | -- | -- | -- |
| **Cold Rolled SAE 960X (P-Ti)** | | | | | | |
| YS | 65.6 | 58.0 | 7.6 | 1.13 | 2.5 | 0.018 |
| $\sigma_{.08}$ | 76.2 | 70.8 | 5.4 | 1.08 | 1.8 | 0.011 |
| K | 126.0 | 115.0 | 11.0 | 1.10 | 3.7 | 0.013 |
| n | 0.194 | 0.186 | -- | -- | -- | -- |
| **Galvanized SAE 960X (P-Cb)** | | | | | | |
| YS | 66.4 | 60.9 | 5.5 | 1.09 | 1.8 | 0.013 |
| $\sigma_{.08}$ | 70.2 | 67.4 | 2.8 | 1.04 | 0.9 | 0.006 |
| K | 120.4 | 115.3 | 5.1 | 1.04 | 1.7 | 0.006 |
| n | 0.178 | 0.179 | -- | -- | -- | -- |
| **Exp. Cold Rolled Lean Dual Phase 60** | | | | | | |
| YS | 53.7 | 46.8 | 6.9 | 1.15 | 2.3 | 0.020 |
| $\sigma_{.08}$ | 76.1 | 69.2 | 6.9 | 1.10 | 2.3 | 0.014 |
| K | NA | 113.4 | -- | -- | -- | -- |
| n | NA | 0.192 | -- | -- | -- | -- |
| **Exp. Cold Rolled Lean Dual Phase 80** | | | | | | |
| YS | 67.0 | 61.5 | 5.5 | 1.09 | 1.8 | 0.012 |
| $\sigma_{.08}$ | 96.9 | 89.7 | 7.2 | 1.08 | 2.4 | 0.011 |
| K | 142.4 | 132.3 | 10.1 | 1.08 | 3.4 | 0.011 |
| n | 0.148 | 0.148 | -- | -- | -- | -- |
| **Hot Rolled & Pickled SAE 980X** | | | | | | |
| YS | 95.3 | 88.9 | 6.4 | 1.07 | 2.1 | 0.010 |
| $\sigma_{.08}$ | 116.5 | 107.9 | 8.6 | 1.08 | 2.9 | 0.011 |
| K | 160.1 | 151.0 | 9.1 | 1.06 | 3.0 | 0.008 |
| n | 0.126 | 0.129 | -- | -- | -- | -- |

in ksi, one MPa = 6.87 psi

Table III - Strain Rate Sensitivity Rate by the Jump Method at $\sigma_{.08}$ ksi

| | 100"/min | 0.1"/min | 100-0.1 | 100/0.1 | m´ | m |
|---|---|---|---|---|---|---|
| Cold Rolled AISI 1006 AK | 50.3 | 45.7 | 4.6 | 1.10 | 1.5 | 0.014 |
| Cold Rolled SAE 950X (P-Cb) | 74.7 | 71.8 | 2.9 | 1.04 | 1.0 | 0.006 |
| Cold Rolled SAE 960X (P-Ti) | 74.4 | 71.6 | 2.8 | 1.04 | 0.9 | 0.006 |
| Galvanized SAE 960X (P-Cb) | 72.6 | 71.0 | 1.6 | 1.02 | 0.5 | 0.003 |
| Exp. Cold Rolled DPL-60 | 75.5 | 71.7 | 3.8 | 1.05 | 1.3 | 0.007 |
| Exp. Cold Rolled DPL-80 | 95.6 | 92.1 | 3.5 | 1.04 | 1.2 | 0.005 |

semi-log or a log - log expression. These relationships are shown below:

semi-log

$$m' = (\sigma_2-\sigma_1)/\log(\dot{\varepsilon}_1/\dot{\varepsilon}_2)$$

log-log

$$m = (\log \sigma_2/\sigma_1)/\log(\dot{\varepsilon}_2/\dot{\varepsilon}_1)$$

where $\sigma$ is any stress parameter
$\dot{\varepsilon}$ is the strain rate
and the subscripts represent test conditions

In analyzing the data, both m´ and m were calculated from both the companion specimen data and the jump data.

RESULTS

The data for the companion specimen method are shown in Table II and for the jump

method in Table III. A comparison of the two methods is shown in Table IV.

## DISCUSSION OF RESULTS

The data in Table IV reveals that values of $m'$ or m computed from companion specimen method data are about twice the value obtained from using data produced with the jump method. It is believed that these observations are too consistent and too experimentally different to be artifacts and are thus believed to be real. Such behavior can be rationalized on the basis that the dislocation dynamics in the companion specimen method are different from the jump method. Since it has been established that companion specimen and jump methods produce different results, it is necessary to decide which method is most applicable to collision energy management. Since the normal use for strain rate sensitivity data in collision energy calculations is to modify conventional static data, use of the companion specimen method would seem more appropriate.

In using strain rate sensitivity data such as $m'$ or m, it should also be noted that at high strain rates, m or $m'$ can increase. That is the rate of strain rate strengthening can become greater. This effect is typically observed at higher strain rates than are typical of tensile testing at a crosshead speed of 100 in/min. Thus, the data presented in Tables II and III should be used as a lower bound approach.

OTHER DATA - Other data from the literature for this same strain rate range are included for comparison with the data of this paper and as a convenience for the reader. Included are data for various hot-rolled steels shown in Table V from Chatfield and Rote(2), in Table VI for hot-rolled bar steels from R. B. Wilson(3), in Table VII for aluminum-killed cold-rolled steel in hydraulic bulge testing from D. V. Wilson(4) and in Table VIII for various steels by the jump method from Waddington et al(5) and Ayres et al.(6) Other somewhat related data that are not directly comparable can also be found in a paper by Davies and Magee.(7)

In comparing the other data, with the work of this paper, several comparisons are possible. For cold-rolled, aluminum-killed AISI 1006 steel, data are available from this study, from Ayres and from D. V. Wilson. In comparing the companion specimen method data of this paper with the hydraulic bulge data of D. V. Wilson in Table VII, these data compare well. Specifically, both sets of data exhibit progressive decreases in m value as the strain at which the flow stress is taken increases. At a strain of 0.08 this work gives an m value of 0.025 which is in contrast to a value of 0.018 at a strain of 0.20 from Wilson. The strain rate sensitivity for the K value (strain of one) from this work is somewhat higher than would be expected from the work of Wilson, but the K value is extrapolated from strains in the range of 0.01 to about 0.2. Thus it is believed that the agreement is excellent.

With regard to the jump method data of Ayres et al in Table VIII the results are much less comparable, but it is not known if the SAE 1010 steel used by Ayres was aluminum-killed. In contrast, the data of Chatfield and Rote in Table V for a hot-rolled, aluminum-killed low-carbon steel are very comparable to the results of this investigation with regard to both the yield strength and the K value.

With regard to the hot-rolled steels, it is possible to compare the data for the hot-rolled pickled and oiled data of this experiment with the results of Chatfield and Rote in Table V using the companion specimen method. With regard to these data, the results of this experiment are about half those reported by Chatfield and Rote. This difference could be explained by differences in composition, hot rolling or the processing associated with pickling. Thus, in general, the results of this investigation would seem to be in reasonable agreement with the work of others. However, as a result of differences in both steels and test methods, strain rate sensitivity data should be taken only as approximate values.

RELATIONS TO PRACTICE - Normal tensile data are taken at strain rates of 0.05 to 0.5 in/min. If it is desired to modify these data for 30 mph collisions, several steps must be taken to utilize the m or m data. In comparable terms, 30 mph is 31,680 in/min. Table IX shows the increase in properties that would be expected for an increase in strain rate comparable to an increase in deformation rate from 0.1 in/min to 31,680 in/min (30 mph). Data from the companion specimen method was used to compute Table IX. It should be noted, however, that the actual strain rates in a 30 mph collision could vary over a wide range depending on how the deformation energy was absorbed through the structure. As can be seen from Table IX, the strength increases resulting from the increased strain rate are quite significant, ranging from 10 to 20 ksi for steels which originally ranged in strength from about 20 ksi to 150 ksi. Thus, the proportional rate of increase tends to decrease as the strength of the steel increases or the tensile property inherently exhibits larger stress values (K compared to yield strength).

With regard to the weight of steel needed to absorb the kinetic energy of a 2500 lb. car moving at 30 mph, the decrease in weight

Table IV - Comparison of Strain Rate Sensitivity for $\sigma_{.08}$ by the Jump and Companion Specimen Methods

| | $m'$ (ksi) | | $m$ | |
|---|---|---|---|---|
| | Jump | Companion Specimen | Jump | Companion Specimen |
| Cold Rolled AISI 1006 AK | 1.5 | 2.8 | 0.014 | 0.025 |
| Cold Rolled SAE 950X (P-Cb) | 1.0 | 2.5 | 0.006 | 0.015 |
| Cold Rolled SAE 960X (P-Ti) | 0.9 | 1.8 | 0.006 | 0.011 |
| Galvanized SAE 960X (P-Cb) | 0.5 | 0.9 | 0.003 | 0.006 |
| Exp. Cold Rolled DPL-60 | 1.3 | 2.3 | 0.007 | 0.014 |
| Exp. Cold Rolled DPL-80 | 1.2 | 3.4 | 0.005 | 0.011 |

Table V - Strain Rate Sensitivity Data by Companion Specimen Method for Various Hot Rolled Steels From Chatfield & Rote (Ref. 2)

| Strength Parameter | Crosshead Speed in/min | Property at Indicated Crosshead Speed (ksi) | Property at 0.5"/min (ksi) | Difference (ksi) | Ratio | $m'$ (ksi) | $m$ |
|---|---|---|---|---|---|---|---|
| Hot Rolled AK | | | | | | | |
| YS | 670 | 51.3 | 36.0 | 15.3 | 1.42 | 4.9 | 0.049 |
| K* | 670 | 79.1 | 71.9 | 7.2 | 1.10 | 2.3 | 0.013 |
| Hot Rolled AK Annealed and Temper Rolled | | | | | | | |
| YS | 815 | 49.9 | 30.6 | 19.3 | 1.63 | 6.0 | 0.066 |
| K | 815 | 79.6 | 66.1 | 13.5 | 1.20 | 4.2 | 0.025 |
| Hot Rolled HSLA-40 | | | | | | | |
| YS | 632 | 50.8 | 38.1 | 12.7 | 1.33 | 4.1 | 0.040 |
| K | 632 | 79.1 | 68.9 | 10.2 | 1.15 | 3.3 | 0.020 |
| Hot Rolled HSLA-45 #1 | | | | | | | |
| YS | 814 | 61.1 | 47.3 | 13.8 | 1.29 | 4.3 | 0.034 |
| K | 814 | 99.4 | 81.3 | 18.1 | 1.22 | 5.6 | 0.027 |
| Hot Rolled HSLA-45 #2 | | | | | | | |
| YS | 553 | 53.7 | 44.7 | 8.8 | 1.20 | 2.9 | 0.026 |
| K | 553 | 107.2 | 95.7 | 11.5 | 1.12 | 3.8 | 0.016 |
| Hot Rolled HSLA-50 | | | | | | | |
| YS | 702 | 63.3 | 51.4 | 11.9 | 1.23 | 3.8 | 0.029 |
| K | 702 | 115.6 | 103.9 | 11.7 | 1.11 | 3.7 | 0.014 |
| Hot Rolled HSLA-80 #1 | | | | | | | |
| YS | 795 | 91.3 | 78.0 | 13.3 | 1.17 | 4.2 | 0.021 |
| K | 795 | 136.5 | 119.5 | 17.0 | 1.14 | 5.3 | 0.018 |
| Hot Rolled HSLA-80 #2 | | | | | | | |
| YS | 800 | 95.2 | 80.6 | 14.6 | 1.18 | 4.6 | 0.022 |
| K | 800 | 132.2 | 111.2 | 21.0 | 1.19 | 6.6 | 0.024 |

* K not given, calculated from

$$K = \frac{TS}{\varepsilon_u^{\varepsilon_u}} \; ; \; \varepsilon_u = \ln(1 + e_u)$$

where $e_u$ is the uniform elongation.

Table VI - Strain Rate Sensitivity Data by the Companion Specimen Method for Hot Rolled Plain Carbon Bar Products From R. B. Wilson (Ref. 3)

| | Crosshead Rate 500"/min | 0.5"/min | Difference (ksi) | Ratio | m' (ksi) | m |
|---|---|---|---|---|---|---|
| **Hot Rolled AISI 1008 Bar** | | | | | | |
| YS(ksi) | 50.0 | 36.5 | 13.5 | 1.37 | 4.5 | 0.046 |
| K (ksi) | 105.3 | 101.1 | 4.2 | 1.04 | 1.4 | 0.006 |
| n | 0.206 | 0.252 | -- | -- | -- | -- |
| **Hot Rolled AISI 1018 Bar** | | | | | | |
| YS(ksi) | 55.6 | 42.9 | 12.7 | 1.30 | 4.2 | 0.038 |
| K(ksi) | 139.7 | 133.0 | 6.7 | 1.05 | 2.2 | 0.007 |
| n | 0.218 | 0.245 | -- | -- | -- | -- |
| **Hot Rolled AISI 1024 Bar** | | | | | | |
| YS(ksi) | 57.8 | 48.9 | 8.9 | 1.18 | 3.0 | 0.024 |
| K(ksi) | 145.4 | 138.0 | 7.4 | 1.05 | 2.5 | 0.008 |
| n | 0.213 | 0.230 | -- | -- | -- | -- |
| **Hot Rolled AISI 1045 Bar** | | | | | | |
| YS(ksi) | 75.9 | 62.0 | 13.9 | 1.22 | 4.6 | 0.029 |
| K(ksi) | 205.3 | 194.1 | 11.2 | 1.06 | 3.7 | 0.008 |
| n | 0.220 | 0.230 | -- | -- | -- | -- |

Table VII - Strain Rate Sensitivity in Hydraulic Bulge Tests for Strain Rates in the Range of $10^{-4}$ to $10^{-1}$ $sec^{-1}$ for an Aluminum Killed Drawing Quality Steel From D. V. Wilson (Ref. 4)

| True Thickness Strain | m |
|---|---|
| 0.2 | 0.018 |
| 0.3 | 0.016 |
| 0.4 | 0.013 |
| 0.55 | 0.0096 |

Table VIII - Strain Rate Sensitivity Data by the Jump Method for Various Sheet Steels From References 5 and 6

| Steel | Reference | m |
|---|---|---|
| Interstitial Free (Cold Rolled) | A | 0.0074 |
| Alloy Dual Phase 80 (Hot Rolled) | A | 0.0066 |
| HSLA 50 (Hot Rolled) | A | 0.0058 |
| HSLA 80 (Hot Rolled) | A | 0.0047 |
| SAE 1010 (CR) | B | 0.009 |
| Renitrogenized SAE 1010 + (CR) | B | 0.005 |
| Lean Dual Phase 80 (CR) | B | 0.005 |
| Lean Dual Phase 80 + 2% Prestrain & Age (CR) | B | 0.006 |

A Comparison of a dual phase steel with other Formable Grades, E. Waddington, R.M. Hobbs, and J. L. Duncan, J. of Applied Metalworking, January, 1980.

D High Strength Low C Sheet Steel by Thermomechanical Treatment: III-Eng. Properties, R.A. Ayres et al, GMR-2375.

Table IX - Increase in Strength Properties for an Increase in Strain Rate Proportional to 30 mph and 0.1" min Deformation Rates

| Property (ksi) | 0.1"/min | Estimated for 31,680 in/min (30 mph) | Difference (ksi) |
|---|---|---|---|
| **Cold Rolled AISI 1006 AK** | | | |
| YS | 23.5 | 43.3 | 19.8 |
| $\sigma_{.08}$ | 44.1 | 59.5 | 15.4 |
| K | 79.8 | 92.4 | 12.6 |
| **Cold Rolled SAE 950X (P-Cb)** | | | |
| YS | 52.2 | 62.1 | 9.9 |
| $\sigma_{.08}$ | 71.2 | 85.0 | 13.8 |
| K | 103.1 | 122.4 | 18.7 |
| **Cold Rolled SAE 960X (P-Ti)** | | | |
| YS | 58.0 | 71.8 | 13.8 |
| $\sigma_{.08}$ | 70.8 | 80.7 | 9.9 |
| K | 115.0 | 135.4 | 20.4 |
| **Galvanized SAE 960X (P-Cb)** | | | |
| YS | 60.9 | 70.8 | 9.9 |
| $\sigma_{.08}$ | 67.4 | 72.4 | 5.0 |
| K | 115.3 | 124.8 | 9.4 |
| **Exp. Cold Rolled Lean Dual Phase 60** | | | |
| YS | 46.8 | 59.4 | 12.6 |
| $\sigma_{.08}$ | 69.2 | 81.8 | 12.6 |
| **Exp. Cold Rolled Lean Dual Phase 80** | | | |
| YS | 61.5 | 71.4 | 9.9 |
| $\sigma_{.08}$ | 89.7 | 102.9 | 13.2 |
| K | 132.3 | 151.0 | 18.7 |
| **Hot Rolled & Pickled SAE 980X** | | | |
| YS | 88.9 | 100.4 | 11.6 |
| $\sigma_{.08}$ | 107.9 | 123.8 | 16.0 |
| K | 151.0 | 167.5 | 16.5 |

will be proportional to the increase in K value. In this calculation, the effect of n value is neglected because on average, it seems to decrease or stay the same. In such circumstances, neglecting the effect of a change in n value will have no effect or underestimate the benefit that might be attained. Thus at a collision strain of 0.1 for steel relatively unstrained in the forming process, the weight reductions would range from 13 to 15% for the cold-rolled steels and be about 10% for the SAE 980X hot-rolled steel and the SAE 960X galvanized steel.

For calculations where yielding is important, the effects can be even more pronounced, ranging from almost an 85% increase for the cold-rolled aluminum-killed AISI 1006 steel in the as-produced condition to a 13% increase for the hot-rolled, pickled SAE 980X steel. After cold work from forming, the expected percentage strength increases would be less pronounced. In assessing the increases in yield strength and K value, it should also be re-emphasized that these estimates are lower bounds.

## CONCLUSIONS

1. It has been shown that the effectiveness of steel in absorbing collision energy depends strongly on the strength of the steel and the strain level attained in the collision deformation, as well as on the amount of steel that is deformed. The effect of collision deformation strain is particularly pronounced. For example, for a 2500 lb. car at 30 mph,

neglecting strain rate effects, about 250 lbs. of steel is required to absorb the collision energy if the strain is 0.025, but if the strain is 0.1 or 0.2, then only 46 or 20 lbs. respectively are required.

2. Strain rate data. These data suggest that a lower bound for strain rate corrections for collision deformation energy is 9 to 16%. In this calculation, it is assumed that the strain rates increase proportionately to the increase in deformation rates from static tensile deformation to 20 mph deformation.

3. Use of SAE 960X to SAE 980X type steels can reduce the weight of steel that must be deformed by 40 to 65% compared to cold-rolled drawing quality steel.

4. Strain rate sensitivity as measured by the companion specimen method is approximately twice that measured by the jump method. It is believed that the companion specimen method measurements are more realistic for use in adjusting static tensile data for energy management calculations for high speed automotive collisions.

ACKNOWLEDGEMENTS

Thanks are due to J. McWilliams and R. W. Thompson for providing the experimental results and to R. W. Thompson for reviewing the manuscript.

REFERENCES

1. B.S. Levy another paper at the 1981 Annual Meeting.
2. D.A. Chatfield and R. R. Rote, SAE 740177, February 25-March 1, 1974.
3. R. B. Wilson, private communication.
4. D.V. Wilson, Metals Technology, July, 1980, p. 282-292.
5. E. Waddington, et al., J. of Applied Metalworking, January, 1980.
6. R. A. Ayres, General Motors Report, GMR-2375.
7. R. G. Davies & C. L. Magee, J. of Engineering Materials and Technology, April, 1975, p. 151-155.

APPLIED MECHANICS REVIEWS

VOL. 31, NO. 3 MARCH 1978

# Metallic Energy Dissipating Systems



W. JOHNSON and S. R. REID

UNIVERSITY ENGINEERING DEPARTMENT
UNIVERSITY OF CAMBRIDGE*

## Abstract

The review is principally devoted to identifying pertinent references and summarizing operative plastic deformation modes so that energy absorption capability can be assessed in the simple structural elements of which most energy absorbers are composed.

## Introduction

The development and detail design of mechanical devices for dissipating kinetic energy in a controlled manner or at a predetermined rate has become increasingly more important to the engineer. Advances in technology have led to higher speeds and more massive vehicles (e.g. motor cars and aircraft) which can cause more serious damage to people, the environment, and to the costly structures themselves. The public, now more than ever, is educated and vocal enough to be able to demand higher degrees of personal and public protection [1] and to be able to exact greater legal penalties for mechanical failures [2]. All these factors make up-to-date acquaintanceship with the design of passive safety measures, especially energy absorbers, a prerequisite for their application in this field.

Crashworthiness is a well-established subject of study especially in the USA, though its treatment as a single discipline has yet to be generated. *In vivo* impact situations consist largely of a miscellany of different entities. Only artificial impact situations are capable of being scientifically well-structured. This applies particularly to the treatment of problems of plastic deformation in structures whose function is to collapse in an envisaged manner when subjected to a specific load that may be encountered in the exceptional circumstance of an unintentional collision. The theory of metal plasticity is now a highly developed discipline in certain areas and, for that in which we now describe its application, it can be taken to provide fairly reliable predictions though there are certain limitations and these are discussed below. The application of its laws and its methods of analysis, especially when backed-up by experiment, can be depended upon to satisfactorily facilitate the dimensioning of parts of crashworthy and energy-absorbing structures with the aid of engineering experience. We do not discuss here the biomechanics of fast arresting situations – this has long been the subject of STAPP [3] Conferences. There are other aspects of the kinetic energy dissipating situation which are not fully discussed here due to lack of space. Among these are the use of nonmetallic materials [4,5] the energy absorbing capability or response of particular vehicles to deformation or penetration [4, 6] and the general philosophy of design in this area of engineering [7].

This review is principally concerned with the relatively slow speed (of the order of, say, 50 m/sec) dynamic impact of metallic structures and dwells on the large deformation plasto-mechanics of the simple structure elements frequently used as parts of complete devices. The design aim is to dissipate kinetic energy irreversibly rather than convert and store it elastically and in particular, restitution is to be avoided. The aim is to safeguard people, cargo, machinery or even the vehicle itself from suffering an excessively high rate of retardation or degree of damage. Devices used to this end are usually one-shot items, i.e., once having been deformed, they are discarded and replaced. Frequently, they are proportioned so as to possess a more-or-less rectangular force-displacement characteristic; they are a special kind of load-limiter. Their repeatability and reliability in use are also of great importance [8]. The cost of these devices must always be kept in mind and searches for high energy absorption-per-unit-weight or volume (which is often said to be very important in aircraft) may well be justified. However, after application, i.e., in post-traumatic collision situations, views about cost may well have changed. References [4, 5 and 7-11] are useful general starting points for all aspects of crashworthy impact situations.

*See end of article for authors' affiliation and address.

### Metal Processing Adaptations

Several designs of energy-absorbers have been based upon simple metal-forming or metal-working processes such as billet compression [12], tube expansion [5], plastic torsion of bars [8, 64] and extrusion [65]. With regard to the latter, Ezra and Fay [8] point out that many different extrusion devices utilizing nonmetallic working material have been proposed. The one suggested recently by Robinson and Greenbank [65] uses lead as the deforming medium and has an almost ideal rectangular force displacement characteristic, as shown in Fig. 8. This device has been suggested for use in the protection of structures from earthquake damage.

Another metal-working process which appears to have been used in various forms is metal-cutting. A metal-shearing device and one which machines grooves in tubes are described in reference [8]. Recently Kirk [66] has described a metal-skinning device in which energy dissipation is effected by pulling a round rod through a circular tool. This latter device was for use as an emergency overshoot stopping device in the U.S. Capitol Subway System.

A perusal of any of the standard textbooks (e.g., reference [67]) on the mechanics of metal-processing operations will instantly suggest to a reader devices for plastically absorbing energy and provide mechanics adequate for design calculations.

### Dynamic Effects, Influence of Strain-Rate and Strain-Hardening

The deformation characteristics of the energy-absorbers described above need to be incorporated into calculations of the arrest of a lift in uncontrolled descent, say, or the deceleration of a vehicle in a crash situation. Such matters form an essential part of the subject of crash-worthy calculations but their detailed treatment is outside the scope of the present review; however, see for example reference [68]. There are nonetheless a number of points relating to likely calculations to which attention must be drawn.

At the outset it was stated that many of the characteristics of the devices described derive from their response under quasi-static loading conditions. When these devices are used as impact energy absorbers where the loading is dynamic, a consideration which should always be kept in mind is the influence of strain-rate on the plastic yielding of the material, though its effects can indeed be exaggerated. Strain-rate is most important in its effects on initial yield or collapse load. But when large strains are involved, increases in stress level even for increases of several orders of magnitude in strain-rate are usually modest [43]. This is, however, an area of extensive research in its own right and reference [69] provides an impression of the scope of some of the general problems which exist.

Also, as has been noted above, many devices undergo large plastic deformation. Strain-hardening often plays a significant role, though this is often neglected in obtaining order of magnitude estimates of the response, as illustrated by equations (2-5). In simple terms, for bending devices say, one would expect strain-hardening to be important when the mode of deformation involves a number of stationary plastic hinges (see reference [21]).

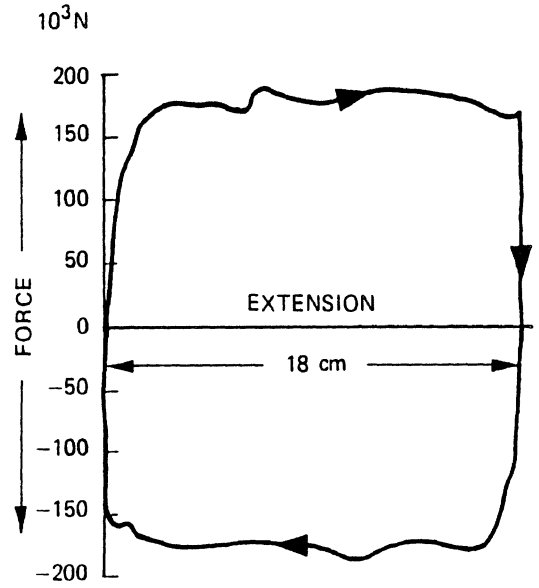


FIG. 8b FORCE-DISPLACEMENT CHARACTERISTIC

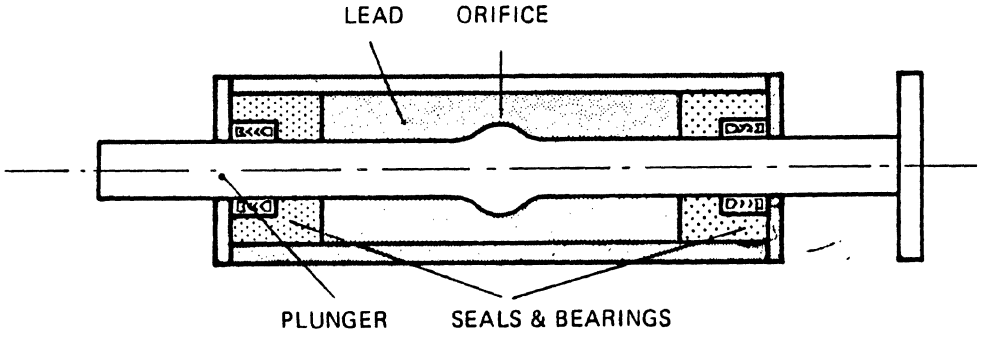


FIG. 8a LEAD EXTRUSION DEVICE DUE TO ROBINSON AND GREENBANK [65]

Broadly speaking, both strain-hardening and strain-rate increase the effective yield stress of the material. A reasonably straightforward formula representing this increase, which has been found to be useful in certain beam problems [9] is,

$$\frac{\sigma}{\sigma_0} = \left[1 + \left(\frac{\dot{\epsilon}}{D}\right)^{1/p}\right](1 + \nu\epsilon), \tag{8}$$

where $D$, $p$ and $\nu$ are material constants and $\sigma$ and $\sigma_0$ are the current and quasi-static yield stresses, respectively.

There are other strain-rate effects which can also occur such as delayed yield [63], although this is more often associated with impulsive loading at rates in excess of those usually encountered in the context of energy absorption.

Nonlinearities in the load-deflection response of a device and time-dependent phenomena such as the dependence of yield stress on strain-rate have also been treated by defining equivalent mass-nonlinear spring-dashpot systems (see for example references [49, 50].

Finally, the possibility must be considered that the mode of deformation of a device may alter under dynamic loading conditions. The buckling of rectangular cross-section tubes under axial compression provides a good example of this. Such behavior is usually the result of the inertia of the deforming element playing a significant role, but this is often assumed not to be the case for energy-absorbers [37]. A number of examples of such phenomena are to be found in the area of high speed impact (see chapter 5, reference [43] where, for example, modes of deformation frequently involve plastic hinges which travel relative to the structure thus providing a continuously changing mode of deformation. In reference [5] it is suggested that a desirable feature of an efficient energy absorber is that "the rapid loading rate expected in crashes should not cause significant change in the (static) force-versus-deformation trace"; clearly the example of the square tube violates this. Recently, Kukkola [70] has shown how *short*, square tubes can be used to satisfy this condition.

### Miscellaneous Non-metallic Systems

The remarks above apply almost wholly to metal energy-absorbing structures. But other media (necessitating other designs or layouts) may be more efficacious in certain circumstances.

Many sophisticated models for determining the arrest of bodies when cushioned against various media (idealized mathematically as springs and dashpots) have been the subject of many papers, reports and books. We shall only instance here the compendious book of Kornhauser [10], though its particular accent on energy-absorption is very different from ours.

Desighs of sophisticated sand-drag type systems for arresting tube trains (hopefully at a rate of about $1g$) are known to be under consideration. The $1g$ level is that which could be tolerated without serious injury to most of the passengers and often without a significant amount of damage to the vehicle. The use of gravel beds for arresting aircraft landing in distress has likewise been investigated and for the same reasons, by the Royal Aircraft Establishment, U.K. (see reference [4] for a summary of this work).

The energy dissipating capability of clays, powders and soils has long been the object of study mainly because of their ballistic associations, though it is important to have some knowledge of them for other purposes [43].

Kinetic energy dissipation systems which do not involve metals are usually developed by testing. As with sand-drag systems, there is usually insufficient knowledge of the properties and mechanics pertaining to the dynamic effects of the materials involved to make strong, rational, theoretically disciplined approaches.

The protective packaging of goods and instruments against damage in transit due to an unintentional blow or fall has long received much attention. But packaging principles appear to be greatly based on experience, e.g., "In all forms of packaging it is customary to have the heavier pieces at the bottom and the lighter pieces at the top" [71]. Heavy articles are generally less susceptible to damage and should therefore be located in the region where the greatest impacts in setting-down will be felt. Following this principle also reduces any tendency to topple-over by lowering the center of gravity as much as possible.

Typical cushioning materials are straw, fiberboard, woodchips and sawdust, wood-wool, polyurethane foam and polystyrene, rubber, corrugated cardboard and paper, moulded paper and flexible rods. These materials are used not only for cushioning, but also for protectively locating and suspending items.

A packaged material can be protected by:

(1) load spreading, i.e., spreading the forces at impact over a large area so that pressure is reduced;

(2) blocking and bracing, i.e., locating supports in contact with the stronger parts of the article so that on impact, forces are directed to these parts; and

(3) shock reduction, i.e., by cushioning the article.

The maximum retardation which may be applied to a given article without damaging it is known at the *fragility factor* of the article. This factor is expressed in multiples of $g$.

The thickness of a cushion, $t$, which exerts a constant force of resistance as it is compressed down to zero thickness is just $t = h/G$, where $G$ is the retardation in $g$ units and $h$ the height of drop. However, for many cushion materials, resistance is proportional to compression and the compressed mass occupies a finite thickness. Accordingly, it is usual to write $t = ch/G$ where $c$ is a *cushioning factor.*

Bulletin of the JSME, Vol.19, No.134, August, 1976

629.11.012.8:539.4.019.1



# Dynamic Analysis of Impact Attenuation Systems Utilizing Plastic Deformations ( Case in Which Effect of Strain-rate Sensitivity Is Considered )*

By Ken-ichiro OHMATA**

An impact attenuation system whose idealized static load-displacement curve consists of an elastic range and unrestricted plastic flow is represented by a dynamically equivalent model which takes into account elasticity, viscosity, plasticity and strain-rate sensitivity of the structure, and its dynamic response to the impact by a moving mass is analyzed. The theoretical results are in fair by good agreement with the experimental results on mild-steel simply supported beams.

An analysis is also made by regarding the equivalent model of the impact attenuation systems as Bingham's model, and the results are compared with the theoretical results by the author's model and the experimental results. Moreover, comparisons between the experimental and theoretical results on plastic impact of beams given by Parkes and the theoretical predictions by author's model are made.

## 1. Introduction

Various impact attenuation systems utilizing plastic deformations have been designed in order to protect the vehicle occupants in car collision. When we study the safety of a car with such an impact attenuation system, maximum impact force, impact duration and the shape of impact pulse are essential factors. In the preceding paper[1], a structure whose load-displacement curve due to geometry change after initial yield is expressed approximately by a cubic curve is represented by a dynamically equivalent model, and its dynamic response to the impact of a moving mass is analyzed disregarding the effect of strain-rate sensitivity. For some materials such as mild-steel, however, there is a marked increase in yield point with strain rate.

In this paper, a structure whose idealized static load-displacement curve consists of an elastic range and unrestricted plastic flow is represented by an equivalent model which takes into account the effect of strain-rate sensitivity together with elasticity, viscosity and plasticity, and its response to the impact is analyzed. The theoretical results are compared with the results of impact tests on the simply supported beams of mild-steel and the experimental and theoretical results given by Parkes[2].

* Received 16th April, 1974.

** Lecturer, Faculty of Engineering, Meiji University, Kawasaki.

In the field of rheology, equivalent models have been used to describe the behaviour of materials and Bingham's model is well known as the model of visco-elastic-plastic substance. In this report, an analysis is also made by regarding the equivalent model of the impact attenuation system as Bingham's model, and the results are compared with the theoretical results by the author's model and the experimental results.

## 2. Dynamic analysis by author's model

Consider a structure (an impact attenuation system) having the idealized load-displacement curve as shown in Fig. 1 and being impacted by a heavy striking mass m. It is well known to describe the behaviour of materials by suitable combinations of springs, dashpots and sliders. If we apply such a model expression to a structure having the deformation characteristic shown in Fig. 1, its equivalent system may be represented as Fig. 2. In Fig. 2, k is the spring constant and $F_p$ is Coulomb

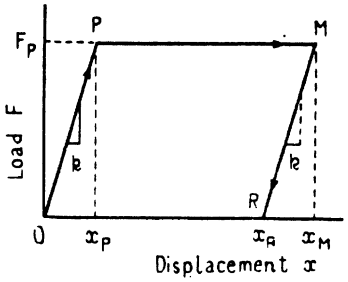


Fig. 1 Static load-displacement curve

friction force, and they correspond to the values in Fig. 1. Moreover, c is the equivalent viscous damping coefficient and the mass of the structure is ignored.

### 2.1 First stage (Elastic stage)

Let $t=0$ and $x=0$ at the moment when a striking mass impinges on the point S with speed $v_0$. We may consider a free vibration system shown in Fig. 3 as long as the spring force kx is small in comparison with $F_p$. Assuming $c<2\sqrt{mk}$, the motion of the striker and the impact force F′ exerted on the striker are

$$\left.\begin{aligned} x &= \frac{v_0}{q} e^{-\alpha t} \sin qt \\ \dot{x} &= \frac{\nu v_0}{q} e^{-\alpha t} \cos(qt+\gamma) \\ \ddot{x} &= -\frac{\nu^2 v_0}{q} e^{-\alpha t} \sin(qt+\eta) \\ F' &= -m\ddot{x} = \frac{kv_0}{q} e^{-\alpha t} \sin(qt+\eta) \end{aligned}\right\} \quad (1)$$

where

$$\left.\begin{aligned} &\alpha = \frac{c}{2m}, \qquad \nu = \sqrt{\frac{k}{m}}, \qquad q = \sqrt{\nu^2-\alpha^2} \\ &\gamma = \tan^{-1}\frac{\alpha}{q}, \qquad \eta = \tan^{-1}\frac{2q\alpha}{q^2-\alpha^2} \end{aligned}\right\} \quad (2)$$

and the spring force is

$$f = kx = \frac{kv_0}{q} e^{-\alpha t} \sin qt \quad (3)$$

When $f=F_p$, deformation enters the second stage. The condition that the deformation should enter the second stage is $f_{max}>F_p$, i.e.

$$\frac{mv_0\nu^2}{qF_p} > \frac{\nu}{q} \exp\frac{\alpha}{q}\left(\frac{\pi}{2}-\gamma\right) \quad (4)$$

In this case the time $t_p$ at the moment when the first stage ends is obtained by the following relation.

$$e^{-\alpha t_p} \sin qt_p = qF_p/mv_0\nu^2 \quad (5)$$

Calculating $t_p$ from Eq. (5) for a given value of $mv_0\nu^2/qF_p$ and substituting it into Eq. (1), we obtain the velocity of the striker $v_p$ when $t=t_p$. The displacement of the striker $x_p$ and the impact force $F_p'$ at this moment are

$$x_p = F_p/k, \qquad F_p' = F_p + cv_p \quad (6)$$

$F_p'$ corresponds to the dynamic yield load and $F_p'/F_p = 1+cv_p/F_p$ coincides with the ratio of the dynamic yield stress $\sigma_y'$ to the static yield stress $\sigma_y$.

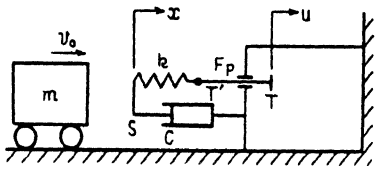


Fig. 2 Equivalent system (Author's model)

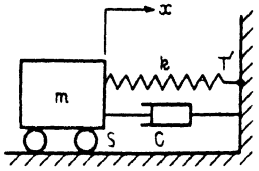


Fig. 3

### 2.2 Second stage (Plastic stage)

In this stage, we must consider a system shown in Fig. 2. The equation of motion is

$$m\ddot{x}+c\dot{x} = -F_p \quad (7)$$

Considering the initial conditions ( i.e., for $t=t_p$, $x=x_p$, $\dot{x}=v_p$ ), we obtain the solution of Eq. (7) as

$$\left.\begin{aligned} x &= x_p + \frac{1}{2\alpha}\left(v_p+\frac{F_p}{c}\right) \\ &\quad \times[1-\exp\{-2\alpha(t-t_p)\}] - \frac{F_p}{c}(t-t_p) \\ \dot{x} &= \left(v_p+\frac{F_p}{c}\right)\exp\{-2\alpha(t-t_p)\} - \frac{F_p}{c} \\ F' &= (F_p+cv_p)\exp\{-2\alpha(t-t_p)\} \end{aligned}\right\} \quad (8)$$

Setting $\dot{x}$ of Eq. (8) equal to zero yields the time at which the striker reaches its maximum position.

$$t_M = t_p + \frac{1}{2\alpha}\ln\left(1+\frac{cv_p}{F_p}\right) \quad (9)$$

Hence, by Eq. (8) the maximum displacement $x_M$ and the impact force $F_M'$ at this moment are

$$\left.\begin{aligned} x_M &= x_p + \frac{1}{2\alpha}\left\{v_p - \frac{F_p}{c}\ln\left(1+\frac{cv_p}{F_p}\right)\right\} \\ F_M' &= F_p \end{aligned}\right\} \quad (10)$$

### 2.3 Rebounding stage

After the striker reached the maximum displacement, we may consider the system shown in Fig. 3 again since the spring is about to return to its original length while the point T′ will remain at rest. In this case, however, the equilibrium position of the system is

$$x_R = x_M - x_p \quad (11)$$

Applying the initial conditions that $x=x_M$, $\dot{x}=0$ when $t=t_M$, we find the motion of the striker and the impact force to be

$$\left.\begin{aligned} x &= \frac{1}{2\alpha}\left\{v_p - \frac{F_p}{c}\ln\left(1+\frac{cv_p}{F_p}\right)\right\} \\ &\quad + \frac{\nu x_p}{q}\exp\{-\alpha(t-t_M)\}\cos\{q(t-t_M)-\gamma\} \\ \dot{x} &= -\frac{F_p}{mq}\exp\{-\alpha(t-t_M)\}\sin q(t-t_M) \\ F' &= \frac{\nu F_p}{q}\exp\{-\alpha(t-t_M)\}\cos\{q(t-t_M)+\gamma\} \end{aligned}\right\} \quad (12)$$

At the moment when $F'=0$, the striker leaves the structure. The time of this moment is

$$t_R = t_M + \frac{\pi}{2q} - \frac{\gamma}{q} \tag{13}$$

$t_R$ corresponds to the impact duration and $x_R$ in Eq.(11) corresponds to the permanent deformation of the structure at the point of application of the load.

If the striker is a falling weight, the effect of its own weight must be considered. In that case it is necessary to replace the equation of motion at the first stage by

$$m\ddot{x}+c\dot{x}+kx = mg$$

and the equation of motion at the second stage by

$$m\ddot{x}+c\dot{x} = -F_p+mg$$

and the equilibrium position at the rebounding stage by

$$x_R = x_M - x_p + x_{st} \qquad (x_{st} = mg/k)$$

## 3. Determination of equivalent viscous damping coefficient

We assume the yield stress-strain-rate law to be of the following form[3].

$$\left.\begin{aligned} &\sigma_y' = \sigma_y\{1+(\frac{\dot{\varepsilon}}{D})^n\} = \sigma_y\{1+(\frac{\dot{x}}{DL})^n\} \\ &\left(\begin{array}{l}\text{for aluminum,} \quad n=1/4,\ D=6500/s \\ \text{for mild-steel,} \quad n=1/5,\ D=40/s\end{array}\right) \end{aligned}\right\} \tag{14}$$

Hence, the dashpot resistance in Fig. 2 is more correctly expressed by a term proportional to the nth power of the velocity. Then, let us consider the equivalent viscous damping in that case.

It will be seen from the results in Chapter 2 that the velocity change of the striker up to the maximum position is expressed approximately by a cosine curve in the elastic stage and by an exponential function in the plastic stage, as shown in Fig. 4 by the solid and dot-dash curve. For simplicity, however, let us regard the velocity change of the striker up to the maximum position as linear, as shown in Fig. 4 by the solid line. Namely

$$\dot{x} = v_0(1-t/t_M) \tag{15}$$

The energy dissipated up to the maximum displacement due to an equivalent viscous damping force $F_D = c\dot{x}$ is

$$D_0 = \int_0^{x_M} F_D\,dx = \int_0^{t_M} c\dot{x}^2\,dt = \frac{1}{3}cv_0^2 t_M \tag{16}$$

When the damping force is expressed by the equation $F_D = C_n\dot{x}^n$, it becomes

$$D_0 = \int_0^{t_M} C_n\dot{x}^{n+1}\,dt = \frac{1}{n+2}C_n v_0^{n+1} t_M \tag{17}$$

The equivalent viscous damping is found by equating the energy dissipated up to the maximum displacement by the viscous damping to that of the actual damping force. From Eqs. (16) and (17)

$$c = \frac{3D_0}{v_0^2 t_M} = \frac{3}{n+2}C_n v_0^{n-1} \tag{18}$$

As an example, let us consider a simply supported beam struck by a heavy mass m at its midpoint with initial velocity $v_0$, as shown in Fig. 5. The beam has a solid circular cross-section of diameter d. When a static load acts on the midpoint of the beam and the maximum bending moment ( $M_{max} = FL/4$ ) reaches a fully plastic moment of the section of the beam ( $M_p = d^3\sigma_y/6$ ), a plastic hinge forms at the midpoint and collapse occurs. The load at this moment corresponds to the static yield load and is given by

$$F_p = 4M_p/\ell = 2d^3\sigma_y/3\ell \tag{19}$$

When the beam is struck by a moving mass, the dynamic load in the plastic stage is given by replacing $\sigma_y$ in Eq. (19) with $\sigma_y'$ of Eq. (14).

$$F' = F_p\{1+(\frac{\dot{\varepsilon}}{D})^n\} \tag{20}$$

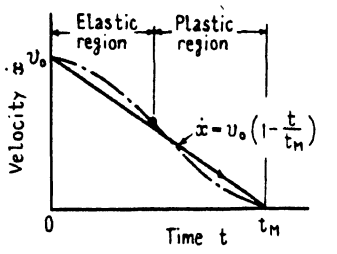


Fig. 4 Velocity change of striker

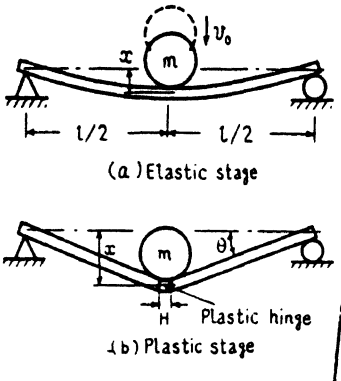


Fig. 5

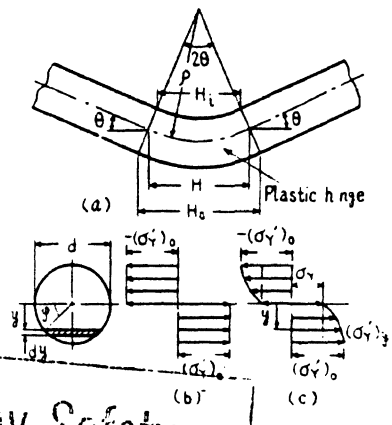


Fig. 6

Let us next consider the case in which the dashpot resistance in Fig. 2 is expressed by $F_D = C_n\dot{x}^n$. The impact force in the plastic stage is

$$F' = F_p + C_n\dot{x}^n \tag{21}$$

Comparing Eq. (20) with Eq. (21), we find

$$C_n\dot{x}^n = F_p(\dot{\varepsilon}/D)^n \tag{22}$$

It is necessary to find out the relationship between the strain rate $\dot{\varepsilon}$ and the transverse velocity $\dot{x}$ at the midpoint of the beam in order to find out the value of $C_n$ from Eq. (22). Using the relationship between the maximum strain rate and the transverse velocity in the elastic range ( in the outer fibres of the midpoint, $\dot{\varepsilon} = 6d\dot{x}/\ell^2$ ), we obtain

$$C_n = F_p\left(\frac{6d}{D\ell^2}\right)^n \tag{23}$$

For large deformation, assuming the shape of the deflection curve as shown in Fig. 6, the relationship between the mean rate of strain in the outer fibres of the hinge and the transverse velocity under the load is represented approximately in the following form[4]:

$$\dot{\varepsilon} = 2d\dot{x}/\ell H \tag{24}$$

where H is the length of the plastic hinge determined experimentally. Substituting Eq. (24) into Eq. (22), we obtain

$$C_n = F_p\left(\frac{2d}{D\ell H}\right)^n \tag{25}$$

Substituting Eqs. (23) or (25) into Eq. (18), we obtain the approximations of the equivalent viscous damping coefficient c. In the case of a rectangular cross-section of width b and depth d, it is only necessary to put $F_p = bd^2\sigma_y/\ell$ in Eqs. (23) and (25).

In the above discussion, the value of c was determined by assuming the dynamic stress distribution at the hinge as shown in Fig. 6(b). However, if the dynamic yield stress is expressed by Eq. (14), this stress distribution may be represented as shown in Fig. 6(c). Therefore, let us consider the value of c for the stress distribution shown in Fig. 6(c). Assuming the configuration of the beam after the hinge has formed is as shown in Fig. 5(b), the resisting moment in the hinge is given by

$$M_p' = \int_A (\sigma_y')_y\, y\,dA = \int_A \sigma_y\left\{1+\left(\frac{\dot{\varepsilon}_y}{D}\right)^n\right\} y\,dA, \tag{26}$$

where $\dot{\varepsilon}_y$ is the strain rate at the distance y from the neutral axis of the hinge. Since $\varepsilon_y = y/\rho$, $2\theta\rho = H$ and $\ell\theta/2 \fallingdotseq x$, $\dot{\varepsilon}_y$ and $\dot{x}$ are related approximately by

$$\dot{\varepsilon}_y = 4y\dot{x}/\ell H \tag{27}$$

Substituting Eq. (27) into Eq. (26) and using the relationships $y = (d/2)\sin\phi$, $dA = d\cos\phi\, dy = (d^2/2)\cos^2\phi\, d\phi$, we have

$$M_p' = \frac{d^3}{2}\sigma_y\int_0^{\pi/2}\left\{1+\left(\frac{2d}{D\ell H}\right)^n\dot{x}^n\sin^n\phi\right\} \times\sin\phi\cos^2\phi\, d\phi = \frac{d^3\sigma_y}{6} \times\left\{1+\frac{3\pi}{4(n+3)}\zeta(n)\left(\frac{2d}{D\ell H}\right)^n\dot{x}^n\right\} \tag{28}$$

in which

$$\zeta(n) = \frac{4}{\pi}\int_0^{\pi/2}\sin^{n+1}\phi\, d\phi = \frac{2}{\sqrt{\pi}}\cdot\frac{\Gamma\left(\frac{n+2}{2}\right)}{\Gamma\left(\frac{n+3}{2}\right)} \tag{29}$$

where $\Gamma$ denotes a gamma function. The dynamic load in the plastic stage is given by

$$F' = F_p\left\{1+\frac{3\pi}{4(n+3)}\zeta(n)\left(\frac{2d}{D\ell H}\right)^n\dot{x}^n\right\} \tag{30}$$

Hence, we have

$$C_n = \frac{3\pi\zeta(n)}{4(n+3)}F_p\left(\frac{2d}{D\ell H}\right)^n \tag{31}$$

For a rectangular cross-section of width b and depth d, this becomes

$$C_n = \frac{2F_p}{n+2}\left(\frac{2d}{D\ell H}\right)^n \tag{32}$$

The values of c calculated from Eqs. (23), (25) and (31) for a simply supported beam impacted by a freely falling striker of w = 25.5kg are given in Table 1. The beam is mild-steel (ss41) for which $\sigma_y = 28\text{kg/mm}^2$ and which has a solid circular cross-section of diameter d = 6/8in$\phi$, and $\ell$=100cm. In these calculations, the length of the hinge H was taken as the average of the lengths at the outer surface and inner surface measured by means of brittle lacquer (TENS-LAC, 7L-500-60A). Table 1 also shows the experimental values of c. These values were calculated from the following relation:

$$c = (F_p' - F_p)/v_p \tag{33}$$

Table 1 Values of equivalent viscous damping coefficient

| Height of fall h (cm) | Initial velocity* $v_0$ (cm/s) | Maximum impact force $F_p'$ (kg) | Length of plastic hinge: Inner surface $H_I$ (cm) | Outer surface $H_O$ (cm) | Mean value H (cm) | Equivalent viscous damping coefficient c (kg·s/cm): $c = 1.362C_n v_0^{-0.8}$ Eq. (23) | Eq. (25) | Eq. (31) | Experimental** Eq. (33) |
|---|---|---|---|---|---|---|---|---|---|
| 50 | 313.1 | 191.3 | 7.0 | 16.2 | 11.6 | 0.217 | 0.268 | 0.237 | 0.222 (0.202) |
| 70 | 370.4 | 193.0 | 11.0 | 19.2 | 15.1 | 0.189 | 0.222 | 0.196 | 0.190 (0.176) |
| 100 | 442.8 | 193.8 | 14.2 | 21.8 | 18.0 | 0.164 | 0.186 | 0.164 | 0.156 (0.149) |
| 150 | 542.2 | 201.5 | 20.8 | 27.4 | 24.1 | 0.124 | 0.149 | 0.132 | 0.139 (0.135) |

* Calculated from $v_0 = \sqrt{2gh}$ ** ( ):Calculated by assuming $v_p = v_0$

where $F_p'$ is the experimental maximum impact force.

In calculating $v_p$ in above equation, the value of c was calculated from Eq.(23). Furthermore, the values of c obtained by assuming $v_p = v_0$ are given in the parentheses of Table 1. It will be seen from Table 1 that the values of c obtained by use of Eq. (23) show good agreement with the experimental values in a wide range of deformations, those by Eq. (31) being slightly greater and those by Eq. (25) fairly greater than the experimental values. Moreover, it is evident that the length of the plastic hinge H changes depending on the degree of impact, although it was assumed to be constant in the derivation of Eqs. (25) and (31).

## 4. Dynamic analysis by Bingham type model

Next, let us consider Bingham's model as the equivalent model of the structure having the static characteristic shown in Fig. 1. The equivalent system is shown in Fig. 7.

### 4.1 First stage (Elastic stage)

Let $t=0$ and $x=0$ at the moment when a striker impinges on the point S with speed $v_0$. As long as the spring force kx is small in comparison with $F_p$, we may consider a system shown in Fig. 3 except that there is no damping. Hence the motion of the striker and the impact force F' are

$$\left.\begin{aligned} &x = \frac{v_0}{\nu}\sin\nu t, \qquad \dot{x} = v_0\cos\nu t \\ &\ddot{x} = -v_0\nu\sin\nu t \qquad (\nu = \sqrt{k/m}) \\ &F' = -m\ddot{x} = kx = mv_0\nu\sin\nu t \end{aligned}\right\} \quad (34)$$

When $mv_0\nu/F_p > 1$, the deformation enters the second stage, and the time $t_p$ and the velocity of the striker $v_p$ at that moment are given by

$$\left.\begin{aligned} &t_p = \frac{1}{\nu}\sin^{-1}\frac{F_p}{mv_0\nu} \\ &v_p = v_0\cos\nu t_p = \frac{F_p\nu}{k}\sqrt{\left(\frac{mv_0\nu}{F_p}\right)^2 - 1} \end{aligned}\right\} \quad (35)$$

### 4.2 Second stage (Plastic stage)

In this stage, we may consider a system shown in Fig. 7. The equation of motion is

$$\left.\begin{aligned} &m\ddot{x} + k(x-u) = 0 \\ &k(x-u) = c\dot{u} + F_p \end{aligned}\right\} \quad (36)$$

From the first of Eqs. (36), we find

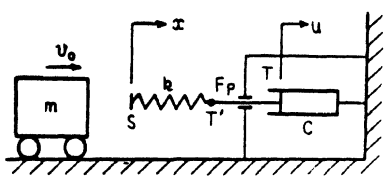


Fig. 7 Equivalent system (Bingham type model)

$$u = \ddot{x}/\nu^2 + x \quad (37)$$

Substituting Eq. (37) into the second of Eqs. (36), we obtain

$$\dddot{x} + 2\xi\nu\ddot{x} + \nu^2\dot{x} = -2\xi\nu^3 x_p \quad (38)$$

where

$$\nu = \sqrt{\frac{k}{m}}, \qquad \xi = \frac{\sqrt{mk}}{2c}, \qquad x_p = \frac{F_p}{k} \quad (39)$$

If $\xi > 1$, the general solution for Eq. (38) is

$$\begin{aligned} x = {} & A_1\exp\{-\nu(\xi+\sqrt{\xi^2-1})(t-t_p)\} \\ & + A_2\exp\{-\nu(\xi-\sqrt{\xi^2-1})(t-t_p)\} \\ & + A_3 - 2\xi\nu x_p(t-t_p) \end{aligned} \quad (40)$$

$$\begin{aligned} \dot{x} = {} & -\nu[A_1(\xi+\sqrt{\xi^2-1}) \\ & \times\exp\{-\nu(\xi+\sqrt{\xi^2-1})(t-t_p)\} \\ & + A_2(\xi-\sqrt{\xi^2-1})\exp\{-\nu(\xi-\sqrt{\xi^2-1}) \\ & \times(t-t_p)\}] - 2\xi\nu x_p \end{aligned} \quad (41)$$

$$\begin{aligned} \ddot{x} = {} & \nu^2[A_1(\xi+\sqrt{\xi^2-1})^2 \\ & \times\exp\{-\nu(\xi+\sqrt{\xi^2-1})(t-t_p)\} \\ & + A_2(\xi-\sqrt{\xi^2-1})^2 \\ & \times\exp\{-\nu(\xi-\sqrt{\xi^2-1})(t-t_p)\}] \end{aligned} \quad (42)$$

Substituting the initial condition for this stage (i.e., for $t=t_p$, $x=x_p$, $\dot{x}=v_p$, $\ddot{x}=-\nu^2x_p$) into Eqs.(40)~(42), we find the values of $A_1$, $A_2$ and $A_3$ to be

$$\left.\begin{aligned} A_1 &= \frac{\nu x_p\{2\xi(\xi-\sqrt{\xi^2-1})-1\}+v_p(\xi-\sqrt{\xi^2-1})}{\nu(\xi-1+\sqrt{\xi^2-1})(\xi+1+\sqrt{\xi^2-1})} \\ A_2 &= \frac{\nu x_p\{2\xi(\xi+\sqrt{\xi^2-1})-1\}+v_p(\xi+\sqrt{\xi^2-1})}{\nu(\xi-1-\sqrt{\xi^2-1})(\xi+1-\sqrt{\xi^2-1})} \\ A_3 &= x_p - A_1 - A_2 \end{aligned}\right\} \quad (43)$$

The maximum acceleration ( the maximum impact force ) occurs at the moment when $d\ddot{x}/dt = 0$ and the time of this moment $t_f$ is given by

$$t_f = t_p + \frac{1}{2\nu\sqrt{\xi^2-1}}\ln\frac{-A_1(\xi+\sqrt{\xi^2-1})^3}{A_2(\xi-\sqrt{\xi^2-1})^3} \quad (44)$$

Substituting Eq. (44) into Eq. (42), we obtain the maximum acceleration as

$$\left.\begin{aligned} \ddot{x}_f = {} & \nu^2K^{-1/2}[1+(\xi/\sqrt{\xi^2-1})] \\ & \times\{A_1(\xi+\sqrt{\xi^2-1})^2 + A_2(\xi-\sqrt{\xi^2-1})^2K\} \end{aligned}\right\}$$

where

$$\left.K = \frac{-A_1(\xi+\sqrt{\xi^2-1})^3}{A_2(\xi-\sqrt{\xi^2-1})^3}\right\} \quad (45)$$

The time $t_M$ at which the striker reaches its maximum position is found by setting $\dot{x}=0$.

$$\begin{aligned} & A_1(\xi+\sqrt{\xi^2-1})\exp\{-\nu(\xi+\sqrt{\xi^2-1})(t_M-t_p)\} \\ & + A_2(\xi-\sqrt{\xi^2-1})\exp\{-\nu(\xi-\sqrt{\xi^2-1})(t_M-t_p)\} \\ & + 2\xi x_p = 0 \end{aligned} \quad (46)$$

If the kinetic energy of the striker is large (so that $t_M-t_p$ is large) and $\xi$ is large, the first term of Eq. (46) is negligible compared to the second and third terms. Hence

$$t_M = t_p + \frac{1}{\nu(\xi-\sqrt{\xi^2-1})} \ln \frac{-A_2(\xi-\sqrt{\xi^2-1})}{2\xi x_p} \tag{47}$$

Substituting Eq. (47) into Eq. (40), we obtain the maximum displacement $x_M$.

### 4.3 Rebounding stage

After the striker has reached the maximum displacement, we may consider a system shown in Fig. 3 except that there is no damping again. In this case, however, the equilibrium position of the system is

$$x_R = x_M - x_p \tag{48}$$

Hence, the motion of the striker and the impact force $F'$ are

$$\left.\begin{aligned} x &= x_M - x_p\{1-\cos\nu(t-t_M)\} \\ \dot{x} &= -\nu x_p \sin\nu(t-t_M) \\ F' &= F_p\cos\nu(t-t_M) \end{aligned}\right\} \tag{49}$$

At the moment when $x = x_R$, the striker leaves the structure. The time of this moment is

$$t_R = t_M + \pi/2\nu \tag{50}$$

If the striker is a falling weight, it is necessary to replace the equation of motion at the first stage by

$$m\ddot{x}+kx = mg$$

and the equation of motion at the second stage by

$$m\ddot{x}+k(x-u) = mg, \qquad k(x-u) = c\dot{u}+F_p$$

and the equilibrium position at the rebounding stage by

$$x_R = x_M - x_p + x_{st} \qquad (x_{st} = mg/k)$$

## 5. Experimental examples

In order to determine whether the analysis could satisfactorily predict the behaviour of the striker, drop tests on simply supported beams were carried out. The beams are mild-steel (ss41) for which $\sigma_y = 28 kg/mm^2$ and which have a solid circular cross-section of d = 6/8in$\phi$, and $\ell = 100$ cm. The static load-displacement curve of these simply supported beams is shown in Fig. 8 and the shock testing machine used in these tests is shown in Fig. 9. The acceleration exerted on the drop mass (w = 25.5kg) was measured by a piezoelectric accelerometer attached to the drop mass and an oscilloscope, and the time-displacement relation was measured by a high-speed camera. The maximum displacement was measured by two slide-wire displacement transducers too. The striking velocity was calculated from $v_0 = \sqrt{2gh}$ (h: height of fall), since this value agreed well with the measured value (error being 1~2% within the limits of this experiment). Comparisons of the experimental and theoretical results on maximum displacement variation and maximum acceleration variation with height of fall are shown in Figs. 10 and 11, respectively. Figures 12 and

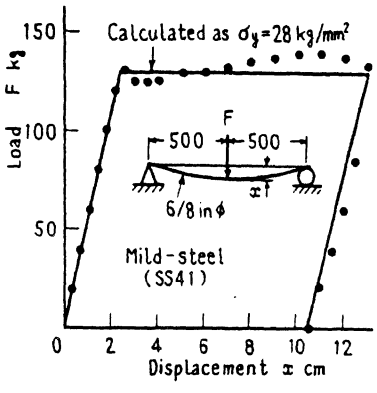


Fig. 8 Static characteristic of simply supported beam

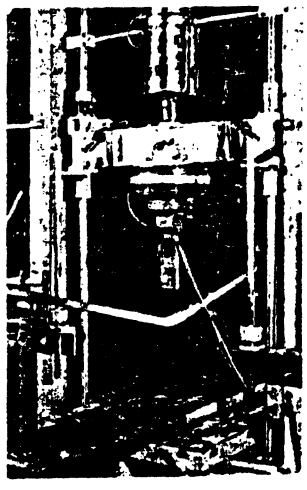

Fig. 9 Shock testing machine

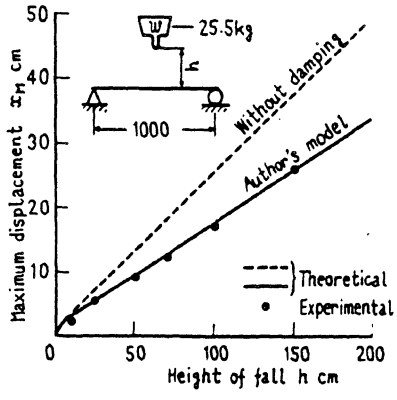


Fig. 10 Relationship between height of fall and maximum displacement

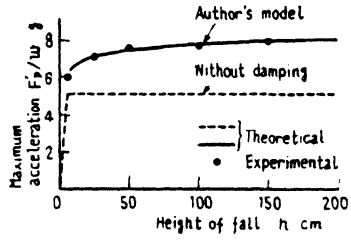


Fig. 11 Relationship between height of fall and maximum acceleration

13 show comparisons of the experimental and theoretical displacement-time histories and acceleration-time histories at which h = 100cm, respectively. In these calculations, the equivalent viscous damping coefficients were calculated from Eq. (23), and the effect of the own weight of the drop mass was considered.

It will be seen from Figs. 10~13 that the theoretical results using the author's model and a Bingham type model fairly well agree with the experimental results, so that the impact system can be explained well by these equivalent models. Bingham type model, however, has the following disadvantages:

(i) The effect of viscosity in the elastic stage is ignored.
(ii) Yield stress has a constant value regardless of strain rate.
(iii) It will be difficult to determine the equivalent viscous damping coefficient analytically.

Therefore, the author's model is superior to the Bingham type model as the equivalent model of the impact attenuation systems utilizing plastic deformations. For reference, the deformed shapes of the beams and the dynamic load-displacement curves at which h = 100cm are shown in Figs. 14 and 15, respectively.

## 6. Comparison of theoretical and experimental results by Parkes with theoretical results using author's model

The problem of the plastic bending of beams under impulsive loading has been studied by many researchers. As one of those studies, let us compare the theoretical and experimental results on a cantilever by Parkes[2] with the theoretical results using the author's model.

Parkes has analyzed the permanent deformation of a cantilever struck transversely at its tip on the assumption that the hinge point moves and compared the

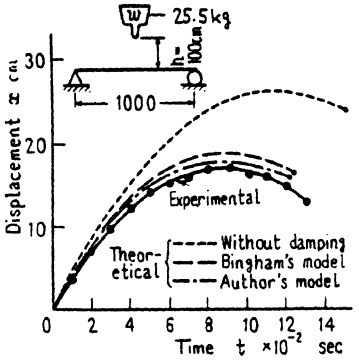


Fig. 12 Displacement-time history

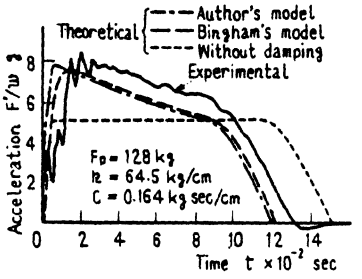


Fig. 13 Acceleration-time history

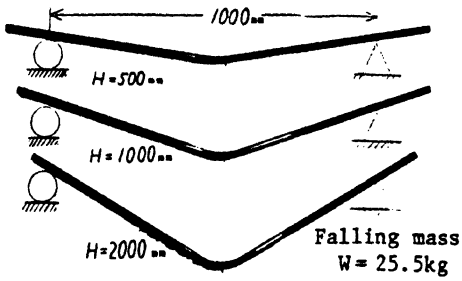


Fig. 14 Deformed shapes of beames

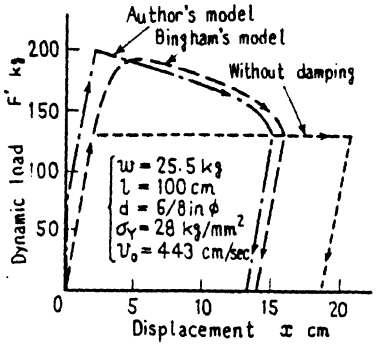


Fig. 15 Dynamic load-displacement curve

Table 2 Permanent deflection of cantilever struck transversely at its tip

| Length $\ell$ (in) | Cross-section b × d (in)(in) | Weight of striker w (lb) | Height of fall h (in) | Initial velocity $v_0$ (ft/s) | Permanent deflection by Parkes $x_R$ (in) | | Theoretical results by author's model | | | |
|---|---|---|---|---|---|---|---|---|---|---|
| | | | | | Experiment | Theory | $F_p$* (lb) | k** (lb/in) | c*** (lbs/in) | $x_R$ (in) |
| 2 | 0.26×0.26 | 4 | 7.55 | 6.4 | 0.22 | 0.21 | 97.0 | 4284 | 1.229 | 0.19 |
| 4 | 〃 | 〃 | 〃 | 〃 | 0.42 | 0.44 | 48.5 | 536 | 0.466 | 0.39 |
| 8 | 〃 | 〃 | 〃 | 〃 | 0.93 | 0.93 | 24.3 | 67 | 0.177 | 0.83 |
| 12 | 〃 | 〃 | 〃 | 〃 | 1.53 | 1.48 | 16.2 | 20 | 0.100 | 1.34 |
| 2 | 0.26×0.26 | 4 | 15.1 | 9.0 | 0.43 | 0.42 | 97.0 | 4284 | 0.936 | 0.37 |
| 4 | 〃 | 〃 | 〃 | 〃 | 0.90 | 0.87 | 48.5 | 536 | 0.355 | 0.82 |
| 8 | 〃 | 〃 | 〃 | 〃 | 2.15 | 1.85 | 24.3 | 67 | 0.134 | 1.81 |
| 12 | 〃 | 〃 | 〃 | 〃 | 3.46 | 2.97 | 16.2 | 20 | 0.076 | 2.98 |

* Calculated as $\sigma_Y = 44090$ lb/in²
** Calculated as $E = 30\times10^6$ lb/in²
*** Calculated from Eq. (23)

results with the experimental results. As one of the extreme conditions he discussed the case of a heavy striker, and a part of his experimental and calculated results is shown in Table 2.

Using the assumption of the plastic-hinge theory, the load-deflection relation of the tip of the cantilever subjected to a static load at its tip becomes similar to that shown in Fig. 1. In the case of a rectangular cross-section of width b and depth d, the values of $F_p$, $x_p$ and k in Fig. 1 are given by

$$F_p = \frac{Mp}{\ell} = \frac{bd^2}{4\ell}\sigma_y, \qquad x_p = \frac{Fp\ell^3}{3EI} = \frac{\sigma_y \ell^2}{Ed}$$

$$k = \frac{Fp}{x_p} = \frac{Ebd^3}{4\ell^3}$$

where $\ell$ is the length of the beam, E is the modulus of elasticity and $\sigma_y$ is the static yield stress of the material. Hence the dynamic response of a cantilever struck transversely at its tip by a heavy striker can be calculated by the results shown in Chapter 2, and the calculated results on the permanent deflection of the tip are given in the final column of Table 2. Furthermore, these results by Parkes and the autor are compared in Fig. 16. It will be seen from Table 2 and Fig. 16 that the theoretical results using the author's model fairly well agree with the theoretical and experimental results by Parkes.

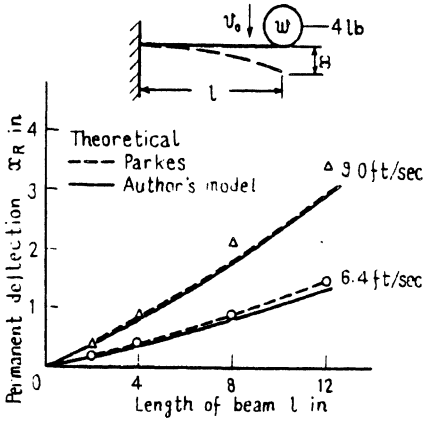


Fig. 16 Permanent deflection of tip of cantilever

## 7. Example applied for impact attenuation system utilizing plastic deformation

In order to protect the vehicle occupants in car collisions, impact attenuation systems having large capacity for energy and buffer quality have been desired. For one-shock having large kinetic energy such as car impact, impact attenuation systems utilizing plastic deformation whose load-displacement curve is nearly square are most effectual. From such a viewpoint, the author et al. have investigated several impact attenuation systems utilizing plastic deformations, and the pipe-ring structure[5] is a typical example of such an impact attenuation system. Another typical example is a cylinder with a hexagonal cross-section given by Fuse and Fukuda[6].

When these structures are crushed between two rigid plates, the idealized load-displacement relations are of the type consisting of an elastic range (OE), restricted plastic flow (EP) and unrestricted plastic flow (PM) as shown in Fig. 17. When the deformations are very large, it will be rational to assume that the load-displacement relations for these structures are OP'MR in Fig. 17. Using this assumption, we may apply the above results to these structures. Let us next compare the results of drop tests for a pipe-ring structure with the theoretical results using the author's model.

It is well known[7] that when a ring structure with a solid cross-section is crushed between rigid plates, the influence of geometry change after initial yield results in an increased load-carrying capacity. In the case of the ring having a thin-walled cylindrical cross-section, however, the load does not increase after initial yield because of buckling failure at the sections on the horizontal axis of symmetry, and its idealized load-displacement relation is of the type shown in Fig. 17[5]. In this case the characteristic values in Fig. 17 are given by

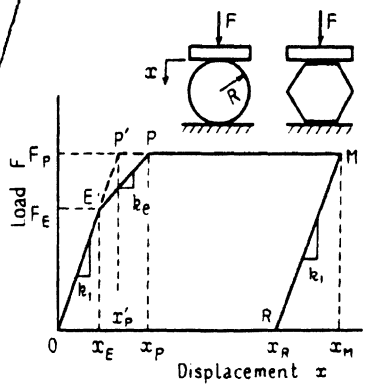


Fig. 17 Static load-displacement curve

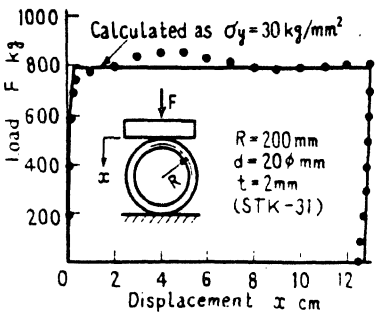


Fig. 18 Static characteristic of pipe-ring structure

$$F_\varepsilon = \frac{\pi M_p}{R}, \qquad x_\varepsilon = 0.4675 \frac{M_p R^2}{EI}$$

$$k_1 = 6.7199 \frac{EI}{R^3}, \qquad F_p = \frac{4M_p}{R}$$

$$x_p = 1.1416 \frac{M_p R^2}{EI}, \qquad x_p' = 0.5952 \frac{M_p R^2}{EI}$$

where EI is the flexural rigidity of the cross-section, R is the mean radius of the ring, and $M_p$ is the fully plastic moment of the cross-section of the ring

$$M_p = \frac{d^3}{6} \{1-(1-\frac{2t}{d})^3\}\sigma_y$$

in which d is the outer diameter and t is the thickness of the ring and $\sigma_y$ is the static yield stress of the material. Figure 18 shows the static load-displacement curve of a ring made of an STK-31 pipe having d = 20mm, t = 2mm, R = 200mm and $\sigma_y$ = 30kg/mm². Figures 19 and 20 show comparisons of the experimental and theoretical displacement-time histories and acceleration-time histories for the case that the ring is struck by dropping a 25.5kg weight from h = 200cm, where the calculated values took account of the effect of its own weight and calculating was made using the equivalent viscous damping coefficient obtained experimentally [the value setting $v_p = v_0$ in Eq. (33)]. It will be seen from Figs. 19 and 20 that there is fairly good agreement between the experimental and calculated values, and the theoretical results using the author's model are applicable for structures having the deformation characteristic as shown in Fig. 17.

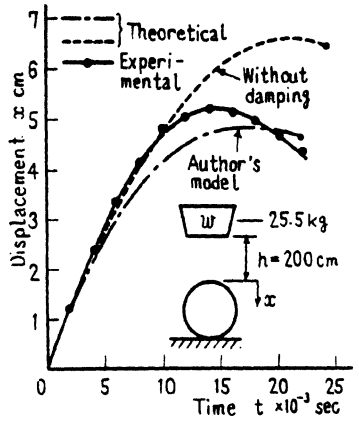


Fig. 19 Displacement-time history

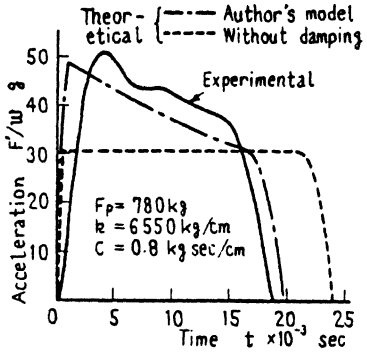


Fig. 20 Acceleration-time history

## 8. Conclusions

In this paper, the dynamic response of a structure whose static load-displacement curve consists of an elastic range and unrestricted plastic flow was analyzed by means of an equivalent model which takes into account elasticity, viscosity, plasticity and strain-rate sensitivity of the structure. The theoretical results agreed fairly well with the experimental results on simply supported beams, and the appropriateness of the author's model was confirmed.

In closing, the author would like to acknowledge the guidance of Professor H. Fukuda. The author also wishes to express his thanks to the personnel of the Computer Centre in Meiji University for their kind cooperation in connection with computation.

## References

(1) Ohmata, K. and Fukuda, H., Bull. JSME, 19-132 (1976-6), 584.
(2) Parkes, E. W., Proc. Roy. Soc. Lond., Ser. A, 228 (1955), 462.
(3) e.g., Perrone, N., Trans. ASME, Ser. E., 32-3 (1965-9), 489.
(4) Parkes, E. W., Proc. Inst. Civil Eng., 10 (1958), 297.
(5) Ohmata, K. and Fukuda, H., Research Reports of Fac. Engng. Meiji Univ. (in Japanese), 28 (1974), 17.
(6) Fuse, H. and Fukuda, H., Trans. Japan Soc. Automot. Engrs. (in Japanese), 3 (1971), 95.
(7) e.g., Deruntz, J. A. Jr. and Hodge, P. G. Jr., Trans. ASME, Ser. E., 30-3 (1963-9), 391.

# IMPACT

## *THE THEORY AND PHYSICAL BEHAVIOUR OF COLLIDING SOLIDS*

by

WERNER GOLDSMITH
*Professor of Engineering Mechanics*
*University of California, Berkeley*


LONDON
EDWARD ARNOLD (PUBLISHERS) LTD.

stress is independent of the previous strain-rate history is probably not completely valid. The observed increase in yield stress of a number of metals under dynamic loading [51, 426] can be accommodated by a suitable choice of the function $g\langle\sigma, \epsilon\rangle$, which will approximate an extension of the elastic line above the static yield stress by any desired amount. This procedure involves the assumption that the material is brought to a state of incipient plastic flow after application of a given elastic strain, regardless of elastic strain rate. Since initiation of plastic flow requires time—as was verified experimentally [59, 77]—the additional strain beyond $\epsilon_Y$ is thus primarily elastic. It is consistent with the preceding discussion that the propagation of a pulse with an intensity greater than $\sigma_Y$ is governed by elastic wave phenomena.

The relations applying to wave propagation, Eqs. (5.38), (5.39), and (5.118), are recapitulated as

$$\frac{\partial \sigma}{\partial x} - \rho \frac{\partial v}{\partial t} = 0 \qquad \frac{\partial \epsilon}{\partial t} - \frac{\partial v}{\partial x} = 0 \qquad E\frac{\partial \epsilon}{\partial t} - \frac{\partial \sigma}{\partial t} = g\langle\sigma, \epsilon\rangle \quad . \quad (5.119)$$

This hyperbolic system of quasi-linear differential equations can be integrated numerically by the method of characteristics. The characteristics in the Lagrange plane are specified by the three families of curves [257]

$$E\,d\epsilon - d\sigma = g\langle\sigma, \epsilon\rangle\,dt \qquad \text{on} \quad dx = 0 \quad . \quad . \quad . \quad (5.120)$$

$$d\sigma - \rho c_0\,dv = -\,g\langle\sigma, \epsilon\rangle\,dt \quad \text{on} \quad dx - c_0\,dt = 0. \quad (5.121)$$

$$d\sigma + \rho c_0\,dv = -g\langle\sigma, \epsilon\rangle\,dt \quad \text{on} \quad dx + c_0\,dt = 0. \quad (5.122)$$

The scheme of characteristic integration for the case when the end $x = 0$ of a bar extending to infinity in the positive $x$-direction suddenly acquires velocity $v_1$ is shown in Figure 122. The elastic wave, governed by Eq. (5.121), travels down the bar with velocity $c_0$. From the shock conditions, Eqs. (5.36), and initial conditions $\sigma = \epsilon = v = 0$ in the undisturbed region, the stress just after the discontinuity is given by

$$\sigma = \rho c_0^2 \epsilon = -\rho c_0 v \quad \text{on} \quad x = c_0 t \quad . \quad . \quad . \quad (5.123)$$

where $v_1 < 0$ for tensile impact. Eliminating $\epsilon$ and $v$ between Eqs. (5.123) and (5.121),

$$\int_{\sigma_0 = -\rho c_0 v_1}^{\sigma} \frac{d\gamma}{g\left\langle \gamma, \dfrac{\gamma}{\rho c_0^2} \right\rangle} = -\tfrac{1}{2}t \quad . \quad . \quad . \quad (5.124)$$

Eqs. (5.36) and (5.124) thus determine the values of $\sigma$, $\epsilon$, and $v$ along the boundary $x = c_0 t$ and this information in conjunction with the condition $v = v_1$ at $x = 0$ permits the determination of the characteristics in the plastic domain. It is necessary to check the plasticity condition $\sigma > f\langle\epsilon\rangle$ at each point of the regime.

For a finite impact duration $\tau$, an unloading wave with characteristic



$dx - c_0\,dt = 0$ emanates from point $(0, \tau)$. The construction of the net up to this line has been described previously. The characteristics in the unloading region, where $g\langle\sigma, \epsilon\rangle = 0$, are

$$\left.\begin{aligned} \sigma - E\epsilon &= \text{constant} \quad \text{on} \quad x = \text{constant} \\ \sigma - \rho c_0 v &= \text{constant} \quad \text{on} \quad x - c_0 t = \text{constant} \\ \sigma + \rho c_0 v &= \text{constant} \quad \text{on} \quad x + c_0 t = \text{constant} \end{aligned}\right\} \quad (5.125)$$

together with the boundary condition $\sigma = 0$ on $x = 0$ and the known values on the elastic–plastic boundary, which determine the constants in

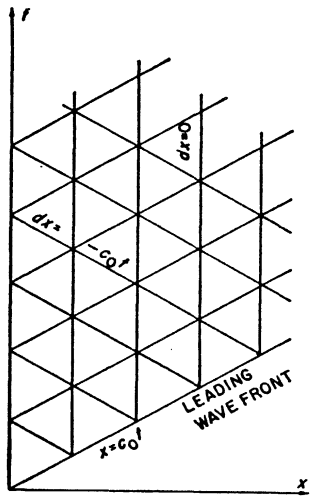


Figure 122. Characteristic Plane for a Strain-rate Dependent Material [257]

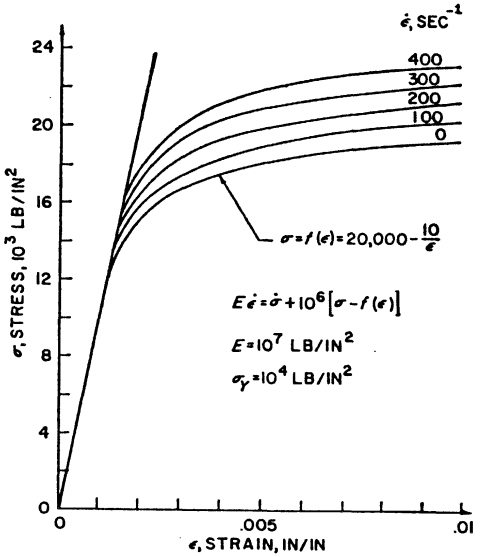


Figure 123. Strain-rate Dependent Stress–Strain Diagram Hypothesized for Aluminium [258]

Eqs. (5.125). The unloading shock wave is progressively absorbed by the plastic pulse and may die out completely. In this case the elastic–plastic boundary does not continue along the unloading characteristic, but is specified by characteristics in the elastic and plastic regions together with the static relation $\sigma = f\langle\epsilon\rangle$.

Numerical integrations have been carried out by this method [258] for a semi-infinite bar of aluminium subjected to a tensile impact velocity of −50 ft/sec at the free end of the bar. Function $g\langle\sigma, \epsilon\rangle$ was chosen as linear with overstress, so that Eq. (5.118) is expressed as

$$E\dot{\epsilon} = \dot{\sigma} + k^*[\sigma - f\langle\epsilon\rangle] \quad . \quad . \quad . \quad . \quad (5.126)$$

The static stress–strain relation for the material was assumed in the simple form

$$f\langle\epsilon\rangle = 20{,}000 - \frac{10}{\epsilon} \quad . \quad . \quad . \quad . \quad (5.127)$$

TABLE 20. STATIC AND DYNAMIC TENSILE PROPERTIES OF SOME METALS [69, 76]

| Material | Heat treatment | Static proportional limit, $10^3$ lb/in$^2$ | Ultimate strength, $10^3$ lb/in$^2$ | |
|---|---|---|---|---|
| | | | Static | Dynamic |
| Ingot Iron | Annealed | 16·0 | 37·1 | 57·4 |
| SAE 1015 | Annealed | 29·3 | 50·6 | 63·5 |
| SAE 1022 | Cold-rolled | 64·5 | 84·0 | 105·0 |
| SAE 1022 | Annealed | 41·0 | 65·0 | 82·7 |
| SAE 1022 | Quench and Tempered | 135·0 | 153·4 | 177·4 |
| SAE 1040 | Annealed | 43·0 | 78·1 | 91·8 |
| SAE 1045 | Normalized | 55·5 | 97·8 | 105·7 |
| SAE 1045 | Quench and Tempered | 132·3 | 142·9 | 169·0 |
| SAE 1095 | Normalized | 74·0 | 144·6 | 151·0 |
| SAE 2345 | Austempered $R_C$ 35 | 121·0 | 155·7 | 182·0 |
| SAE 2345 | Quench and Tempered $R_C$ 35 | 135·0 | 145·3 | 175·3 |
| SAE 4140 | Austempered $R_C$ 31 | 82·0 | 139·8 | 150·7 |
| SAE 4140 | Quench and Tempered $R_C$ 31 | 123·5 | 134·3 | 151·0 |
| SAE 5150 | Austempered $R_C$ 31 | 102·5 | 148·5 | 165·3 |
| SAE 5150 | Quench and Tempered $R_C$ 32 | 124·0 | 139·0 | 148·1 |
| Type 302 Stainless Steel | As received | 44·0 | 93·3 | 110·8 |
| Commercial Copper | Annealed | 4·0 | 29·9 | 36·7 |
| Commercial Copper | Cold-rolled | 30·0 | 45·0 | 60·0 |
| 1100 Aluminium Alloy | Annealed | 1·7 | 11·6 | 15·4 |
| 1100 Aluminium Alloy | ½ Hard | 12·0 | 17·2 | 22·1 |
| 2017 Aluminium Alloy | As received | 38·0 | 59·9 | 63·8 |
| 2024 Aluminium Alloy | As received | 47·0 | 65·2 | 68·6 |
| 2024 Aluminium Alloy | Annealed | 14·0 | 34·0 | 45·0 |
| Magnesium Alloy (Dow Metal F) | As received | 25·5 | 35·9 | 51·8 |
| Magnesium Alloy (Dow Metal J) | As received | 29·9 | 43·8 | 51·4 |

| Elongation in 8 in, % | | Energy per unit volume, ft-lb/in$^3$ | | Reduction of area, % | | Observed limiting impact velocity, ft/sec | Computed critical impact velocity,* ft/sec |
|---|---|---|---|---|---|---|---|
| Static | Dynamic | Static | Dynamic | Static | Dynamic | | |
| 25·7 | 16·2 | 726 | 440 | 69 | 71 | 100 | § |
| 28·0 | 30·0 | 1028 | 1323 | 69 | 63 | 100 | § |
| 6·0 | 15·0† | 401 | 1180† | 66 | 66 | 100 | 95 |
| 25·5 | 27·7 | 1240 | 1750 | 69 | 69 | 160 | § |
| 2·9 | 5·9 | 332 | 780 | 53 | 62 | >200 | 120 |
| 20·4 | 20·7 | 1235 | 1510 | 51 | 53 | >200 | § |
| 13·0 | 15·3 | 955 | 1253 | 57 | 57 | >200 | § |
| 5·7 | 9·2‡ | 670 | 1230‡ | 61 | 59 | 190 | 88 |
| 7·6 | 10·7 | 888 | 1239 | 24 | 24 | >200 | 232 |
| 6·4 | 9·9‡ | 759 | 1448‡ | 68 | 67 | >200 | 171 |
| 8·4 | 14·1‡ | 1007 | 1840‡ | 60 | 61 | >200 | 161 |
| 8·5 | 10·4‡ | 946 | 1231‡ | 32 | 57 | >200 | 225 |
| 8·5 | 14·7‡ | 866 | 1761‡ | 75 | 68 | 175 | 132 |
| 5·8 | 10·8‡ | 636 | 1334‡ | 62 | 63 | >200 | 181 |
| 8·5 | 13·3‡ | 1004 | 1596‡ | 61 | 63 | 170 | 159 |
| 58·5 | 46·6 | 3940 | 3840 | 69 | 64 | >200 | 490 |
| 32·7 | 43·8 | 631 | 1010 | 64 | 69 | >200 | 231 |
| 2·5 | 10·7† | 71 | 425† | 44 | 46 | 50 | 42 |
| 23·0 | 30·0 | 190 | 340 | 81 | 78 | >200 | 176 |
| 4·6 | 17·0† | 58 | 250† | 76 | 80 | 110 | 36 |
| 14·2 | 17·0 | 594 | 854 | 41 | 41 | >200 | 307 |
| 11·3 | 13·5 | 589 | 749 | 33 | 37 | >200 | 290 |
| 6·7 | 9·9 | 164 | 337 | 37 | 45 | >200 | 174 |
| 8·3 | 9·6‡ | 245 | 394‡ | 24 | 31 | >200 | 232 |
| 9·6 | 10·9‡ | 339 | 454‡ | 19 | 33 | >200 | 303 |

* Based on static stress–strain curve and strain-rate independent theory of plastic wave propagation.
† Maximum value at limiting velocity.
‡ Considerable scatter in elongation and energy curves below limiting velocity. Value reported is the average below limiting velocity.
§ Existence of a yield point prevents establishment of a theoretical failure velocity.

for specimens of 0·300 in diameter and a gauge length of 8 in.[69, 76] While wave propagation effects were considered in the reduction of the data, the results may have been influenced by bending and equipment effects. However, although somewhat different results might be obtained with another type of apparatus, Table 20 gives a good indication of the general trend of material properties under tensile impact conditions. The dynamic ultimate strength was determined from the average value of the maximum plateau in the stress–time curve measured by a dynamometer in series with the specimen. The reported energy per unit volume is a first-order approximation, being computed as the product of the impact velocity and the total area under the stress–time curve. For almost all materials tested, the dynamic ultimate strength exceeded the static value, but remained relatively constant above impact velocities of 25 ft/sec; this variation is indicated in Figure 256 for one steel and one aluminium alloy.



Curves of total specimen elongation and energy absorbed per unit volume as a function of impact velocity exhibited three characteristic shapes. The first of these, illustrated in Figure 257, exhibits a constant plateau of elongation and energy up to a limiting value of the impact velocity, followed by a marked decrease in the value of the parameters. The second type, exemplified in Figure 258, shows a progressive increase in the magnitudes of the ordinates up to a maximum at the limiting velocity, beyond which these quantities decline. The third group of curves, found principally for quenched and tempered and austempered steels and magnesium alloys, are not too well defined below the limiting value of impact velocity. Consequently, the average values recorded for these curves are not as significant as the magnitudes obtained from the other types of diagrams. The existence of the limiting impact velocity is obscured unless the ratio of gauge length to test bar diameter is sufficiently

specimens indicated no significant difference in their yield point strength, as indicated in Figure 266,[421] although the micro-hardness of steel bars strained dynamically was found to be greater than when strained under static conditions an equal amount.[170] This observation is at variance with the results of static tests on specimens previously subjected to a compressive impact, where the yield stress was reduced below that of an unstrained specimen.[60]

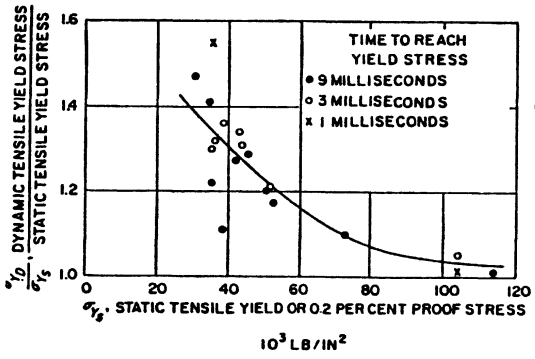


Figure 265

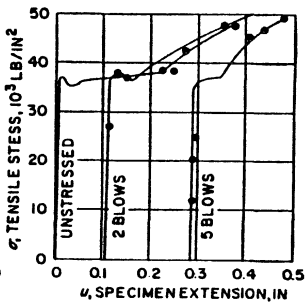


Figure 266

Figure 265. Ratio of Dynamic to Static Tensile Yield or Proof Stress as a Function of Static Tensile Yield or Proof Stress for Various Steels [50, 420]

Figure 266. Results of Static Tensile Tests on ¼-in-diameter, 8-in-long 0·22% Carbon Steel Specimens after being Prestressed by Repeated Impact [421]

## 7.4. Dynamic Compressive and Torsion Tests

While the objectives of dynamic tensile and compressive tests of materials are identical, there necessarily exist some differences between the two types of investigations with regard to the manner of load application. Some experiments have been carried out with devices compressing the specimen between two movable anvils which approach each other at a constant rate.[3, 248, 304] However, most of the tests utilized an impact technique consisting either of a modification of the Hopkinson bar method or the projecting of the test piece against a hard target. In the Hopkinson bar arrangement a stress wave is initiated in an anvil bar by the dropping of a weight, the impact of a bullet, or the detonation of an explosive charge, and this pulse is employed to load a specimen sandwiched between the anvil bar and an extension.[18, 57, 58, 59, 60, 232, 255] This technique possesses a considerable advantage over corresponding methods of tensile testing in that a much closer control over axiality of loading can be exercised. However, care must be taken to avoid the use of specimen geometries and conditions at the interface which might prevent free lateral expansion of the test piece and might introduce deviations from a state of plane stress in



the specimen. Bending effects can be minimized in direct drop tests by curving one of the colliding surfaces.

Again, wave phenomena encountered in all impact tests must be properly accounted for in the analysis of the data, and conditions of uniform strain or strain rate cannot be produced in the specimen by such methods. Unlike tensile specimens, which fail either by necking or brittle fracture, a metallic test bar subjected to uniform, uni-axial dynamic compression will fail either by barrelling, column action, or shear effects, and at much higher strain magnitudes. In most other respects, however, the dynamic behaviour of metals in tension and compression is very similar.

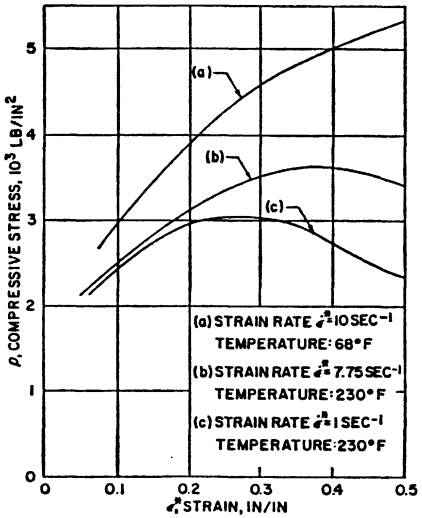


Figure 267. Dynamic Compressive Stress–Strain Curves for Pure Lead Subjected to Constant Applied Strain Rates at Two Different Test Temperatures [248]

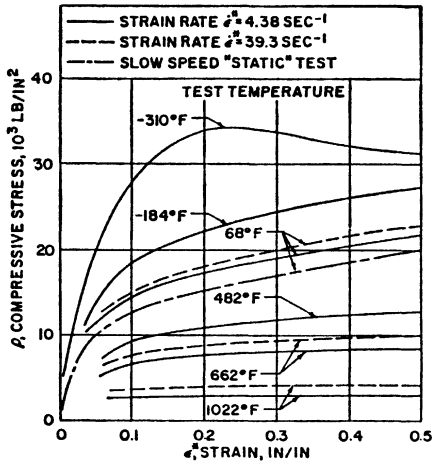


Figure 268. Dynamic Compressive Stress–Strain Curves for 99% Pure Aluminium, Annealed at 752° F, Subjected to Constant Applied Strain Rates at Various Test Temperatures [3]

The stress–strain curve, including the yield stress and ultimate strength, is elevated compared to that under static conditions, and materials with a definite yield point exhibit a time delay before the onset of plastic deformation, as indicated in Figure 253. Similarities have also been observed in micro-structural changes under the two types of impact load.

The results of some slow-speed tests on lead, aluminium, copper, and steel at several temperatures and constant true strain rates are presented in Figures 267, 268, 269, and 270.[3, 248] Barrelling was prevented by grooving and lubricating the specimens at the contact surfaces, and the time rate of decrease of specimen length was maintained constant by a cam controlling the motion of the compressing anvils. As in the corresponding tension tests, the stresses required to produce a given plastic strain increase with strain rate and a reduction of test temperature.

The action of single compressive pulses plastically straining specimens located between two anvil rods of a Hopkinson bar arrangement has also been employed to derive dynamic stress–strain curves for various materials. Transducers are mounted on sections of the anvil bars which remain elastic throughout the test cycle and which are of the same diameter as the test piece. In one series of experiments explosively generated pulses were measured by means of parallel and circumferential condenser microphones whose output was converted to stress–time and strain–time

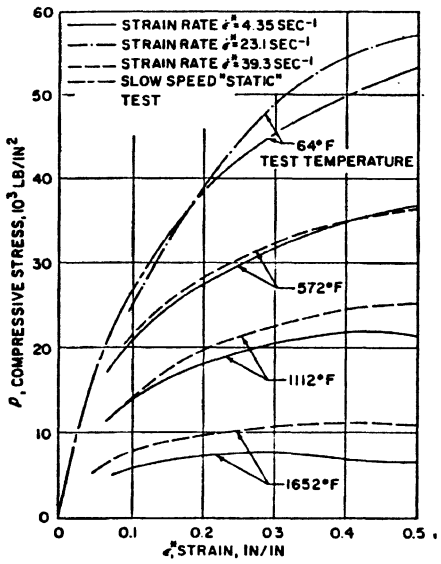


Figure 269. Dynamic Compressive Stress–Strain Curves for Commercially Pure Copper, Annealed at 1112° F, Subjected to Constant Applied Strain Rates at Various Test Temperatures [3]

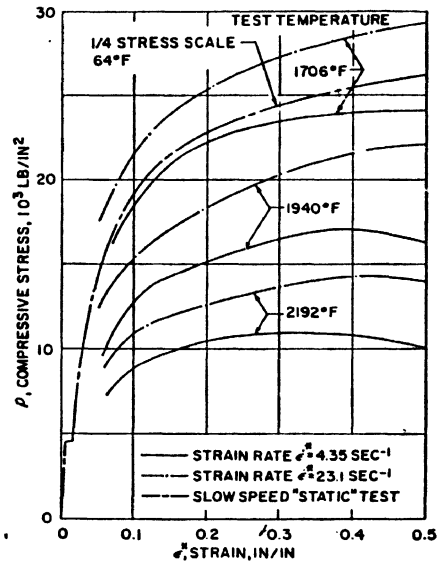


Figure 270. Dynamic Compressive Stress–Strain Curves for 0·17% Carbon Steel, Annealed at 1634° F, Subjected to Two Constant Rates of Applied Strain at Various Test Temperatures [3]

diagrams.[223] A remarkable difference was observed in the dynamic compressive behaviour of soft metals and plastics in that the latter exhibited virtually complete recovery immediately subsequent to unloading, while almost no recovery was noted in the case of the metals.

In another group of tests stress waves were produced by dropping a weight from various heights on the curved end of one of the anvil bars, and strain histories were recorded by means of strain gauges mounted on both anvil rods near the interface of a steel specimen.[59, 355] For this case, the stress and particle velocity history at both faces of the specimen were calculated from the strain gauge records by means of the method of characteristics, using Eq. (5.60). A representative set of such curves for a ½-in × ½-in mild steel specimen of 0·24% carbon content is shown in Figure 271; the close agreement between the stress histories at the upper



and lower specimen surfaces indicate that the inertial effects of the specimen are small. The average strain-rate history for the specimen, presented in Figure 272, is computed as the ratio of the difference of particle velocity at the upper and lower face and original length of the specimen, so that $\left.\frac{d\epsilon^*}{dt}\right|_m = (v_u - v_L)/L_0$. Integration of Figure 272 and combination with the data shown in Figure 271 provides the stress–strain curve exhibited in Figure 273, where the strain must be considered as an average value for the test bar at any time. The results of static tests on the original and previously dynamically strained specimens are included for comparison. The results of similar tests on medium carbon steel (0·32% carbon) at several impact velocities and test temperatures are presented in Figures 274 and 275.

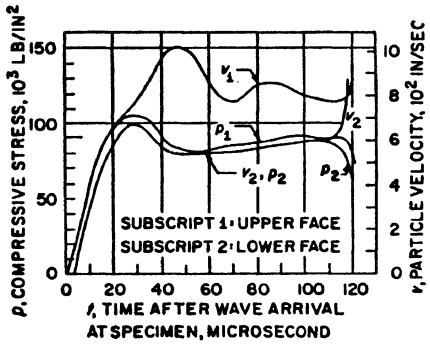


Figure 271

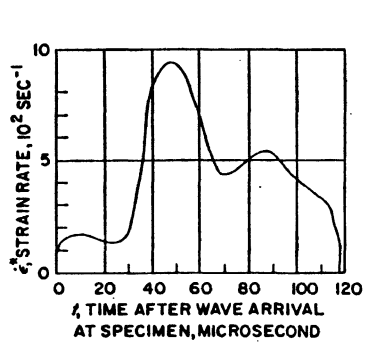


Figure 272

Figure 271. Stress and Particle Velocity Histories at the Upper and Lower Faces of a ½-in × ½-in Mild Steel Specimen Containing 0·24% Carbon, Annealed at 1652° F, Due to a Compressive Impact [59]

Figure 272. Strain-rate Curve Corresponding to Figure 271 [59]

It may be noted that the dynamic compressive yield stress of mild carbon steel is raised by a factor varying between 2 and 3 over the corresponding static yield stress, but that the ratio of these stresses decreases with increasing strain. The dynamic yield stress for a given material is increased both with impact velocity—and hence, strain rate—and a decrease in test temperature, exactly as in the case of tensile tests. A time delay before the initiation of plastic flow was observed in all dynamic tests, as may be seen from the numbers along the curves, which represent the time in microseconds to reach a given state.

The data of Figure 273 indicate that the static strength of a dynamically shocked specimen is less than the strength of the corresponding annealed test bar. This conclusion was confirmed in similar experiments involving the determination of the static stress–strain curve of a 0·32% carbon steel

# Advanced Anthropomorphic Test Device (AATD) Development Program

Phase 1 Reports: Concept Definition

## AATD SYSTEM TECHNICAL CHARACTERISTICS, DESIGN CONCEPTS, AND TRAUMA ASSESSMENT CRITERIA

John W. Melvin
Albert I. King
Nabih M. Alem

Contract No. DTNH22-83-C-07005
Task E-F
Final Report
September 1985

THE UNIVERSITY OF MICHIGAN
Department of Mechanical Engineering
& Applied Mechanics

1200±180 N/cm (685±103 lb/in). This nonlinear overall load–deflection response can also be represented in a continuous manner by a load–deflection relationship given by

$$F_F = (48 \pm 7 \text{ N/cm}^2)d_F^2 \quad \text{or} \quad (69 \pm 10 \text{ lb/in}^2)d_F^2$$

where $F_F$=frontal load, and $d_F$=frontal deflection. This is based on the mean nonlinear (deflection squared) spring from the curve–fitting of the Kroell response data (see Table 9).

The static normal belt–load/chest–deflection response at mid–sternum should approximate a linear stiffness of 676±101 N/cm (386±58 lb/in) for deflection up to 2.54 cm (1 in). The corresponding stiffness value for the upper lateral regions of the front of the chest, with clavicular structures in place, should be 948±142 N/cm (541±81 lb/in), while the lower lateral regions of the front of the chest should exhibit a stiffness in the range of 400±60 N/cm (228±34 lb/in). The tests to determine these static responses to shoulder–belt loading should duplicate the techniques of L'Abbé et al. (1982).

The static lateral force–deflection characteristics of the chest have not been studied. If the chest were a linear elastic structure, theoretical calculations for a ring–like structure with the dimensions of the AATD chest predict a slightly higher stiffness (on the order of 1.24 times) for the lateral direction than the frontal, due to the more curved nature of the lateral aspects of the chest. Thus, the static lateral force–deflection response of the chest for loading by a 15.2–cm (6–in) diameter rigid disc should be similar to that for frontal loading but with 19% lower deflection for a given load. This would give an overall static load deflection relationship of the form

$$F_L = (74 \pm 11)d_L^2$$

where $F_L$=lateral load (N), and $D_L$=lateral deflection (cm).

**Dynamic Load–Deflection Response.** The dynamic response of the chest to flat rigid–disc frontal impacts has been discussed extensively by Melvin et al. (1985). The summary response curves for apparent initial stiffness and plateau forces as functions of impactor velocity (Figures 3–2 and 3–3 of Task B report) can be represented by the following equations:

$$S_{AI} = 0.263 + 0.603(V\text{-}1.3) \qquad (V > 1.3 \text{ m/s})$$

and

$$F_P = 1 + 0.750(V\text{-}3.73) \qquad (V > 3.73 \text{ ms})$$

where: $S_{AI}$ = apparent initial stiffness, kN/cm
$F_P$ = plateau force, kN
$V$ = impactor velocity, m/s

The variations of the test subject mass from that of the AATD specifications must be accounted for through scaling of the data using the factor $\lambda_1 = \sqrt[3]{\lambda_m}$. For the stiffness data $(S_{AI})_{scaled} = \lambda_1(S_{AI})_m$, whereas for the force plateau data $(F_P)_S = \lambda_1(F_P)_m$. This scaling does not change the form of the above relationships, only the parameter values. The scaled relationships are

$$S_{AIS} = 0.255 + 0.603(V - 1.1) \qquad (V > 1.1 \text{ m/s})$$

$$F_P = 1.1 + 0.750(V - 3.47) \qquad (V > 3.47 \text{ m/s})$$

The equations can be combined to define an equivalent deflection $d_{PI}$ at which the plateau would theoretically begin. This idealized response would be characterized by the equation:

$$F_P = S_{AI} d_{PI} \quad \text{or} \quad d_{PI} = \frac{F_P}{S_{AI}}$$

The maximum deflection of the chest occurs when the impactor velocity and the chest reach a common velocity. Thus, the force at maximum deflection is primarily a static response. Accordingly, the deflection at the end of the plateau region can be estimated by the combination of the plateau force at a given velocity and the associated static deflection needed to produce a static force level equal to the plateau force. This can be expressed by the equation

$$F_P = S_E d_{PF}^2 \quad \text{or} \quad d_{PF} = \sqrt{F_P / S_E}$$

where $S_E$ equals the coefficient of the nonlinear static elastic response of the chest and is equal to $(48 \pm 7)$ N/cm$^2$ for frontal loading. Figure 16 shows the resulting idealized response curves (with $\pm 15\%$ ranges) generated from the above equations for three impactor velocities: 4.3, 6.7, and 10 m/s (14, 22, and 32.8 ft/s). The first two velocities are those of the present Part 572 test procedure. The corresponding values for defining the curves are given in Table 10. The impactor mass should be 23.4 kg (51.5 lb).

The results of the curve-fitting analysis of the Kroell data, Table 9, also yield characteristic values for velocity and acceleration coefficients that can be used, along with the nonlinear static spring coefficient, as guides to the nature of the parameters needed for a properly responding thorax design. The mean value of the linear velocity coefficient is $4.85 \pm 0.73$ N·s/cm ($2.77 \pm 0.42$ lb·s/in), and the mean value of the linear acceleration coefficient is $0.30 \pm 0.045$ kg ($0.67 \pm 0.1$ lb).

There are limited data on the lateral impact response of the chest under loading conditions similar to those used in frontal testing. Stalnaker et al. (1973) reported on cadaver tests using the same test techniques. The test methods were quite different from those employing a moving-mass impactor of the type used in present ATD certification procedures. Consequently, Neathery (1974) concluded that the data were not strictly comparable to the traditional Kroell data. The Stalnaker data can, however, be used to indicate general similarities and differences between frontal and lateral loading. In particular, Stalnaker found that, under identical input conditions, the apparent initial lateral stiffness $(S_{AI})_L$ of the chest was approximately 63% of the apparent initial frontal stiffness $(S_{AI})_F$ and that the plateau force levels were approximately the same. This implies that the linear velocity coefficient would be similar to the frontal coefficient but that the effective initial mass involved in the response may be lower than that for frontal loading due to the geometric differences between the front and the side of the thorax. This information along with the lateral static chest response relation can be applied by the previously described methods for defining the idealized thoracic frontal response to generate analogous lateral response specifications. Figure 17 shows the resulting idealized response curves (with $\pm 15\%$ ranges) generated from that analysis for the same three impactor velocities 4.3, 6.7, and 10 m/s (14, 22, and 32.8 ft/s). The corresponding values for defining the curves are given in Table 11.

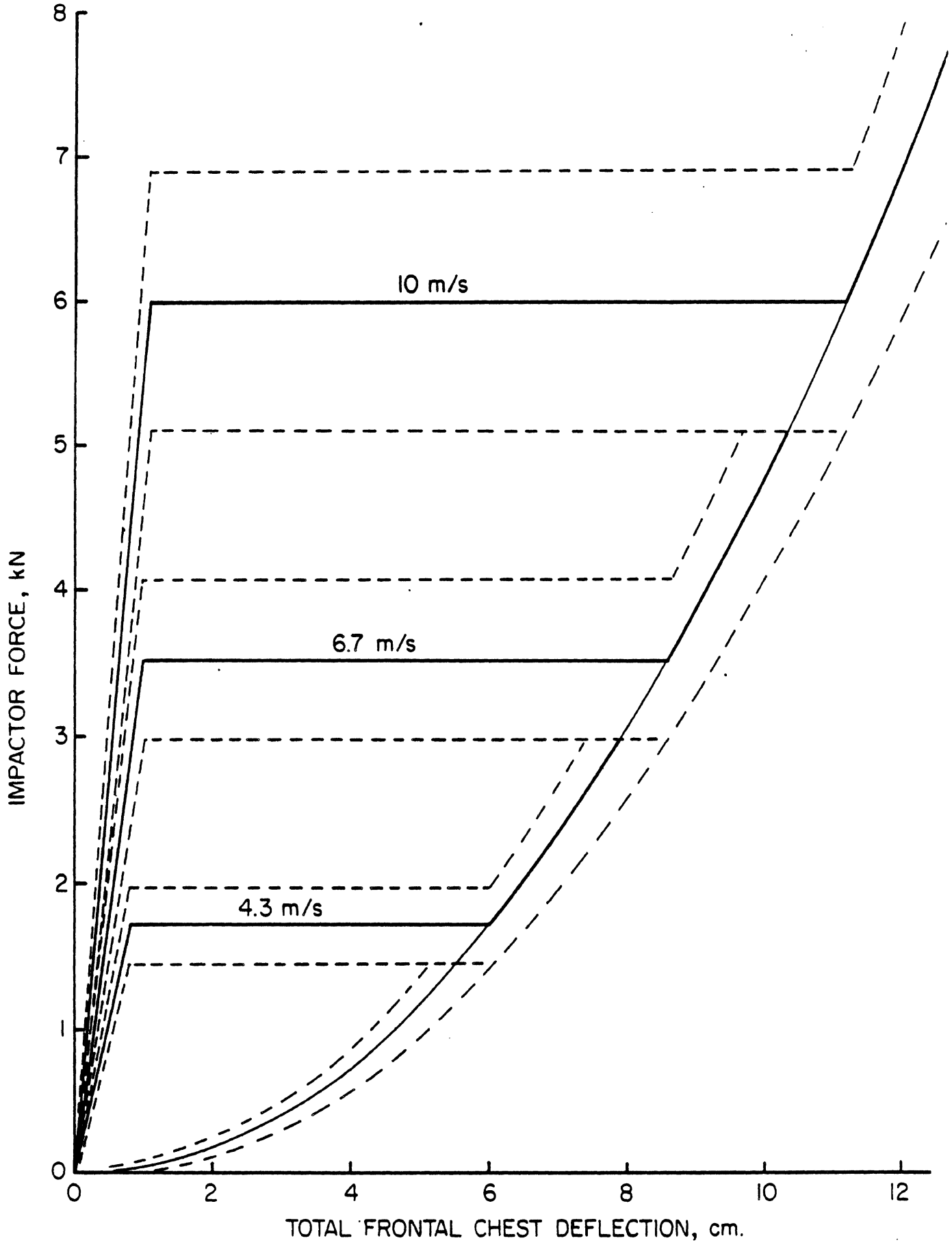


FIGURE 16. AATD frontal thoracic impact response—loading only (15.2-cm rigid disc, 23.4-kg impact mass).

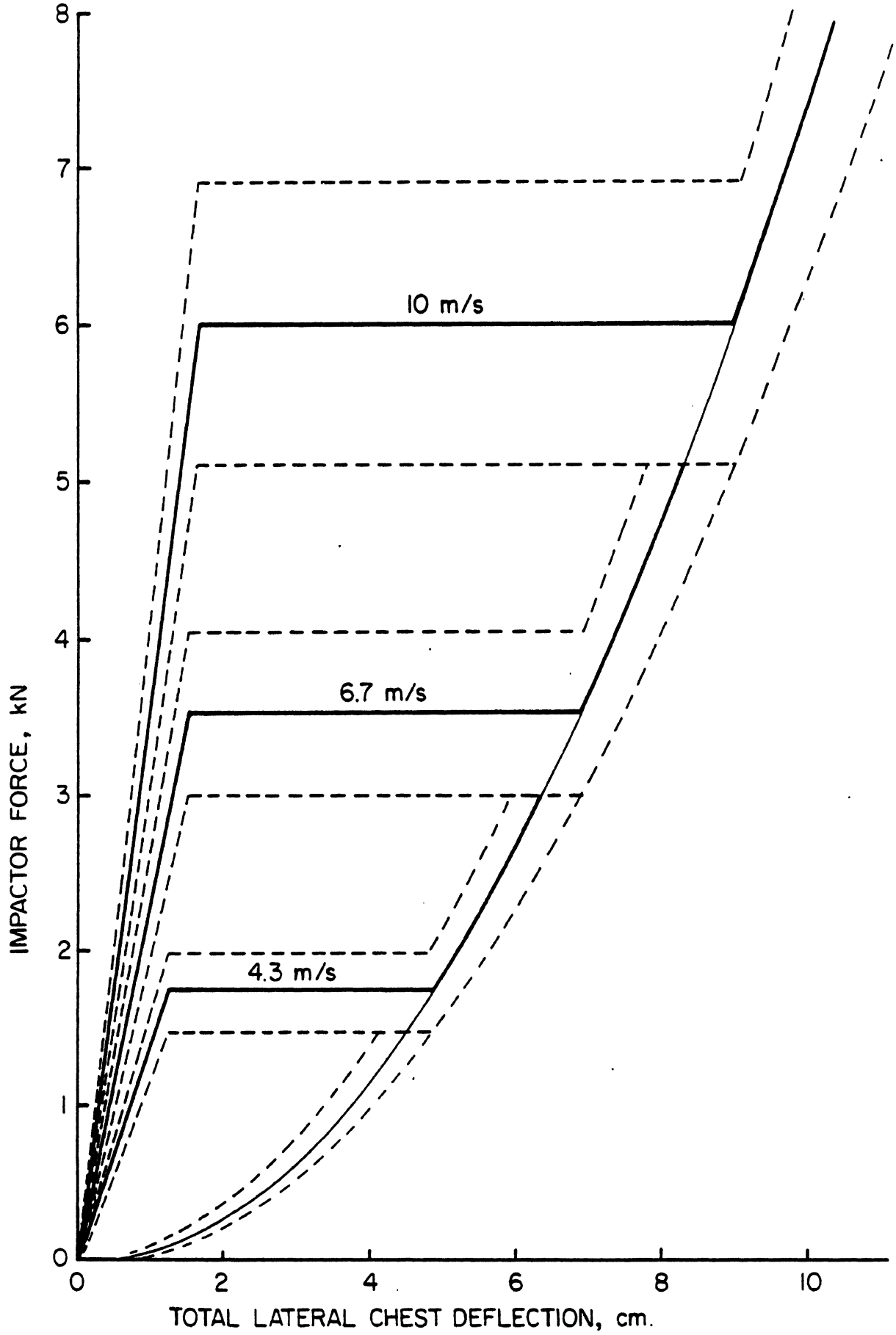


FIGURE 17. AATD lateral thoracic impact response—loading only (15.2-cm rigid disc, 23.4-kg impact mass).

TABLE 10

AATD IDEALIZED FRONTAL THORACIC IMPACT RESPONSE PARAMETERS
(Rigid disc impactor, 15.2-cm diameter and 23.4-kg mass)

| Impactor Vel (m/s) | $S_{AI}$ (kN/cm) | $F_P$ (kN) | $d_{PI}$ (cm) | $d_{PF}$ (cm) |
|---|---|---|---|---|
| 4.3 | 2.18±0.33 | 1.72±0.26 | 0.79 | 6.0 |
| 6.7 | 3.63±0.54 | 3.52±0.53 | 0.97 | 8.6 |
| 10.0 | 5.62±0.84 | 6.00±0.90 | 1.07 | 11.2 |

TABLE 11

AATD IDEALIZED LATERAL THORACIC IMPACT RESPONSE PARAMETERS
(Rigid disc impactor, 15.2-cm diameter and 23.4-kg mass)

| Impactor Vel (m/s) | $S_{AI}$ (kN/cm) | $F_P$ (kN) | $d_{PI}$ (cm) | $d_{PF}$ (cm) |
|---|---|---|---|---|
| 4.3 | 1.38±0.21 | 1.72±0.26 | 1.25 | 4.8 |
| 6.7 | 2.29±0.34 | 3.52±0.53 | 1.54 | 6.9 |
| 10.0 | 3.55±0.53 | 6.00±0.90 | 1.69 | 9.0 |

The response of the thorax to frontal and lateral impact loads has been defined above for loading only. The unloading behavior of the thorax has been shown by Kroell et al. to dissipate the energy of deformation. In crash testing, the unloading response is not as critical as the loading response, as long as sufficient energy dissipation occurs. This may be specified in terms of a hysteresis ratio, which is the ratio of the area bounded by the loading and unloading portions of the force-deflection curve to the area under the loading portion of the curve. For sufficient response, this ratio should be more than 75% but less than 85%.

The response of the thorax to oblique impacts that are between the frontal and lateral directions has not been quantified by similar methods. Nusholtz et al. (1983b) reported on low-level (2-m/s) impacts in the frontal, lateral, and 45° oblique directions in terms of point-of-impact impedance. These non-injurious impacts produced similar mechanical impedance values in all three directions in the same test subject. Thus it is likely that the oblique response of the thorax is bounded by the frontal and lateral responses.

SAE Technical Paper Series

790324



# High and Low Rate Force-Deformation Characteristics of Motorcycle Helmets

**Herbert B. Kingsbury and Wayne C. Herrick**
Dept. of Mechanical and Aerospace Engrg., Univ. of Delaware, Newark, DE
**Dinesh Mohan**
Research Dept., Insurance Institute for Highway Safety, Washington, DC

**Congress and Exposition**
**Cobo Hall, Detroit**
**February 26-March 2, 1979**

SOCIETY OF AUTOMOTIVE ENGINEERS, INC.
400 COMMONWEALTH DRIVE
WARRENDALE, PENNSYLVANIA 15096

790324

# High and Low Rate Force-Deformation Characteristics of Motorcycle Helmets

**Herbert B. Kingsbury and Wayne C. Herrick**
Dept. of Mechanical and Aerospace Engrg., Univ. of Delaware, Newark, DE
**Dinesh Mohan**
Research Dept., Insurance Institute for Highway Safety, Washington, DC

A NUMBER OF PERFORMANCE STANDARDS for motorcycle helmets are currently in use in various countries or have been proposed [1]*. Helmets sold in the United States must meet Federal Motor Vehicle Safety Standards (FMVSS) 218 [2] which, in turn, is based on ANSI Z 90.1 [3]. Other standards include Snell 1975 [4], CSA AD230 in Canada, and BSI 200, in Great Britain.

All of these standards require the helmet provide some minimum level of impact load attenuation to a dummy headform. The allowed impact level is phrased either in terms of maximum force or of accelerations over various time intervals. Each of these standards generally includes a helmet retention requirement as well as a requirement for penetration and abrasion resistance. Each code is quite specific concerning method of impact load application and construction of the headform on which the helmet will be mounted during testing. Most standards are also different from all other standards in the above respects.

Although performance standards are necessary, helmet manufacturers quite naturally tend to design helmets to meet these artificial, although very specific, performance criteria rather than to provide optimum protection for the actual human motorcyclist.

A practical way to determine the actual effect of present motorcycle helmets in head impact attenuation would be to employ a mathematical model of the human head-torso structure, such as the HSRI MVMA 2-D [5], combined with a mathematical representation of the helmet structure. Such a tool, once developed, could also be used to determine head impact response for a range of impact velocities as well as to determine the effect of structural and material changes on helmet effectiveness.

To carry out such a study it is first necessary to determine the load-deformation characteristics of actual helmets at loads and deformation rates comparable to those encountered under service conditions.

This paper reports on the results of a test program carried out to determine these data for a variety of helmet types. Use of the resulting load deformation data to determine head accel-

*Numbers in brackets refer to the list of references.

ABSTRACT

The load-displacement characteristics of fifteen motorcycle helmets were determined at displacement rates from quasi-static to 5M/S. Seven of these helmets had polycarbonate outer shells while the remaining shells were of fiberglass construction. The stiffness of helmets with polycarbonate shells was found to be more uniform, both with loading rate and magnitude of load, than that of fiberglass shell helmets.

Use of these data to predict helmeted head force and acceleration after impact with a rigid surface is illustrated using a mathematical model.

0148-7191/79/0226-0324$02.50

eration response at impact is illustrated by means of a simple dynamical model of the torso-head-helmet system.

EQUIPMENT AND PROCEDURE

In this series of tests, motorcycle helmets were mounted on a headform in a hydraulic test machine in order to investigate their load-deformation characteristics under quasi-static and high rate conditions.

The fifteen helmets studied were designed to protect three quarters of the head and face (Table 1). This type of helmet is more popular among the average motorcycle rider than the more expensive full-coverage type. The helmets are of trilaminar construction with an inner foam-backed cloth lining for comfort and fit, a middle shell of expanded bead polystyrene and an outer shell molded of either polycarbonate polymer or varying numbers of layers of fiberglass. The cost of these helmets ranges from $16 to $60. The less expensive helmets have polycarbonate outer shells while the expensive ones are constructed of fiberglass with the cost being proportionate to the number of fiberglass layers incorporated. The four helmet brands used in this investigation were chosen because of their ready availability in local stores and their representation of the entire price spectrum. According to the manufacturers' labels, all of these helmets exceed the A.N.S.I. Z-90.1 standard which is similar to Federal Motor Vehicle Safety Standard (FMVSS) 218.

The test unit employed is a large-displacement, high-velocity, servo-hydraulic system manufactured by the Instron Corporation (Figure 1). In closed loop control the unit is capable of developing displacement rates of .85 M/s while in open loop with no load rates of 17 M/s can be achieved. Maximum piston displacement is 40 cm and maximum piston force in tension or compression is 24.5 KN. Stroke, velocity, strain and load control is accomplished through signals generated in the control console.

The force on the helmet was measured by a piezoelectric force link mounted on the upper crosshead of the load frame. A linear voltage differential transformer (LVDT) connected to the piston provided a record of piston and helmet displacement. Signals from the force link and the LVDT were displayed on a dual channel digital recording oscilloscope (500 NS per point response time). This arrangement allowed simultaneous monitoring of helmet force and displacement. A permanent record of these data from which load displacement curves could be constructed was made by recording the traces on an x-y plotter.

To provide a flat loading surface for the helmet, a 15 cm x 15 cm square of aluminum plate was drilled and tapped in the center and attached to the force link on the upper crosshead of the load frame.

Table 1 - Helmet Brands Tested

| Brand | Manufacturer | Model | Outer Shell Material |
|---|---|---|---|
| Norcon (N) | Norcon Mfg. Co. Forest Lake, MN. | X-200 | Polycarbonate |
| Hondaline (H) | American Honda Motor Co. Gardena, CA. | Stag | Fiberglass |
| Bell (B) | Bell Helmets, Inc. Long Beach, CA. | R/T | Fiberglass |
| Electro (E) | Electrofilm, Inc. No. Hollywood, CA. | PRO | Fiberglass |

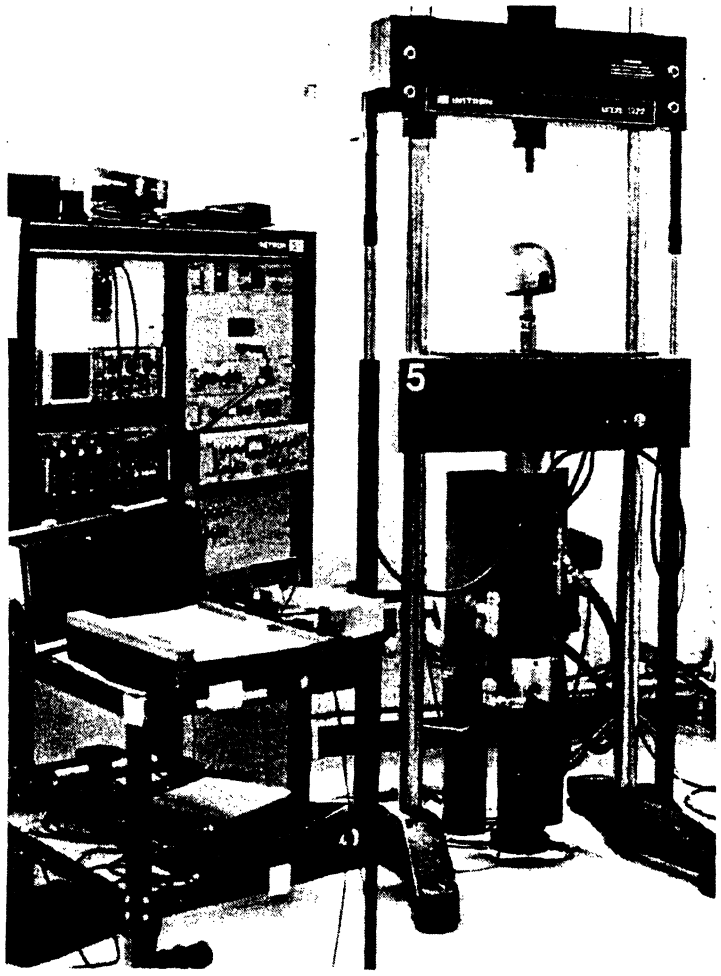

Fig. 1 - Test facility

Helmets were tested while mounted on a rigid magnesium headform conforming to FMVSS 218 (Figure 2). Helmets of medium size provided the best fit on the 55 cm circumference headform.

The orientation of the headform and that of helmet was adjusted in the machine so that a tangent drawn through the top center surface of

the helmet was parallel to the horizontal aluminum plate attached to the load cell (Figure 2). Before each helmet was placed on the test machine the combined thickness of the polystyrene and outer shell was measured with a dial gage. The thickness was measured again immediately after loading (Table 2).

Both quasi-static and high rate dynamic tests were performed (Table 2). To carry out the quasi-static tests, the machine piston was first adjusted until the helmet and force plate surfaces just made contact as indicated by load cell reading. The piston was slowly raised (.065 cm/sec) and the force and displacement signals recorded on the oscilloscope. In order not to exceed the rated load limit of the force link loading was stopped at a force of approximately 24 KN. Eight helmets were tested in this manner.

Seven helmets were tested dynamically. One helmet (#9) was tested at maximum velocity closed loop while the remainder were tested at maximum velocity open loop. In the open loop dynamic tests the piston was allowed to accelerate over 12.5 cm of stroke to reach a speed of 5m/s which is comparable to the impact speed of the FMVSS 218 test. Maximum force in the open loop mode of operation was determined by the dynamic interaction of the helmet with the test system but was generally in the range 22 KN to 24 KN.

TEST RESULTS

Typical quasi-static test force-time and displacement-time traces for a polycarbonate shell helmet (helmet #2) are shown in Figure 3. Corresponding data for a fiberglass helmet (#3) are shown in Figure 4. As noted in the preceding section, the initial point of the quasi-static displacement-time traces represent the position of the piston where first contact of helmet and force plate surfaces causes the load signal to begin. In common with all low speed force-time traces, Figures 3 and 4 show a force relaxation while displacement was held at its maximum value. The impact velocities of the seven dynamic tests are listed in Table 2. These values were calculated from the regions of constant slope on the displacement-time traces.

Helmet #9 was tested at maximum velocity under closed loop control. The resulting loading rate was 20% of that obtained in the open loop test. The force-time and displacement-time traces for this helmet (Figure 5) resembles the traces of the quasi-static tests.

Figure 6 shows typical force-time, displacement-time traces for a polycarbonate helmet (#17) loaded at maximum rate under open loop control. The peaks marked A and B are the initial loading of the helmet while the remaining oscillations are the results of dynamic mechanical interaction of the helmet with the test system. Figure 7 is an oscilloscope display

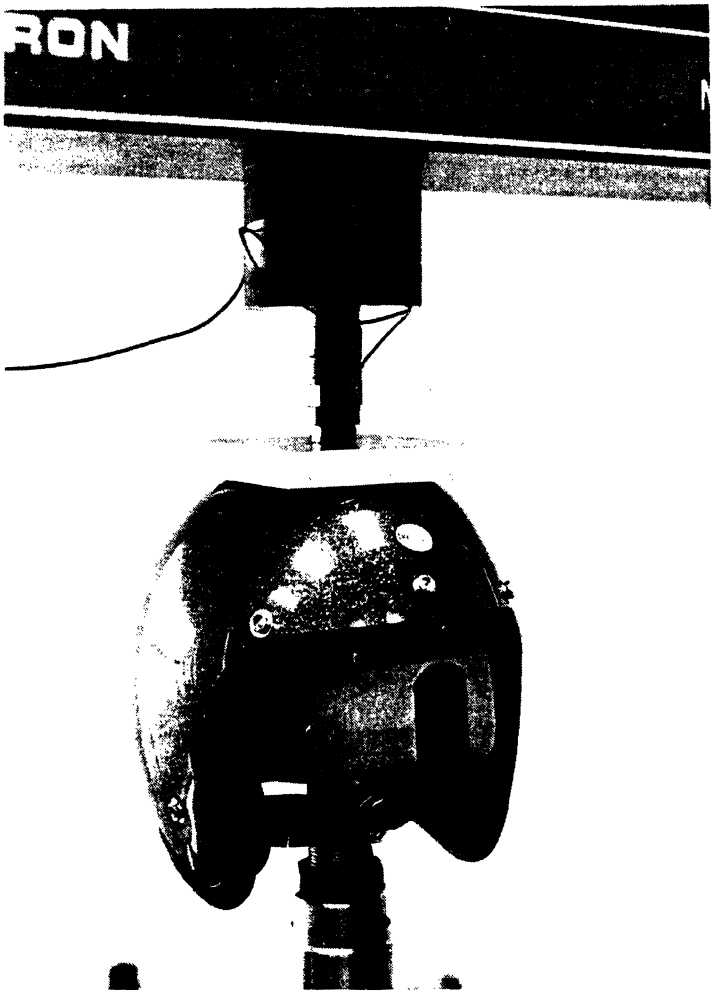


Fig. 2 - Helmet on headform under load

expansion of peaks A and B of Figure 6. The portion of the force-time trace up to the maximum of peak B was used to plot the load-displacement curves for each of the tests. Peak A is postulated to be caused by the initial strike and rebound of the helmet acting as a rigid body supported by the flexible comfort liner acting as a spring. The headform then overtakes the rebounding helmet leading to the true loading peak (peak B). The subsequent high rate force time traces were recorded at a rate sufficient to capture only the initial helmet loading (peaks A and B).

Figures 8, 9 and 10 show data collected from high rate dynamic testing of fiberglass helmets. The data of these figures represent the same segment of the loading event as the expanded trace in Figure 7. The irregularities in the force-time traces in these figures are a result of failure of the fiberglass outer shell. The helmets represented in Figures 8 and 10 exhibit multiple failures while Figure 9 shows only one large failure. Irregularities in the force-time traces as noted above were not observed in the quasi-static tests on fiberglass

Table 2

| Helmet # | Brand | Test | Initial Thickness (cm) | Maximum Force (KN) | Δt (cm)† |
|---|---|---|---|---|---|
| 1 | N | Static | | | |
| 2 | N | Static | 3.6 | 20.5 | 1.4 |
| 3 | E | Static | 3.6 | 23.7 | 1.4 |
| 4 | B | Static | 3.0 | 22.7 | .7 |
| 5 | E | Static | 3.6 | 22.6 | 1.4 |
| 6 | B | Static | 2.8 | 22.4 | .9 |
| 7 | H | Static | 3.6 | 21.7 | .8 |
| 8 | H | Static | 3.0 | 22.4 | .8 |
| 9 | N | Dynamic (0.8 M/S) | 3.8 | 14.9 | .8 |
| 12 | H | Dynamic (5 M/S) | 3.3 | 24.0* | 1.3 |
| 13 | N | Dynamic (5.5 M/S) | 3.6 | 24.0* | 1.4 |
| 14 | B | Dynamic (3.5 M/S) | 3.0 | 24.0* | .9 |
| 15 | N | Dynamic (4 M/S) | 3.8 | 24.0* | 1.7 |
| 16 | E | Dynamic (5 M/S) | 3.3 | 24.0* | .8 |
| 17 | N | Dynamic (3 M/S) | 3.6 | 24.0* | 1.2 |

*Stall load of test machine.
†Decrease in liner thickness.

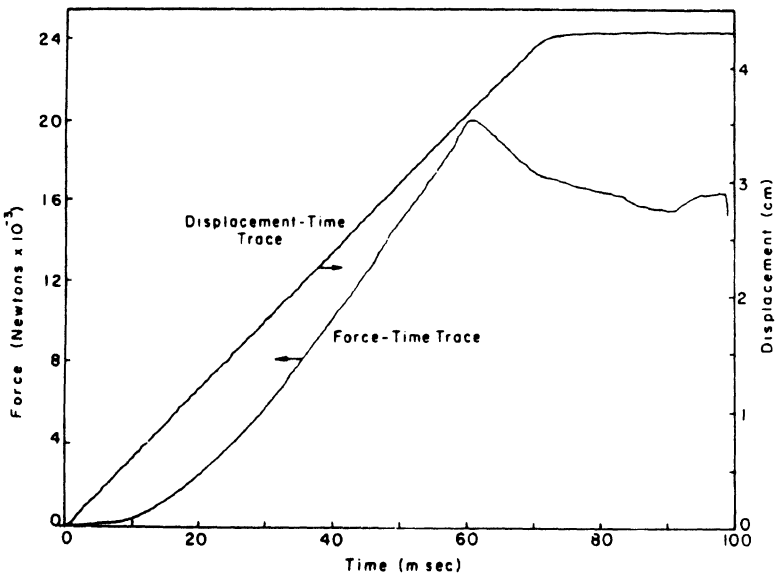


Fig. 3 - Displacement and force traces for helmet #2

helmets nor in any of the tests on the polycarbonate helmets. This suggests a rate dependent mode of failure for the fiberglass helmets.

Each pair of force and displacement traces were cross-plotted to yield the force-deformation curves shown in Figures 11 through 14. These data were plotted for loading up to the maximum force indicated on the force-time trace. The very low initial slope in the initial 5 to 10 mm displacement of the quasi-static load-displacement curves was produced by compression of the soft foam backed cloth lining the inner surface of the helmet. Its contribution to the overall effectiveness of the helmet for head impact force attenuation is negligible.

In order to obtain a single valued force-displacement curve from the dynamic test data, the curve leading to the second loading peak (peak B) was extrapolated back to zero force and peak A neglected. This was considered permissible since peak A is caused by the helmet as a rigid mass supported by the soft liner impacting with the load cell. Since that portion of the response curve corresponds to the very low stiffness initial region of the quasi-static load-displacement curve, no important information is lost. Small irregularities in the

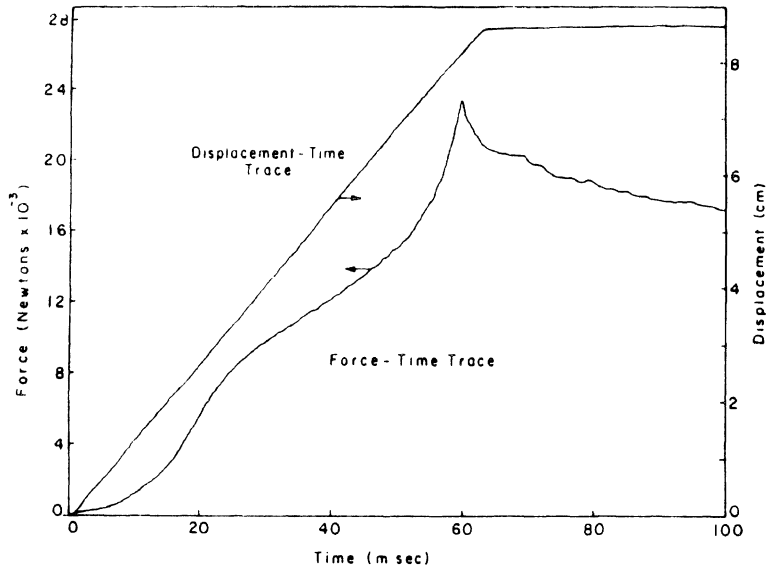


Fig. 4 - Displacement and force traces for helmet #3

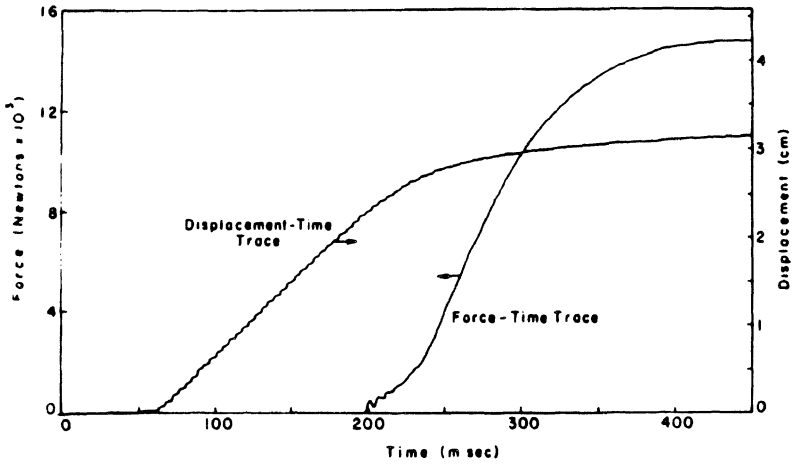


Fig. 5 - Displacement and force traces for helmet #9

force-time data, as previously discussed, were neglected in the construction of the load-displacement curves.

Finally, some helmets of each brand were retested quasi-statically and dynamically in order to ascertain the effect of initial loadings on the subsequent load-displacement curve. The resulting load-displacement curves are presented in Figures 15 and 16.

The quasi-static force-displacement curves of Figures 11 through 14 show an initial region (~8 mm) of very small slope (.03 MN/M) corresponding to the deformation of the soft "comfort liner" of the helmets. This region of low modulus is absent from the high-rate curves because of the previously discussed procedure for constructing those traces. Since the small stiffness region will have little effect on the force attenuation characteristics of the helmet, it is not included in the bilinear representation of helmet stiffness described below.

In order to provide a basis for comparison of the various helmet force-displacement curves as well as a convenient representation of these data for use in mathematical modeling of the helmet structure, the test results were fitted to a bilinear representation.

Table 3 lists the values for the initial stiffness ($K_{21}$), the approximate point of inflection ($\delta$) and the second slope ($K_{22}$). The stiffnesses were calculated by passing a straight line through the region of interest and determining the slope of this line. $K_{21}$ was computed over the first region of appreciable stiffness. $\delta$ was calculated to be the displacement over which $K_{21}$ extended. $K_{22}$ was taken as the slope of the curve following the inflection point up to a force of 20KN. Table 4 lists the stiffnesses by helmet brand and type of test and also indicates the average static and dynamic stiffnesses for the polycarbonate and fiberglass shell helmets.

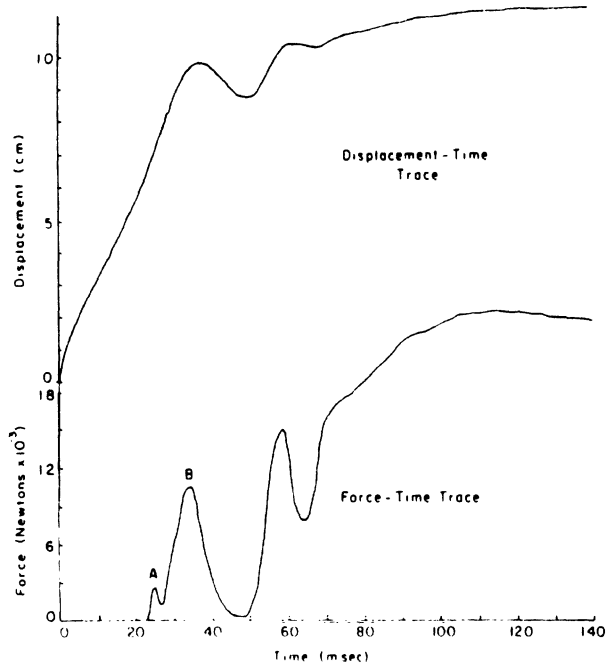


Fig. 6 - Displacement and force traces for helmet #17

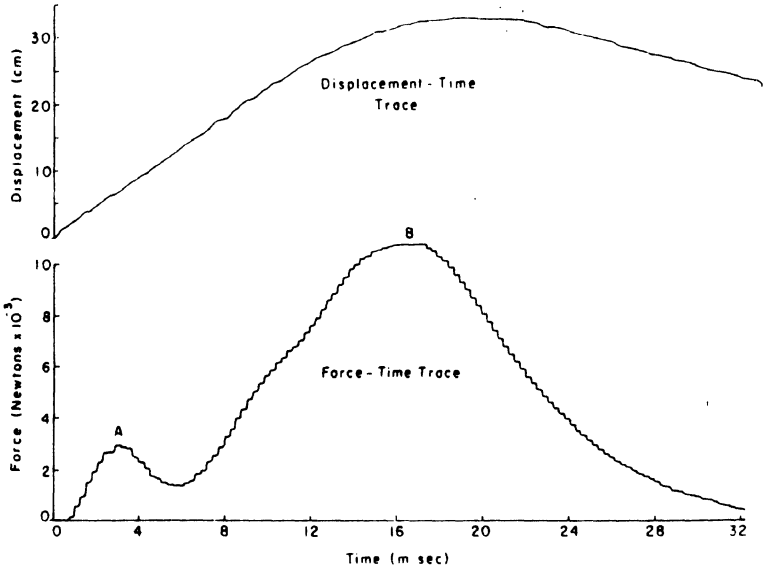


Fig. 7 - Expanded displacement and force traces for helmet #17

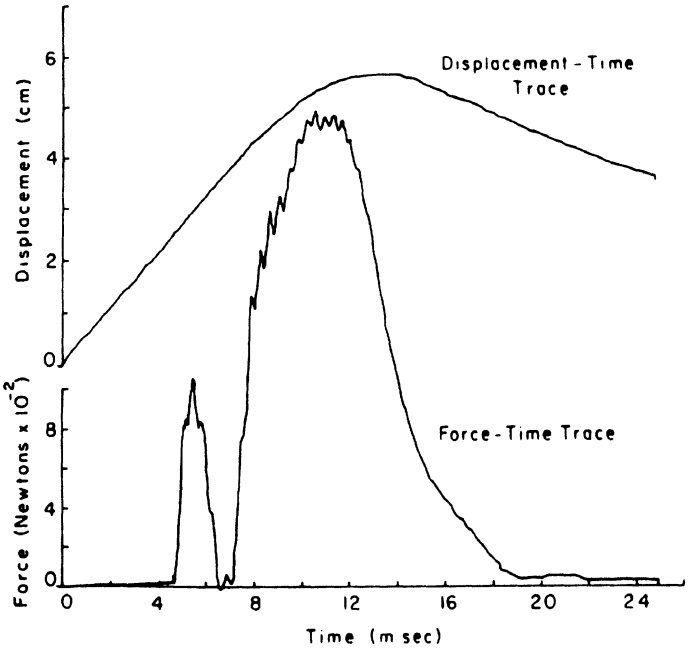


Fig. 8 - Displacement and force traces for helmet #12

## MODEL STUDY OF IMPACT RESPONSE

Mathematical models of varying complexity of the human head encased in a protective helmet have been developed by a number of investigators including Lombard [6], Liu et al [7], and Berger [8]. Although these headhelmet models may be used in the study of attenuation of many types of head impacts, their utility for investigation of head impact after free fall is limited by their failure to account for the force exerted on the head by the impacted surface as the remainder of the body is brought to rest.

A recent study by Mohan et al [9] of head acceleration upon impact after free fall using a nine degree-of-freedom computer model (Bowman et al [5]) indicates the torso contributes in

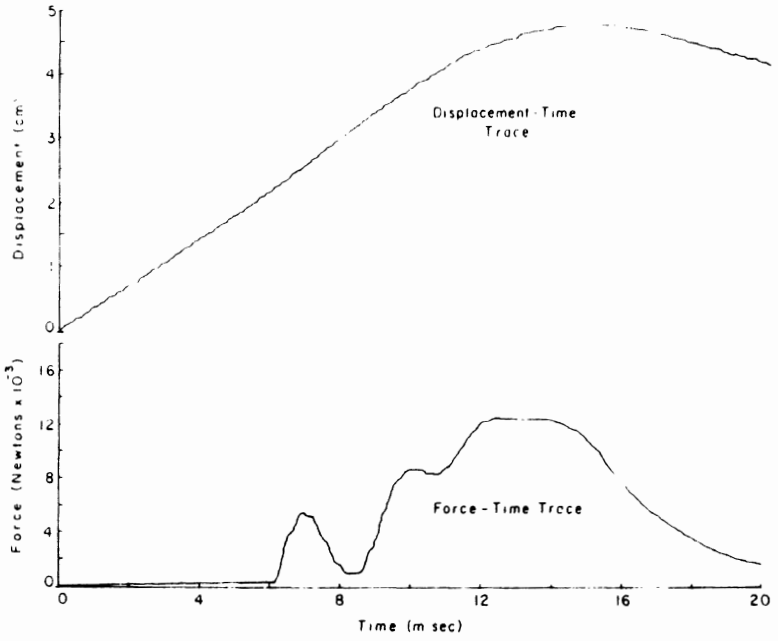


Fig. 9 - Displacement and force traces for helmet #14

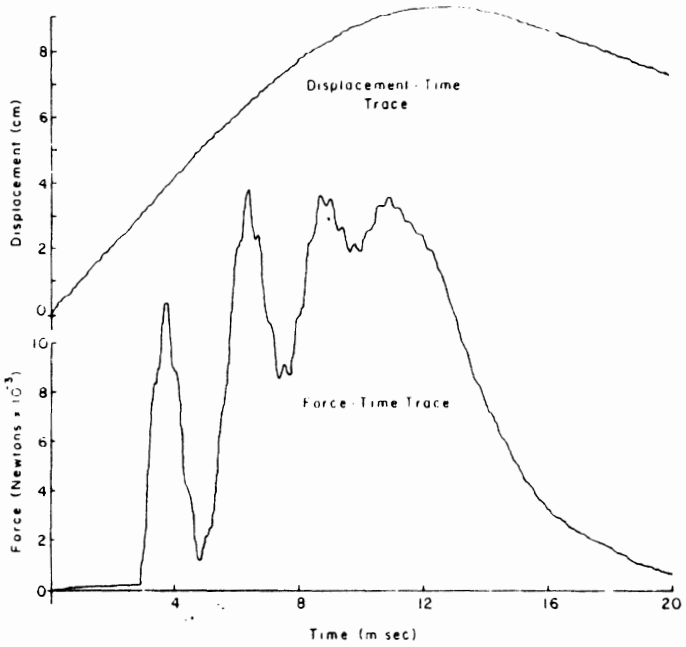


Fig. 10 - Displacement and force traces for helmet #16

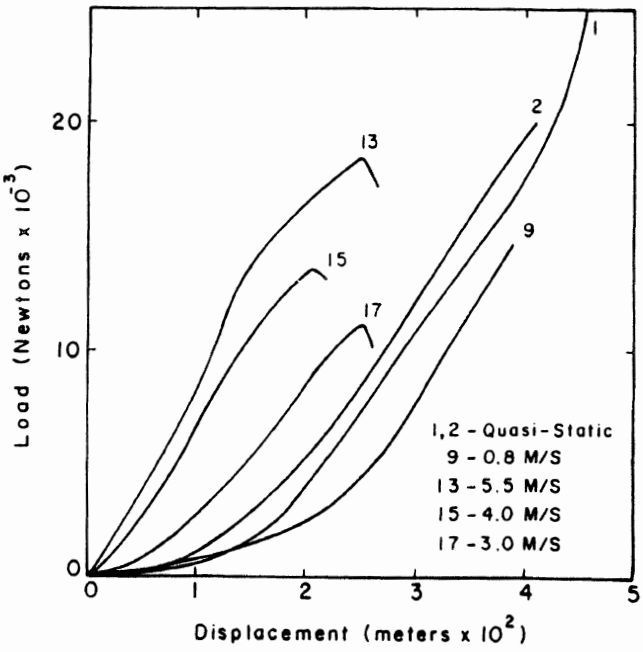


Fig. 11 - Load-deformation curves for polycarbonate shell helmets

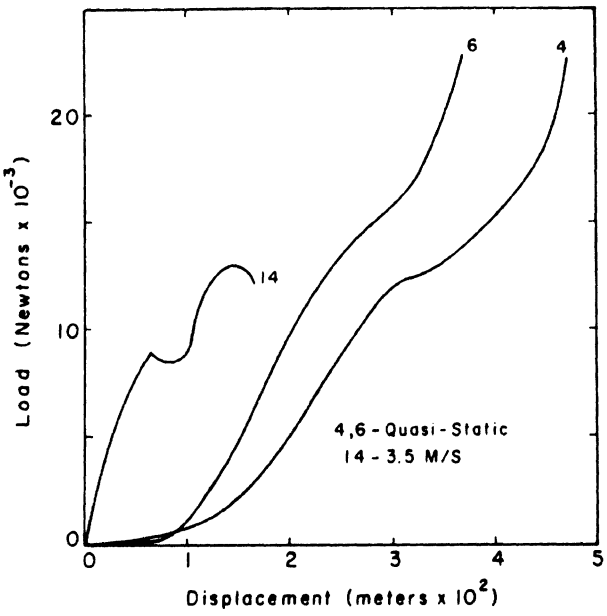


Fig. 12 - Load-deformation curves for brand B fiberglass shell helmets

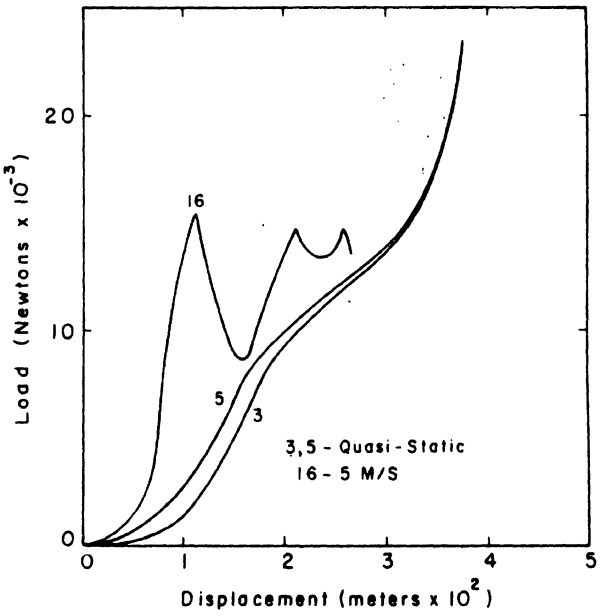


Fig. 13 - Load-deformation curves for brand E fiberglass shell helmets

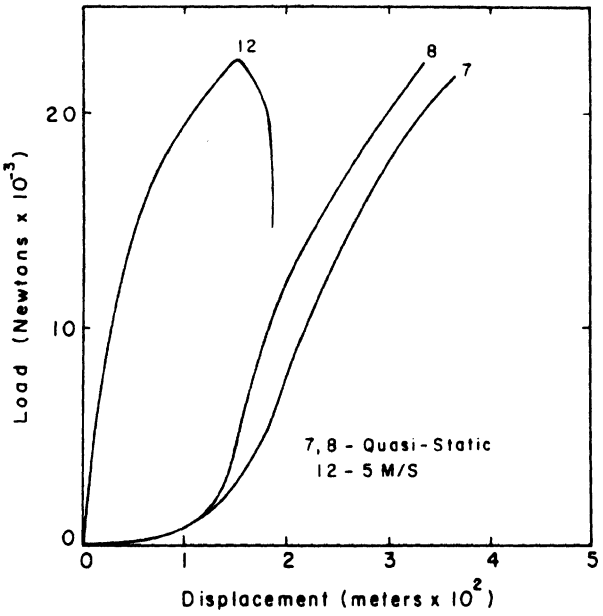


Fig. 14 - Load-deformation curves for brand H fiberglass shell helmets

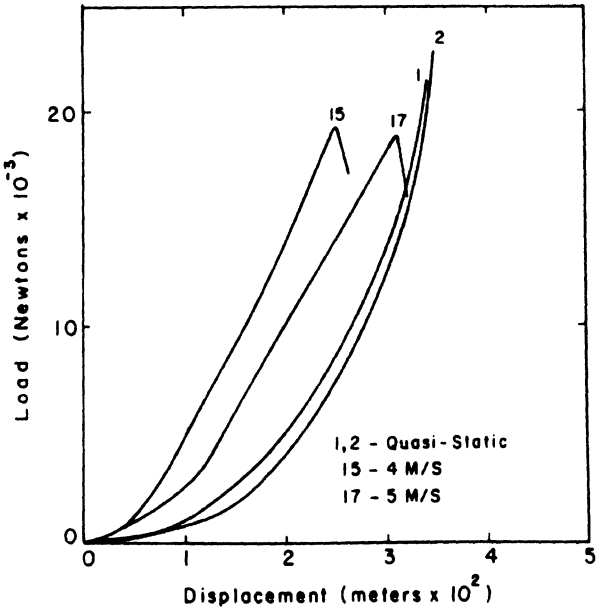


Fig. 15 - Second loading load-deformation curves for polycarbonate shell helmets

a most pronounced way to the total head acceleration pattern.

Mohan's results show an essentially two peak head deceleration response curve consisting of a first peak centered at 3 ms followed, after some irregularity, by a second peak at 7 to 10 ms. The magnitude of each of these peaks are from 400 G's to 800 G's. It is postulated that the first peak represents the mass of the head impacting on the rigid surface. Then, as the head starts to recover from its initial deceleration, the full mass of the torso impinges upon the head causing further deceleration of the center of the head.

Given the pronounced two peak patterns to the head deceleration curve obtained from a general degree-of-freedom computer model, it is reasonable to expect that a relatively simple, two degree-of-freedom model should be able to produce the essential results obtained from the more complex one. By the addition of a mathematical representation of a motorcycle helmet to this simple model, the effect of various parameters of helmet design may then be studied easily and relatively inexpensively.

Two mathematical models were developed on the basis of the physical models shown in Figure 17. The first of these, consisting of two

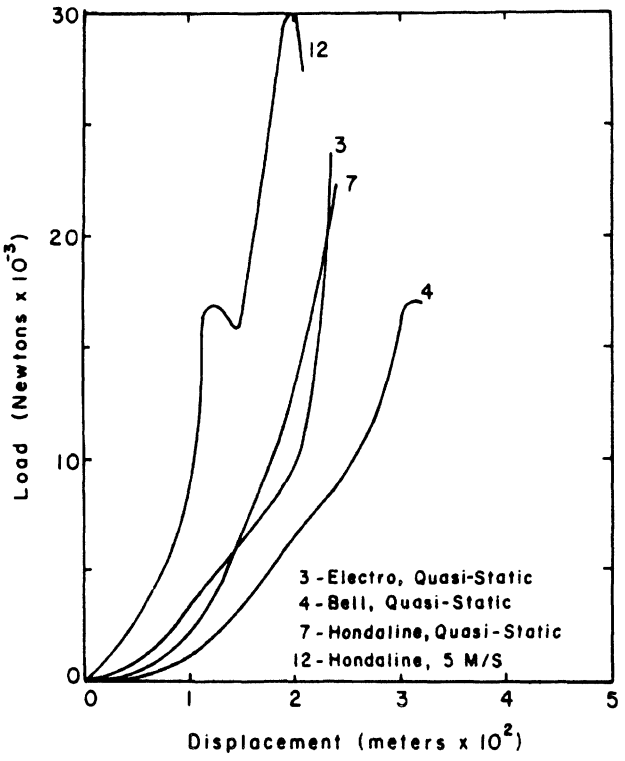


Fig. 16 - Second loading load-deformation curves for fiberglass shell helmets

masses and two stiffness elements (springs), was used to obtain the effective torso mass ($M_T$) and stiffness ($K_N$) required to reproduce the two peak characteristics determined by Mohan et al [9]. In this model, as in all others, the head mass ($M_H$) and stiffness ($K_H$) were taken from measured values reported in Mohan et al [9]. The value of head mass used was 4.5 kg and the head stiffness was modeled as a bilinear spring with initial spring constant of 2.8 MN/M and second constant of 1.4 MN/M with inflection at 1.1 mm.

The second model was used to represent the torso-head-helmet system. In this model, the helmet is represented as a bilinear spring ($K_2$) with arbitrary inflection point ($\delta_2$) in series with the bilinear head spring ($K_H$).

Typical head acceleration and deformation curves calculated using the two degree-of-freedom model of the head and torso are shown in Figures 18 and 19. For these calculations the initial velocity of the torso-head system is 10 M/S. It was found that several combinations of $M_T$ and $K_N$ yield a double-peaked deceleration curve similar in magnitude and duration to those calculated by the more complex model and that the relative magnitudes of the two maxima could easily be varied. In subsequent calculations using the model containing representation of the helmet stiffness, $M_T$ and $K_N$ are taken to be 5 kg and 2.5 MN/M respectively.

Figures 20 through 22 show the calculated response of the head and helmet when the helmet

Table 3 - Stiffness, From Figures 13 Through 16

| Helmet # | Brand | $K_{21}$ $\frac{MN}{M}$ | $\delta$ (mm) | $K_{22}$ (MN/M) |
|---|---|---|---|---|
| 1 | N | 0.67 | | 0.67* |
| 2 | N | 0.69 | | 0.69 |
| 3 | E | 1.04 | 6.0 | 0.79 |
| 4 | B | 0.87 | 12.5 | 0.54 |
| 5 | E | 0.93 | 9.5 | 0.69 |
| 6 | B | 1.09 | 10.0 | 0.77 |
| 7 | H | 1.18 | 13.0 | 0.69 |
| 8 | H | 1.70 | 8.0 | 0.72 |
| 9 | N | 0.25 | 15.0 | 0.76 |
| 12 | H | 2.95 | 4.0 | 0.77 |
| 13 | N | 0.96 | 14.0 | 0.56 |
| 14 | B | 1.55 | 6.0 | 0.90 |
| 15 | N | 0.75 | | 0.75 |
| 16 | E | 2.75 | 5.0 | 0.0 |
| 17 | N | 0.68 | | 0.68 |

*To 20 KN

Table 4 - First and Second Stiffness by Manufacturer and Type (From Table 3)

| Brand (Test) | Helmet | $K_{21}$ (MN/m) | $\delta$ (mm) | $K_{22}$ (MN/m) |
|---|---|---|---|---|
| N (static) | 1 | 0.67 | | 0.67 |
| N (static) | 2 | 0.69 | | 0.69 |
| N (slow dynamic) | 9 | 0.25 | 15 | 0.76 |
| N (dynamic) | 13 | 0.96 | 14 | 0.56 |
| N (dynamic) | 15 | 0.75 | | 0.75 |
| N (dynamic) | 17 | 0.68 | | 0.68 |
| B (static) | 4 | .87 | 12.5 | 0.54 |
| B (static) | 6 | 1.09 | 10.0 | 0.77 |
| B (dynamic) | 14 | 1.55 | 6.0 | 0.90 |
| E (static) | 3 | 1.04 | 6.0 | 0.79 |
| E (static) | 5 | .93 | 9.5 | 0.69 |
| E (dynamic) | 16 | 2.75 | 5.0 | 0.0 |
| H (static) | 7 | 1.18 | 13 | 0.69 |
| H (static) | 8 | 1.70 | 8 | 0.72 |
| H (dynamic) | 12 | 2.95 | 4 | 0.77 |
| average polycarbonate (static) | | 0.68 | | 0.68 |
| average polycarbonate (dynamic) | | 0.65 | | 0.69 |
| average F.G. (static) | | 1.14 | | 0.70 |
| average F.G. (dynamic) | | 2.42 | | |

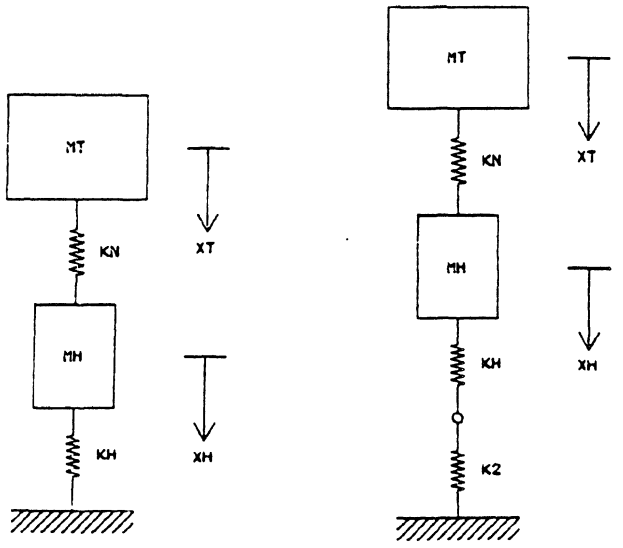


Fig. 17 - Two mass models with bilinear head stiffness (left) and with bilinear head and helmet stiffness (right)

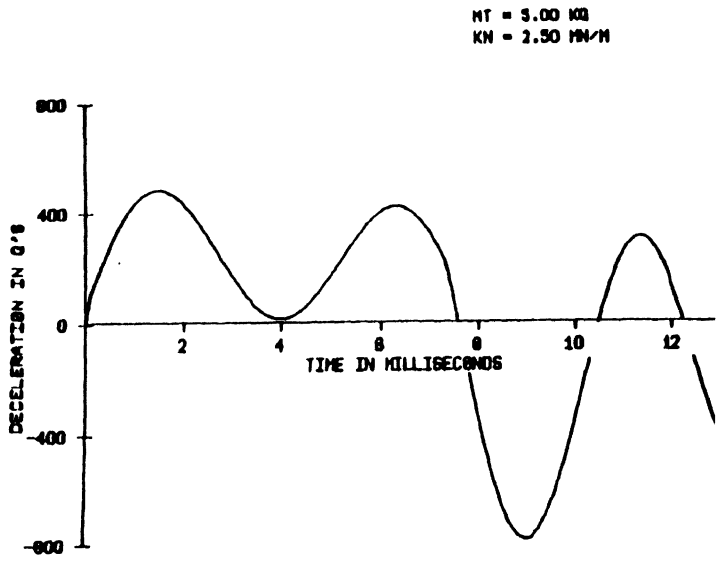


Fig. 18 - Head deceleration after impact without helmet ($V_o$ = 10M/S)

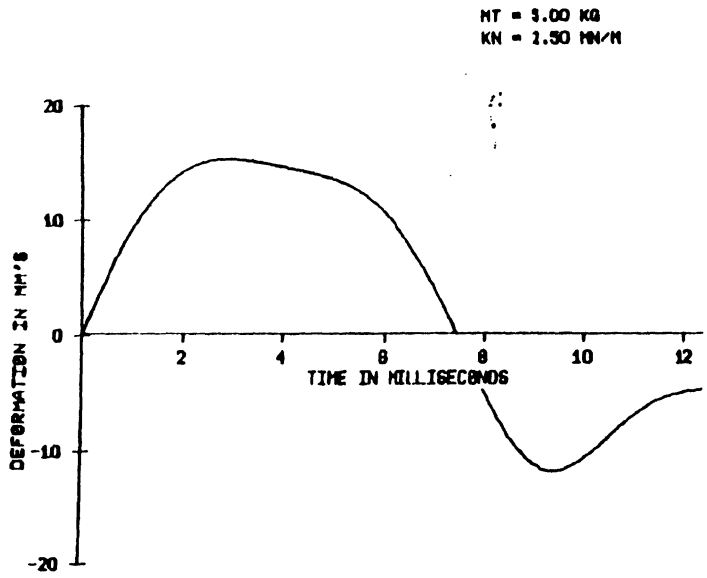


Fig. 19 - Head deformation after impact without helmet ($V_o$ = 10M/S)

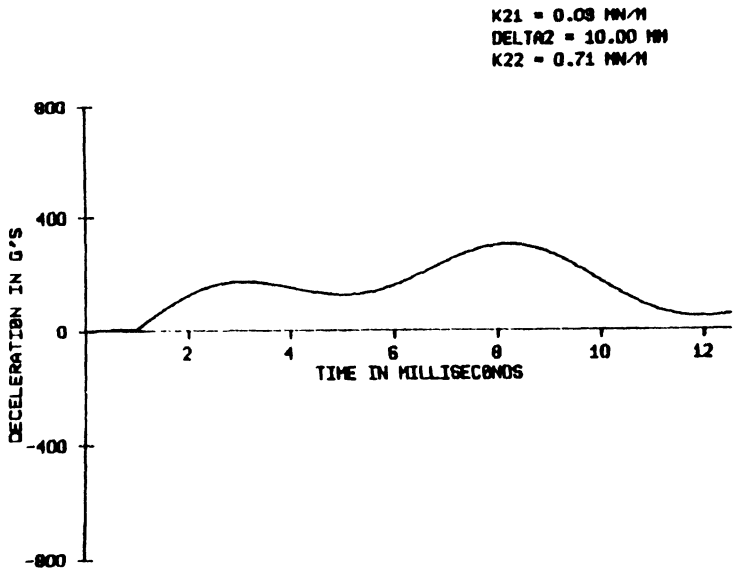


Fig. 20 - Head deceleration after impact with helmet ($V_o$ = 10M/S)

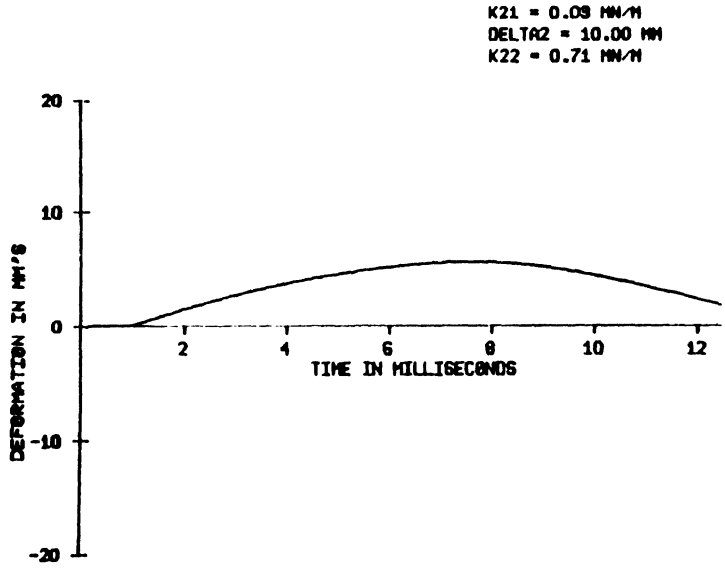


Fig. 21 - Head deformation after impact with helmet ($V_o$ = 10M/S)

is assumed to have an initial region (~8mm) of very low stiffness (~0.03 MN/M) corresponding to deformation of the soft "comfort liner" material followed by a second region of much greater slope (0.71 MN/M). It is seen that the low stiffness portion of the helmet liner has negligible effect on head acceleration or deformation.

Figures 23 through 25 show the response when the helmet force deformation curve is represented as a bilinear spring with initial modulus of 1.0 MN/M and final modulus of 0.71 MN/M based on the measured data. It is seen that the response curve of Figures 23 are very similar to those of Figures 20 when the initial low acceleration region of the latter is neglected.

The effect of the helmet can be determined by comparing Figures 20 through 25 with Figure 18.

With the helmet in place (on the model), maximum head acceleration is decreased from 500 G's to 300 G's. In the 10 ms following impact, total duration above the 200 G level is decreased from 4.5 ms to 3 ms and the time above 150 G's from 7 ms to 5 ms. The helmet has the effect of lowering but lengthening the initial acceleration response trace.

Maximum head deformation is decreased by the presence of the helmet from 15 mm to 10 mm. The helmet deformation is about 3cm which is slightly more than the permanent helmet shown in Table 1.

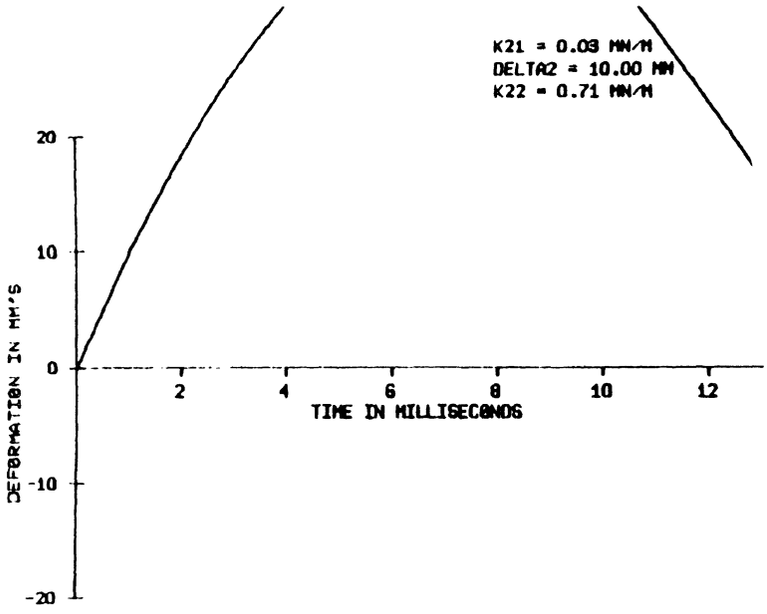


Fig. 22 - Helmet deformation after impact with helmet ($V_o$ = 10M/S)

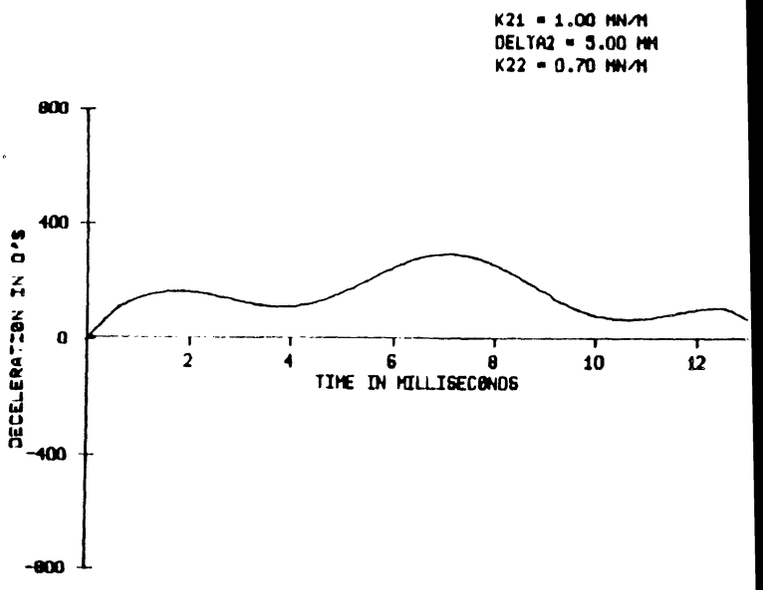


Fig. 23 - Head deceleration after impact with helmet ($V_o$ = 10M/S)

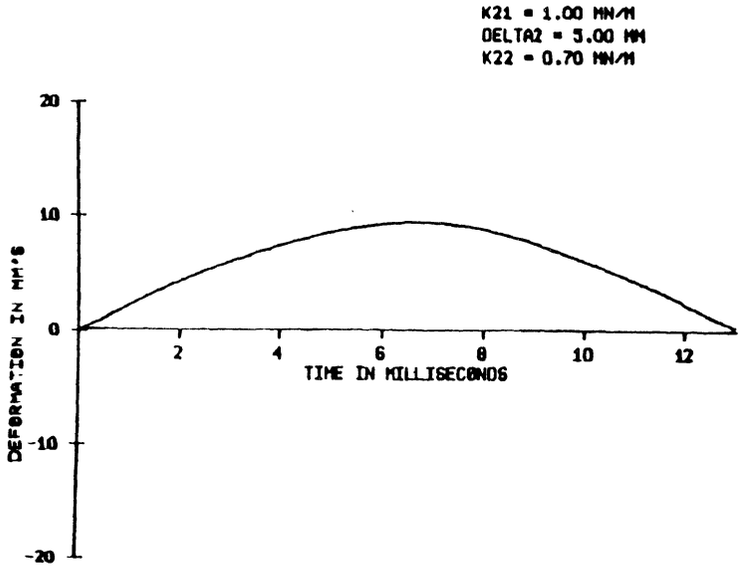


Fig. 24 - Head deformation after impact with helmet ($V_o$ = 10M/S)

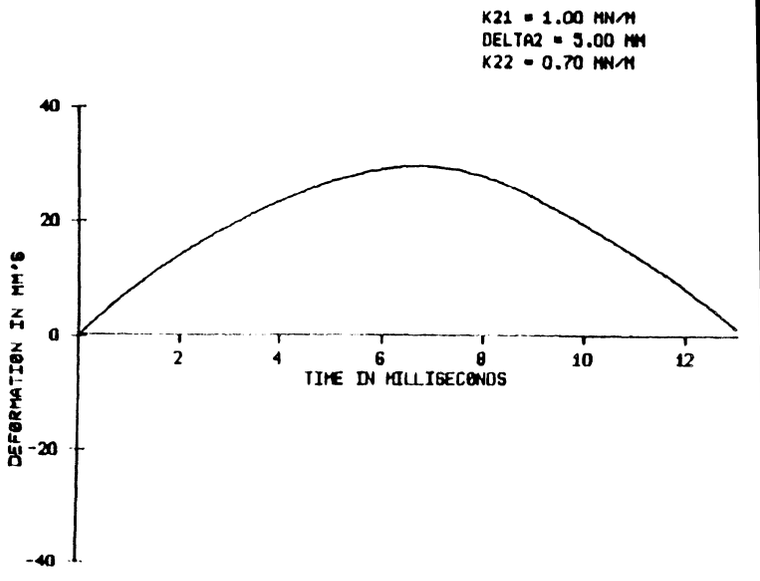


Fig. 25 - Helmet deformation after impact with helmet ($V_o$ = 10M/S)

## CONCLUSIONS

It is seen from Table 4 that the first and second stiffnesses of the polycarbonate helmets are very similar as are the static and dynamic stiffnesses. From these tables, as well as from examination of the load-deformation and load-time traces, helmets with polycarbonate shells tend to behave uniformly and consistently with both rate and magnitude of loading.

As a group, the fiberglass shell helmets are significantly more rigid than those with polycarbonate shells. Their stiffness is also much more load and rate dependent. The dynamic response to load of fiberglass helmet #16 was particularly different from its quasi-static character. Although the average slopes, from beginning to end of the curves, are comparable, the dynamic curve has a much greater slope initially followed by a very irregular region of small average slope. The high initial stiffnesses of both helmets #16 and #12 might adversely affect the deceleration response of the encased head at impact.

Table 3 shows $K_{21} > K_{22}$ for eleven helmets, $K_{21} = K_{22}$ for three helmets and $K_{21} < K_{22}$ for one helmet. Therefore, within the load range employed, most of the helmets appear to behave as the skull does; with a larger initial stiffness followed by a smaller secondary

stiffness. Certainly it is to be expected that at higher loads the helmets will become increasingly more rigid. The complete definition of the force-deformation curves will be the subject of future work.

From Figures 15 and 16 it is determined that the slope of the load-displacement curves for all helmets became steeper when the helmets were loaded for a second time. This increase in stiffness (20%-400%), which is due to permanent compression of the polystyrene liner caused by the initial loading, emphasizes the importance of helmet replacement after a severe impact.

Comparison of Figure 18 with Figures 20 and 23 reveals the effect of the helmet on head acceleration at impact is to decrease the magnitude of the peak deceleration while increasing the duration of the deceleration period. The corresponding decreased in force acting on the head is indicated by the magnitude of head deformations of Figures 19, 21 and 24.

It is clear from these results that a major function of the helmet is to act as an energy storage element interposed between the head and the impacted surface. Contrary to many statements in the literature, the role of the helmet as an energy dissipation device is probably not of major significance.

REFERENCES

1. J.A. Newman, "Safety Helmets for Motorcycle Riders: An Evaluation of Safety Standards." Proc. of the Annual Conference Traffic Injury Research Foundation of Canada, Ottawa, 1976.
2. FMVSS 218 "Motorcycle Helmets." Federal Register V 38 No. 160, August 1973.
3. "Specifications for Protective Headgear for Vehicular Users." ANSI Z 90.1-1971, American National Standards Institute, Inc., New York, 1971.
4. "Standard for Protective Headgear." Snell Memorial Foundation, Sacramento, CA., 1975.
5. B.M. Bowman, R.O. Bennett and D.H. Robbins, "MVMA Two-Dimensional Crash Victim Simulation, Version 3." Final Report to Motor Vehicle Manufacturers Association, VM-HSRI-BI-74-1, 3 Vols., Highway Safety Research Institute, The University of Michigan, Ann Arbor, 1974.
6. C.F. Lombard, "Investigation of Fabrication and Impact Protection of the Human Head and Neck." Northrop Space Laboratories, Hawthorne, Calif., 1966.
7. Y.K.N. Liu, P.E. Kravesh and C.H. Beck, "Optimal Protection in Direct Closed Head Impact." Proc. 28 Conference Alliance for Engineering in Medicine and Biology, Chevy Chase, MD. p. 167, 1975.
8. R.E. Berger, "Considerations in Developing Test Methods for Protective Headgear." NBSIR 76-1107, U.S. Dept. of Commerce, National Bureau of Standards, Washington, D. C., 1976.
9. D. Mohan, B. Bowman, R.G. Snyder and D.R. Foust, "A Biomechanical Analysis of Head Impact Injuries to Children." Insurance Institute for Highway Safety, Washington, D.C., 1978.

HS-806-960
TSC-NHTSA-85-4

# Crash Padding Research
## Volume I: Material Mechanical Properties

Oscar Orringer
Kevin T. Knadle
John F. Mandell

Transportation Systems Center
Cambridge MA. 02142

July 1986
Final Report



U.S. Department of Transportation
**National Highway Traffic Safety Administration**

Office of Research and Development
Office of Crashworthiness Research
Washington DC 20590

## SUMMARY

Selection of materials for energy-absorbent performance is an important consideration for automobile interior padding, which must provide the greatest occupant protection for the least padding thickness possible. Rational selection requires an understanding of which material properties, as measured in standard laboratory tests, correlate well with impact performance in crash situations. Such understanding can be gained by characterizing a material in the laboratory, constructing a performance model from the laboratory test results, applying the model to predict the response of the material to impact conditions, and then verifying the prediction by test. This report summarizes the results of the first link in the chain of understanding.

A program of laboratory experiments was undertaken to characterize the dynamic mechanical properties of Uniroyal Ensolite AAC foam rubber. This material is a typical padding product, and has been used by the National Highway Traffic Safety Administration in other experimental investigations of injury mitigation concepts for automobile occupants.

The present test program was designed to evaluate a hypothesis that standard laboratory test methods could be used to measure the properties which correlate with impact performance. The test program thus emphasized the material properties associated with uniform compression of small samples. Additional tests were performed, however, to investigate the material under more complex loading conditions in order to evaluate the potential usefulness of the uniform-compression model.

The results of this research program are as follows:

- Sufficient standard data have been gathered to provide the basics required for modelling the dynamic behavior of Ensolite AAC foam rubber in uniform comparison.
- It appears that useful predictions of impact response should be possible, based on a uniform-compression material model.
- Sufficient nonstandard test data have been gathered to provide for understanding of prediction errors, i.e. to identify any significant material properties not included in the uniform-compression model.
- An experimental protocol applicable to the characterization of other crash padding materials has been established.

# 1. INTRODUCTION

Automobile interior crash padding is used to protect vehicle occupants against serious injury during collisions, when parts of the occupant's body may strike parts of the vehicle's interior structure. The padding should ideally provide high energy absorption at low force levels, but practically its performance is limited for general ride comfort. Material selection for energy-absorbent performance thus becomes an important consideration.

Since an occupant-to-vehicle impact typically consumes only 20 to 50 milliseconds (ms), the dynamic properties of the material at short times (or equivalently, high strain rates) determine its energy-absorption characteristics. Candidate padding materials are typically viscoelastic, i.e. they relax under load, their moduli are time-dependent, and their dynamic properties are strongly dependent on strain rate.

The behavior of real materials is also considerably more complex than the descriptions afforded by simplified hypothesis such as linear viscoelastic models. Hence, standard rheological test methods must be applied to experimentally characterize the behavior of a real material, but the tests must be made at or near strain rates corresponding to typical occupant-to-vehicle impacts. Only after data has been obtained from such tests is it possible to construct a good empirical model of the material behavior.

The present work started with a laboratory experiment program on Uniroyal Ensolite AAC, a recoverable closed-cell foam rubber material which has been used in previous NHTSA investigations of injury-reduction concepts for automobile passenger compartments. This report summarizes the experimental methods which were used to characterize Ensolite foam and the results of the tests.

Experimental data is to be used to define several parameters of an empirical equation representing the time-dependent relaxation, loading, and unloading behavior of the foam. Therefore, to effectively model the impact-rate collision of unrestrained occupants with padded structures, test data should cover peak strains of at least 0.8, strain rate as high as 2000 per second, and relaxation times down to 0.1 ms. The experimental objective is to characterize the compressive response of the material. Specifically, the type of data sought include stress relaxation curves for at least three different strains, and full stress-strain loading and unloading curves at various strain rates from which can be derived stress versus strain rate, percent residual strain versus strain rate, and asymptotic (fully relaxed) stress-strain curves.

Initial attempts to directly measure the material performance could not reach impact rates without introducing spurious test fixture vibrations into the data. Therefore, tests were ultimately conducted at somewhat lower strain rates but also at lower temperatures, and the time-temperature superposition principle was used to extrapolate the data. Unless otherwise noted, the test speciments were cut 1.38 inches in diameter from 0.14 inch thick Ensolite sheets. The tests were performed on both electromechanical (EM) and servohydraulic (SH) machines.

Sections 2 and 3 describe the procedures used and the results obtained in two types of standard materials tests: the stress-relaxation test and the stress-strain test. These results provide the data necessary for fitting a one-dimensional (uniform compression) constitutive equation model to the material. The extent to which such a model is useful for predicting behavior when the material is subjected to nonuniform impact conditions depends upon other properties. Section 4 describes some additional experiments which were performed to address this question.

## 3.1 EXPERIMENTAL PROCEDURE

Stress-strain curves were obtained using the same test apparatus as that described for stress relaxation tests. Specifically, the SH machine performed those tests with strain rates between 1.2 and 73 per second, while the EM machine performed the lower strain-rate tests (down to .0012 per second) including low temperature tests for time-temperature superposition. The strain-rate magnitude was kept constant during each test by using a triangle-shaped displacement-controlled loading and unloading function to a maximum strain between 0.75 and 0.85. No delay was allowed between the loading and unloading stages apart from unavoidable rounding of the triangular shape at the maximum point at the higher displacement rates.

Some stress-strain-time points were also obtained with an impact rig, which allowed specimens to be loaded by a hand-swung hammer to an adjustable maximum strain. A peizoelectric load cell directly below the specimen produced a force-time curve on the digital oscilloscope, from which the force and time at the point of peak strain could be read. The rate of applied strain was assumed to be constant and was calculated as strain/time at the peak point.

## 3.2 TEST RESULTS

The first series of tests measured low strain-rate EM loading-unloading curves at several cold temperatures for the purpose of constructing master curves, as done with the stress-relaxation data. Stacks of four thin foam specimens were subjected to the triangular displacement at strain rates on the order of 0.12 per second. Figure 3-1 illustrates the stress-strain curves obtained from these tests. The strong temperature-dependence of the hysteresis property evident in this plot implies an equivalent dependence on strain rate at fixed temperature.

In order to apply the time-temperature superposition principle to the construction of stress-strain master curves, it is more convenient to plot stress versus strain rate for several different values of strain, i.e. following the format suggested by Equation 4. The loading portions of the three highest temperature stress-strain curves in Figure 3-1 were thus cross-plotted to produce the data points shown in Figure 3-2. These data points correspond to strains of 0.33, 0.50, and 0.75, i.e. the same values used to plot stress-relaxation data, and they have already been time-temperature shifted. Also shown in Figure 3-2 are the master curves which were constructed from the data.

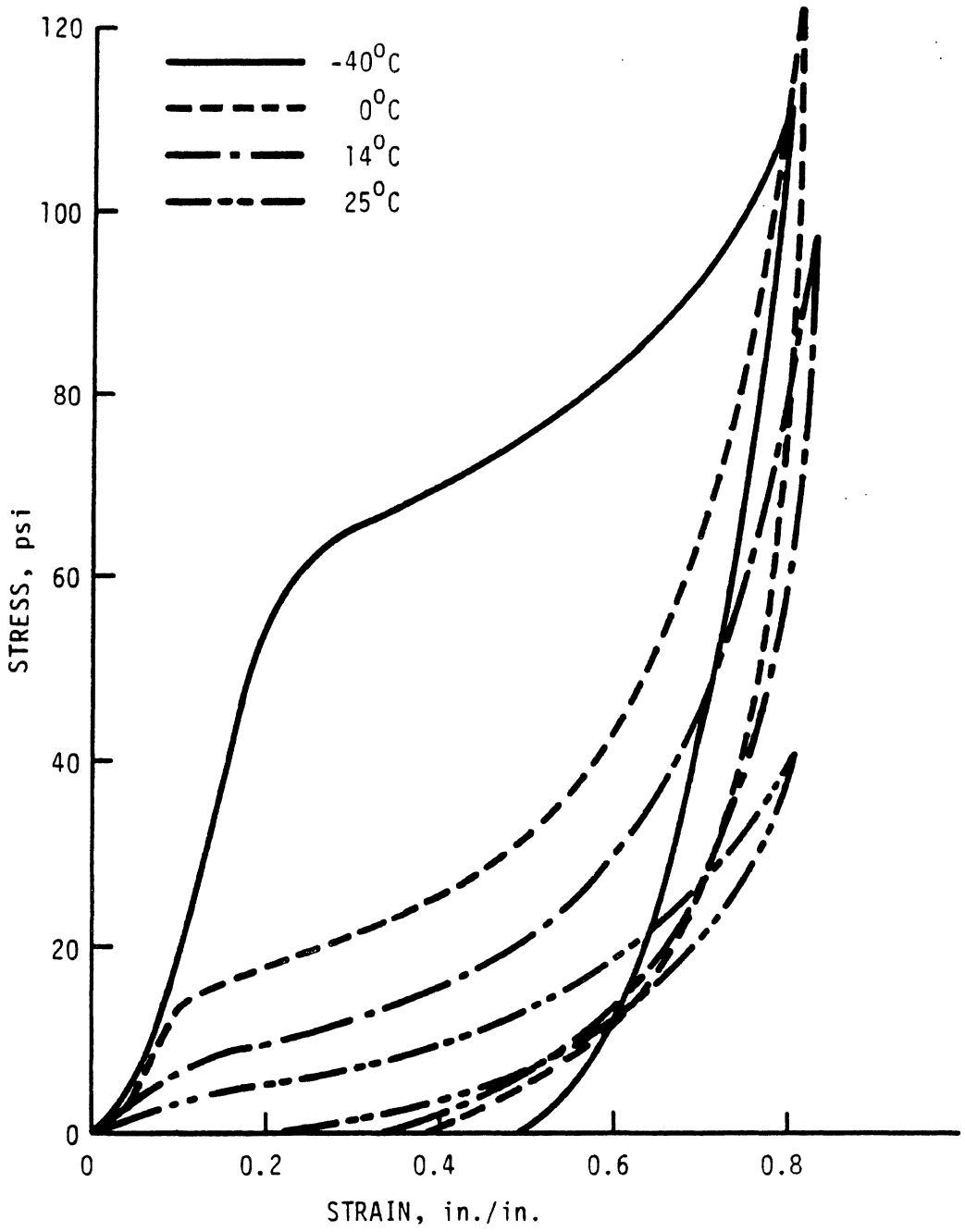


FIGURE 3-1. TYPICAL STRESS-STRAIN CURVES AT LOW STRAIN RATE

TABLE 4-1. EFFECT OF SPECIMEN DIAMETER ON STRESS-STRAIN CURVE*

| STRAIN RATE ($SEC^{-1}$) | Dia (in.) | STRESS (psi) | | |
|---|---|---|---|---|
| | | Strain =0.3 | Strain =0.5 | Strain =0.75 |
| 73 | 2.0 | 18.5 | 30.2 | 85.1 |
| | 1.38 | 19.8 | 29.8 | 70.1 |
| | 1.0 | 19.7 | 29.9 | 68.5 |
| 30 | 3.9 | 21.1 | 30.2 | 63.9 |
| | 2.0 | 17.1 | 25.8 | 72.7 |
| | 1.38 | 16.1 | 26.2 | 71.9 |
| | 1.0 | 17.8 | 25.8 | 59.8 |
| 3.0 | 3.9 | 10.4 | 19.9 | 62.0 |
| | 2.0 | 10.4 | 18.2 | 50.9 |
| | 1.38 | 11.1 | 19.6 | 56.9 |
| | 1.0 | 11.4 | 19.6 | 54.9 |
| | 0.5 | 11.4 | 17.7 | 42.4 |
| 1.2 | 2.0 | 10.2 | 19.0 | 63.0 |
| | 1.38 | 10.6 | 19.5 | 70.3 |
| | 1.0 | 10.7 | 18.9 | 56.0 |

*Compression tests at 25°C; 0.14-inch thick specimen.

## 4.2 PERFORMANCE AT HIGH STRAIN AND LOW TEMPERATURE

The shifting anomaly observed for the long-time tails of stress-relaxation tests at 0.75 strain was studied further. After equilibrating at -20°C for 30 minutes, small rectangular thin-foam specimens were subjected to clamping at 0.75 or larger strain across half their length, with the other half left undeformed. Specimens were held clamped at -20°C for 20 to 30 minutes, released, and immediately sliced lengthwise with a razor to expose a cross-section containing both deformed and undeformed material. The surfaces of the deformed half appeared rough and pitted. Observation of the cross section under a low-power microscope revealed cell-wall crushing (Figure 4-1). The deformed cells were flattened and rough-edged compared to the round bubble shape of normal cells (Figure 4-2). The deformed half of the specimen remained collapsed for a long time. Even after two days strains of 0.15 to 0.25 were still evident. Within a week, however, the two halves were indistinguishable.

# 5. CONCLUSIONS

The research reported herein comprises an investigation of the dynamic properties of Uniroyal Ensolite AAC foam rubber. The research objective was to obtain the minimum data required as a basis for a constitutive equation model which could be used to predict the material response during typical occupant-to-vehicle impacts which may occur in automobile collisions.

Sufficient data has been gathered to provide the basis for one-dimensional (uniform uniaxial) dynamic compression models of Ensolite AAC. The required data has been tabulated in Appendices A and B. The following conclusions can be drawn from the results of the research:

- Ensolite AAC foam is a nonlinear viscoelastic material with dynamic characteristics which depend strongly on strain rate. The strain-rate effect also appears as a time effect, i.e. dynamic response at short times after a loading event is equivalent to dynamic response at high strain rates.

- Both stress-relaxation tests and stress-strain tests at constant strain rate are required to characterize the material in one dimension. The need for both types of test arises from the material nonlinearity.

- It is essential to assess stress-relaxation performance at short times (of the order of 0.1 to 10 milliseconds) and stress-strain curve performance at high strain rates (of the order of 2000 per second) to provide the basis for simulating typical impacts. These performance characteristics cannot be arbitrarily extrapolated from long-time or low-rate data. Some extrapolation is necessary, however, to cover impact rates which cannot be directly tested.

- The time-temperature superposition principle can be used to make the necessary extrapolations, if the principle is carefully applied. Careful application requires auxiliary tests to assess potential deviations.

- The dynamic properties of Ensolite foam are generally time-temperature shiftable, i.e. low-rate or long-time response at low temperature is equivalent to high-rate or short-time response at service temperature. Thus, it is possible to construct master curves for dynamic performance at service temperature. There are, however, two exceptions to this conclusion.

- The first exception involves stress-relaxation performance at times exceeding 100 seconds. At these very long times, Ensolite foam appears to have a decay characteristic different from the short-time characteristic. It is necessary, therefore, to focus on the short-time data in order to estimate asymptotic response parameters that will be useful in models of impact phenomena.

- The second exception involves performance at high strain (strain equal to or greater than 0.75). At these strain levels, Ensolite foam experiences a cell-wall crushing mode at low temperature, but the crushing mode is apparently absent under conditions of high strain rate at service temperature. Auxiliary tests were required to identify the crushing mode.

- Auxiliary tests were also required to show that the material does not possess any other non-shiftable characteristics, such as air-flow effects on stiffness. The presence or absence of such effects can be confirmed by varying the specimen diameter.

- Other auxiliary tests for Poisson's ratio and for different indenter geometries are useful for assessing some of the three-dimensional characteristics of foam-rubber materials.

- Ensolite foam appears to behave like a transversely isotropic material, but does not fully satisfy the static conditions of transverse isotropy. Further study of the viscoelastic effects on this property would be needed to provide the basis for a three-dimensional constitutive equation model.

- Under nonuniform one-dimensional loading, the apparent stiffness of Ensolite foam is increased by shear effects at strains up to 0.8 and by hydrostatic effects at strains exceeding 0.8. However, neither effect appears to influence the characteristic relaxation time.

- It appears that a one-dimensional constitutive equation for Ensolite foam, based on the uniform compression test results, will be useful for predicting occupant-to-vehicle impact responses.

- The sequence of basic and auxiliary tests reported herein form an experimental protocol which can be usefully applied to the characterization of other crash padding materials.

TABLE B-5. SERVOHYDRAULIC STRESS-STRAIN DATA (25°C)

| STRAIN | STRESS (psi) | | | | | | | | | |
|---|---|---|---|---|---|---|---|---|---|---|
| | 1.2/sec | | 3.0/sec | | 7.5/sec | | 30/sec | | 73/sec | |
| | LD | UL | LD | UL | LD | UL | LD | UL | LD | UL |
| 0.050 | 3 | | 4 | | 5 | | 5 | | 5 | |
| 0.010 | 6 | | 7 | | 9 | | 10 | | 13 | |
| 0.150 | 7 | | 8 | | 10 | | 11 | | 15 | |
| 0.200 | 9 | | 9 | | 11 | | 13 | | 15 | |
| 0.250 | 9 | | 10 | | 12 | | 14 | | 17 | |
| 0.275 | | 0 | | | | | | | | |
| 0.300 | 11 | 1 | 11 | 0 | 13 | 0 | 16 | | 18 | |
| 0.350 | 12 | 2 | 13 | 2 | 15 | 1 | 18 | 0 | 20 | |
| 0.400 | 14 | 3 | 14 | 3 | 16 | 3 | 20 | 2 | 22 | 0 |
| 0.450 | 16 | 6 | 17 | 4 | 19 | 4 | 22 | 3 | 25 | 2 |
| 0.500 | 19 | 8 | 20 | 7 | 22 | 6 | 26 | 5 | 28 | 4 |
| 0.550 | 24 | 11 | 24 | 9 | 25 | 9 | 30 | 8 | 33 | 6 |
| 0.600 | 29 | 15 | 28 | 13 | 30 | 12 | 36 | 11 | 39 | 9 |
| 0.625 | 33 | | 31 | | 32 | | 40 | | 42 | |
| 0.650 | 37 | 22 | 34 | 18 | 36 | 17 | 44 | 16 | 46 | 13 |
| 0.675 | 43 | | 39 | | 39 | | 49 | | 51 | |
| 0.700 | 50 | 31 | 43 | 25 | 44 | 22 | 55 | 23 | 57 | 19 |
| 0.750 | 70 | 46 | 57 | 34 | 55 | 30 | 72 | 34 | 72 | 26 |
| 0.775 | 88 | 58 | 66 | 40 | 62 | 35 | 83 | 42 | 82 | 32 |
| 0.800 | 108 | 77 | 78 | 49 | 72 | 41 | 97 | 53 | 96 | 39 |
| 0.825 | 140 | 111 | 95 | 61 | 83 | 49 | 112 | 70 | 112 | 48 |
| 0.830 | 143 | 143 | | | | | | | | |
| 0.833 | | | | | | | 115 | 115 | | |
| 0.850 | | | 119 | 77 | 100 | 60 | | | 133 | 62 |
| 0.875 | | | 151 | 108 | 122 | 76 | | | 154 | 83 |
| 0.887 | | | | | | | | | 158 | 158 |
| 0.885 | | | 159 | 159 | | | | | | |
| 0.900 | | | | | 148 | 109 | | | | |
| 0.906 | | | | | 149 | 149 | | | | |

)T-HS-806-961
)T-TSC-NHTSA-85-5

# Crash Padding Research

## Volume II: Constitutive Equation Models

Oscar Orringer
Kevin T. Knadle
John F. Mandell

Transportation Systems Center
Cambridge MA 02142

August 1986
Final Report



U.S. Department of Transportation
**National Highway Traffic Safety Administration**

Office of Research and Development
Office of Crashworthiness Research
Washington DC 20590

## SUMMARY

Selection of materials for energy-absorbent performance is an important consideration for automobile interior padding, which must provide the greatest occupant protection for the least padding thickness possible. Rational selection requires an understanding of which material properties, as measured in standard laboratory tests, correlate well with impact performance in crash situations. Such understanding can be gained by characterizing a material in the laboratory, constructing a performance model from the laboratory test results, applying the model to predict the response of the material to impact conditions, and then verifying the prediction by test.

Volume I of this series of reports summarized the first link in the chain of understanding: results of laboratory tests to determine the dynamic properties of Uniroyal Ensolite AAC foam rubber, a typical crash padding product which the National Highway Traffic Safety Administration has used in other investigations of injury mitigation concepts for automobile occupants.

This report is Volume II of the series, and summarizes the results of the second link. Earlier methods for constructing material performance models were reviewed and were found to be inadequate for representing the impact response characteristics of materials like Ensolite foam rubber. Criteria were then formulated for the more complex type of model required, and two such models were developed. The model developments included organization of curve-fitting procedures which take advantage of all of the relevant materials test data.

When the two models were applied to the Ensolite test data, one was found to accurately represent the material over only a limited range of performance, but the second was found to represent the material well over the entire range of interest. Both models may still be useful for predicting the impact response of Ensolite AAC, and both models can be applied to other materials.

# 1. INTRODUCTION

The first volume of this report summarized the results of laboratory tests to determine the compressive mechanical properties of Uniroyal Ensolite AAC foam rubber, a recoverable closed-cell crash padding material. The principal results were for stress as a function of time after imposition of a fixed strain (stress relaxation) and for stress as a function of strain applied at a fixed rate. The second group of results included measurements of the "residual" strain present at the instant the material had unloaded to zero stress. Both groups of results were extrapolated to typical impact times (0.001 second) and strain rates (2,000 per second) by means of the time-temperature superposition principle, which was used to construct master curves for material behavior at 25°C from results of tests at lower temperatures.

The body of data in Volume I characterizes the material response to two specific types of loading. This characterization of material properties must be generalized, however, to provide a useful basis for predicting the dynamic responses of objects which collide with padded structure. What is sought is an equation of state, or constitutive equation, which describes the possible relationships between current states and incremental changes of stress and strain in the material.

In the typical impact situation, the colliding mass imposes a known initial strain rate on the crash padding material. The mass is decelerated and the strain rate decreases, however, as the padding builds up stress to resist the motion of the mass. The deceleration eventually brings the mass to momentary rest with respect to the padding, the relative motion is then reversed, and finally there occurs an instant when the padding stress has returned to zero. At this last instant, contact between the mass and padding is lost, and the impact event is complete.

To be useful for predicting impact response, a constitutive equation must be able to follow all of the foregoing phases of the motion. This imposes the following three requirements on the properties of the equation itself. First, as a minimum, it must relate the instantaneous rate of change of stress to the instantaneous values of stress, strain, and strain rate. Second, it must embody an unambiguous relationship between loading and unloading, including transitions between these states at zero strain rate. Third, it must account for the presence of residual strain rate in the padding at the end of contact.

In addition to satisfying the foregoing requirements, the constitutive equation must also be consistent with the laboratory test data and should have as simple a form as possible. This volume summarizes the development of such constitutive equation models for the one-dimensional (uniform compression) behavior of Ensolite foam rubber. Section 2 reviews several earlier models which were investigated, but which were found to have various significant limitations. As a consequence of these initial studies, some general mathematical criteria were formulated to govern the construction of multi-parameter empirical models, and two such models were derived. Section 3 discusses these developments, including the analysis procedures used to fit the models to laboratory test data. Section 4 describes the numerical results obtained by applying the curve-fitting procedures to the Volume I test data for Ensolite foam and illustrates the degree of consistency obtained.

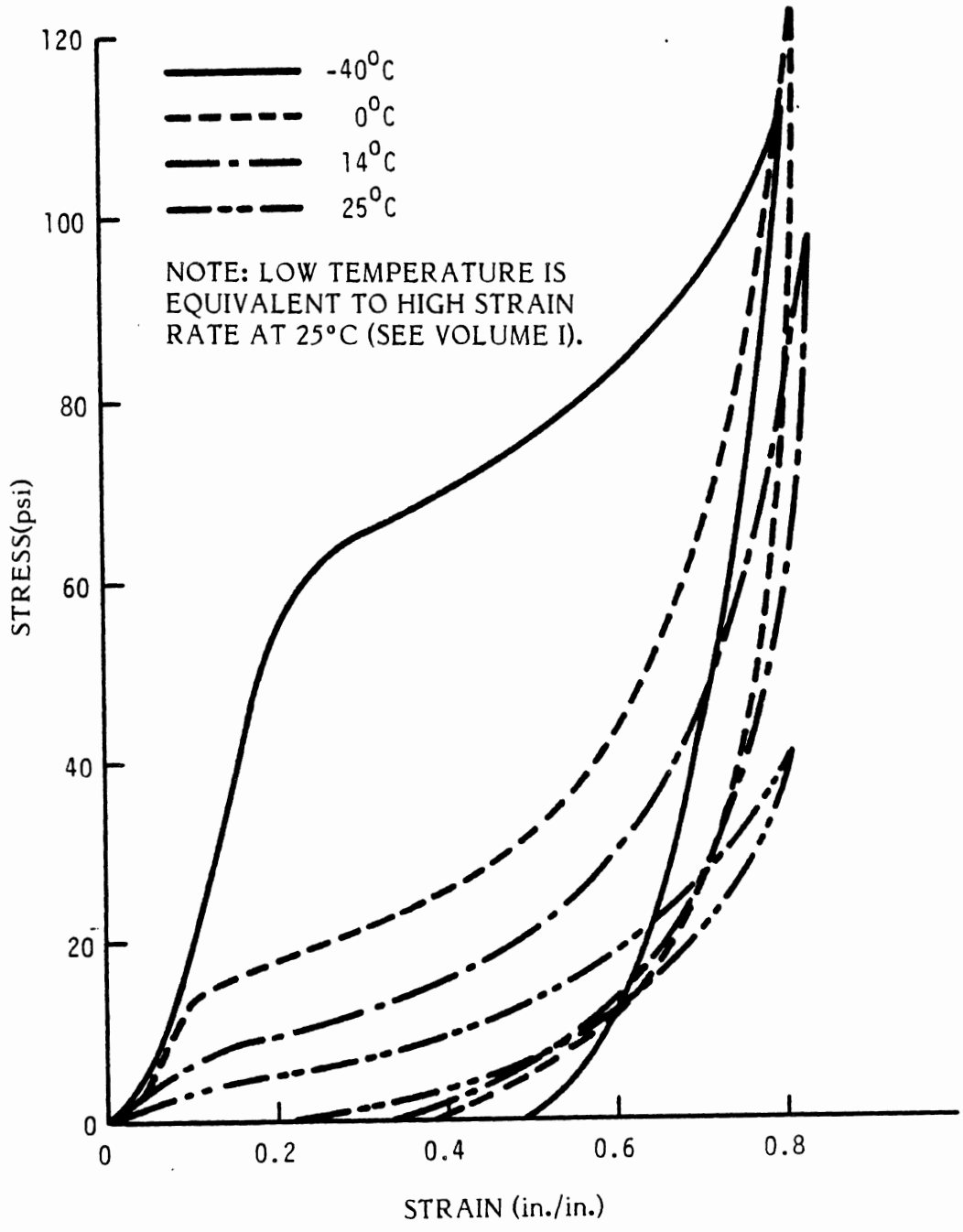


FIGURE 2-8. ENSOLITE AAC FOAM RUBBER STRESS-STRAIN CURVES AT LOW STRAIN RATE

DT-HS-806-962
DT-TSC-NHTSA-86-1

# Crash Padding Research

## Volume III: Impact Analysis and Model Validation

Oscar Orringer
David Y. Jeong
Pin Tong
Kevin T. Knadle
John F. Mandell

Transportation Systems Center
Cambridge MA 02142

July 1986
Final Report



U.S. Department of Transportation
**National Highway Traffic Safety Administration**

Office of Research and Development
Office of Crashworthiness Research
Washington DC 20590

## SUMMARY

Selection of materials for energy-absorbent performance is an important consideration for automobile interior padding, which must provide the greatest occupant protection for the least padding thickness possible. Padding material dynamic properties, including energy absorption, can be determined by laboratory tests on small specimens. Such tests were performed on Uniroyal Ensolite AAC foam rubber padding, and constitutive equations embodying the energy-absorption characteristics of this material were developed. The results of these phases of the work were reported in Volume I and Volume II, respectively.

The present volume summarizes the application of the laboratory material model to the predicton of impact behavior. For this purpose, the material model has been embedded in a simplified dynamic simulation of the occupant-vehicle impact. The simulation is a computer program which predicts force, acceleration, etc., versus time, based on fundamental inputs of the occupant's initial speed, mass, and geometry, the automobile's metal structure stiffness, and the laboratory model of the padding.

The computer simulation has been validated for impact scenarios involving metal structure similar to the automobile dashboard. The validation was accomplished by comparing the simulation predictions with impact test results.

# 1. INTRODUCTION

The first two volumes of this report summarized the characterization of Uniroyal Ensolite AAC foam rubber, a recoverable closed-cell crash padding material. The first volume dealt with the results of laboratory tests to determine the one-dimensional (uniform compression) material dynamic properties. The second volume dealt with the development of constitutive equations to model the observed uniform compression properties. Two empirical models were developed, one with 9 parameters and one with 21 parameters. These models were applied to the Ensolite test data, with the result that the 21-parameter model fit the data well over the entire range of interest, while the 9-parameter model provided a reasonable fit only over a limited range.

This volume summarizes the application of the empirical models to the problem of predicting impact responses. The type of impact problem to be considered involves the collision of an unrestrained vehicle occupant with padded components of an automobile's interior structure during a crash.

The occupant-to-vehicle impact problem can be defined as follows: Let $M_1$ and $M_2$ be the effective masses of the occupant and vehicle, respectively; let $V_1'$ and $V_2'$ be their post-impact velocities. The impact can be assumed to have a short duration, i.e. short enough so that external forces do not substantially change the vehicle velocity during the event.

The impact involves exchange of momentum and kinetic energy between the two bodies and absorption of some kinetic energy by their deformable parts. If the energy absorption is characterized by a coefficient of restitution, C, then the momentum and energy conservation laws can be used to derive the following expressions for the post-impact velocities:

$$V_1' = \left[ (M_1 - M_2\sqrt{C})V_1 + (1 + \sqrt{C})M_2V_2 \right] / (M_1 + M_2) \quad (1)$$

$$V_2' = \left[ (1 + \sqrt{C})M_1V_1 + (M_2 - M_1\sqrt{C})V_2 \right] / (M_1 + M_2) \quad (2)$$

If the occupant's effective mass is small compared to the vehicle mass, and if the impact is described in coordinates at rest with respect to the vehicle, then Eqs. 1 and 2 reduce to $V'_1 \simeq -\sqrt{C}\, V_1$ and $V'_2 \simeq V_2 = 0$. The quantity 1-C is, by definition, the fraction of available kinetic energy that is absorbed by deformations:

$$1\text{-}C = E_{ABSORBED}/E_{AVAILABLE} \tag{3}$$

where

$$E_{AVAILABLE} = \frac{M_1 M_2 (V_1 - V_2)^2}{2 (M_1 + M_2)} \simeq M_1 V_1^2/2 \tag{4}$$

Impact analysis of crash pads has two objectives. The first is to estimate the coefficient of restitution or the equivalent post-impact velocities. These results can be used as inputs to computer programs such as the NHTSA Crash Victim Simulator[1], which predicts the path of an unrestrained occupant engaging in multiple impacts with different parts of the automobile's passenger compartment. The second objective is to estimate the force-time history of the pad's reaction on the occupant. Such force-time histories can be used as inputs to biomechanical models [2] from which injury severity indices are calculated.

Either objective requires analysis of both the loading and unloading phases, although the requirements for model accuracy are more stringent for the second objective than for the first. The loading phase encompasses the instant of contact to the point at which the pad reaches maximum compression. The unloading phase begins at the maximum-compression point and ends when the rebounding occupant loses contact with the pad.

The analysis is performed by coupling the occupant's equations of motion with the constitutive equation of the padding material. The equations of motion supply the strain and strain-rate fields imposed on the pad, while the constitutive equation supplies the reaction stress field and the net force on the occupant. In general, the part of the occupant's body involved in the impact is a flexible curved surface, and the resulting interaction is more complex than the one-dimensional uniform compression tests used to determine padding material properties. Section 2 summarizes the development of impact analysis procedures. The development emphasizes a simplified case in which the occupant is replaced by a rigid sphere, although other cases have been discussed elsewhere [3].

The rigid-sphere approximation is a useful device in two important ways. First, it is reasonable to treat the occupant as a rigid body in some cases, for example, impacts that involve the occupant's head. In such cases, the skull and its thin covering of skin are much less flexible than, say, the padding which covers the dashboard. Second, solid metal projectiles with spherical surfaces can be used in validation experiments to check the analysis method. Section 3 summarizes the procedures and results of a series of such validation experiments. Section 4 compares the test results with predictions made by the impact analysis method.

Report No. NA-69-5
(DS-69-10)



# FINAL REPORT

Project No. 510-002-04X

# DYNAMIC TEST CRITERIA FOR AIRCRAFT SEATS





OCTOBER 1969



DEPARTMENT OF TRANSPORTATION
FEDERAL AVIATION ADMINISTRATION
National Aviation Facilities Experimental Center
Atlantic City, New Jersey 08405

# INTRODUCTION

## Purpose

The purposes of the project reported herein were (1) to establish background for dynamic test criteria for the type certification of aircraft seats and restraint devices, (2) to determine test methods which demonstrate compliance with the dynamic criteria, (3) to express the present static test load requirements for aircraft seats and restraint devices specified in the Federal Aviation Regulations (FAR) in terms of the dynamic criteria, and (4) to relate the static test load requirements to an actual crash environment utilizing the dynamic criteria.

## Background

FAR's 25.561 and 25.785, and Technical Standards Orders (TSO) C-22 and C-39 specify design loads for aircraft seats and restraint devices for which the aircraft occupant is to be restrained and protected even though parts of the aircraft would be damaged. These design loads are expressed in static "inertia forces" based on the combined weight of the seat and occupant, with the occupant weight taken as 170 pounds. The specified inertia forces have remained unchanged since 1957, and their values are indicated in the test specifications as 9 g's forward, 6 g's downward, 2 g's upward, and 1.5 g's sideward.

Although seats and restraint devices are designed to withstand these inertia forces, there is no way to relate the forces with the crash environments that would produce them. The dynamic test criteria establish a relationship between inertia forces and crash environments by specifying tests in terms of crash environment inputs, allowing the inertia forces to develop as short-duration response pulses as they would in an actual crash. Utilization of the dynamic test criteria, then, enables the inertia forces on the seat/occupant combination and the seat's capability of restraining the occupant to be expressed in terms of the crash phenomenon, resulting in a more realistic certification procedure.

The dynamic test criteria presented herein can also satisfy the present need for standardization in the aircraft industry in view of the fact that several airlines have for some time required dynamic testing for acceptance of aircraft seats, with the tests being conducted by the seat manufacturers. The test specifications have differed between airlines, and the test methods have differed between manufacturers.

To meet the objectives of the project, it was first necessary to establish a theoretical basis for the dynamic test criteria. The seat types to be tested were then determined along with the test methods which would yield seat response characteristics in a form compatible with the dynamic test theory. Finally, it was necessary to utilize existing crash environment data to relate the results of the dynamic tests with actual crash severity.

Description of Theory for Dynamic Test Criteria: In a static test of a seat, the specified inertia force for the seat/occupant combination provide the input to the seat and are applied at the center of gravity of the seat/occupant combination. The vertical seat leg reactions are a measure of the response of the seat and are directly proportional to the input, or inertia force, from which they can be calculated.

In a dynamic test, the input is the acceleration-time pulse of the sled on which the seat with occupant (dummy) is mounted. An actual crash environment is simulated where the input is the acceleration-time pulse of the aircraft floor in the vicinity of the seat, and the seat/occupant combination is free to respond as a spring-mass system (Figure 1). The vertical seat leg reactions are a measure of the response as they were in the static test. Likewise, the effective inertia force remains proportional to the reactions, but in the dynamic test becomes part of the response and can be calculated from the measured reactions. The direct proportionality between the reactions and the input holds for the dynamic test, as it did for the static test, provided the input is of long duration (Figure 2a). If the input is of short duration, as it is for typical crash environments, the reactions will lag the input and have peak values lower than those indicated by the long-term proportionality (Figure 2b).

Static tests can be related to dynamic tests by utilizing the response level (vertical seat leg reaction level) as a parameter. For a given seat, lap belt, occupant weight, input direction, and peak seat leg reaction level, there exists one static input (inertia force) and an infinite number of dynamic inputs (acceleration-time pulses) which will induce the given peak seat leg reaction level. Since there are an infinite number of dynamic inputs, they can be expressed as a curve, called a sensitivity curve, provided an empirical relationship can be established between the dynamic inputs and the peak seat leg reaction level and provided the dynamic inputs can be expressed in terms of two variables, such as velocity change and average acceleration.

Figure 3 shows a variety of input acceleration-time pulses and their corresponding response curves for a given seat, lap belt, occupant weight and input direction. These response curves can be obtained empirically during the type certification testing of the seat and are the means by which the dynamic inputs and the peak vertical seat leg reaction level can be related. Each seat test produces one point on the curve. Other points are obtained by testing the seat with input pulses of different magnitudes. The response factor C, for each test, can be calculated as follows:

$$C = \frac{G_e}{\bar{G}} \qquad (1)$$

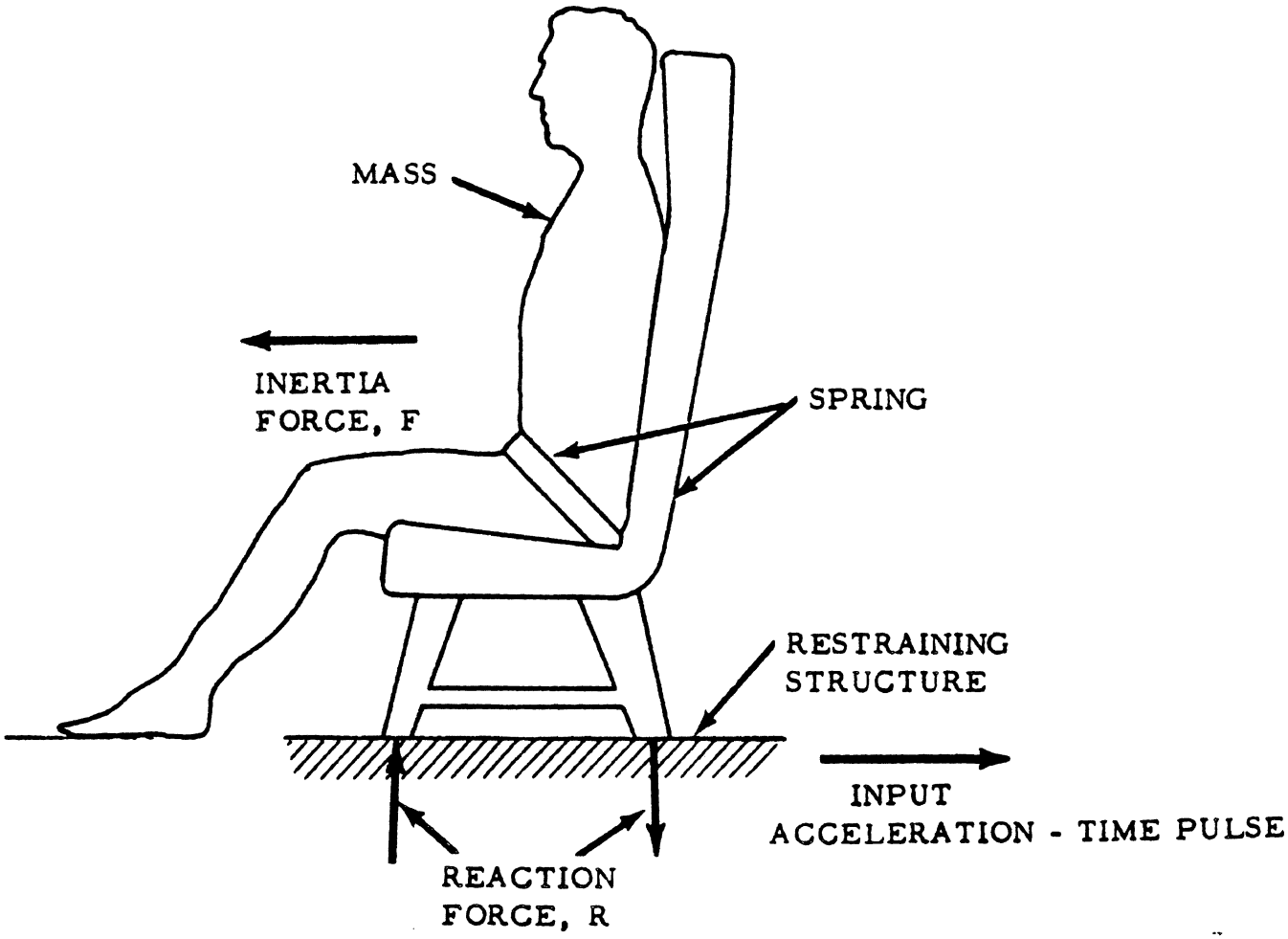


**FIG. 1 SEAT/OCCUPANT SPRING-MASS SYSTEM**

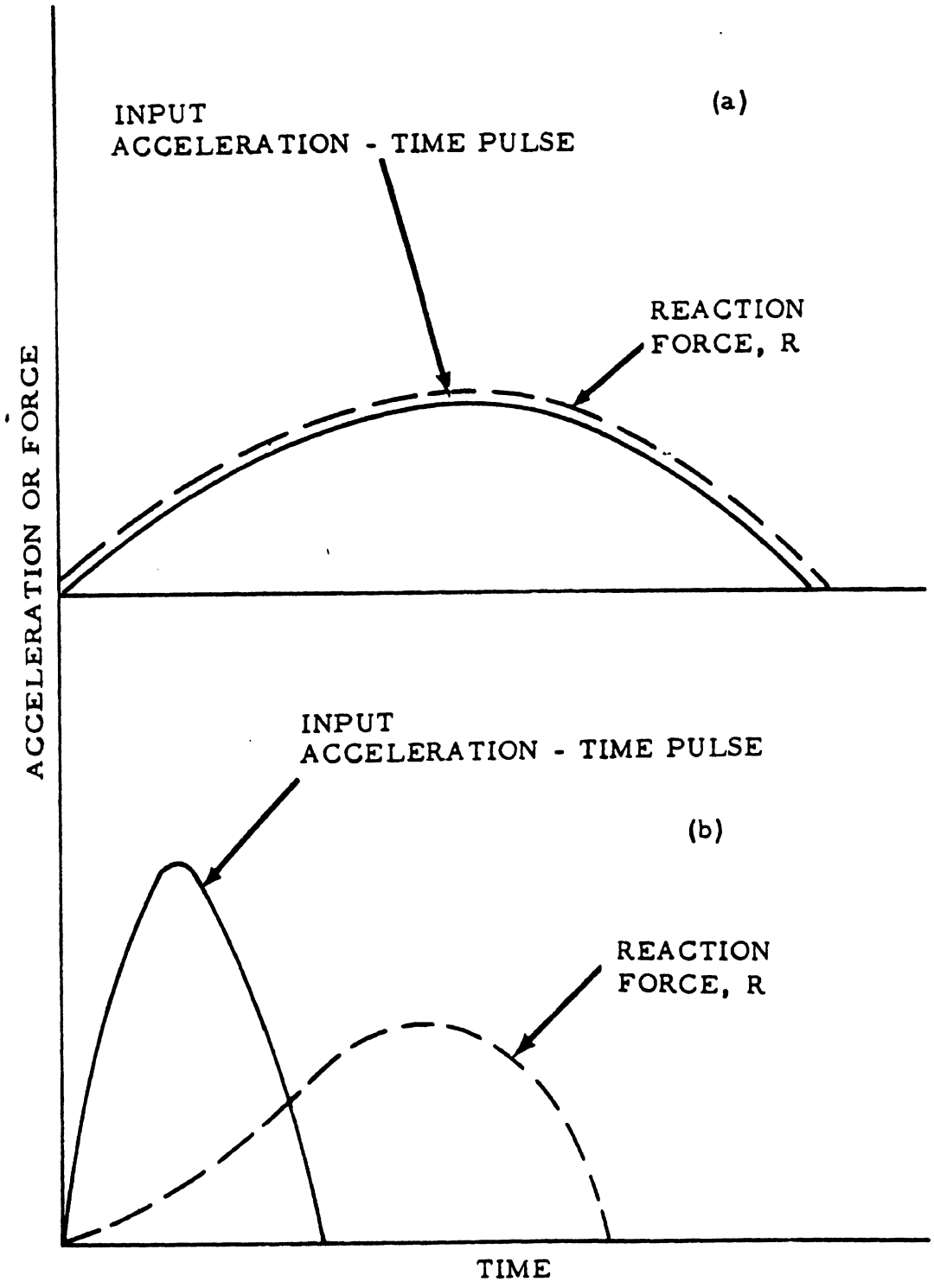


FIG. 2 RELATIONSHIP BETWEEN INPUT PULSE AND REACTION FORCE

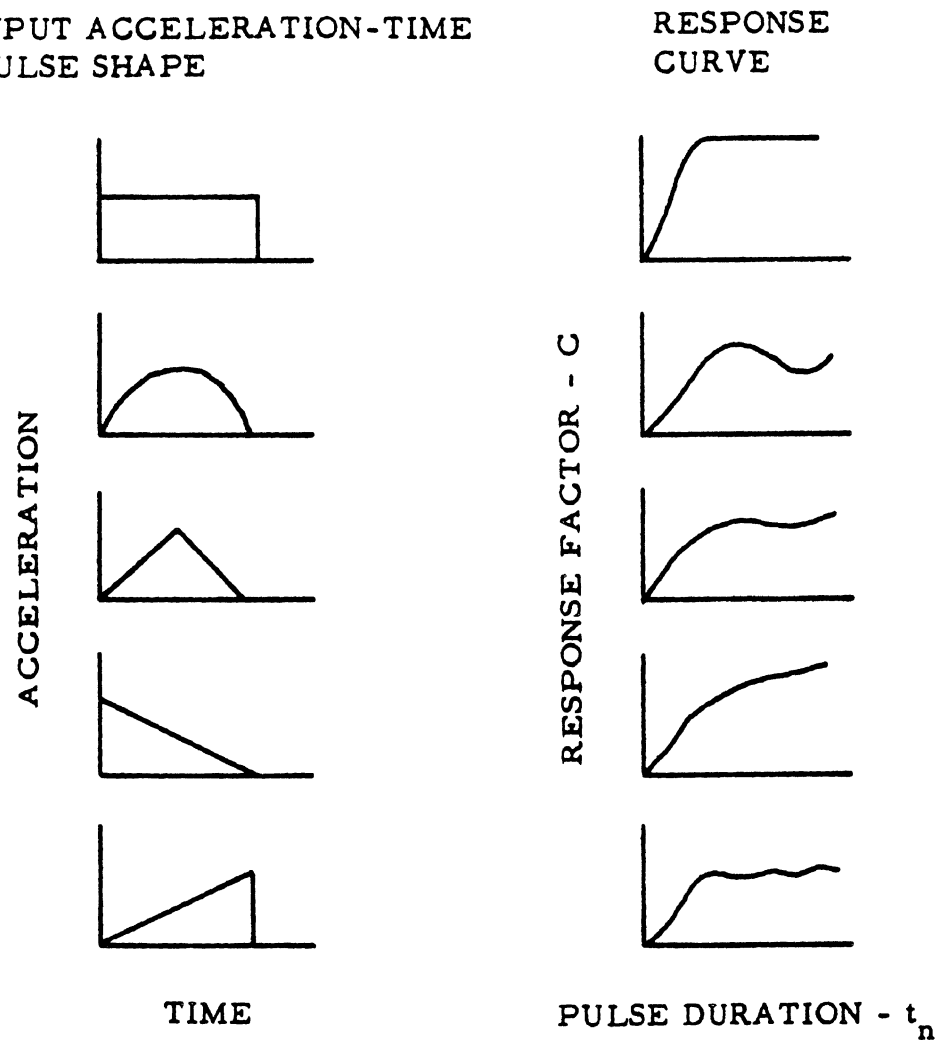


FIG. 3 RESPONSE FACTORS FOR A SIMPLE SPRING-MASS SYSTEM SUBJECTED TO SINGLE PULSES

Where $g_e$ is the effective peak inertia force on the seat/occupant combination calculated from the measured peak vertical seat leg reactions, and $\bar{G}$ is the average acceleration of the input acceleration-time pulse calculated from the measured pulse as follows:

$$\bar{G} = \frac{\Delta V}{g \times t_n} \tag{2}$$

Where g is the gravitational constant, $t_n$ is the measured pulse duration, and $\Delta V$ is the velocity change of the measured pulse obtained by calculating the area under the pulse shape:

$$\Delta V = \int_0^{t_n} f(G)\, dt \tag{3}$$

The variables velocity change and average acceleration ($\Delta V$ and $\bar{G}$) describe an input acceleration-time pulse and can be used to generate sensitivity curves that define an infinite variety of input acceleration-time pulses which induce, or are sensitive to, a given peak response level in the seat (vertical seat leg reaction level) (Figures 4 and 5). Points on sensitivity curves can be calculated from response curves by assuming a constant value for $g_e$, Equation (1), which corresponds to the desired peak response level in the seat, and calculating the corresponding values of $\bar{G}$ and $\Delta V$, Equations (1) and (2), for each assumed value of $t_n$. If the peak response level selected corresponds to the seat leg reaction intensities induced by the standard static test prescribed in the FAR's, any point on the resulting sensitivity curve defines an input acceleration-time pulse which converts the present static test into a dynamic test. The derivation, application, and limitations of the sensitivity curve technique are given in References 1 and 2 and will not be discussed in this report.

It can be seen from Figure 3 that the response curve is a function of the shape of the input acceleration-time pulses that produce it. If, in a given investigation, the input pulses are of the same general shape, as was obtained in this investigation including the results in Reference 3, one response curve will sufficiently define the relationship between the input pulses and the peak response level for each seat and loading direction, thus considerably simplifying the dynamic method.

To use this technique to express the present Federal Aviation Administration (FAA) static test load requirements in terms of dynamic criteria, it was necessary to determine the response characteristics of a representative number of aircraft seat/occupant systems to both statically and dynamically applied loads.

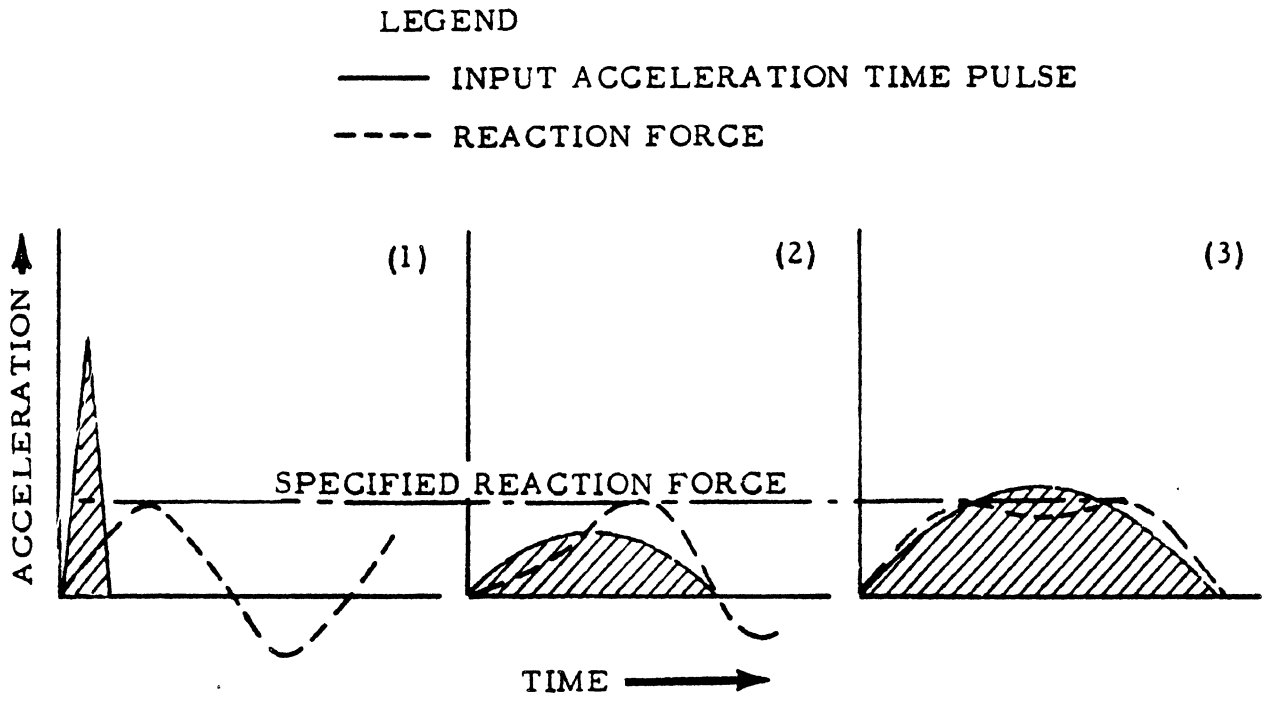


FIG. 4 INPUT PULSES FOR THE SPECIFIED RESPONSE

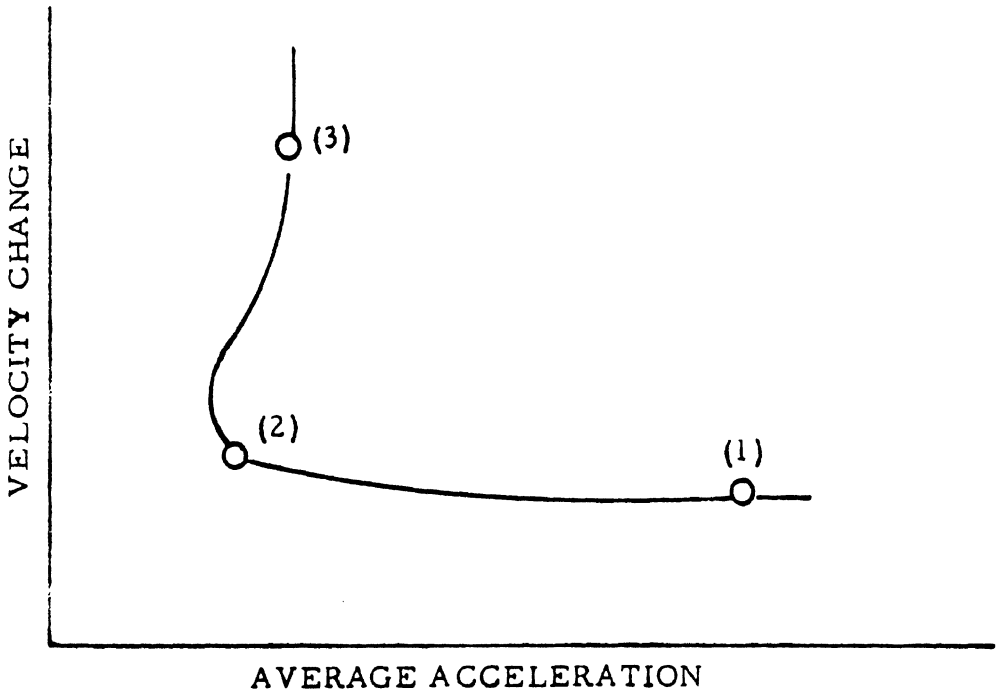


FIG. 5 SENSITIVITY CURVE FOR THE SPECIFIED RESPONSE

Three different types of seats, designated as A, B, and C, were selected to represent the majority of equipment being used by the airlines. All of the seats were three-place tourist class, but differed in construction. Seat A was of tubular construction, floor-mounted; Seat B was of sheet metal construction, floor-mounted; and Seat C was of tubular construction, floor/sidewall mounted (Figures 6, 7, and 8).

The seats were instrumented to measure the data necessary to establish dynamic seat test criteria comparable to the present FAA static test load requirements. It should be noted that these tests were not conducted for the purpose of certifying any particular aircraft seat or to compare static testing with dynamic testing per se. The seat installations on the test facilities simulated, as near as practical, the seat installation in an aircraft, but no attempt was made to simulate the aircraft floor structure because of the difference in the floor construction from aircraft to aircraft. The seat tests were limited to the forward and downward directions only, because of the cost of the test specimens and because these are the most common seat loading conditions which occur in an airplane crash. This, however, did not limit the technique to these particular cases.

Test Methods and Procedures: The static tests were conducted in accordance with the present FAA regulations at the National Aviation Facilities Experimental Center (NAFEC). These tests were conducted to provide load and failure data that could be compared with similar data obtained from the dynamic seat tests. Similarities and differences between the two means of testing were thus noted. The seats were attached to a test stand using instrumented attachment fittings. Body blocks, weighing 170 pounds, were positioned and secured in each seating place with standard airline seat belts. Loads as specified in TSO C-39 were applied to each body block simultaneously by means of hydraulic cylinders. An electrically driven pump supplied the pressure to the hydraulic cylinders, and the load was regulated by a control valve housed in a console. Typical setup positions are shown in Figures 9 and 10.

The input load supplied by the hydraulic cylinders, the seat belt tension, and the reaction forces of the seat attachments were recorded by two oscillographs. Motion picture cameras were positioned to photograph the test from various angles. Time correlation between the cameras and the oscillograph was used. A complete instrumentation description of the static tests is contained in Appendix II.

The horizontal and vertical dynamic tests were conducted under an agreement with the Aerospace Crew Equipment Department (ACED) located at the Naval Air Development Center, Philadelphia, Pennsylvania. Under this agreement, the seats were subjected to several nondestructive dynamic tests where the velocity change was held constant while the average acceleration was varied. The seats were again tested holding the

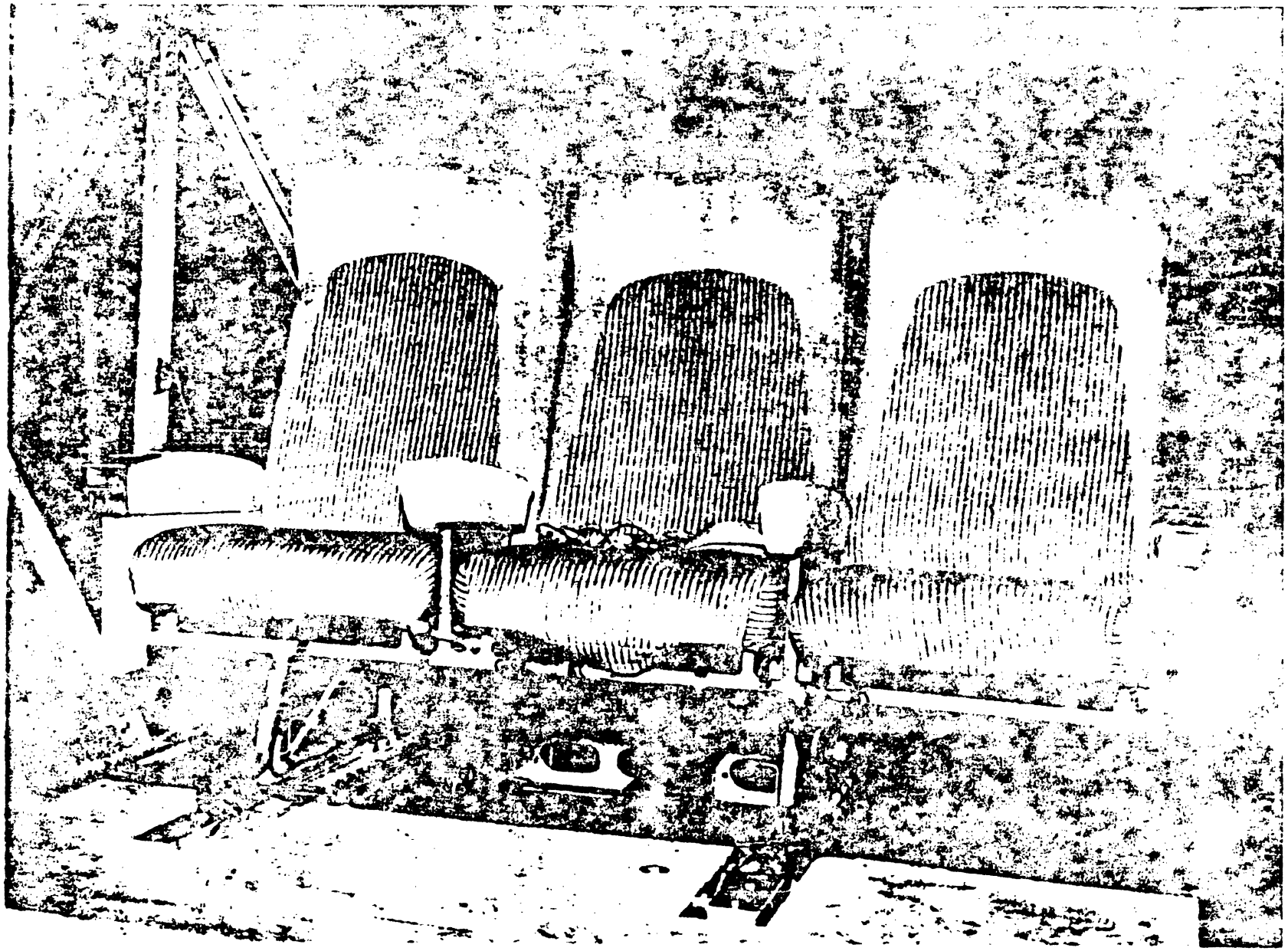

FIG. 6 SEAT A - TUBULAR CONSTRUCTION

average acceleration constant and varying the velocity change. Finally each seat was tested, increasing either the velocity change or average acceleration, until the seat was damaged.

The horizontal tests of Seats A, B, and C and vertical tests of Seat A were conducted on the ACED Horizontal Linear Accelerator. This facility is a hydraulically controlled, pneumatically driven catapult device incorporating a test sled and 386 feet of track. The seats, facing opposite to the direction of acceleration, were mounted to the sled by means of instrumented attachment fittings. Instrumented anthropomorphic dummies, each weighing 170 pounds, were secured in each seating place with standard airline seat belts. Typical test arrangements are shown in Figures 11 and 2-3.

The sled was accelerated by a piston which receives its energy from the expansion of a fixed air mass entrapped in an accumulator. The sled, seat, and dummy accelerations, seat belt tension, and the reaction forces of the seat/floor attachments were transmitted by direct line from the sled and recorded by two oscillographs during the acceleration stroke. Motion picture cameras were positioned on and around the sled to photograph the tests from various angles. A complete instrumentation description of these dynamic tests is contained in Appendix II.

The vertical dynamic tests for Seats B and C were conducted on the ACED 150-Foot Vertical Drop Tower (Figure 12). This facility is a 150-foot tower incorporating a 10- by 10-foot test car which can be dropped from any height up to 112 feet and is arrested by metal straps. Mounting techniques similar to those used on the catapult were incoporated for the installation of the seats on the drop tower test car. Again, anthropomorphic dummies were secured in each seating place with standard airline seat belts.

The car was raised to the desired height then dropped and arrested by the controlled bending of the metal straps. The sled, seat, and dummy accelerations, seat belt tension, and the reaction forces of the seat attachments were transmitted by telemetry to a ground station and recorded on magnetic tape. The tests were photographed from various angles by motion picture cameras mounted on and around the test facility. Refer to Appendix II for instrumentation details of these tests.

Selection of the Acceptable Dynamic Test Methods: To determine methods of testing aircraft seats and occupant restraint devices to show compliance with dynamic seat test criteria, a study was made of existing seat test facilities, both static and dynamic. Since seat testing is primarily conducted by the manufacturer, consideration had to be given to the amount, complexity, and cost of the test equipment and facilities required to certify an aircraft seat under dynamic conditions.

Visits were made to airlines, seat manufacturers, airframe manufacturers, and government test facilities to study the existing static and dynamic seat test requirements and procedures. A variety of test reports and documents was obtained and reviewed, and is contained in the Bibliography.

Seat Strength Versus Crash Loads: The measure of an aircraft seat's capability to restrain its occupant is the maximum load the seat can withstand without failing. Presently, the crash load requirement specifies the strength of a seat in terms of statically applied inertia loads. Unfortunately, an airplane crash is a dynamic phenomenon with a variety of loading conditions which cannot be exactly defined or reproduced by static loading.

By expressing the present FAA crash load requirements in terms of dynamic criteria, a comparison can be made between actual aircraft crash inputs and the present seat strength requirements. This was accomplished by calculating and plotting the sensitivity curves for each seat type and input direction based on the static test load response level and plotting, on the same graph, acceleration-time inputs of the aircraft floor produced in an actual aircraft crash. If all of the data points plotted from the aircraft crash test lie to the left and below the sensitivity curve of a particular seat, the present crash load requirement would be adequate for that particular seat in the given crash. However, if any of the points lie to the right and above the sensitivity curve for a particular seat, the present crash load requirement would not be adequate, since the existing loads required to certify the seat would have been exceeded (Figure 13). This assumes, of course, that all of the dynamically applied inputs used from the actual aircraft crash test were below those that would cause the human tolerance of the seat occupant restrained by a lap belt only to be exceeded.

## DISCUSSION AND RESULTS

### Static and Dynamic Tests

Seventy-four dynamic tests and nine static tests were conducted to establish dynamic seat test criteria.

To use the sensitivity curve approach, it was first necessary to define the response characteristics of each seat/occupant, spring-mass system in both the longitudinal and vertical directions. Knowing the response characteristics for each system, a sensitivity curve was established (for each direction) that represented the applied dynamic inputs that produced the same peak seat leg reaction level as did the FAA-required static test load.

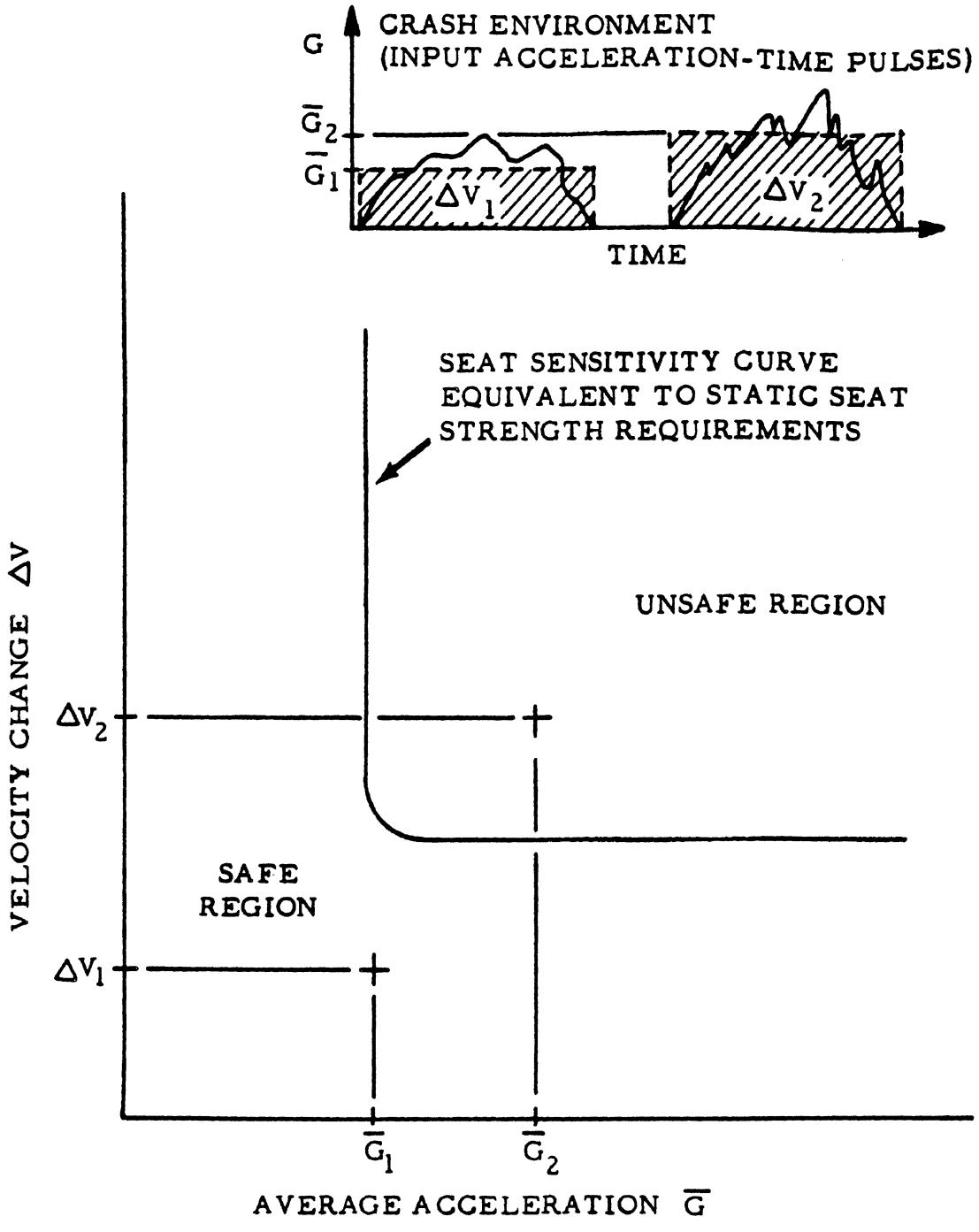


**FIG. 13 SAMPLE SENSITIVITY CURVE RELATING STATIC SEAT STRENGTH REQUIREMENTS TO CRASH ENVIRONMENT**

The spring response characteristics of each seat were defined in terms of the effective peak inertia force on the seat/occupant combination, $g_e$, and the average acceleration of the input acceleration-time pulse, $\bar{G}$, and were expressed as response factor C. Dynamic response curves were plotted for each seat/occupant system in terms of the response factor, C, versus the input acceleration-time pulse duration, $t_n$, whereas in Equation (1), Page 2:

$$C = \frac{\text{Effective Peak Inertia Force}}{\text{Effective Weight}^* \times \bar{G}} = \frac{Wt \times g_e}{Wt \times \bar{G}} = \frac{g_e}{\bar{G}}$$

and where the effective peak inertia force was calculated from the recorded reaction loads. Examination of these response curves, shown in Figures 14 through 19, indicates that each seat has different spring characteristics and that the spring characteristics can change with loading history; i.e., response level. This was most evident in the vertical dynamic tests of Seat A where the anthropomorphic dummy bottomed out on the aft stress tube (Figures 15 and 20). Seat C, because of its unique energy-absorbing design, established two longitudinal response curves as shown in Figure 18.

To derive the sensitivity curves for each seat comparable to the present static load requirements, the values of $\bar{G}$ and $\Delta V$ were calculated for a specified statically applied load; i.e., 9 g's forward, using the respective response curves for each seat to determine the appropriate response factor C.

To calculate $\bar{G}$, Equation (1) was expressed as:

$$\bar{G} = \frac{g_e}{C}$$

where C is determined drom the response curve for an arbitrarily selected pulse duration, $t_n$. The velocity change corresponding to the same duration, $t_n$, was then determined from Equation (3), Page 6:

$$\Delta V = \bar{G} \times g \times t_n$$

* Effective weight is the weight of the seat plus that weight of the anthropomorphic dummies on the seat. In some cases, the dummies' legs were partially supported by the floor, and the effective weight was correspondingly reduced.

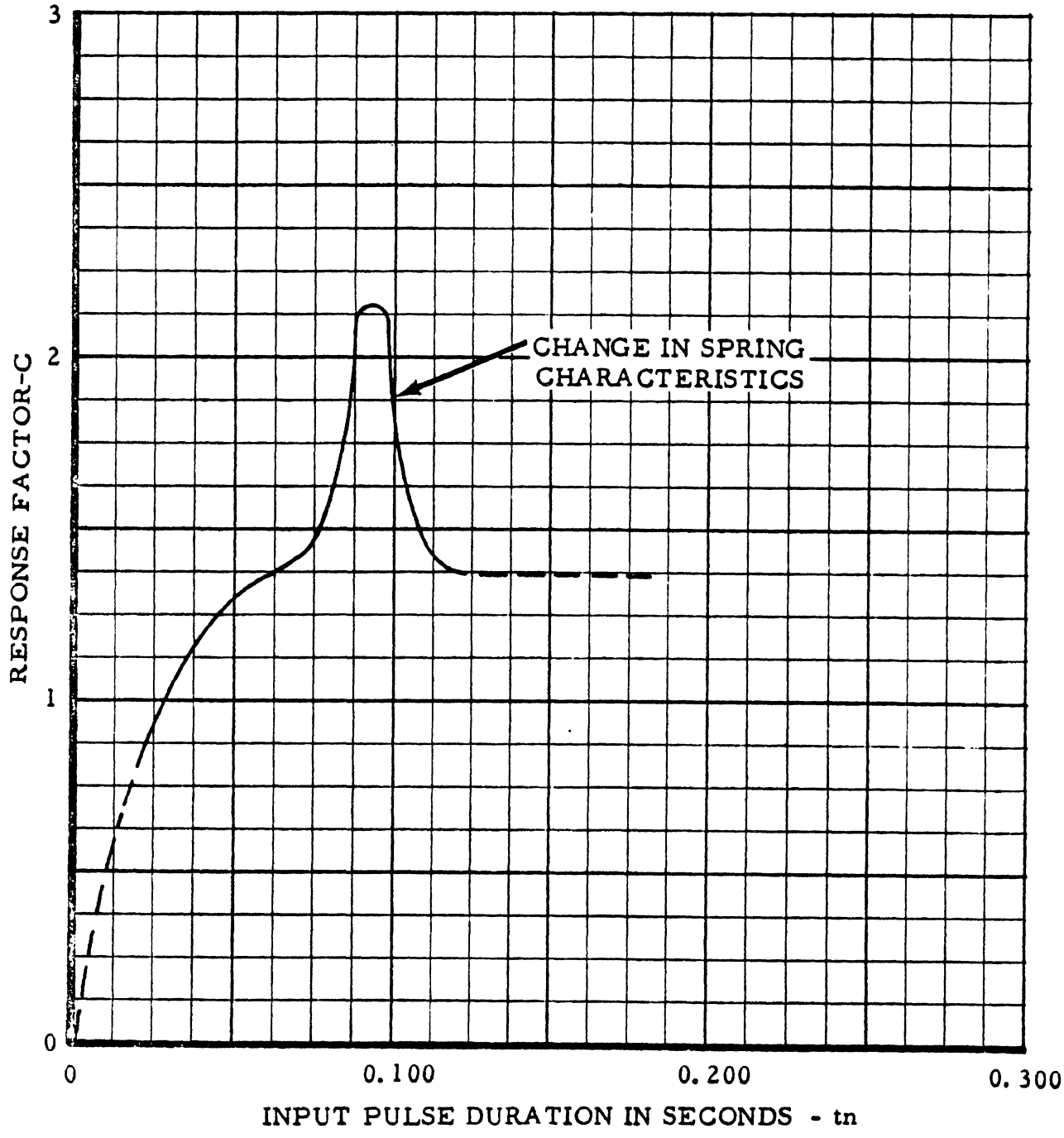


FIG. 15 VERTICAL RESPONSE CURVE FOR SEAT A

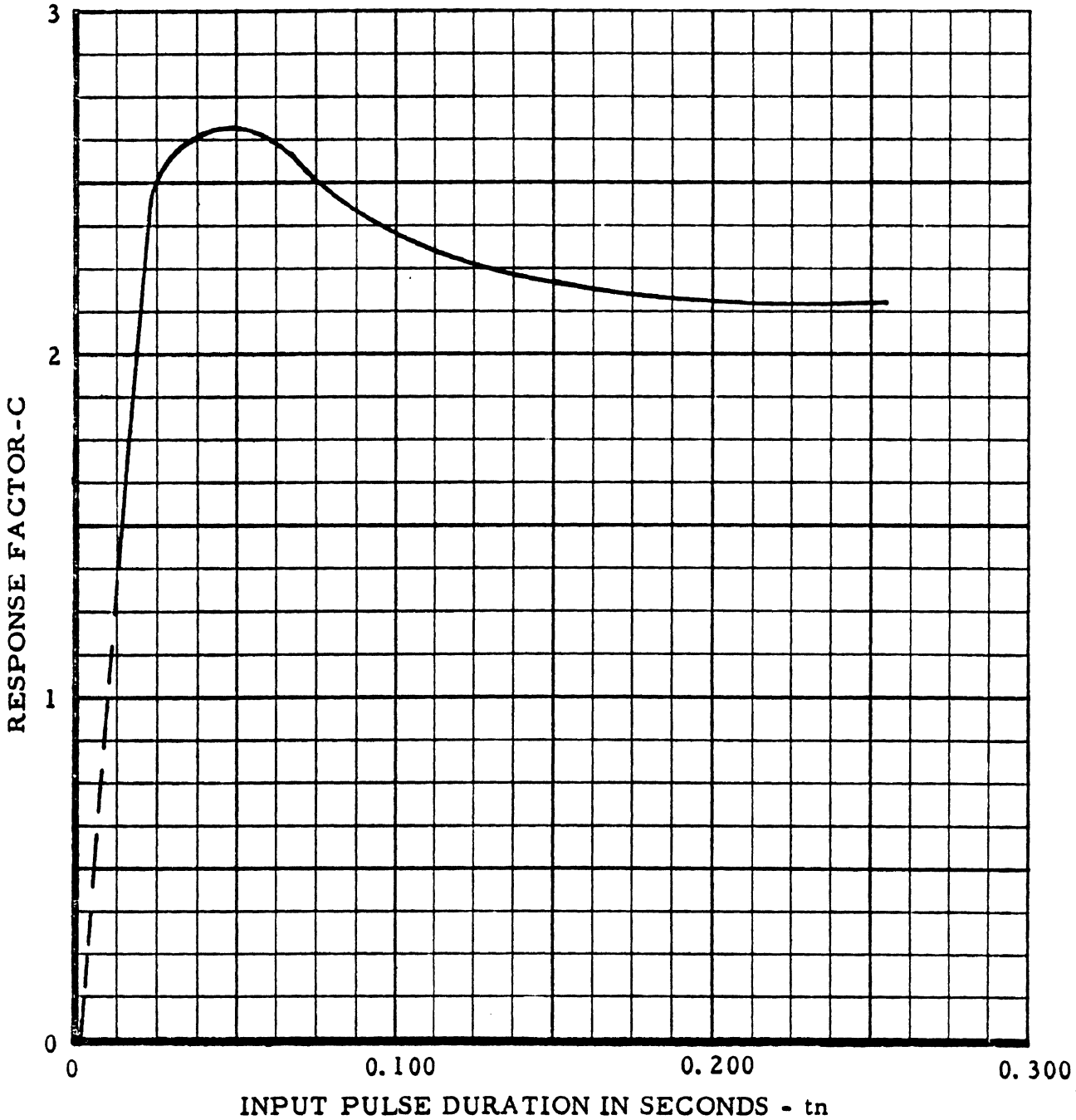


FIG. 17 VERTICAL RESPONSE CURVE FOR SEAT B

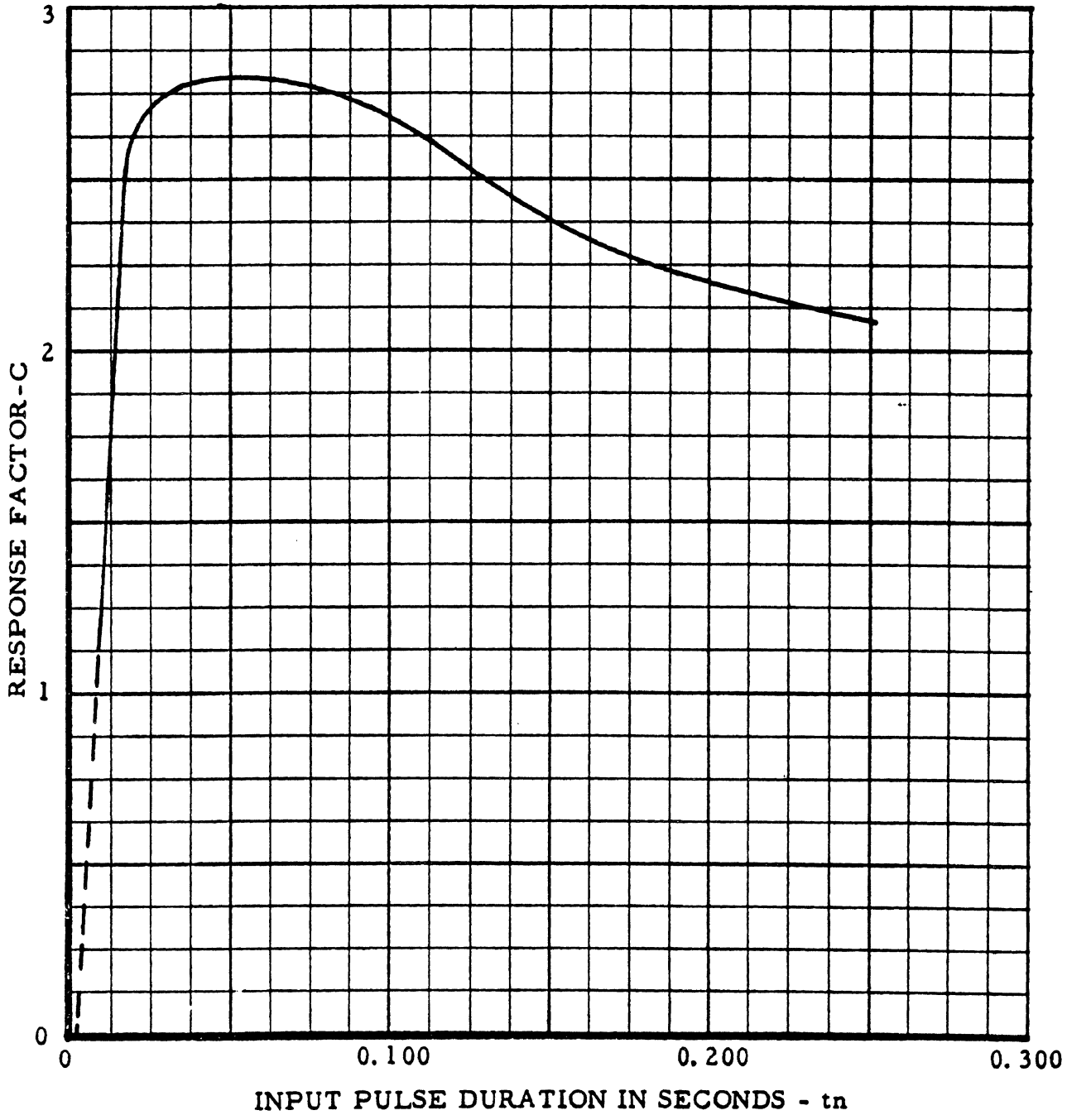


FIG. 19 VERTICAL RESPONSE CURVE FOR SEAT C

The sensitivity curves derived for each seat describe the input acceleration-time pulses which induce the same peak seat leg reaction level as the applied static loads specified in the FAR's. Inspection of Figures 21, 22, and 23 shows clearly that seats certified for the same applied static loads responded quite differently to the same dynamic inputs. This is evident since the spring characteristics of each seat differ as previously mentioned.

Figures 24 and 25 are examples of the data collected from the dynamic tests and demonstrate the value of the sensitivity curve. Note that $\bar{G}$ for Tests 39 and 40 are nearly equal; however, the seat failed during the latter test. This demonstrates how the velocity change affects the loading on the seat. All of the data used in this reported are contained in Appendix III, Data Summary.


Acceptable Dynamic Testing Methods

Dynamic test methods and instrumentation need not be elaborate. The basic test facility would only require a means of accelerating the test article to the specified velocity, a means of decelerating it to obtain the specified acceleration pulse shape and acceleration average, and a means of recording the necessary input and response variables.

The methods of obtaining the desired velocity for the forward and sideward seat tests could range from the use of a simple pendulum or an inclined plane, to the more complex catapults and rocket sleds (Figures 26, 27, and 28). The downward tests, for the best results, were found to be limited to the use of a drop tower. Adequate deceleration can be obtained by the use of shock absorbers, arresting cables, or any energy-absorbing technique which will provide the desired average acceleration and acceleration pulse shape.

Ideally, the instrumentation of the input would be a continuous acceleration-time trace throughout the deceleration or impact cycle. This can be achieved by utilizing one accelerometer, mounted on the test sled, and recording on an oscillograph with timing. The pulse shape can readily be determined, and the three input variables, velocity change, average acceleration, and pulse duration can readily be calculated, Equations (2) and (3). Once confidence can be established in the repeatability of the input pulse shape, the instrumentation can be further simplified to any means of accurately obtaining any two of the three input variables. For example, the velocity change could be reduced to some means of obtaining the velocity just prior to impact. This velocity would represent the velocity change if the seat/occupant system comes to rest at the end of the impact cycle.

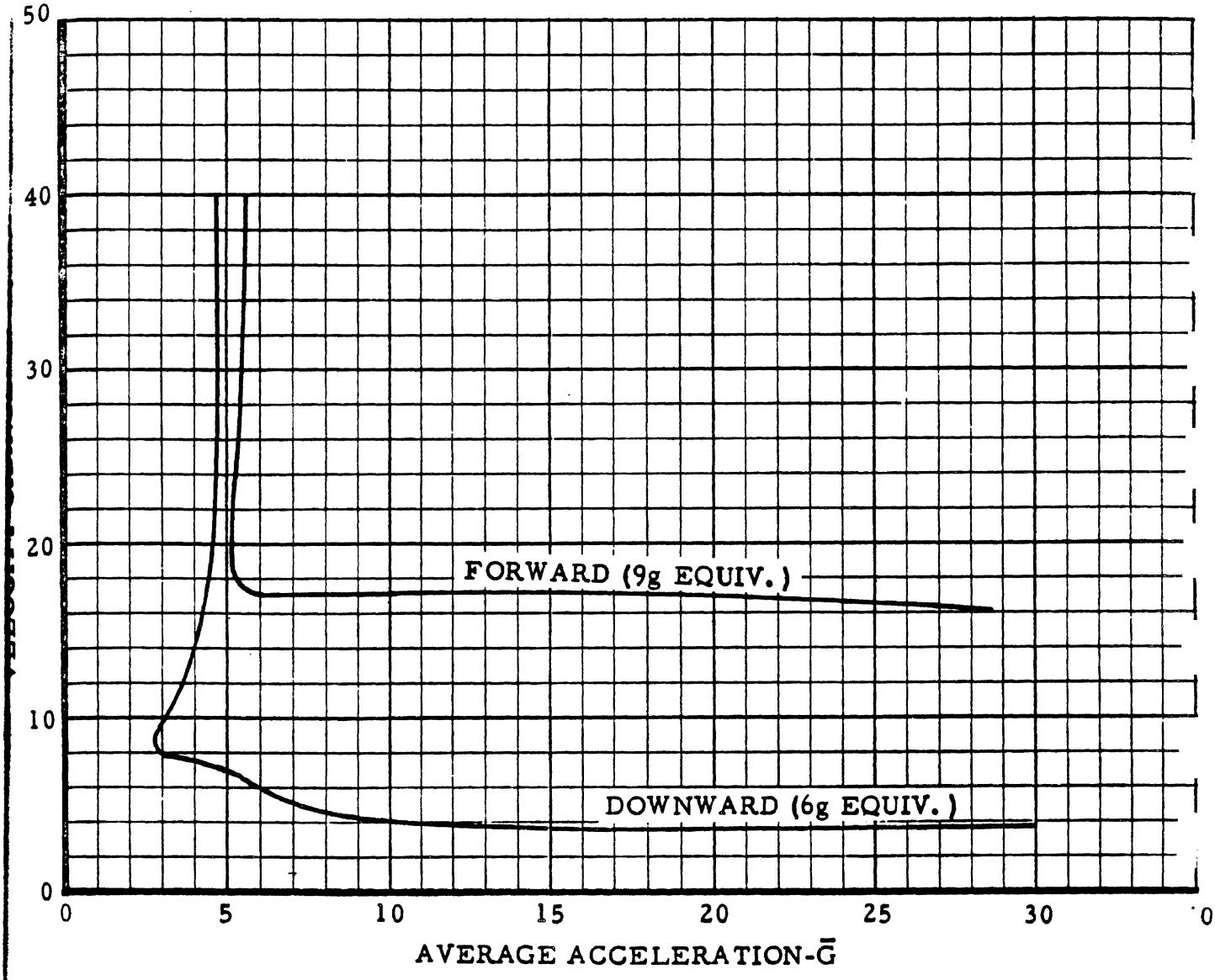


FIG. 21 SENSITIVITY CURVE - SEAT A

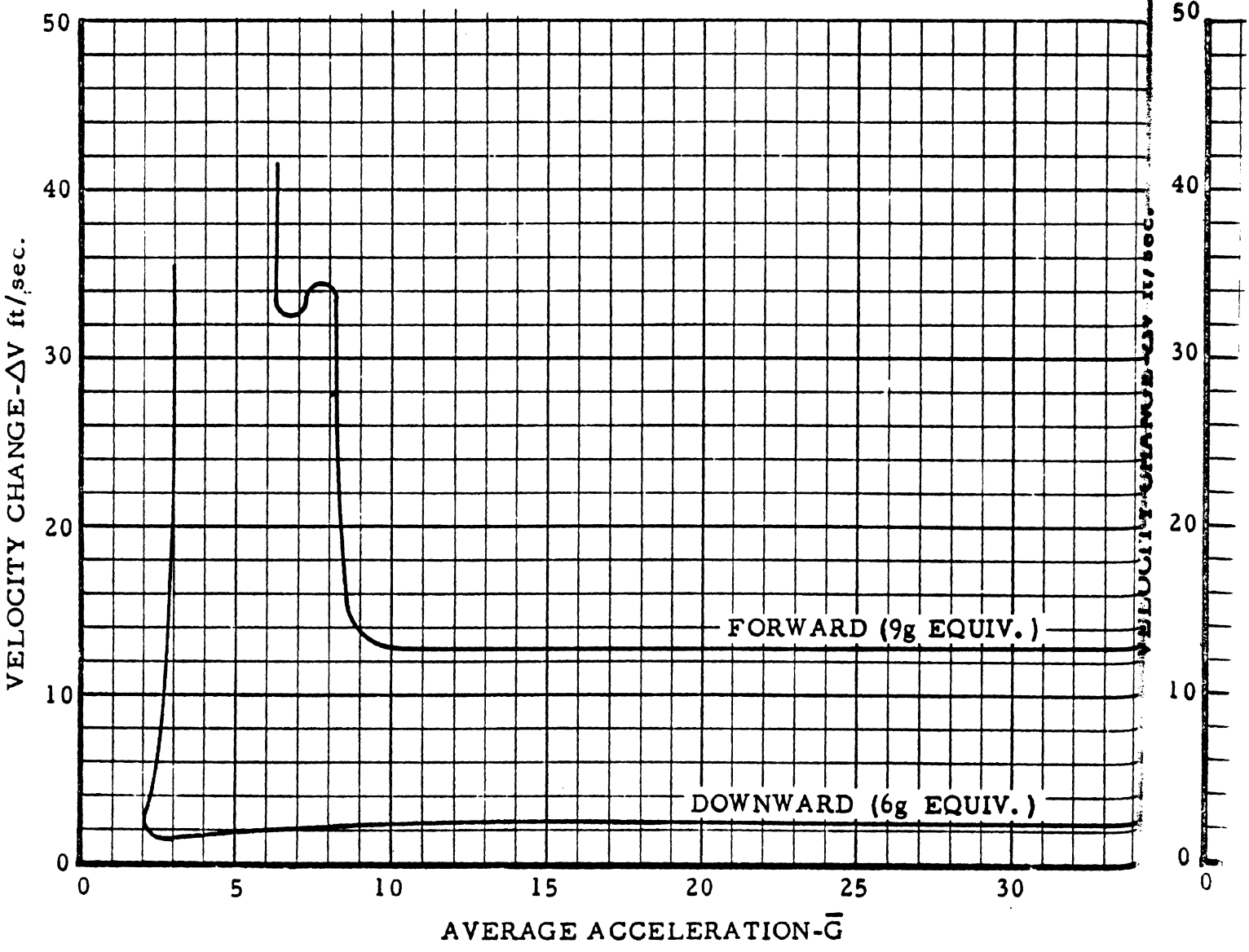


FIG. 22 SENSITIVITY CURVE - SEAT B

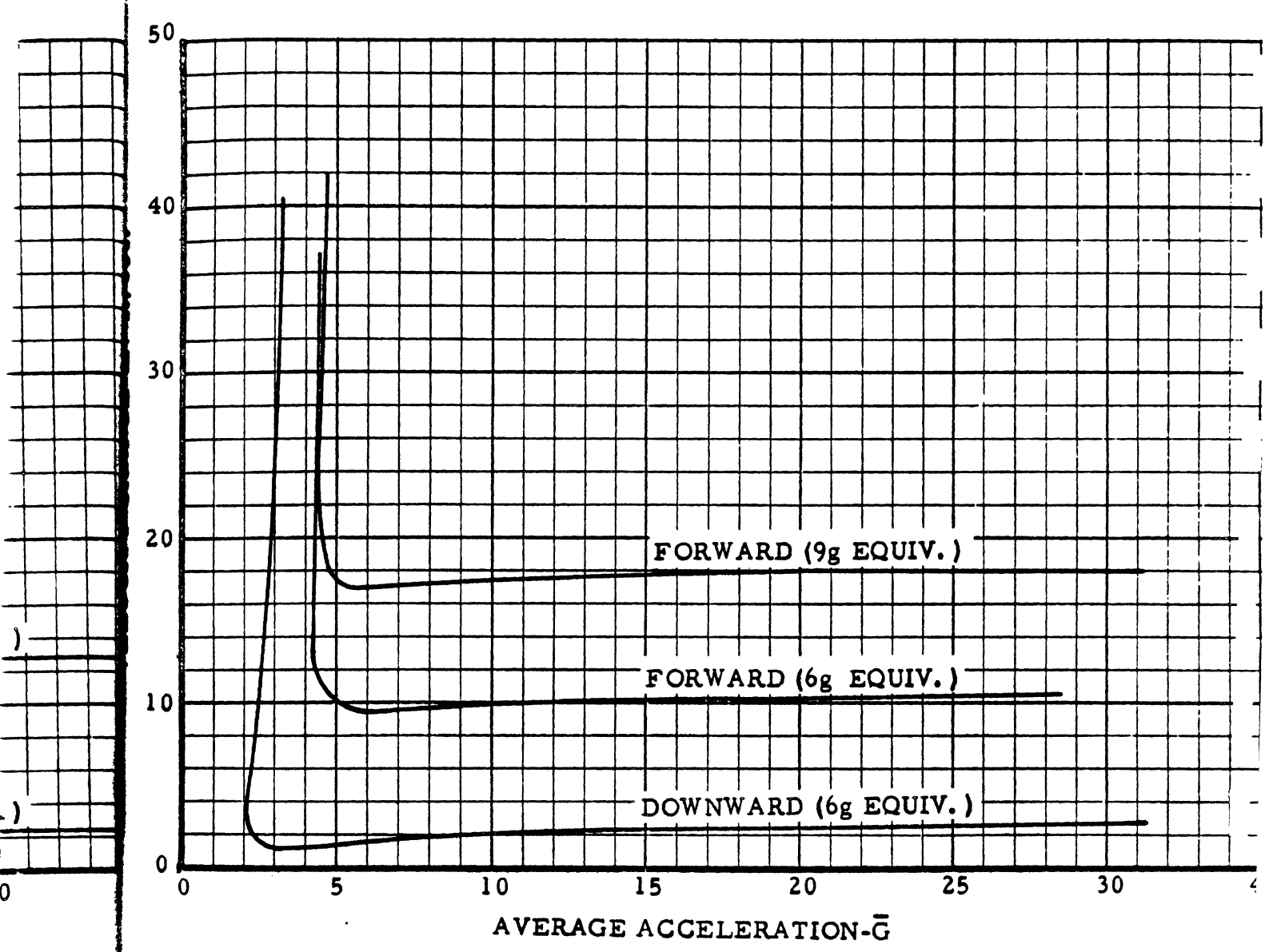


**FIG. 23 SENSITIVITY CURVE - SEAT C**

Instrumentation for the response of the seat/occupant system involves the recording of only the peak seat leg reactions. Continuous traces of the reactions throughout the deceleration cycle are not required. Peak reactions are required for all four legs in the downward and upward tests. For the forward and sideward tests, peak reactions are required for only the two legs subjected to tension. The tension legs are selected to minimize the random effect that occupant rebound may have on the response characteristics of the seat/occupant system. Occupant rebound is otherwise important in the evaluation of human survivability, ultimate damage to the seat, and the restraint capabilities of the seat. The tension legs are the two aft legs for the forward tests, and the aft leg and forward leg on the side opposite to the direction of the inertia force for the sideward tests.

An acceptable method of recording input data would be the use of high-speed photography. This technique would probably be more desirable to the seat manufacturer since it would provide him with a visual account of the test, along with the required data, using a minimum amount of equipment. For this method to be acceptable, time and the required distances must be recorded on the film.

In conducting a dynamic test, the test setup should be similar to that used in the test portion of this project with the exception of the elaborate instrumentation. The seat should be mounted to a rigid test bed using the same tiedowns (track and floor fittings) planned for the seat installation in operational aircraft. A rigid test bed is recommended in lieu of the simulated aircraft floor structure for several reasons:

1. Even though it would be desirable, it is doubtful whether or not the structural response of an aircraft floor could be simulated since such a small portion is required for the seat test installation.

2. The floor response characteristics will vary from aircraft to aircraft and from seat location to seat location in any given aircraft. For example, the transverse beams which support the seat tracks in one aircraft have a spacing of 20 inches. The seat spacing used by most airlines is 34 inches. Since 20 is not a multiple of 34, it is obvious that some seats will be mounted directly over the transverse beams providing a comparatively more rigid installation than those seats straddling the beams.

3. A rigid floor structure will usually create the most severe test condition for a seat and will insure test consistency for better seat evaluation.

The use of anthropomorphic dummies was found to provide more realistic test results because their response and seat pan impression were more representative of that of a human than the body blocks prescribed in the present FAA requirements (TSO-C-39). The most representative human response simulation available is necessary to

accurately evaluate a seat. It was found during the many dynamic tests conducted in this project that many of the forces experienced by the seats were not considered in the initial seat design. For example, a forward seat leg attachment came loose from the floor track due to the dummies' rebound from the initial acceleration inducing a tension force on the attachment (Figure 29). Since all the test conditions for forward facing seats prescribed in the FAR, with the exception of the sideward and upward loads which are comparatively low, places the front legs in compression, it is logical, therefore, that any sizeable tension load in the forward leg could be overlooked.

Another condition which can best be evaluated by use of an anthropomorphic dummy is the possibility of the seat occupant "bottoming out" on the seat's basic frame. Many back injuries have been experienced in aircraft accidents in which high sink rates or vertical decelerations have caused the seat occupant to bottom out on the seat structure. This is especially true of crew members whose seats were mounted on a pedestal. The anthropomorphic dummy provides a more realistic seat pan impression and provides more accurate seat load distribution. The body blocks presently specified have a large seat imprint. Examination of Figures 20 and 30 shows the difference between the results of tests using dummies and those using body blocks.

## Seat Sensitivity Versus Crash Loads

Having established sensitivity curves for Seats A, B, and C comparable to the present FAA static crash load requirements, a comparison of these requirements was made with actual airplane crash inputs and the realism of the present seat strength requirements determined.

The actual crash inputs used for the comparison were those taken from the crash test of a Lockheed 1649A aircraft. The data and a detailed description of the test are reported on in Reference 3. The data used in this report were those longitudinal and vertical acceleration-time histories measured at Fuselage Stations (FS) 195 and 685 when the aircraft impacted a $6^{o}$ and $20^{o}$ slope (Figures 31 and 32).

The most severe longitudinal acceleration-time pulse for each impact was reduced to terms of velocity change and average acceleration. These quantities were then plotted on a composite of each seat's sensitivity curve comparable to a 9-g forward static load. Inspection of the composite plot which is shown in Figure 33 indicates that the present crash load test requirement was not adequate in this crash for most type-certified seats had they been mounted in the crew compartment area, FS 195. However, the requirement was definitely adequate for such seats mounted at the aircraft's center of gravity, FS 685, and aft during the impact with both the $6^{o}$ and $20^{o}$ slopes. Although the horizontal floor acceleration obtained

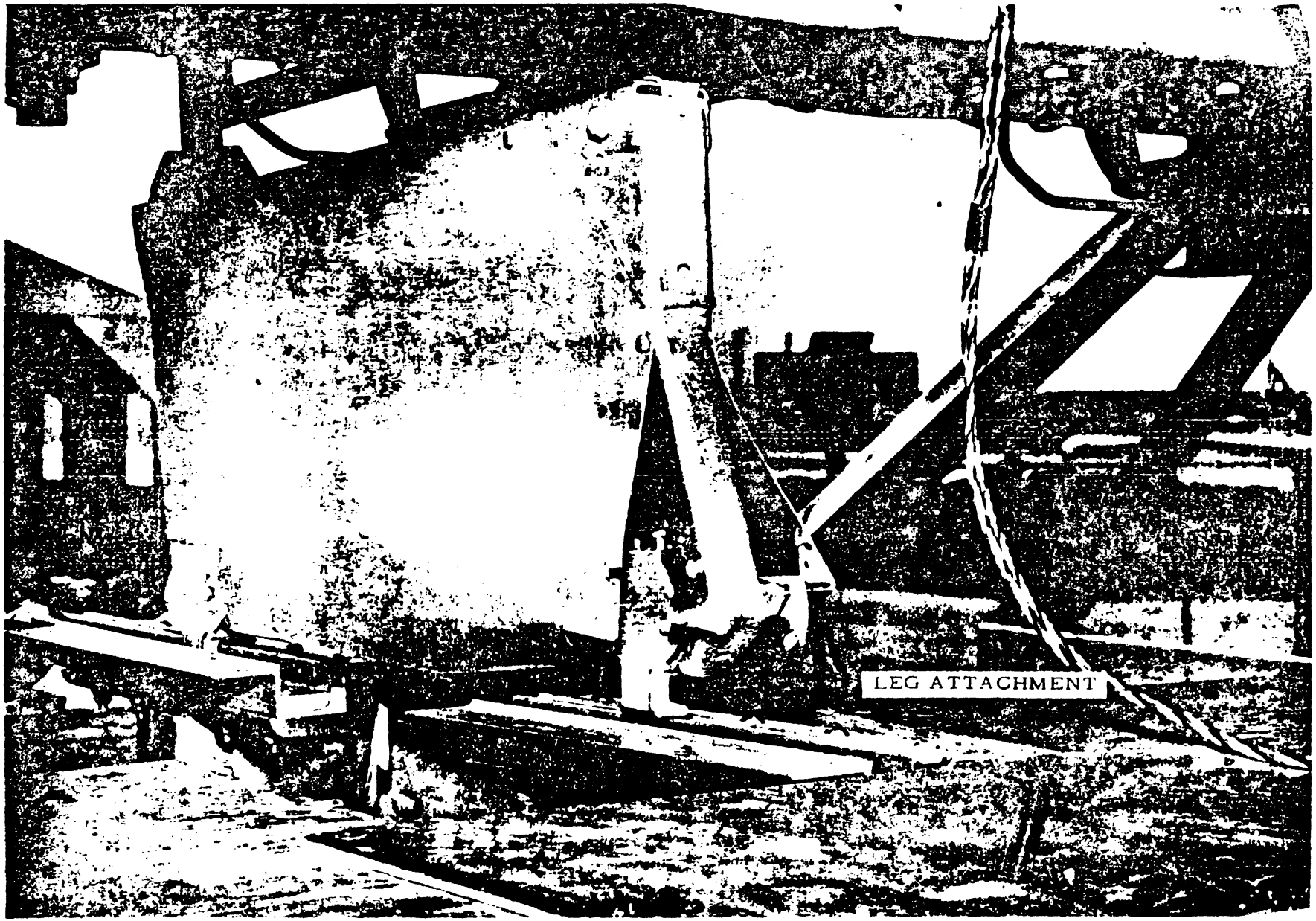


FIG. 29 FORWARD LEG OF SEAT C FOLLOWING FORWARD DYNAMIC TEST

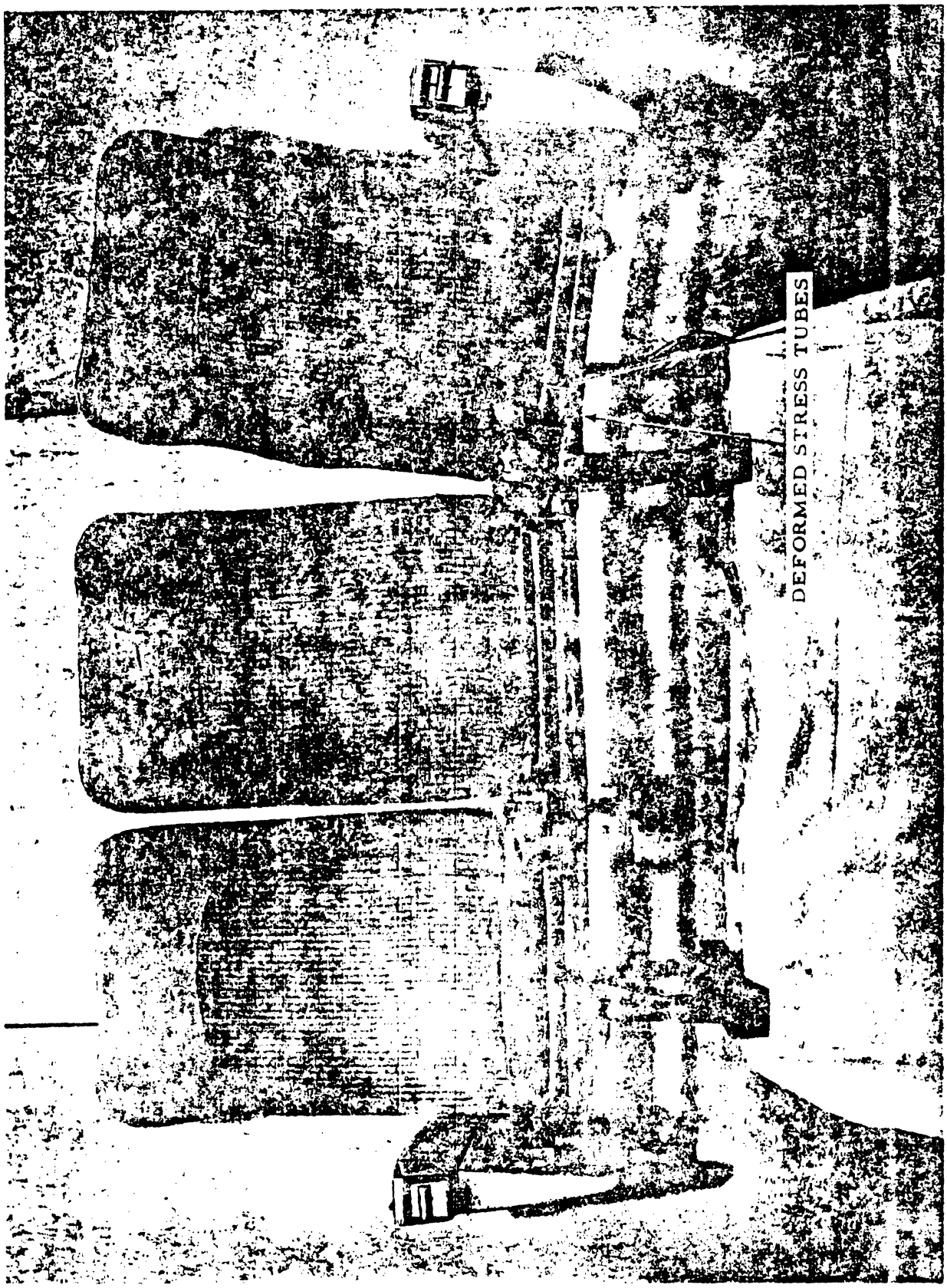
DEFORMED STRESS TUBES

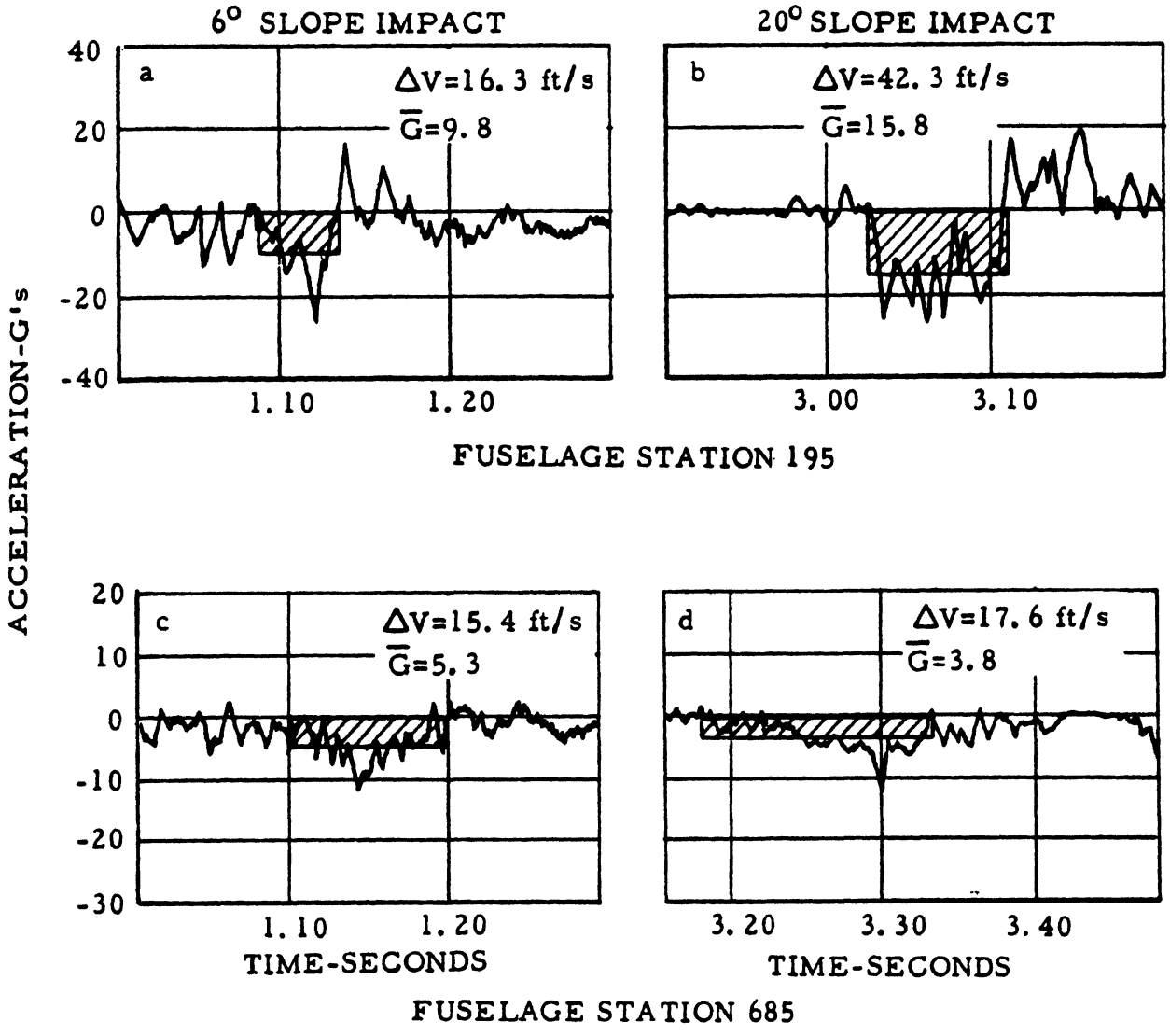


FIG. 31 LOCKHEED 1649A AIRCRAFT LONGITUDINAL FLOOR ACCELERATIONS

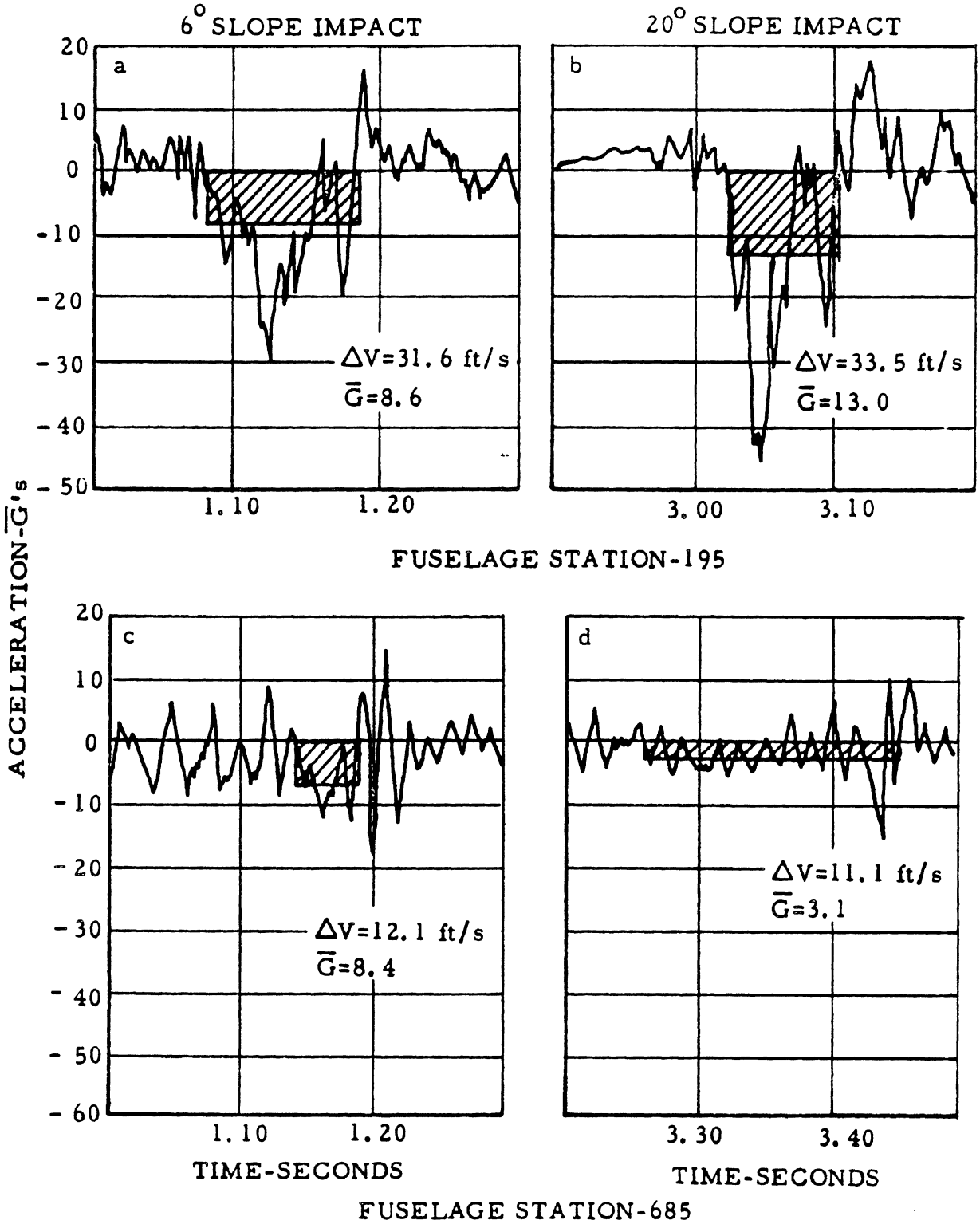


FIG. 32 LOCKHEED 1649A AIRCRAFT VERTICAL FLOOR ACCELERATIONS

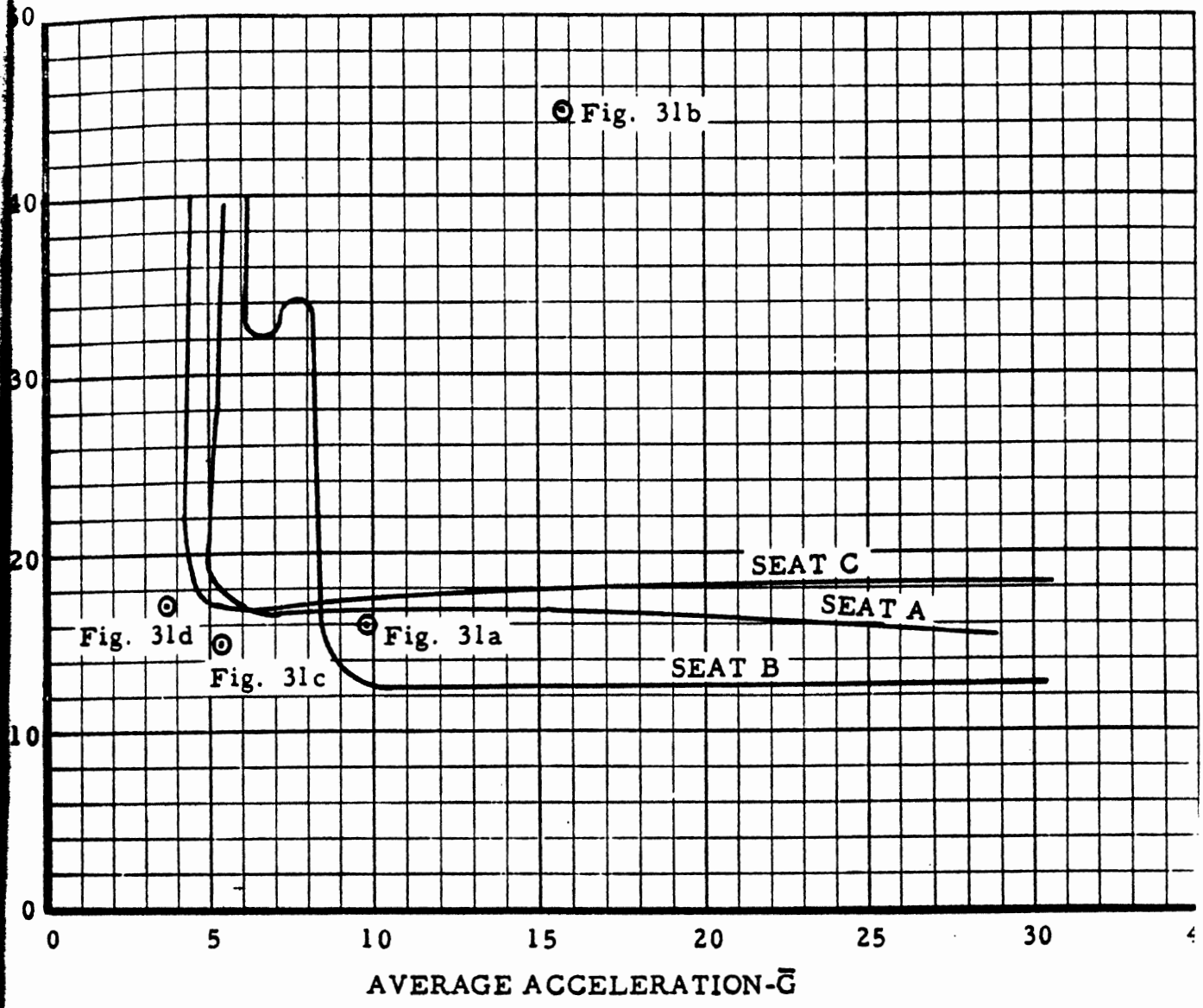


FIG. 33 LONGITUDINAL 9-g SENSITIVITY CURVES

at FS 460 was not analyzed, the fact that a Seat A configuration containing dummy passengers and located at FS 417 did not fail horizontally indicated that the present requirement was probably adequate for type-certified seats had they been mounted anywhere a few feet aft of FS 380 where a complete fuselage break occurred. It should be noted that the velocity change and average acceleration determined from the acceleration-time history, measured on the crew compartment floor, FS 195, during the aircraft's impact with the $6^{o}$ slope, fell below the sensitivity curves (safe region) for Seats A and C, but above and to the right of the sensitivity curve (failure region) for Seat B. This demonstrates the inadequacy of the present static crash load test requirements to define a consistent level of safety for the crash environment, since all of the seats used in the project either met or exceed the test requirements for certification.

Similarly, a composite was made of velocity changes and average accelerations, determined from the vertical acceleration-time histories recorded during the aircraft's impact with the $6^{o}$ and $20^{o}$ slopes, and each seat's sensitivity curve comparable to a 6-g downward static load (Figure 34). Inspection of this composite shows that the present crash load test requirement for this condition was only adequate for Seat A, mounted at the aircraft's center of gravity and aft during the aircraft's impact with the $20^{o}$ slope. The inadequacy of the present crash load test requirement in defining a consistent level of safety for an aircraft crash was again demonstrated, since the velocity change and average acceleration determined from the acceleration-time history measured at the center of gravity during the aircraft's impact with the $20^{o}$ slope was in the safe region for Seat A, but in the failure region for Seats B and C.

## Certification Procedure Utilizing Dynamic Tests

The dynamic test methods should provide the response characteristics of a seat and restraint device in terms of the response curves, and, in the absence of sufficient human survivability data, the present static inertia force requirements should be selected as the peak response level parameters with which the sensitivity curves can be analytically generated from the response curves. The sensitivity curves will define the maximum crash severity level for each input direction at which the occupant can be successfully restrained. At least one test should be performed in each direction for which the seat and restraint device are subjected to the maximum crash severity level. The occupant should be an anthropomorphic dummy equal in weight to the present occupant weight requirement for the static tests (170 pounds).

The test methods should be such that the response curves reflect the effect of the parameters; input pulse shape and response level.

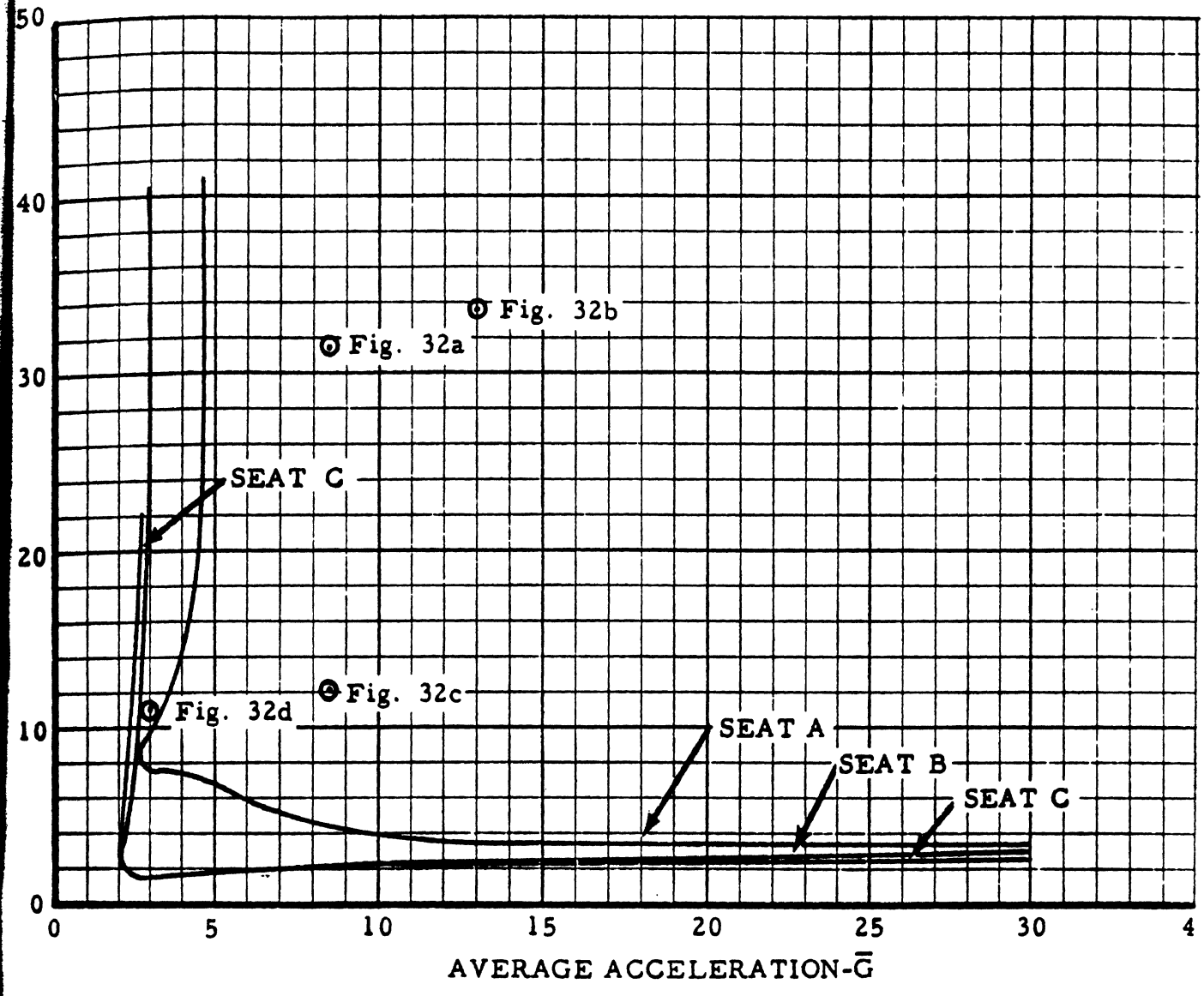


FIG. 34 VERTICAL 6-g SENSITIVITY CURVES

Pulse shapes approximating those encountered in actual crash environments, Reference 3, should be used, and tests producing response levels close to the peak response level requirements should ultimately determine the response curves.

In order to embody the above recommendations, the certification test procedure for each seat/lap belt combination for each input direction should be as follows:

1. Utilizing one seat and lap belt, obtain a response curve using inputs which induce peak response levels within the elastic range of the seat/lap belt system. About five tests are required (Figure 35a). The seat and lap belt can be utilized for additional testing.

2. Generate an approximate sensitivity curve for the peak response level requirement (Figure 35b). Select two inputs each at one of the "asymptote" locations on the sensitivity curve (Figure 35c), and, using two different seats and lap belts, perform two more tests.

3. Permanent deformation characteristics of the seat/lap belt system will probably be noted causing the two additional points to fall off the previously determined response curve (Figure 35d).

4. Adjust the response curve moving the upper portion parallel to itself so that the two points are now on the curve (Figure 35d).

5. Generate a final corrected sensitivity curve from the adjusted response curve for the peak response level requirement (Figure 35e).

6. If the seat leg reaction data from the last two tests indicate that the peak response level requirement had not been reached or exceeded, retest one of the seats at one of the asymptote locations on the corrected sensitivity curve (Figure 35f). If successful restraint of the occupant cannot be obtained, perform the test on a new and previously untested seat and lap belt. Successful restraint of the occupant during the final test together with a documentation of the response and sensitivity curves will certify the seat.

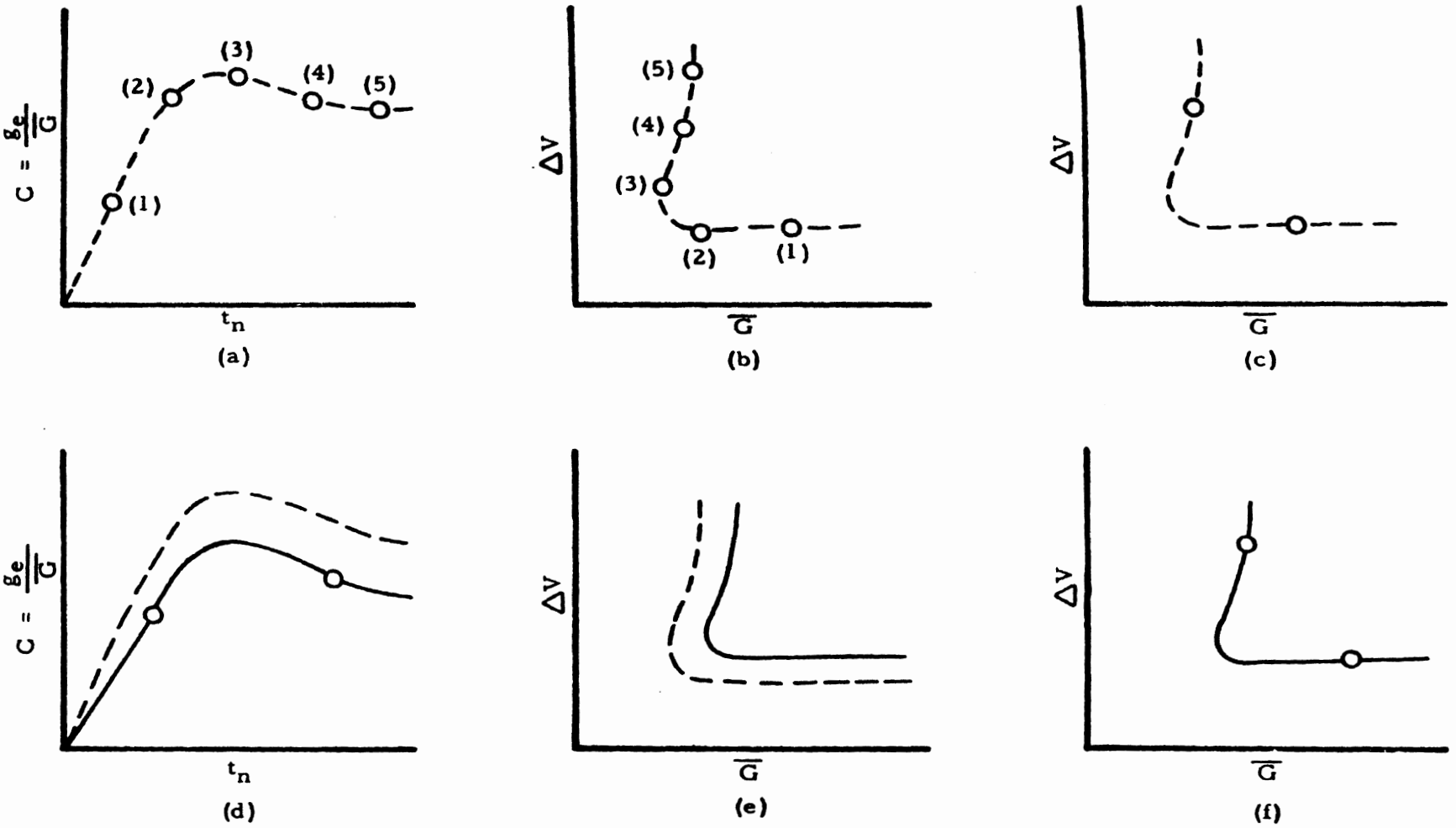


FIG. 35 RESPONSE AND SENSITIVITY CURVES FOR THE TYPE CERTIFICATION OF AIRCRAFT SEAT/LAP BELT SYSTEMS

## CONCLUSIONS

Based on an evaluation of the methods, criteria, and results of both static and dynamic tests of aircraft passenger seats, it is concluded that:

1. Static testing for the type certification of aircraft seats and restraint devices, as specified in the Federal Aviation Regulations and the Technical Standards Orders, cannot of itself be related to crash environments, and, consequently, static test requirements do not correspond to a consistent level of crash severity.

2. Dynamic testing for the type certification of aircraft seats and restraint devices, as governed by the dynamic test criteria established in this report, can be related to crash environments; therefore, dynamic test requirements can be specified in terms of crash severity.

3. Dynamic test methods which demonstrate compliance with dynamic criteria provide a more definitive simulation of the mechanical behavior of the seat/occupant system when subjected to the crash environment. Acceleration-time pulses at the level of the seat leg attachments provide the crash environment inputs allowing the seat/occupant system (seat-anthropomorphic dummy) to respond as a spring-mass system, with the dummy capable of contributing secondary responses such as the bottoming out of the occupant on the seat structure and the reversing of inertia loads due to occupant rebound.

4. Dynamic test methods can be kept relatively simple requiring only basic test facilities, equipment, and instrumentation. The instrumentation should provide the seat leg reaction peaks (peak response level) and any two of the three input variables: velocity change, average acceleration and pulse duration.

# INTERNATIONAL CONFERENCE ON

# VEHICLE STRUCTURES

## I Mech E CONFERENCE PUBLICATIONS 1984–7

Sponsored by The Automobile Division of
The Institution of Mechanical Engineers
and
The Impact Centre, Cranfield Institute of Technology

Co-sponsored by The Institution of Body Engineers
and held under the patronage of
Fédération Internationale des Sociétés d'Ingénieurs
des Techniques de l'Automobiles (FISITA)

Cranfield Institute of Technology
16–18 July 1984

MEP

Published for
The Institution of Mechanical Engineers
by Mechanical Engineering Publications Limited
LONDON

C173/84

# Influence of inertia in structural crashworthiness

S R REID, BSc, MA, PhD, CEng, FIMechE and C D AUSTIN, MSc
Department of Engineering, University of Aberdeen

SYNOPSIS The effects of inertia on the modes of collapse of two classes of structure are described and discussed. Systems of structural elements which have a monotonically increasing load-deflection curve deform under the influence of structural waves when subjected to impact loading. The behaviour of tubular columns is dominated by the effects of instability which are also strongly influenced by the inertia of the structure.

## 1 INTRODUCTION

As a first step in assessing the behaviour of the whole or part of a vehicle structure under impact loading conditions, the quasi-static load deflection characteristics of the structure are often examined (1). In a few cases simple plastic methods of analysis can be used to estimate collapse loads and to calculate load-deflection relationships. For the rest, the data are acquired from programmes of crushing tests.

Quasi-static characteristics are obviously easier to acquire than the equivalent dynamic ones. This is especially so if one is interested in such details as transient loads and geometry which can only be captured using sophisticated instrumentation when the loading is of the type encountered during impact. Despite the different conditions which apply, the procedure of using quasi-static data provides a good initial estimate of the energy absorbing capacity of the critical components especially when some allowance is made to account for the enhancement of the yield stress of the material stemming from the higher strain rates which occur during impact.

The approximation is particularly useful when embodied into computer codes which take into account the presence and distribution of significant concentrated masses in the vehicle structure such as the engine (2). The inertia of such 'rigid' components affects significantly the distribution of deformation within the crushed structure as well as the loads transmitted to the occupants. The main effects of inertia will be modelled by such codes with reasonable accuracy provided that the masses of the 'rigid' components are large compared with those of the deformable components since the latter are usually represented as massless, non-linear springs. However it should be noted that treatments such as that described in (2) often use dynamic enhancement factors to scale the static non-linear spring characteristics attributed to the deformable elements. The source of these factors is sometimes unclear.

Notwithstanding the extensive use of quasi-static characteristics, it is clear from a number of studies that the inertia of the deformable structure itself can have a significant effect during impact. However, depending upon the nature of the structure, inertia influences its transient behaviour in different ways. Because of the complexity of the problem, a general classification of the behaviour of structures under impact load is difficult. Some progress can be made by considering separately those structures whose quasi-static load-deflection curves increase monotonically as shown in Fig.1 (Type I) and those for which the load reduces after reaching some critical value (Type II) as shown in Fig.2. Such a classification has been suggested recently by Calladine and English (3) when discussing two particular components. The work of Calladine and English addresses the important problem of deriving useful data from small-scale models of energy-absorbing structures and show why Type II structures are more sensitive to the effect of impact speed than Type I structures.

Whilst adopting a similar classification in this paper, we wish to draw attention to phenomena which are somewhat different from those discussed in (3). Attention will be directed to *assemblies* of Type I structures in which the shape of the load-deflection curve leads to the hypothesis that deformation results from the initiation, propagation and reflection of a structural shock wave (4), a hypothesis which is supported by the evidence of high speed films (5,6,7). Type II structures include those whose behaviour is dominated by an initial buckling process. These have been considered extensively in the context of vehicle structures and particular attention has been directed to thin-walled tubular components (1,8,11). With regard to the use of this type of structure as an energy-absorber, an overriding consideration is whether or not the structural response is stable. This term needs to be clarified when used in the context of impact energy absorption since it has slightly different connotations from its standard use in structural mechanics. As far as Type II structures are concerned they are all unstable in the sense that the load carrying capacity reduces after the first peak load is

reached. However this does not necessarily mean that the structure is ineffective as an energy-absorber. The performance of a circular metal tube shown in Fig.2 is an example of a buckling structure that in global terms is stable in the sense that its load-deflection curve oscillates about a well-defined mean. It is a particularly efficient energy absorber and has led to a lot of work on the use of thin-walled tubular components of different cross-sectional shapes (structural columns) as energy absorbers.

Thornton et al (11) have discussed the question of the stability of structural columns. In their terminology, instability means a change from an axial crushing mode, which is globally stable in the sense described above, to an Euler buckling mode in which the column bends about a certain cross-section and the load carrying capacity falls away rapidly (see Fig.2). The latter mode of deformation represents poor energy management in terms of the energy absorbed per unit mass of the component. The analysis of quasi-static column stability is complex, as shown in (11). However it is also clear that lateral inertia plays an important role when the axial load is applied dynamically (3,8,9,12). Its effect will be to modify the geometry of the mode of stable collapse as well as the conditions under which instability occurs.

Another aspect of instability is the fact that structural columns are sensitive to the axiallity of the load. Instability (i.e. local bending failure as opposed to progressive collapse) is more likely to occur when the column is loaded obliquely. Clearly one would wish to explore possible ways in which a progressive mode of deformation could be generated for a column under oblique loading in order to improve its energy absorbing capacity. Selective weakening of the column and foam filling are two possibilities which are described below.

In the next section the behaviour of assemblies of Type I structures is described with reference to the occurrence of structural wave propagation. This is followed by a section dealing with certain aspects of the deformation of structural columns. In both cases emphasis is placed upon the phenomenology of the impact behaviour rather than theoretical models, reference being made to the latter where appropriate.

## 2 STRUCTURAL WAVE PROPAGATION

Consider a circular metal tube or ring under lateral loading as an example of a Type I structure. The behaviour of this component and a number of variants of it has been described at length in (7). Fig.1 shows a typical load-deflection curve for a tube crushed between flat plates. Plastic collapse occurs at a load $P_o$ and this is followed by a phase in which the load increases at an ever increasing rate (curve is convex to the deflection axis) as a result of changes in geometry and the effects of strain hardening.

Fig.3(a) shows a sledge apparatus used for high speed crushing of ring systems (5). Fig. 3(b) shows the effect of crushing three different systems of rings by a sledge moving at a speed of approximately 34 m/s. Each system was supported at the left hand end by a rigid surface whilst impact occurred at the other (proximal) end. It is shown in (4) and (5) that the deformation occurs as the result of the propagation of a plastic structural shock wave which passes from ring to ring proceeding from the proximal end to the support where it undergoes reflection and travels part way back along the system until the sledge is brought to rest. The speed of propagation of the shock and the deformation in each ring are governed by the mass of the ring and the shape of load-deflection curve. In (4) a theory is established based upon an analogy with shock wave proagation in metal rods which shows good agreement with the experimental data. The agreement is improved by the inclusion of elastic effects as discussed in a recent paper (13). The significance of the work is that the ring inertia plays a leading role in establishing the pattern of deformation in the system as well as the level of the load pulse transmitted through the system. The structural waves travel at speeds which are of the order of the impact speed which is two orders of magnitude less than typical wave speeds in metals. The deformation does not occur uniformly throughout the system. Rather the deformation occurs element by element which can lead to unusual patterns of deformation as can be seen in the top system in Fig.3(b) where a wrap-around mode has occurred. Similarly when plates are inserted in the system the speed of propagation is altered so that, comparing the lower two systems in Fig.3(b), the distribution of deformation is altered. When the wave is slowed down, more of the deformation is focussed at the impact end, the deformation time is lengthened and consequently (from overall momentum considerations) the mean force exerted on the support is reduced.

Wave effects in the more complex system shown in Fig.4 (a model of a modular crash cushion (6)) have proved beneficial from the point of view of directional sensitivity. Fig.4(a) shows the quasi-static response of a triangular array of rings to a crushing load inclined at $15^{\circ}$ to the axis whereas Fig.4(b) shows the dynamic response at an equivalent level of deformation. Because of the relatively low speed of propagation of structural wave through the system, the distribution of deformation is significantly different. Under quasi-static loading there appears to be a 30% reduction in energy absorbing capacity when the load is applied obliquely to the system. When the system is crushed dynamically this reduction is not apparent. The different mode of deformation leads to more extensive deformation of those elements close to the point of impact and, because the load-deflection curve is non-linear, to a greater amount of energy absorption by these elements compared with their contribution in the quasi-static case. The inertia effects therefore compensate for the apparent directional sensitivity, a result which has been confirmed in full-scale testing of these systems.

With regard to vehicle structures as opposed to vehicle arresting systems, the tubular ring energy absorber shown in Fig.5 is interesting since it shows a similar pattern of deformation to that of the top system in Fig.3(b). It consists of six layers each of which is made up of four sections of metal tubes

welded together to form a square (see Fig.5(c)). Under lateral compression the tube sections crush but provide mutual constraint which leads to higher collapse loads and greater energy absorption capacity than a single tube of equal length. The static load-deflection curve for a single tube is shown in Fig.6(a). The deformation of the system shown in Fig.5(b) followed impact by a 82kg mass travelling at 10.5 m/s which led to a 25% reduction in the height of the system. On the assumption that the response is quasi-static an increase in load of 33% over the initial collapse load would be anticipated whereas the load trace shown in Fig.6(b) shows a fairly uniform load transmitted to the base on which the system is mounted. This is clearly a function of the mode of deformation. A form of wrap-around is evident in this system and leads to non-uniform deformation from layer to layer. It should be noted that an initial transmitted load of 60 kN is attained compared with a quasi-static collapse load of 33 kN. This is principally due to the effect of strain rate on the yield stress of the material.

These examples demonstrate that the internal exchange of momentum within the system which leads to these wave-like responses can have significant effects on the transmitted forces as well as the overall energy absorbing capability of the system.

## 3 AXIAL AND OFF-AXIAL LOADING OF TUBULAR COLUMNS

The effect of loading rate on the response of some simple Type II structures has been investigated both experimentally and theoretically. The more complete treatments have been given for simple struts (including edge loaded plates) (3,8,12) and circular metal cylinders under axial loading (9) (see also (1)).

As far as non-circular tubular columns are concerned, Postlethwaite and Mills (9) make some interesting comments about tubes of rectangular cross-section under axial impact. At high impact velocities short wavelengthcrumpling occurs at the proximal end followed by longer wavelength buckles whereas under static loading similar tubes failed in an Euler buckling mode. The authors have obtained similar results recently, the onset of bending instability being delayed by the effect of lateral inertia (see Fig.7(a) and (b)).

Thornton et al (11) give a detailed account of the behaviour of tubular columns under quasi-static loading and draw attention to the question of instability as defined in the Introduction. Whilst this is a major consideration from the point of view of producing a reliable design, it is clear that stability under axial loading is improved when the loads are applied dynamically. Attention is drawn to this fact in (11) and reference is made to a paper by Thornton and Dharan (14) in which the change of collapse mode under dynamic loading is discussed.

One way of improving the stability of rectangular tubular columns is to use foam filling as can be seen in Fig.7(c). The presence of the polyurethane foam produces a substantial increase in the mean collapse load as well as a stable mode of crushing. A full account of the response of tubular columns to axial impact will be described in a future paper.

Finally the question of off-axial or oblique impact of tubular columns is briefly considered. With regard to car front structures a lot of emphasis has been placed on the use of tubular columns to provide the prime means of impact energy absorption. Provided that the impact is head-on, longitudinal tubular columns respond well. However if the impact occurs at an angle to the axis of the vehicle, e.g. a corner impact on the front of the car, then much of the energy absorbing capacity may not be realised. A longitudinal column will fold in an Euler-type isolated hinge mode which is inefficient in terms of total energy absorption.

Recently the authors have explored the possibility of generating progressive modes of collapse in tubes by introducing slots in the tube on the side closest to the impact barrier as shown in Fig.8. Once more inertia controls the propagation of a bending wave along the tube. In model impact tests performed using the sledge apparatus shown in Fig.3(a), slotted aluminium tubes fixed at an angle into sledges were fired at a rigid barrier over a range of velocities. On impact the tip of the tube bends inwards towards the barrier whilst the supported end remains undeformed. Progressive bending occurs down the tube during which a substantial fraction of the kinetic energy is absorbed before root rotation finally occurs. It should be noted that equivalent static tests result in simple bending about the supported end, inertia is an essential feature of the dynamic mode of deformation. For comparison, the response of an unslotted tube is shown in Fig.8(b). Whilst a degree of deformation occurs at the impact end due to the effect of friction, this is minimal. The proximal end slides along the barrier and root rotation occurs. It should be noted that axial impact of slotted tubes results in a similar mode of collapse to that shown in Fig.8(a) and the available energy is absorbed in a stable and satisfactory manner.

The use of selective weakening of the sort described above would appear to be an effective way to cope with off-axial loading of tubular columns because of the effects of inertia in controlling the axial transmission of bending deformation.

## 4 DISCUSSION AND CONCLUSIONS

Some of the effects of inertia in the crushing of two major types of structure have been described. It should be noted that the dynamic nature of the loads on the structures will also produce yield stress enhancement due to the strain rate sensitivity of the material. A comparison of the relative importance of inertia and strain rate effects is complex even for relatively simple structures. Such considerations have been made for a Type I structure by Reid and Bell (13) and for a Type II structure by Calladine and English (3).

The examples given above illustrate some of the significant effects that inertia has on the

gross deformation of metal structures. For Type I structures the finite time it takes for deformation to propagate through such structures plays a key role in determining the nature of the deformation mode as well as the amplitude and duration of the transmitted force pulse. The control of the deformation by the insertion of discrete masses provides one way of tuning the system to give a preferred mode of collapse.

Tubular columns particularly of rectangular section are commonly used in vehicle structures. The problem of instability often leads to the use of relatively thick-walled components. It is clearly of interest to establish the ways in which the combination of inertia effects, selective weakening and perhaps foam filling influence the behaviour over a range of loading conditions in the search for efficient energy absorbing structures especially for small cars.

## 5 ACKNOWLEDGEMENTS

The authors wish to express their thanks to Dr. C.R. Calladine and Mr. R.W. English for a copy of reference (3) and to Mr. R. Smith and Mr. M.D. Gray for conducting experiments on the tubular rings and rectangular tubes respectively. Support from the Departments of Energy and Transport through a grant administered by the Transport and Road Research Laboratory is gratefully acknowledged as is support from NATO (Grant 04981).

## REFERENCES

(1) JOHNSON, W. and REID, S.R. Metallic Energy Dissipating Systems, Applied Mechanics Review, 1978, 31, 277-288.

(2) EMMERSON, W.C. and FOWLER, J.E. The application of computer simulations in vehicle design, Proceedings 5th International Conference on Experimental Safety Vehicles, London, U.S. Department of Transportation, U.S. Government Printing Office, Washington DC (050-003-00210), 712-720, 1974.

(3) CALLADINE, C.R. and ENGLISH, R.W. Strain rate and inertia effects in the collapse of two types of energy-absorbing structure, to be published, Int. J. Mech. Sci., 1984.

(4) REID, S.R., BELL, W.W. and BARR, R.A. Structural plastic shock model for one-dimensional ring systems, Int. J. Impact. Eng., 1983, 1, 175-191.

(5) REID, S.R. and REDDY, T.Y. Experimental investigation of inertia effects in one-dimensional metal ring systems subjected to end impact. I: Fixed ended systems, Int. J. Impact. Eng., 1983, 85-106.

(6) CARNEY, J.F., AUSTIN, C.D. and REID, S.R. Modelling of steel vehicular crash cushion, J. Transportation Engineering, A.S.C.E., 1983, 109, 331-346.

(7) REID, S.R. Laterally compressed tubes as impact energy absorbers, Structural Crashworthiness, ed. N. Jones and T. Wierzbicki, Butterworths, London, 1983, 1-43.

(8) POSTLETHWAITE, H.E. and MILLS, B. Use of collapsible structural elements as impact isolators, with special reference to automotive applications, Part 1 : Development of an impact analysis for struts, J. Strain Analysis, 1970, 5, 58-64.

(9) POSTLETHWAITE, H.E. and MILLS, B. ditto, Part 2 : Impact analysis of sheet metal structures, J. Strain Analysis, 1970, 5, 65-73.

(10) WIERZBICKI, T. Crushing behaviour of plate intersections, Structural Crashworthiness, ed. N. Jones and T. Wierzbicki, Butterworths, London, 1983, 66-95.

(11) THORNTON, P.H., MAHMOOD, H.F. and MAGEE, C.L. Energy absorption by structural collapse, Ibid, 96-117.

(12) ABRAHAMSON, G.R. and GOODIER, J.N. Dynamic flexural buckling of rods within an axial compression wave, J. Appl. Mech., 1966, 33, 241-247.

(13) REID, S.R. and BELL, W.W. Response of one dimensional ring systems to end impact, 3rd Int. Conf. on the Mechanical Properties of Materials at High Rates of Strain, Oxford, 9-12 April, 1984.

(14) THORNTON, P.H. and DHARAN, C.K.H. The dynamics of structural collapse, Mat. Sci. and Engineering, 1975, 18, 97-106.

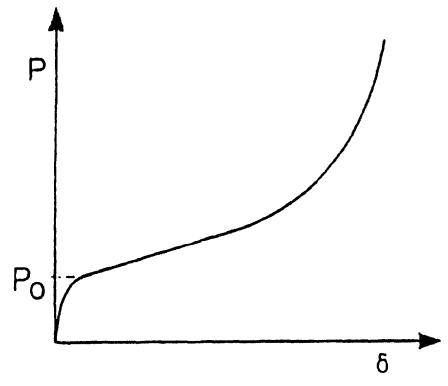


Fig 1 Type I structure – monotonically increasing load–deflection curve

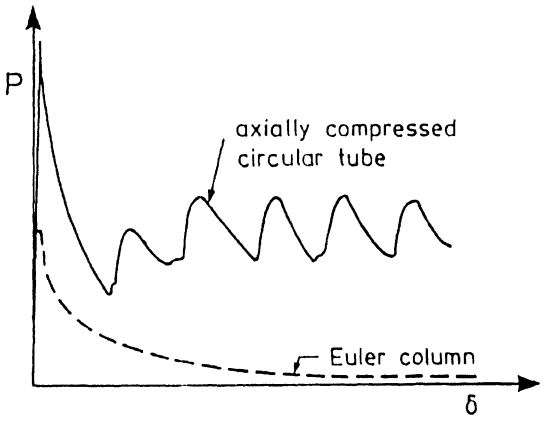


Fig 2 Type II structures – initial buckling followed by stable post-buckling (axial buckling of circular tube) or unstable (Euler column) behaviour

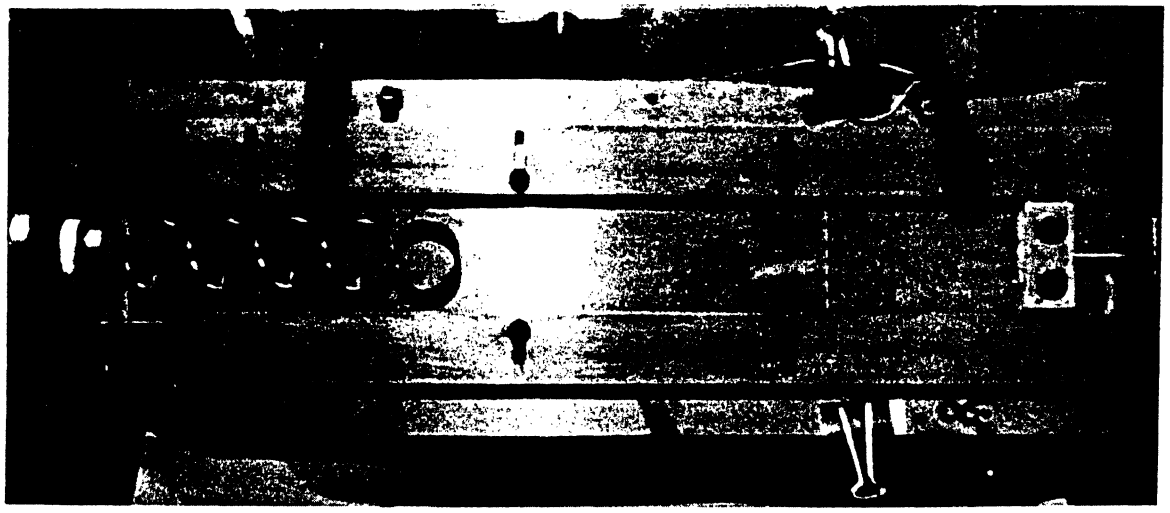

Fig 3(a) Sledge apparatus for high speed compression tests (see (5))

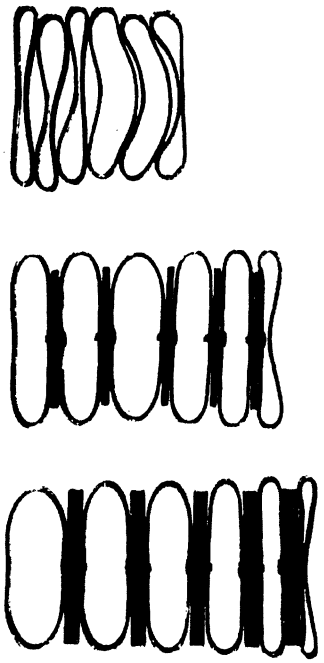

Fig 3(b) Free ring system and two plated systems (see (5))

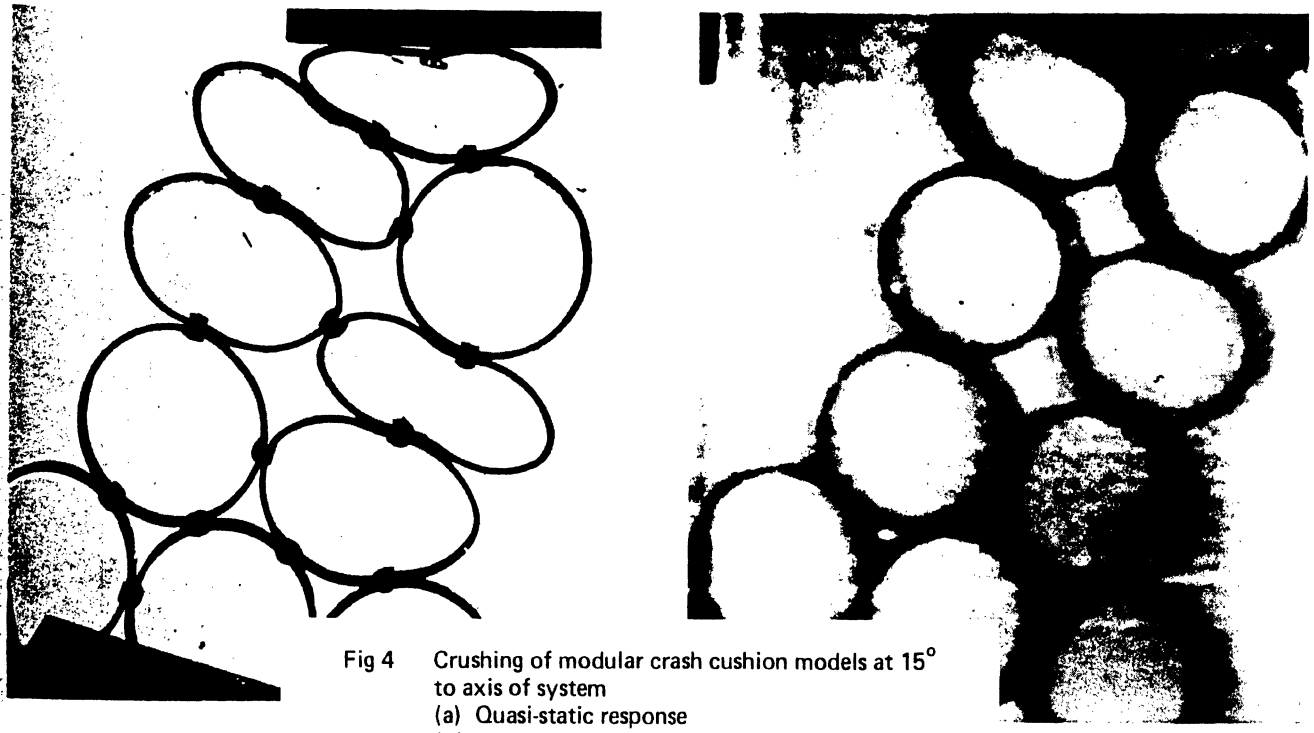

(a) (b)

Fig 4 Crushing of modular crash cushion models at 15° to axis of system
(a) Quasi-static response
(b) Dynamic behaviour

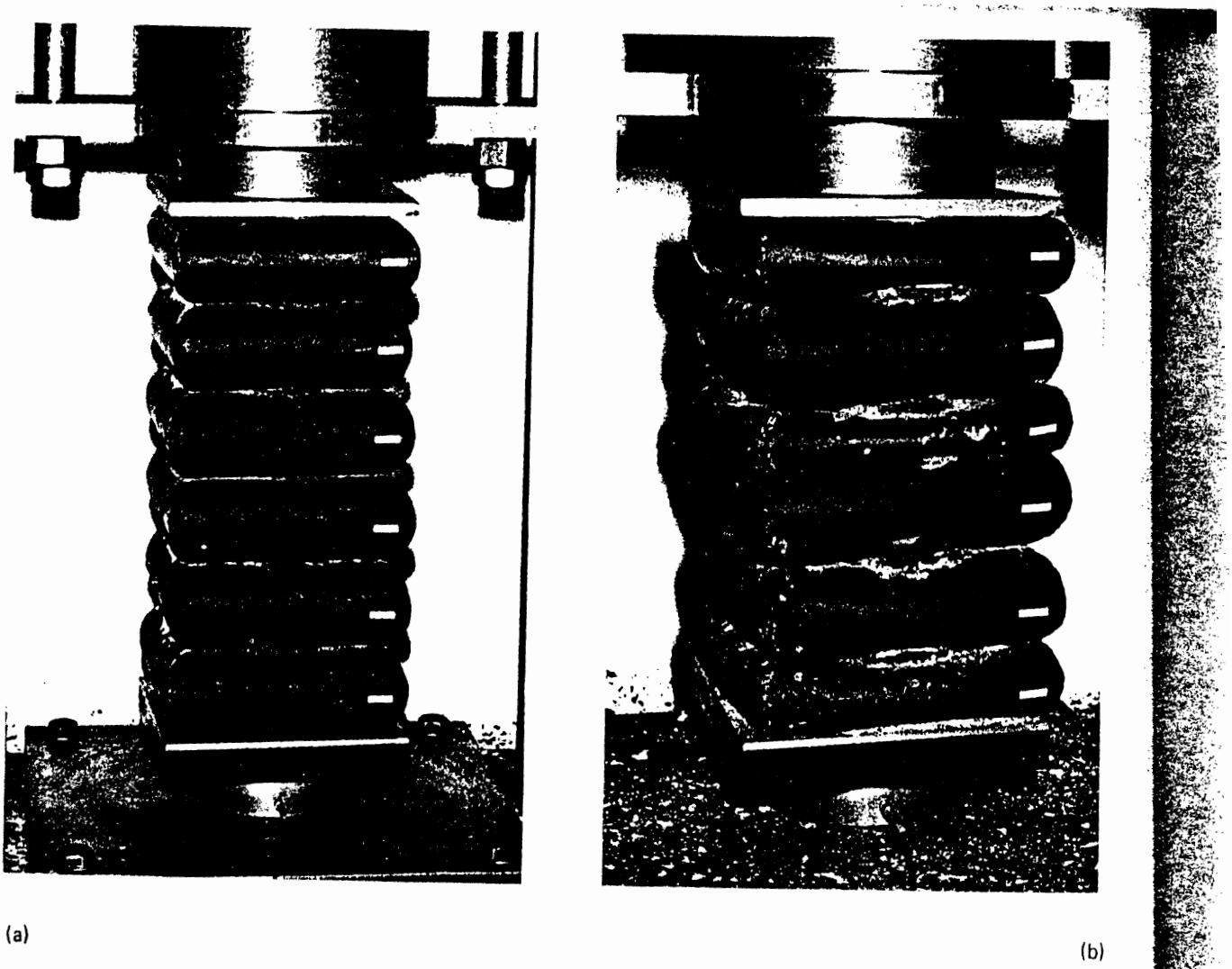

(a)

(b)

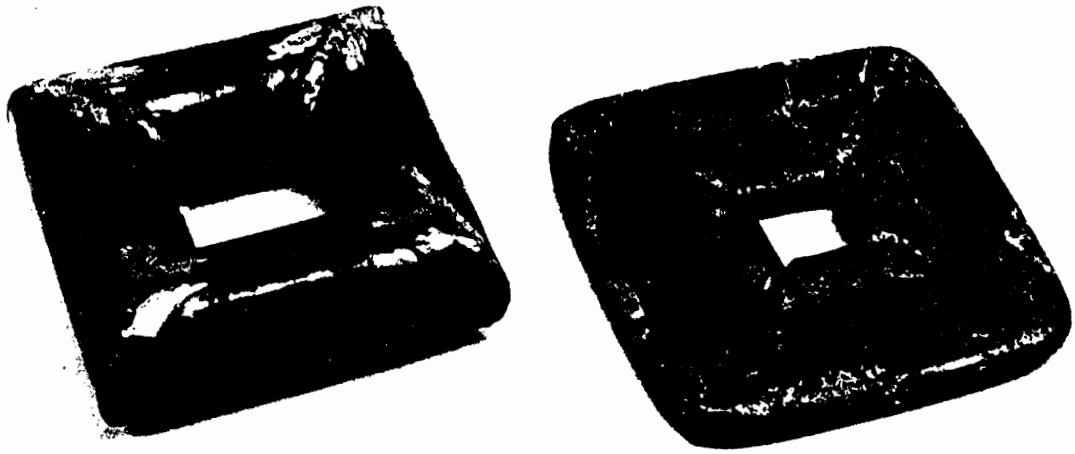

(c)

Fig 5 Six-layer tubular ring system
(a) Before impact
(b) After impact
(c) Single tubular ring before and after ring impact

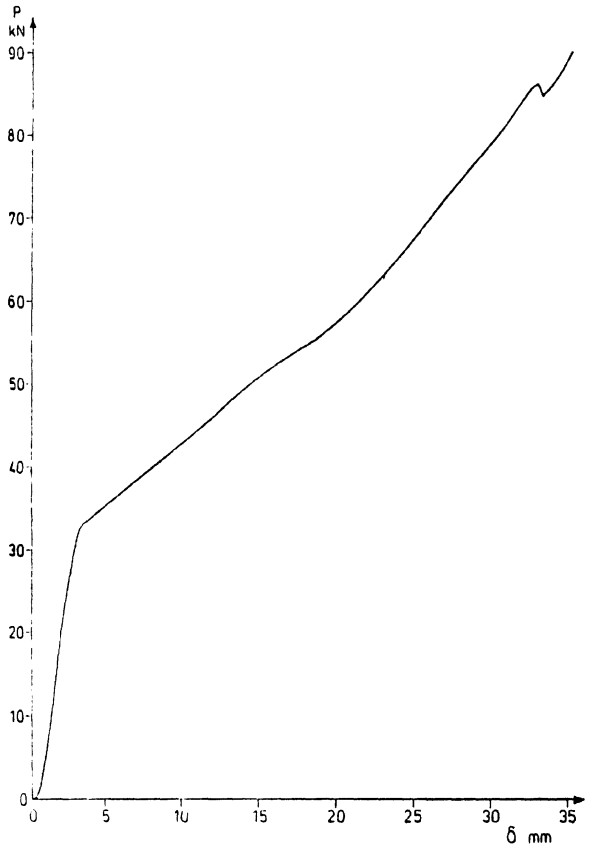


Fig 6(a) Quasi-static load-deflection curve for tubular ring (50.8mm diameter tube)

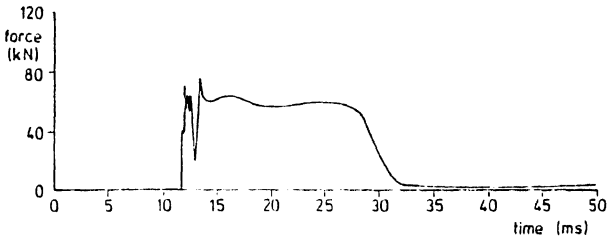


Fig 6(b) Load-pulse transmitted to load-cell in base of system shown in Fig 5(a)

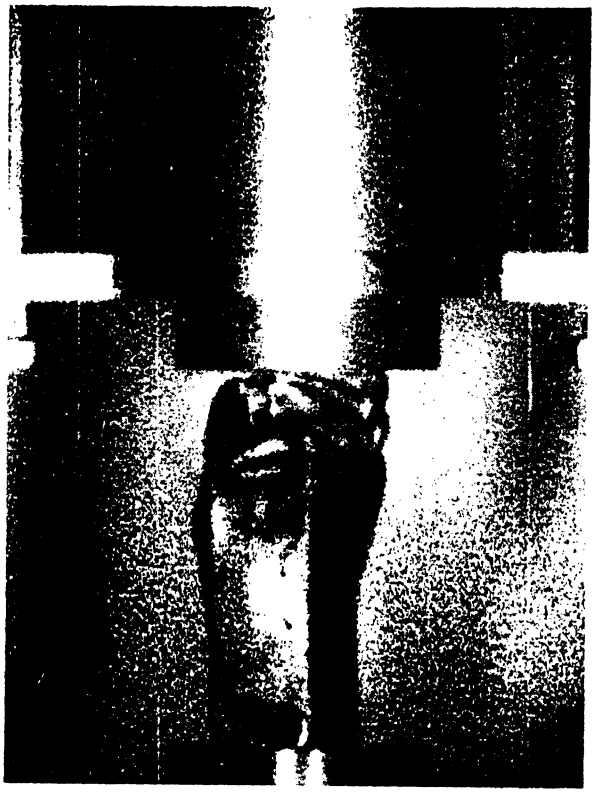

(b)

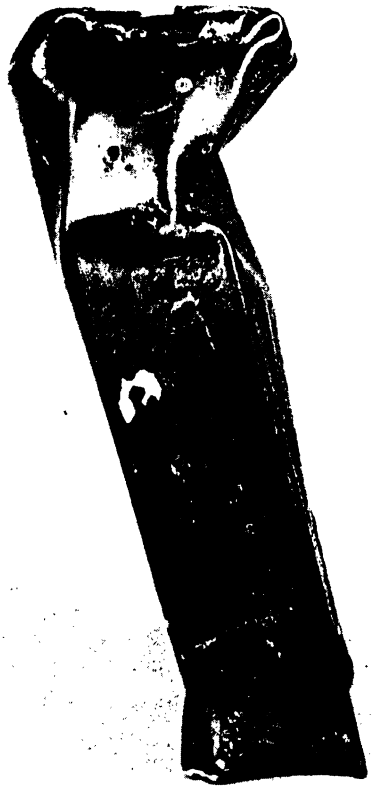

(a)

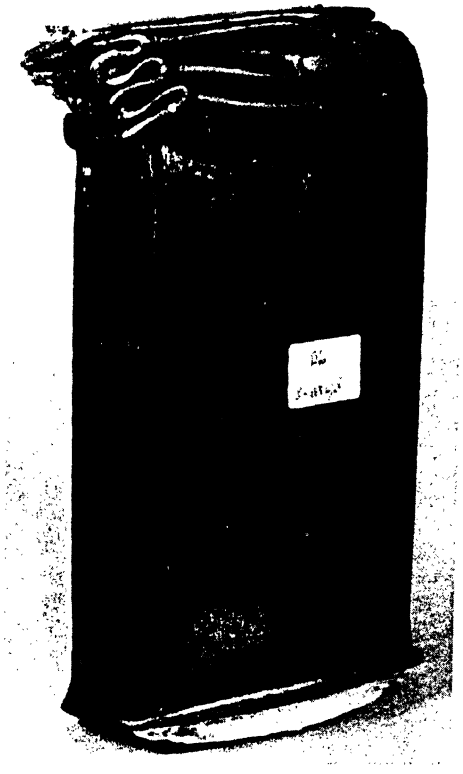

(c)

Fig 7 Rectangular cross section thin-walled sheet metal tubes under axial loading (section 101.6 mm x 50.8 mm, 1 mm wall thickness)
(a) Quasi-static mode of collapse
(b) Still from high-speed film of axial impact test
(c) Final state of foam-filled tube (foam density = 188 kg/m$^3$

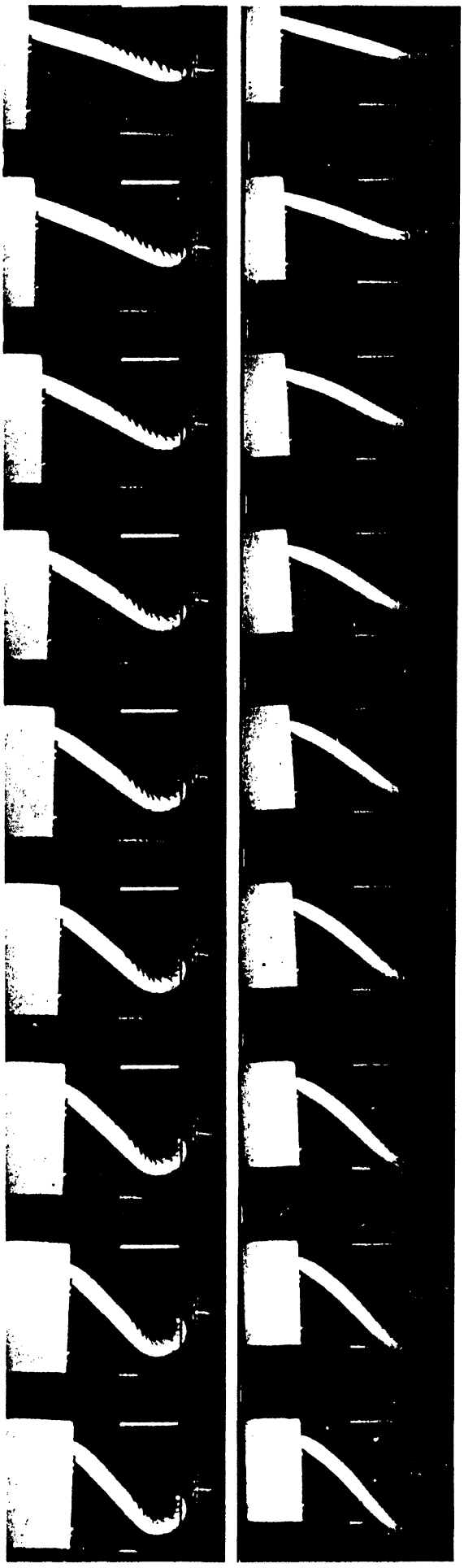

(a) (b)

Fig 8 Oblique impact of aluminium tubes
(a) slotted
(b) plain tubes



5

**Sponsored by:**
The U.S. Department of Transportation

**Hosted by:**
The U.K. Department of the Environment
and
The Society of Motor Manufacturers and Traders, Ltd.

**Held at:**
London, England
June 4 - 7, 1974

# FIFTH INTERNATIONAL TECHNICAL CONFERENCE ON EXPERIMENTAL SAFETY VEHICLES


U.S. DEPARTMENT OF TRANSPORTATION
NATIONAL HIGHWAY TRAFFIC
SAFETY ADMINISTRATION





For sale by the Superintendent of Documents
U.S. Government Printing Office, Washington, D.C. 20402
Price $10.20 Stock Number 050-003-00210

# THE APPLICATION OF COMPUTER SIMULATIONS IN VEHICLE SAFETY

W. C. EMMERSON
*Manager, Engineering Development*
J. E. FOWLER
*Project Leader*
British Leyland Motor Corporation Limited

## INTRODUCTION

In the development of a new vehicle numerous experimental tests have to be carried out to ensure acceptable performance in all respects, and this requires the production of many expensive prototype vehicles. Fortunately much of the performance testing is non-destructive and therefore a particular prototype can be used for a number of different purposes. However, in the case of safety requirements many of the tests are destructive in nature, and each new requirement can seriously effect the development lead time and cost. It was therefore decided that there was a need to develop techniques which were basically non-destructive, so that assessments could be made of various design schemes to ensure that new models would comply with future safety requirements.

The approach adopted at British Leyland in 1968 was to develop computer systems which simulate the various safety performance requirements. These systems would enable an assessment to be made of the survival criteria for pedestrians, vehicle occupants and the vehicle structure. Some of the computer programs developed have been used in the joint work undertaken with the Transport and Road Research Laboratory (T.R.R.L.), and reference is made to this work in the paper to be presented by P M Finch (Ref. 1). The present paper elaborates on the various simulation models which have been developed, and illustrates their application to the safety projects undertaken with T.R.R.L.

All the computer programmes for assessing the structural performance of the vehicle have been developed in British Leyland and include the analysis of Front, Rear and Side impacts. Using the various vehicle simulation models, assessments can also be made of vehicle to vehicle impacts under any combination of these three impact conditions. In the analysis of occupant and pedestrian survival criteria it has been found that the Calspan program (Refs. 2 and 3) is suitable, and in the case of occupant analysis the input information used is the output from the vehicle impact simulation programmes in terms of deceleration/time characteristics.

The project work undertaken jointly between T.R.R.L. and British Leyland, which is described in (Ref. 1) was all based on developments of the Morris Marina. The simulation models and results presented in this paper are also based on this vehicle, although other vehicles have been analysed in a similar way.

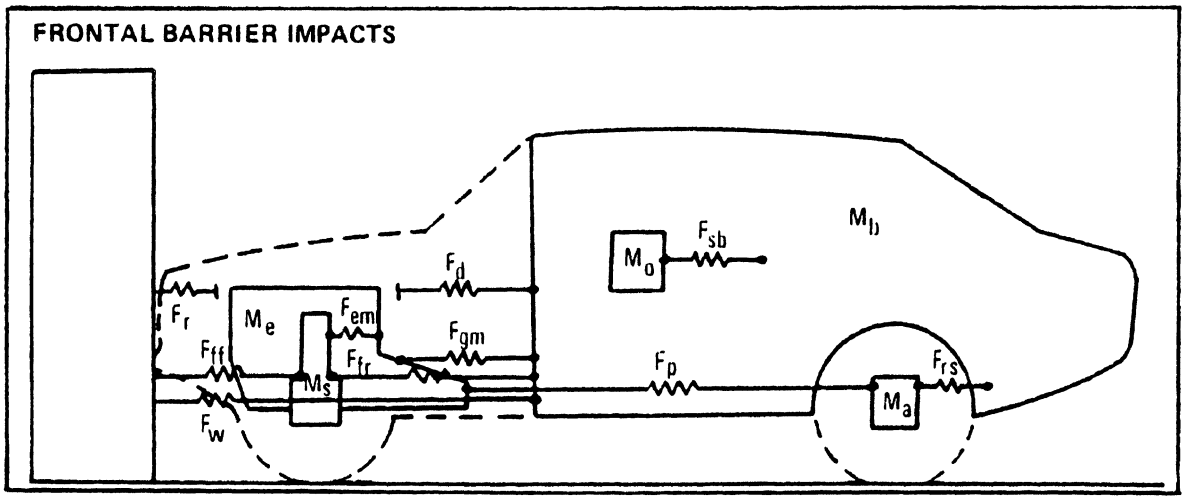


*Figure 1. Frontal Barrier Test. Simulation model of standard Morris Marina*

The mass distribution of the Marina was analysed and divided into a number of well defined and where possible discrete masses. These masses were considered to be connected by non-linear, plastically deforming "spring" elements representing parts of the structure. The idealized model of the standard Marina is shown in Figure 1. (The notation used is described in the Appendix). For this model the equations of motion, on which the simulation programme is based, are as follows:–

$$M_b\ddot{x}_b + F_w + F_d + F_{gm} + F_{fr} + F_{rs} + F_{sb} = 0 \quad . \quad . \quad . \quad (1)$$

$$M_o\ddot{x}_o - F_{sb} = 0 \quad . \; . \; . \quad (2)$$

$$M_e\ddot{x}_e + F_{em} + F_r - F_d - F_{gm} - F_p = 0 \quad . \; . \; . \quad (3)$$

$$M_a\ddot{x}_a + F_p - F_{rs} = 0 \quad . \; . \; . \quad (4)$$

$$M_s\ddot{x}_s + F_{ff} - F_{fr} - F_{em} = 0 \quad . \; . \; . \quad (5)$$

The forces in the equations (1) to (5) represent the dynamic forces produced instantaneously during the impact, and are functions of the relative displacement between the masses (i.e. relative crush) and the rate of crush. The following empirical relationship is used to relate the dynamic forces to the static crush characteristics:–

$$F_{dynamic} = F_{static}\left[1 + \lambda \frac{\dot{x}}{Vo}\right] \qquad \text{where } \lambda \text{ is}$$

the "dynamic magnifier", $\dot{x}$ is the rate of element deformation and Vo is the reference velocity at which $\lambda$ has been determined. The value of $\lambda$ varies for different types of construction and for different parts of the structure. The actual values used are usually based on previous comparisons between theory and experiment.

In the case of the standard base line Marina the static stiffness of the "spring" elements were determined experimentally by slow crushing in a specially designed crush rig (Ref. 1). Figure 2 shows a typical stiffness characteristic which in this case is for the Marina front end forward of the front wheel centre line.

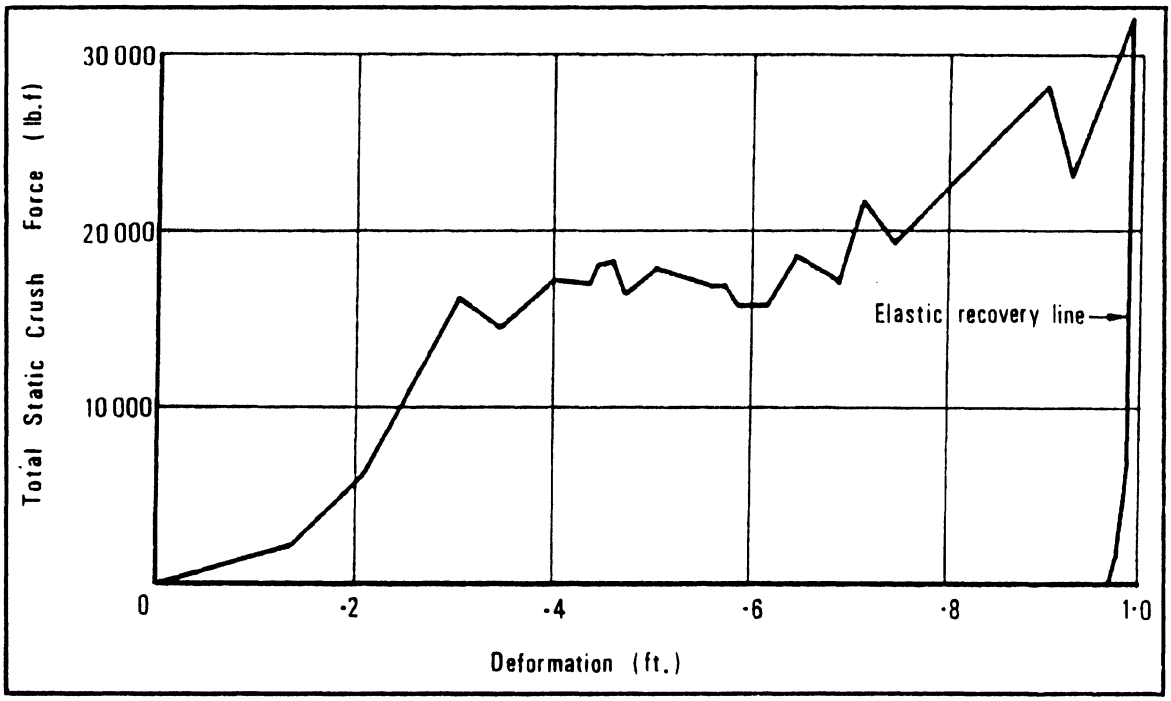


*Figure 2. Stiffness Characteristic of Morris Marina Front Half of Front End*

This graph clearly shows the inherent non-linearity of the structure, which is the main reason why normal analytical techniques are not adequate, and why a mathematical model of the system must be made for use in a computer simulation.

A flow diagram for the complete programme is shown in Figure 3. The most critical part of the programme, and the part that largely determines its success, is in the calculation of the dynamic forces. The measured static characteristics are input to the computer in a tabular form. The instantaneous static force is then calculated from the relative displacement and modified according to the rate of crush. The rebound characteristic is equally important and its position varies according to the maximum displacement reached. The rebound point is detected by the point at which the vehicle velocity is zero. Each component force is determined in a subroutine (Macro). A series of these routines have been written to cover most of the different types of structural elements that could be encountered. These were developed independently to the main programme. Furthermore, these subroutines can be used for any type of vehicle impact simulation and are not restricted to frontal impacts.

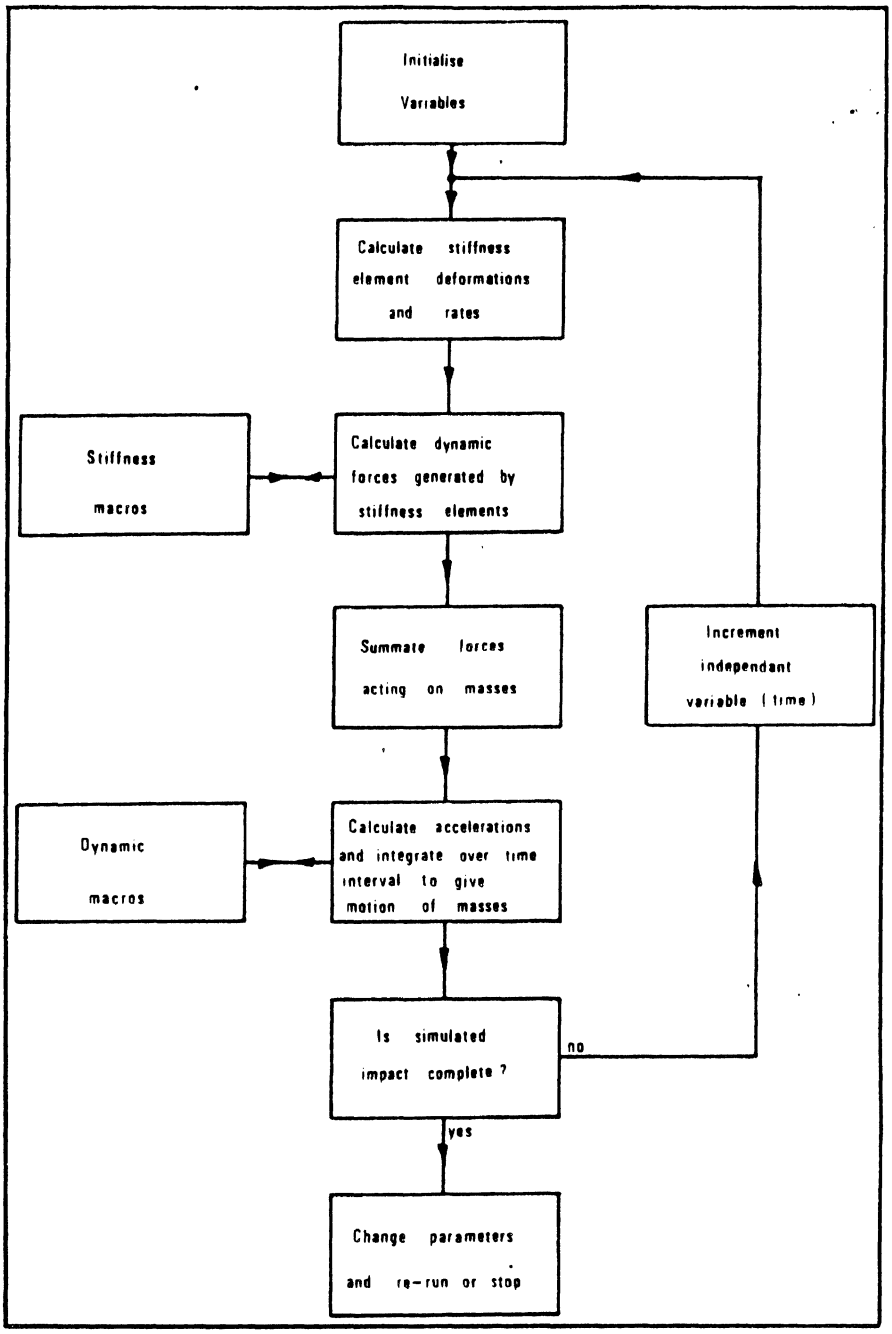


*Figure 3. Basic Program Flow Diagram*

The output from the programme can be any of the displacements, crush distances, velocities, accelerations or forces specified as variables and these can be plotted if required.

The occupants are represented by a single mass restrained by a single stiffness element as shown in Figure 1. This is obviously a simplification of real occupants, but its purpose is to approximate the effects of the occupants on the crashing vehicle and not vice versa. For accurate simulation of the effects on the occupants a separate occupant simulation programme is available which uses the vehicle simulation results as input data. The simplified representation of the occupants does give, however, an indication of how near to the optimum is the shape of the vehicle deceleration envelope. The occupants' peak acceleration being regarded as a vehicle "severity index".

A more detailed and technical description of the simulation techniques employed can be found in (Ref. 4).

Static crush tests were conducted on the standard Marina and the simulation model validated against the results of a barrier test. A comparison of the computer simulated and experimental test deceleration plots is shown in Figure 4. Once satisfactory results had been achieved the proposed changes to the standard Marina could be evaluated with the programme.

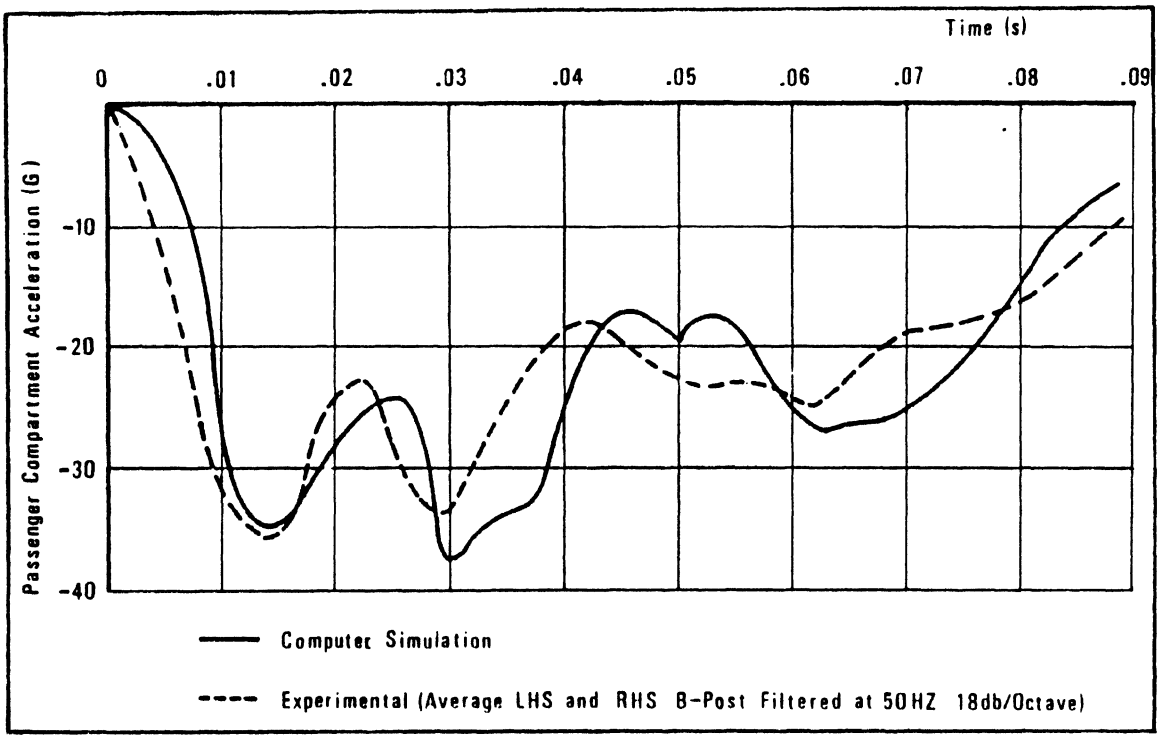


*Figure 4. Comparison of Results for a 40 mph Frontal Barrier Test on a Standard Morris Marina*

The main vehicle modifications considered were:–

a Front end structure incorporating curved longitudinals.
b Increased engine to dash clearance.
c Increased dash and tunnel stiffness.
d Hydraulic low speed bumper system.
e "Metalastik" and deformable cylinder bumper system.
f "Cable Belt" bumper system.
g Independent rear suspension.
h One-piece versus two-piece propeller shaft.
i Engine restraint systems for low speed impacts.
j Wheelbase increase by moving front wheels forward.
k Waist level longitudinal rails in doors.

Various combinations of these changes were simulated, in some cases the advantages gained by one modification would be reduced by the interaction with the effects of another. Based on these simulation results it was decided to build the first modified vehicle (Phase I) to include modifications (a), (b), (c), (f), (i) and (k) given above. It should be noted that the effects of the modifications evaluated were specific to the modified Marina and may not be desirable for vehicles with different stiffness or mechanical layouts. The simulation model representing the vehicle in the Phase I condition is shown in Figure 5, and the comparison of the simulated and experimental results is shown in Figure 6. The close agreement between these results indicates the usefulness of the simulation technique during the design of the vehicle. An important advantage is the exact repeatability obtained and the facility to change one variable at a time while the others remain exactly constant. This is extremely difficult with experimental testing due to the inherent scatter in results.

The above list of modifications (a) to (k) include both high speed and low speed design features. The high speed requirements are basically concerned with occupant survival, whereas the low speed features are to minimise vehicle damage. It is of interest to describe further some of the work on low speed impacts.

Bumper system evaluation was simulated using a model similar to that shown in Figure 5, but with a freedom for engine pitch included. With low speed no damage impacts the restraint of the engine is equally as important as the design of the bumper and back-up system itself. Forward acting engine restraints are necessary to prevent the engine penetrating the radiator and possible damage to the engine mountings. The type of restraint and its point of reaction on the engine is of prime importance and this

SAE Technical Paper Series

810475

# Static-to-Dynamic Amplification Factors for Use in Lumped-Mass Vehicle Crash Models

Priyaranjan Prasad
and Arvind J. Padgaonkar
Ford Motor Co.

International Congress and Exposition
Cobo Hall, Detroit, Michigan
February 23-27, 1981



SOCIETY OF AUTOMOTIVE ENGINEERS, INC.
400 COMMONWEALTH DRIVE
WARRENDALE, PENNSYLVANIA 15096

# Static-to-Dynamic Amplification Factors for Use in Lumped-Mass Vehicle Crash Models

**Priyaranjan Prasad and Arvind J. Padgaonkar**

Ford Motor Co.

IN ORDER to reduce expensive and time-consuming crash tests in the early design/development stages of a vehicle, simple, lumped-mass mathematical models were developed by Kamal (1)* and Battelle Columbus Laboratories (2). Although these models are collinear, therefore one dimensional, they have proven to be useful tools in studying the effect of mass and stiffness change of the various structures undergoing collapse in frontal barrier crashes on the crash response of the passenger compartment.

The lumped mass models consist of rigid masses representing the passenger compartment, engine, cross-member, and bumper for frontal mode. The rigid masses are connected by energy-absorbing elements representing the frame, sheet metal, firewall, driveline, radiator, etc. The crush characteristics of the various energy absorbers used in the model are generally obtained by static crush tests of the elements. In order to be able to use the statically obtained crush data for the dynamic simulation, a transformation is required to account for deformation rate effects. Therefore, the key to the use of the lumped-mass models is in obtaining (a) valid static force-deflection relationships and (b) the static-to-dynamic transformations for the various energy absorbers used in the models. The valid static force-deflection relationships are obtained by

*Numbers in parentheses designate References at end of paper.

## ABSTRACT

One-dimensional, lumped-mass models for predicting the dynamic response of vehicles in crashes have been used extensively in recent years. The energy-absorbing characteristics, i.e., the load/deflection data, for use in the models are determined from static crusher tests of actual vehicle components. In order to account for the crush rate effects on the structure, a transformation is needed to extrapolate the statically obtained data to the dynamic case. The transformation factors -- the static-to-dynamic amplification factors -- are empirically derived and have been reported by some investigators to be linearly and by others to be logarithmically related to crush rate. This paper reports on the development of dynamic amplification factors for vehicles with framed structures, e.g., light trucks and S-framed cars, and unibody cars. The factors were developed by exercising lumped-mass models with various forms of dynamic amplification factors and comparing the model results with results from crash tests. The factors that best explained the crash tests are different for different construction vehicles.

0148-7191/81/0223-0475$02.50

carefully matching the crush modes produced during the static crush tests with those observed during full-scale crash tests. However, considerable variations in approach exist in determining the static-to-dynamic transformation factors. Some organizations use logarithmic factors and some use linear factors to account for the deformation rate effects. There is also a considerable difference in the magnitude of the factor used. The determination of these factors has been essentially an empirical process based on comparisons of model results with crash test results.

This paper reports on the authors' experience with the use of a modified Battelle crash simulation model in conjunction with static crush tests and the development of static-to-dynamic transformation factors. During this study, static crush and dynamic crash tests of various unitized body and S-frame vehicles were studied. Also studied were four vehicles utilizing frames constructed from open C-sections.

The first part of this paper reports on an extensive literature review carried out with emphasis on crush rate effects on structures. The second part of the paper describes the methodology used for determining the crush rate effects on automobile structures.

## LITERATURE REVIEW

A review of the literature shows that there are two main factors affecting the behaviors of structures under impact loading. The first factor is the sensitivity of material properties to strain rate. The second factor is the effect of wave propagation and inertial effects within the structure itself.

## MATERIAL STRAIN RATE SENSITIVITY STUDIES

The experiments performed by Manjoine (3) showed that the values of yield point strain depend upon the rate of strain. The results of his experiments showed that not only the yield point but also the ultimate strength and the total elongation depended on the strain rate. In general, these quantities increased with increases in strain rates. For mild steels, the yield point was elevated from around 28,000 psi (193 MPa) at $9.5 \times 10^{-7}$ per sec. strain rate to around 75,000 psi (517 MPa) at 300 per sec. strain rate.

More recent investigations into the strain rate effects of steel have been reported by Lake and Grenawald (4) and Saxena and Chatfield (5). The strain rate effect of various materials, including steel, has also been reported by Davies and Magee (6). Under the loading conditions investigated, a logarithmic relationship was found between tensile strength and strain rate. The sensitivity of yield strength to strain rate decreased with increasing quasi-static yield strength. Results of Lake and Grenawald (4) show that the rate sensitivity, as measured by the ratio of the yield strength at the highest and the lowest strain rates (static), varies from around 1.1 for steels with 130 ksi (896 MPa) static yield strength to around 2.15 for steels with 28 ksi (193 MPa) static yield strength. Based upon the above studies, it would seem that tensile static and dynamic tests performed on the materials used in manufacturing the vehicles would give sufficient data for the "dynamic amplification factors" to be used in mathematical models of the type being considered in this report. The validity of using tensile test data in complex bending tests was demonstrated by Davies and Magee (7). Also, tests performed on collapse characteristics of corrugated tubular sections by Thornton (8) have shown that the dynamic response of such structures is governed by the strain rate sensitivity of the material. The structural rate effects do not affect the collapse process because the geometry of the design predetermines the locations for the formation of plastic hinges. However, earlier tests on tubular structures by Macaulay and Redwood (9) where the crush modes were not predetermined -- as in the structures tested by Thornton (8) -- showed that the material strain rate sensitivity could not explain the increase in energy absorption observed in the dynamic tests. More recent tests on tubular structures by Vankuren and Scott (10) also show the trends observed by Macaulay and Redwood (9). Therefore, it appears that the inertial rate effects are important in structures in which the crush modes are not predetermined by design.

## STRUCTURAL RATE EFFECT STUDIES

The effects of wave propagation and inertia of a structure during dynamic collapse have been studied by several researchers. An exhaustive review of such studies has been reported by Thornton and Dharan (11). Of particular importance to our study is the result of several investigators that during dynamic buckling of columns, lateral inertia forces of the column prevent excessive deflections even when the axial forces exceed the Euler buckling loads. Therefore, it is possible to exceed the buckling loads observed in static tests during the dynamic buckling process. The implication of the above result is that the force-deflection re-

lationship determined statically may not be valid dynamically even if the material strain rate effects are taken into account. Also, important is the dependence of the buckle wavelength on impact velocity (9) in thin-walled tubular structures during the dynamic crumpling process. The structural rate effects have been studied on simple structures experimentally and theoretically. Very little data are currently available on automobile-type structures. The impact response of curved box beam-columns was studied by Ni (12) both experimentally and theoretically with a mathematical model. It is not clear whether the data from the above study can be extrapolated to all thin-walled structures and sheet metal commonly used in automotive construction. It is expected that with the development of large deformation, elastic-plastic finite element/difference models, the structural rate effects can be studied.

## RATE EFFECTS IN AUTOMOTIVE-TYPE STRUCTURES

The few studies on full-scale automobile collisions that are available are generally at 30 mph (48 km/h) and the conclusions regarding rate effects may be valid only for the speed tested. Of the two common rate factors in use, one is linear and the other logarithmic in shape. Both account for a 30 percent increase in energy absorbed from the static case to the dynamic case at 30 mph (48 km/h) impact velocity. The linear factor was suggested by Kamal (1) and the logarithmic one by Battelle (2). Support for the linear factor can come from the results of Ohokubo, et al. (13) from tests on closed hat-section members, and Vankuren and Scott (10). Support for the logarithmic factor would come from the material strain rate sensitivity tests. Other forms involving powers of deformation rate have been suggested by Wierzbicki and Akerstrom (14) and Tani and Funahashi (15) for the static to dynamic load factors. A summary of the various forms of the factors is given below:

$$F_D = (1 + \alpha_3 \dot{\Delta})\, F_s \qquad (1)..1$$

$$F_D = (\alpha_1 + \alpha_2 \log V_0)\, F_S \qquad (16)..2$$

$$F_D = (\alpha_4 + \alpha_5 \log \dot{\Delta})\, F_S \qquad (16)..3$$

$$F_D = \left\{1 + \left(\frac{\dot{\Delta}}{L.D}\right)^q\right\} F_S \quad \text{For max.load} \qquad (15)..4$$

$$F_D = \left\{1 + \left(\frac{C\dot{\Delta}}{L.D}\right)^q\right\} F_S \quad \text{For mean load} \qquad (15)..5$$

Where, $F_D$ = dynamic force

$F_S$ = static force

$\alpha_i$ = coefficient (empirical)

$V_o$ = initial collision velocity

$\dot{\Delta}$ = deformation rate

L = initial length of member

D = empirical constant (40.4/ sec. sec. for mild steel)

C = empirical constant (0.01 for mild steel)

q = empirical constant (0.2 for mild steel)

As can be seen from the above expressions, various ways are used to account for the crush rate effects in structures. All the above expressions are empirically derived from test data on simple structures. Depending on the equation selected (eqns. 1 to 5), the Dynamic amplification factor currently used can range between 1.3 to greater than 2.0 at a rate of 44 fps (13.2 m/s). The validity of these amplification factors during crash of vehicles involving complex buckling modes needs further study.

## CONCLUSIONS FROM THE LITERATURE SURVEY

The sensitivity of material properties to strain rate, and the complexities arising from wave propagation and inertial effects within the structure, make it difficult to extrapolate the results obtained from quasi-static tests to dynamic tests. Although many empirical methods are currently in use to transform static data for use in dynamic cases, no unique method has been established. It appears that in collapse of structures in which the collapse modes have been pre-established due to the geometry of the structures, the material strain rate sensitivity factors are sufficient to transform statically obtained data to dynamic data. However, in structures where the crush modes are not predetermined, the inertial effects also have to be taken into account.

## DEVELOPMENT OF A DYNAMIC AMPLIFICATION FACTOR FOR USE IN MODELS

During the course of Ford's R.S.V. contract (17), six identical small unitized vehicles were crash tested at 32, 37, and 42 mph (51.2, 59.2, and 67.2 km/h) into a flat, rigid barrier. Also, two identical vehicles were crushed statically to develop a mathematical model to predict the effect

of front-end component changes on the inertial response of the passenger compartment. The above crash tests and static crush tests were used to develop "dynamic amplification factors" for transforming the static data to the dynamic case. The model configuration chosen for the study is shown in Fig. 1. The crusher tests showed that the foreframe and the aftframe were the main energy absorbers.

The crash tests showed that for the first 40 ms, the occupant compartment response was governed mainly by the crush characteristics of the frame rails since the driveline, firewall, and the transmission mounts were not stressed that early in the crash. The sheet metal force levels in the first 40 msecs. were negligible compared to the frame force levels. Various "dynamic amplification factors" were tried for the frame during the simulation runs and compared with the crash tests up to 40 ms. The best results were obtained by using a factor shown in Fig. 2 and an inertia spike in the aftframe in Fig. 3.

During the crash beyond 40 msecs., the firewall and driveline interactions with the engine become important. It was postulated that a material rate sensitivity factor of the type used by Battelle (2) and Calspan (16) would be adequate for the driveline and the firewall since the crush rates are considerably reduced at the time of engine/driveline and engine/firewall

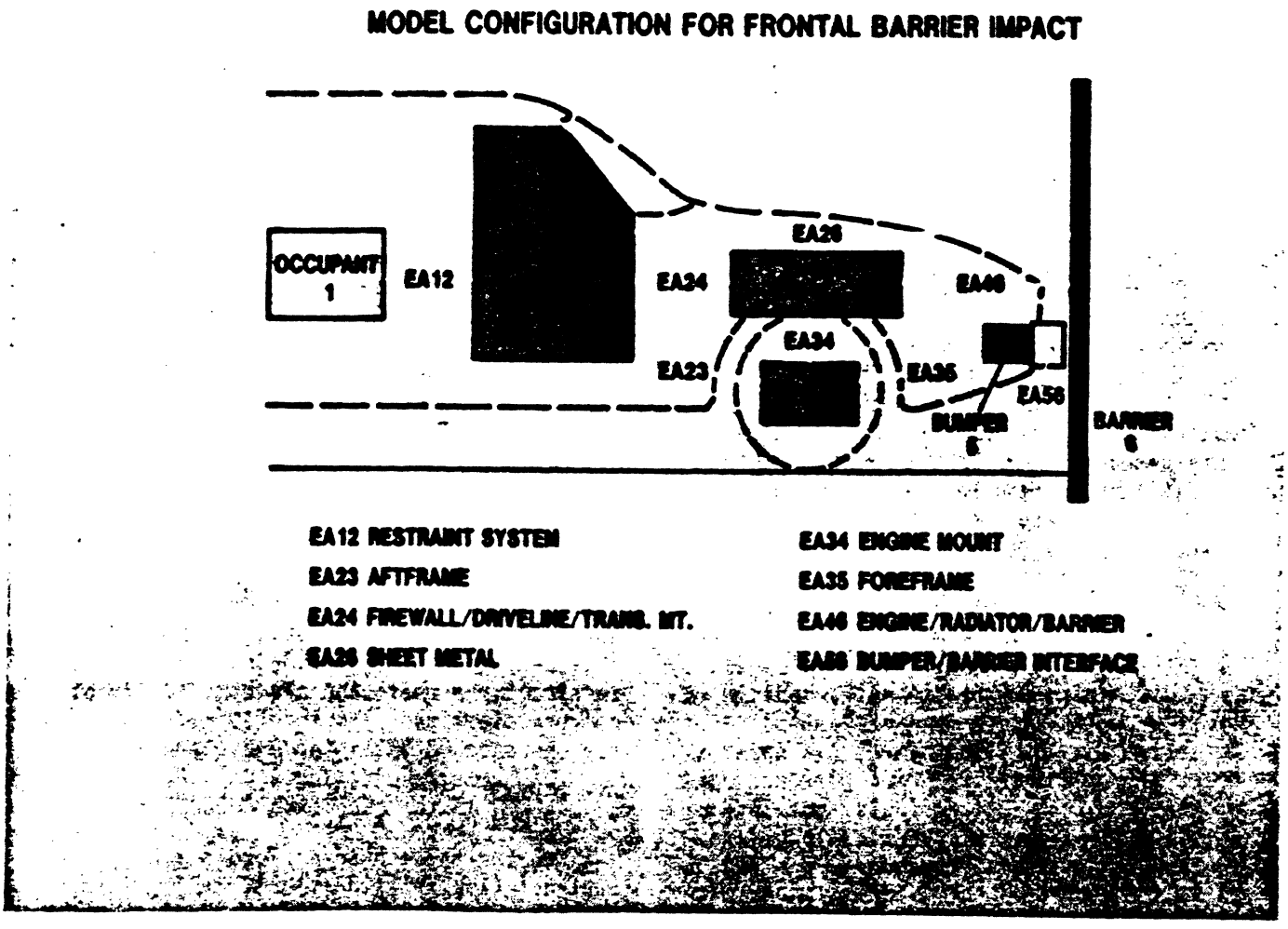


Fig. 1 - Model configuration for frontal barrier impact

interactions when compared with the initial crash velocity.

A comparison of the results of the simulations with the crash test results are shown in Fig. 4 to Fig. 7. A comparison of the component crush and travel between the simulation and the crash tests is shown in Table 1.

It can be seen from the figures that the basic wave shape of the deceleration response of the passenger compartment is predicted well by the model. Exact comparisons with the deceleration pulse can be misleading at times due to the various techniques used to filter the wideband accelerometer data. Potential variation due to filtering can be quantified by considering that the accelerometer-integrated travel of the passenger compartment in the above crash tests shows 2" (5 cm) more travel that the film analysis data across the speed range tested.

Fig. 8 shows a comparison of the model predicted crush and engine intrusion into the passenger compartment with the experimental test results. It can be seen from the figure that the model predicted crush is well within the observed test results across the speed range. The intrusion predicted by the model is within 1.5" (3.75 cm) of that observed in the 42 mph (67.2 km/h) tests and one of the 32 mph (51.2 km/h) tests. At 37 mph (59.2 dm/h), the engine intrusion predicted by the model is 2.5" (6.25 cm) higher than that observed in the crash tests. This lack of correlation can be traced to approximately 3" 97.5 cm) of additional engine travel observed in the crash tests when compared to the simulation results (Table 1).

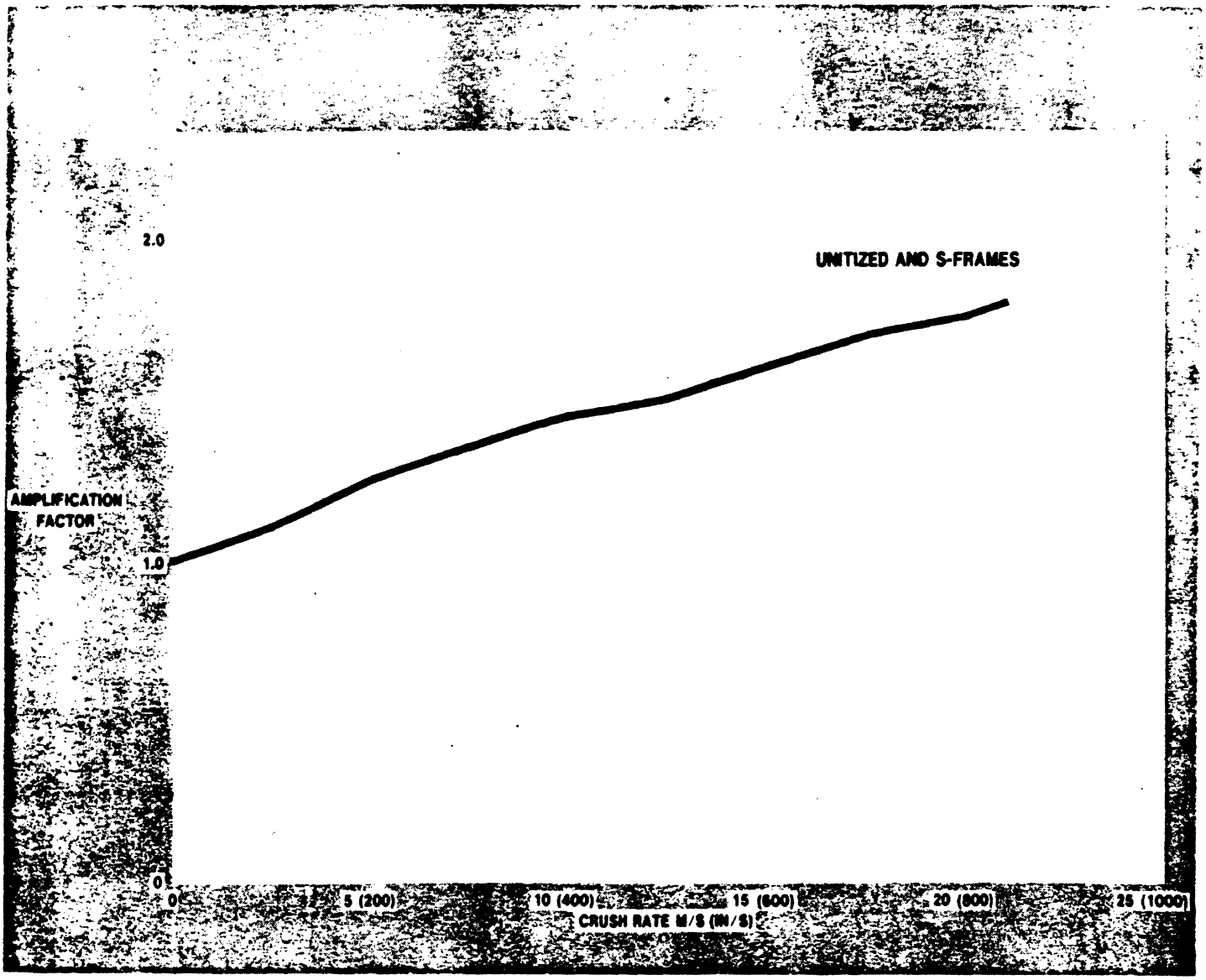


Fig. 2 - Dynamic amplification factor for subcompact vehicle frame

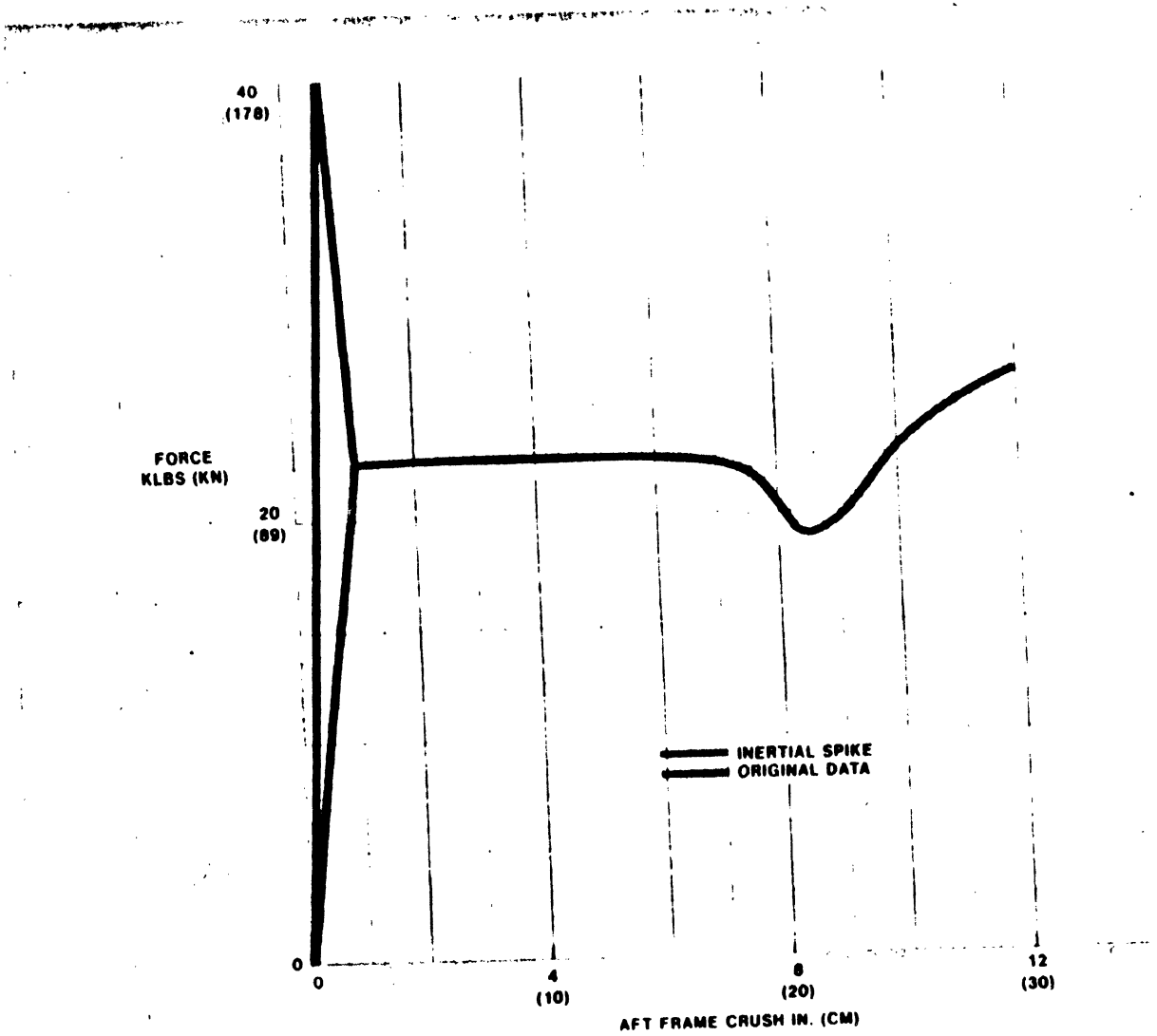


Fig. 3 - Inertial spike in the aft frame

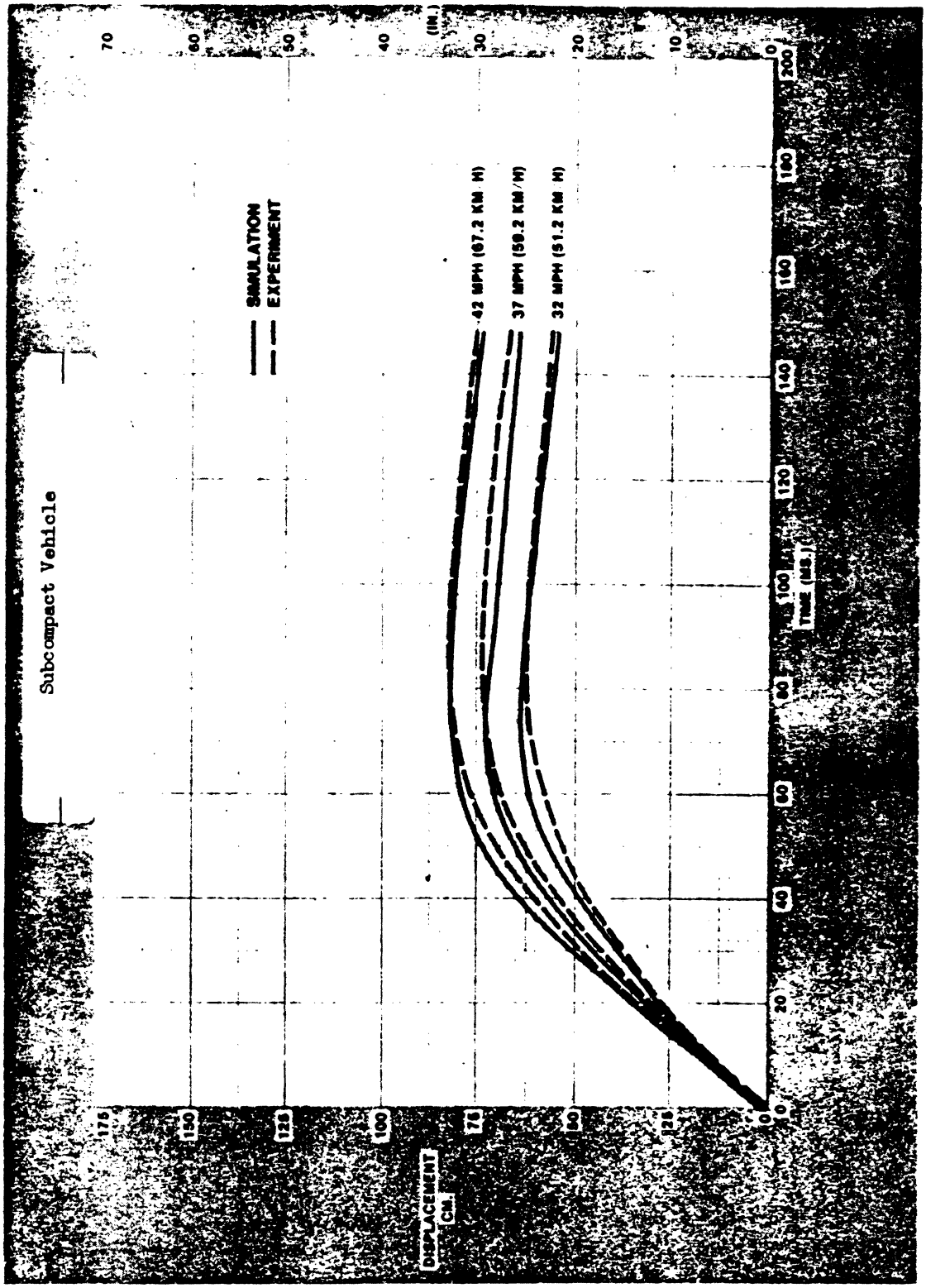


Fig. 4 - Comparison between the simulated and crash test results - passenger compartment travel (film analysis)

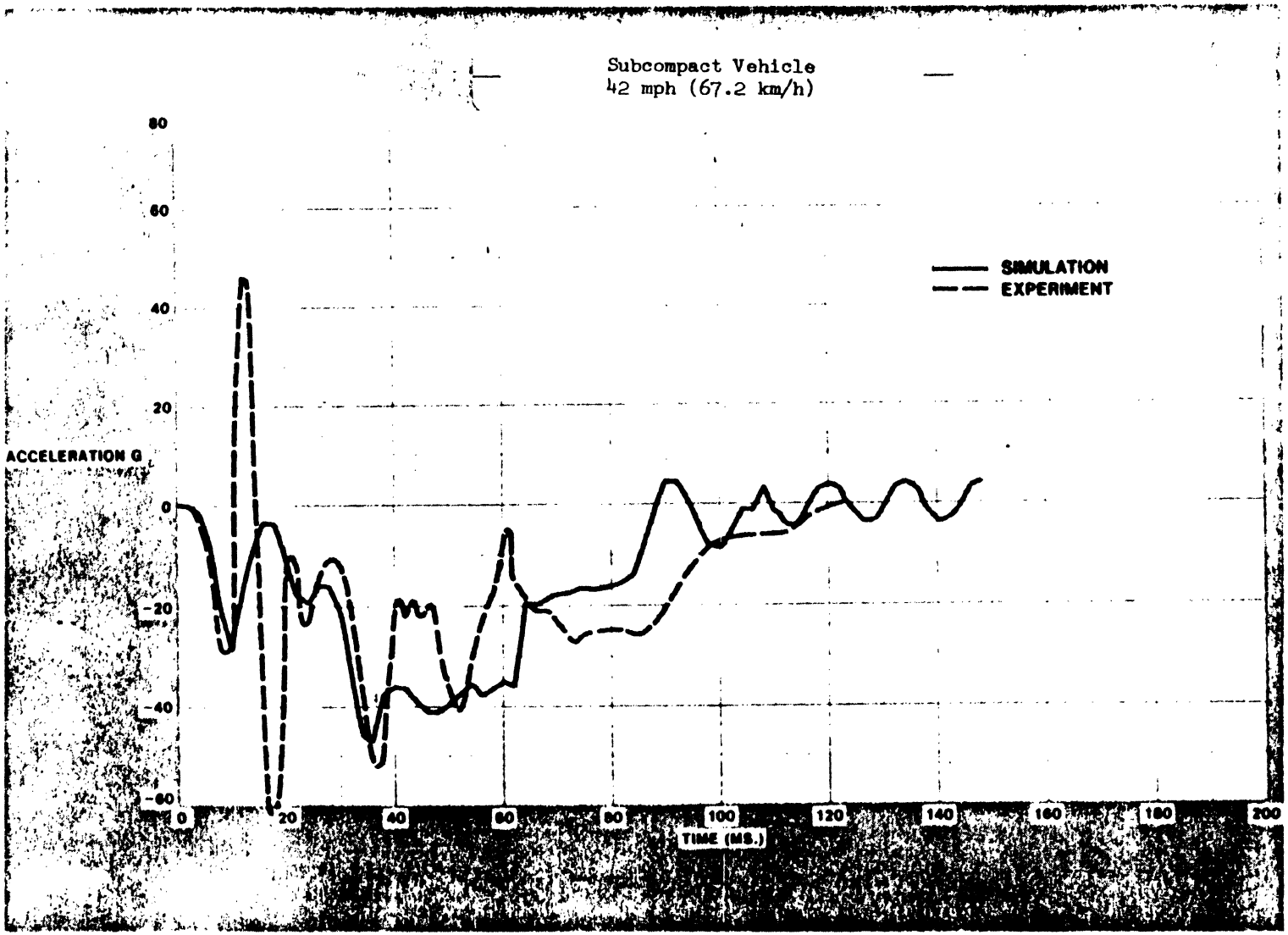


Fig. 5 - Comparison between the simulated and crash test results - passenger compartment deceleration

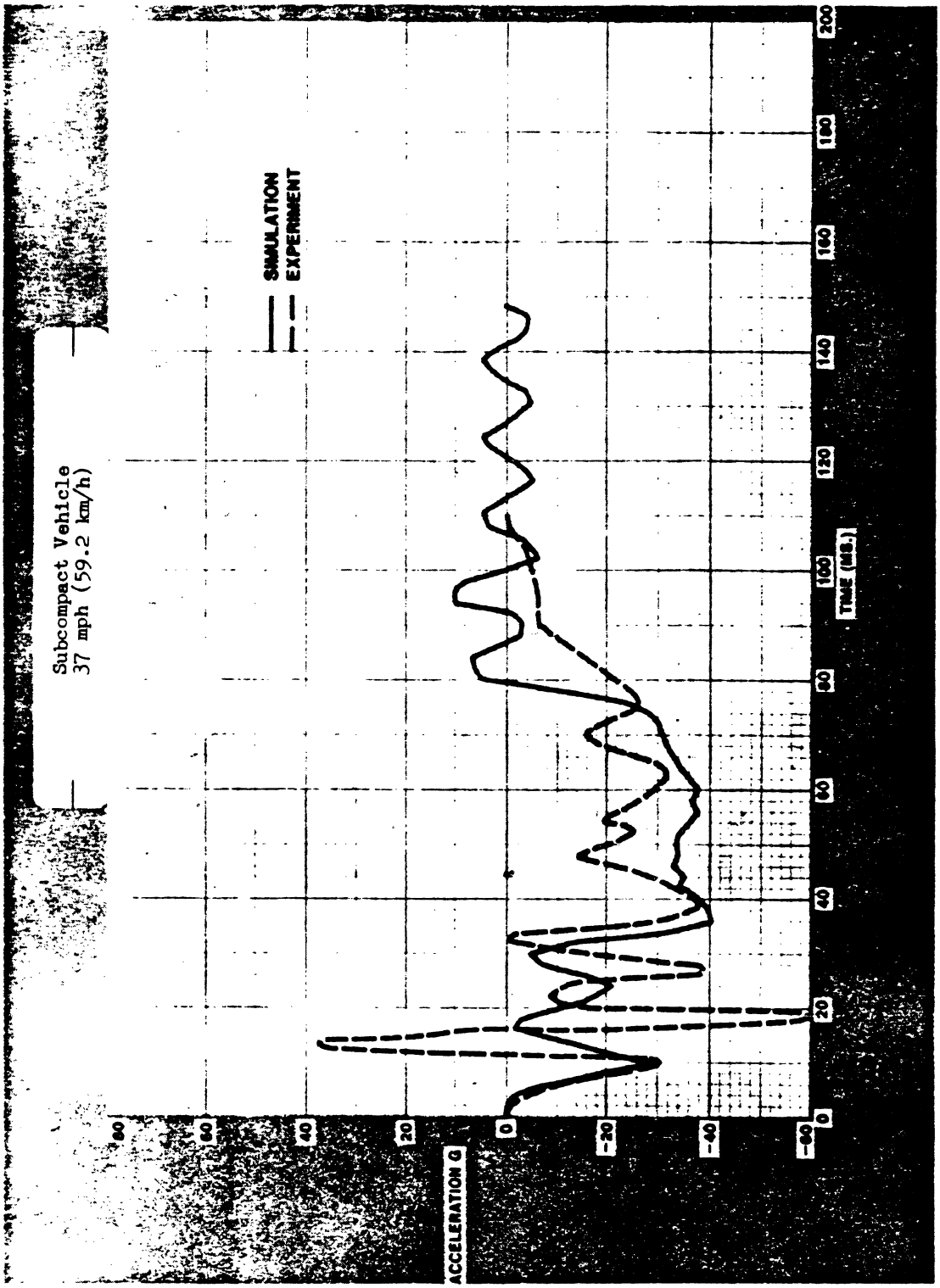


Fig. 6 - Comparison between the simulated and crash test results - passenger compartment deceleration

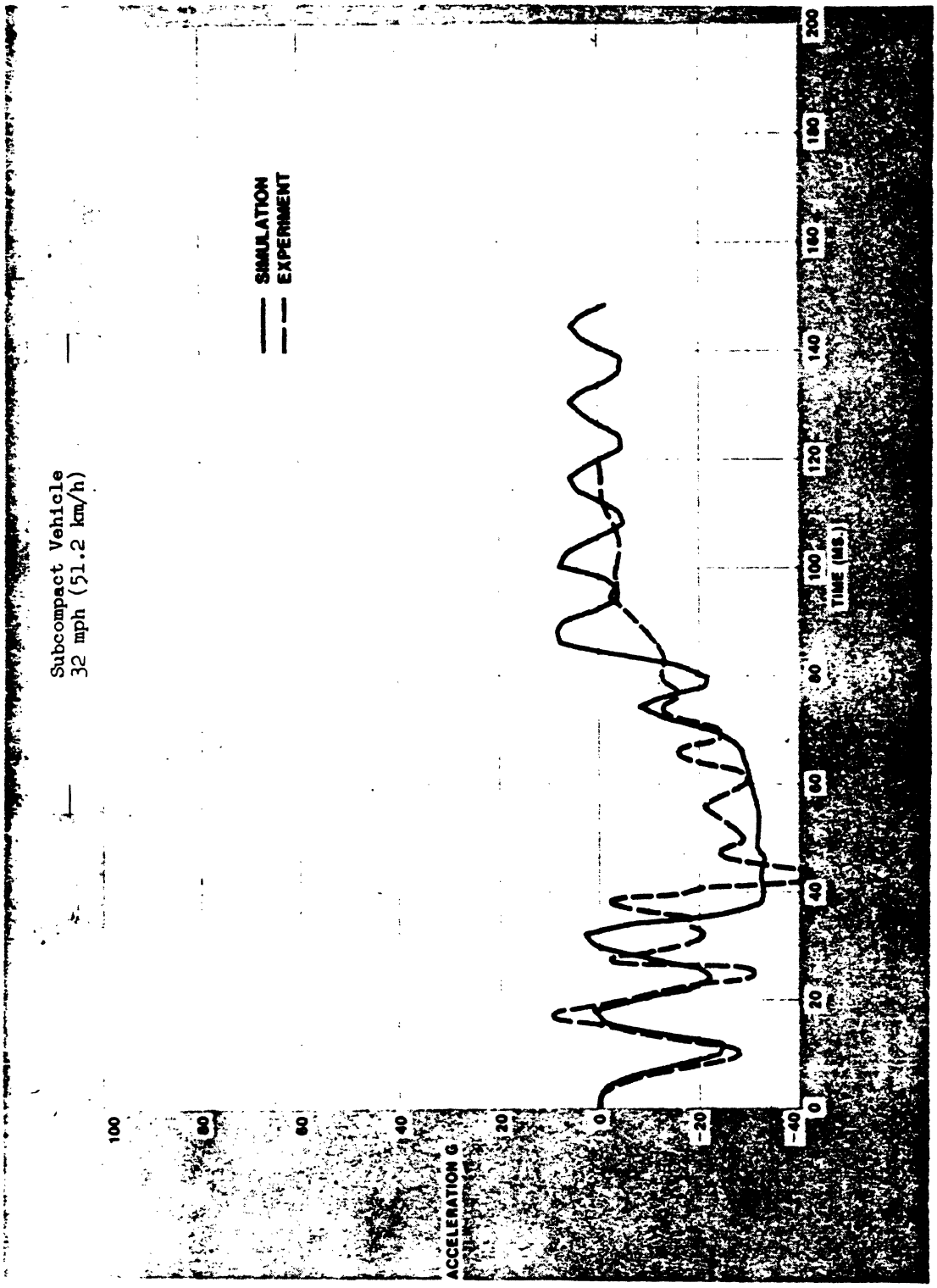


Fig. 7 - Comparison between the simulated and crash test results - passenger compartment deceleration

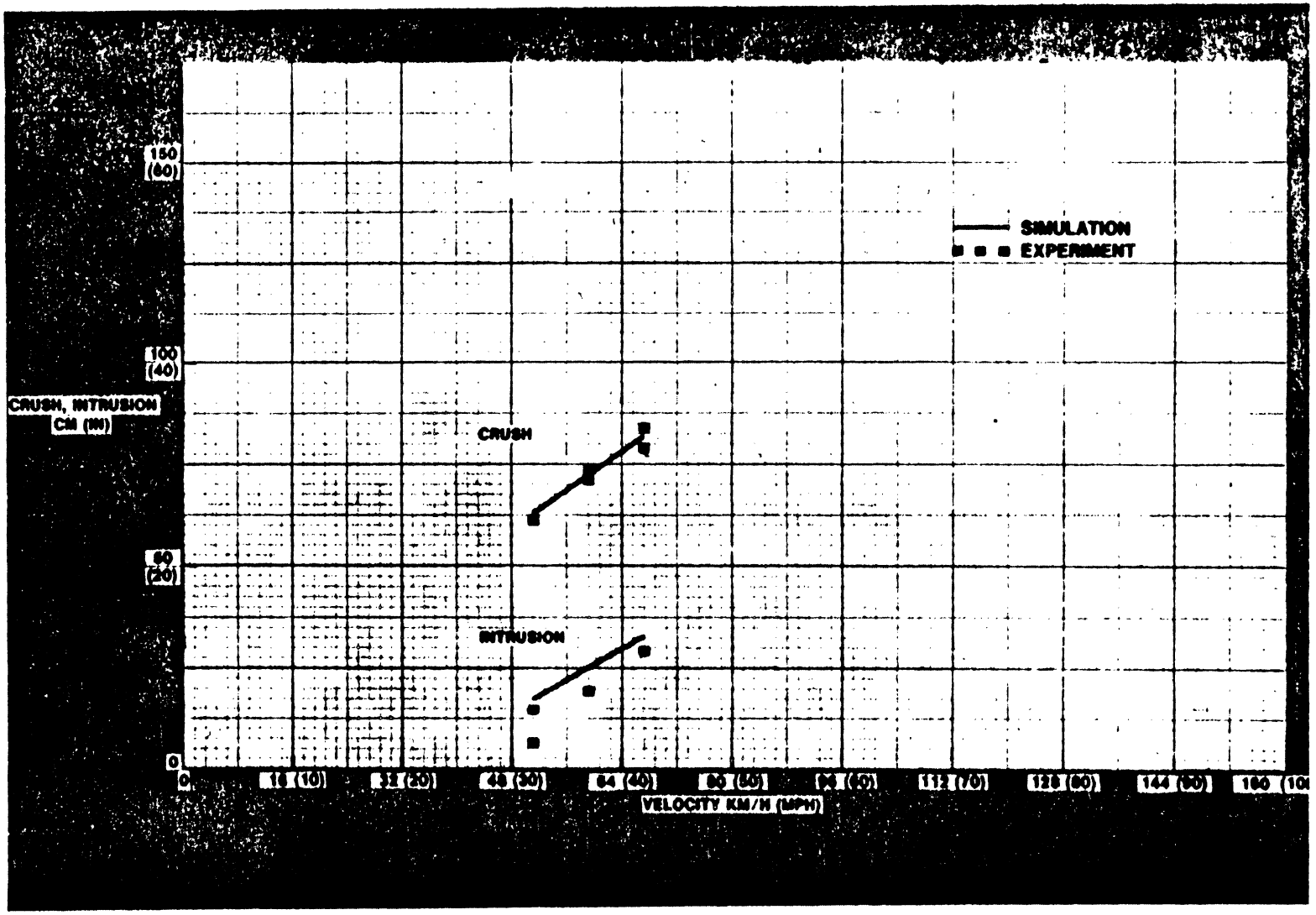


Fig. 8 - Comparison of crush and engine intrusion for subcompact vehicle crashes and simulations

TABLE 1 - COMPARISON OF COMPONENT CRUSH AND TRAVEL BETWEEN CRASHES AND SIMULATIONS FOR THE SUBCOMPACT VEHICLES

| Velocity mph (km/h) | Test/ Simulation | Dynamic Collapse cm. (in.) | Cross-Member Travel cm. (in.) | Engine Travel cm. (in.) | Engine-Dash Intrusion cm. (in.) | Aftframe Crush cm. (in.) | Foreframe Crush cm. (in.) |
|---|---|---|---|---|---|---|---|
| 42 (67.2) | 1 | 79.50 (31.8) | 51.75 (20.7) | 46.25 (18.5) | 30.00 (12.0) | 27.75 (11.1) | 45.50 (18.2) |
| | 2 | 83.25 (33.3) | 59.50 (23.8) | 50.00 (20.0) | 30.00 (12.0) | 23.75 (9.5) | 53.00 (21.2) |
| | Simulation | 82.15 (32.86) | 61.03 (24.41) | 46.85 (18.75) | 33.45 (13.38) | 22.75 (9.10) | 54.35 (21.74) |
| 37 (59.2) | 3 | 71.25 (28.5) | 61.25 (24.5) | 48.75 (19.5) | 19.50 (7.8) | 15.00 (6.0) | 50.00 (20.0) |
| | 5 | 73.75 (29.5) | 61.25 (24.5) | 52.00 (20.8) | 19.00 (7.6) | 12.50 (5.0) | 55.00 (22.0) |
| | Simulation | 72.35 (28.94) | 58.08 (23.23) | 44.38 (17.75) | 25.40 (10.16) | 14.55 (5.82) | 53.58 (21.43) |
| 32 (51.2) | 4 | 61.25 (24.5) | 51.00 (20.4) | 43.25 (17.3) | 15.25 (6.1) | 10.25 (4.1) | 44.75 (17.9) |
| | 6 | 61.25 (24.5) | 55.00 (22.0) | 52.50 (21.0) | 5.75 (2.3) | 6.25 (2.5) | 48.75 (19.5) |
| | Simulation | 63.65 (25.46) | 52.28 (20.91) | 42.08 (16.83) | 19.33 (7.73) | 11.90 (4.76) | 49.03 (19.61) |

## FURTHER VERIFICATION OF THE MODEL

In order to verify the "dynamic amplification factor" determined empirically in the above study for the vehicle frames, the model was exercised with the static crush data of a unitized body compact car with a test weight of 4000 lbs. (1818 kgs). Two crash tests were available at 35 mph (56 km/h) and 30 mph (48 km/h) for comparison with the simulation results. The results of the model simulation and crash tests are shown in Figs. 9-11.

It can be seen from the figures that the dynamic crush predicted by the model is within 1.5% of that observed in the tests and the time to maximum crush predicted by the model is within 3.6 ms.

The model was further exercised with the static crush data of a mid-size car of unitized body construction. The predicted model results are compared with the experimental results in Figs. 12 and 13. The comparison between the model and the test is considered to be good.

Based on the above simulation results, it can be concluded that the "dynamic amplification factor", as shown in Fig. 2, when used in the fore-frames and the aft-frames of unitized vehicles in conjunction with a material rate sensitive factor, shown in Fig. 14, for the sheet metal, firewall and driveline, predict the crash test results with adequate accuracy.

Since a series of crash test results at 8, 25, 30, and 35 mph (13.3, 40, 48, and 56 km/h) of an S-framed vehicle were available in the literature (16) along with the static crush data of the front-end components (16, 18), the model developed for the unitized vehicles was exercised with the published static data. Comparison of the model predicted results and the crash test results are shown in Figs. 15-22.

The 8 mph (13.3 km/h) simulation resulted in approximately 1.25" (3.12 cm) (i.e., 17.8%) more crush when compared with the crash test. It is felt that at this low speed, the effect of the bumper energy absorbers predominate the structural

effects, making valid comparisons between the model and the test difficult. However, the simulation results in the speed range of 25 to 35 mph (40 to 56 km/h) show good correlation with the crash test results. The dynamic collapse predicted by the model is within 5% of that observed in the tests. Also, the predicted time to maximum crush is within 12 msecs. of that observed in tests. The above simulations show that the methods used for transforming the static crush data to the dynamic case in unitized vehicles is also valid in the S-framed vehicles.

## DYNAMIC AMPLIFICATION FACTORS FOR C-FRAMED VEHICLES

The major energy absorber in frontal crashes of the C-framed vehicles investigated in the current study is also the frame. Since studies on the collapse of C-section frames are not available in the literature, it was decided to experiment with various forms and magnitude of dynamic amplification factors in the model to best explain the crash test results. The objective of the study was to develop one dynamic amplification factor for the frames that can explain crashes of all similar framed structures.

As a first step, since static crush and dynamic crash data were available for several vehicles, it was decided to compare the kinetic energy absorbed in the crash tests with the energy absorbed in the static crusher tests for equal front-end crush. The results of the comparison are shown for four tests in Table 2. It can be seen that dynamically, the front-end

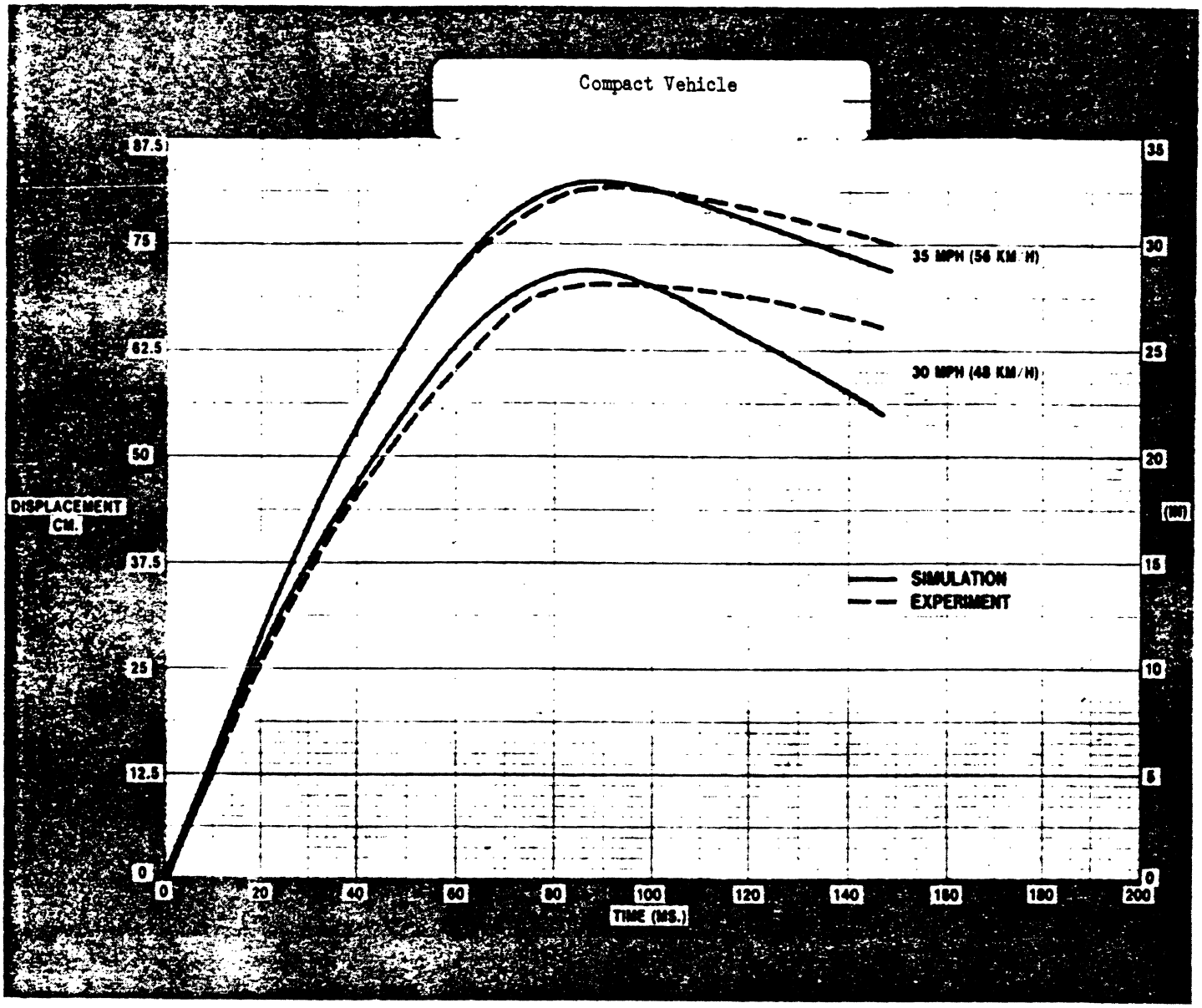


Fig. 9 - Comparison between the simulated and crash test results - passenger compartment travel

structure absorbs 64 percent to 100 percent more energy when compared with the static crush tests. These results are similar to those reported by Ohokubo, et al. (13) for rear-end crashes of sub-compact cars. It became obvious that the dynamic amplification factor developed for the car frames would not be adequate for this series of vehicles.

Once again, in order to maintain consistency with the previous simulations, the "dynamic amplification factor" for the sheet metal radiator, firewall, and driveline were those shown in Fig. 14. The factor for the frame was varied to achieve the best results for the four vehicles. The best results were obtained by using the factor shown in Fig. 23. It can be seen that this factor is much higher that that used for the unitized and the S-framed vehicles. Currently, such an increase in the levels cannot be explained. However, it is hypothesized that since the C-frames were initially straight and the buckling modes involved considerable torsion, the inertial effects during the buckling process were considerable. Also, there is some evidence that the material strain rate effects during shear deformations are higher than those in tensile deformations (19).

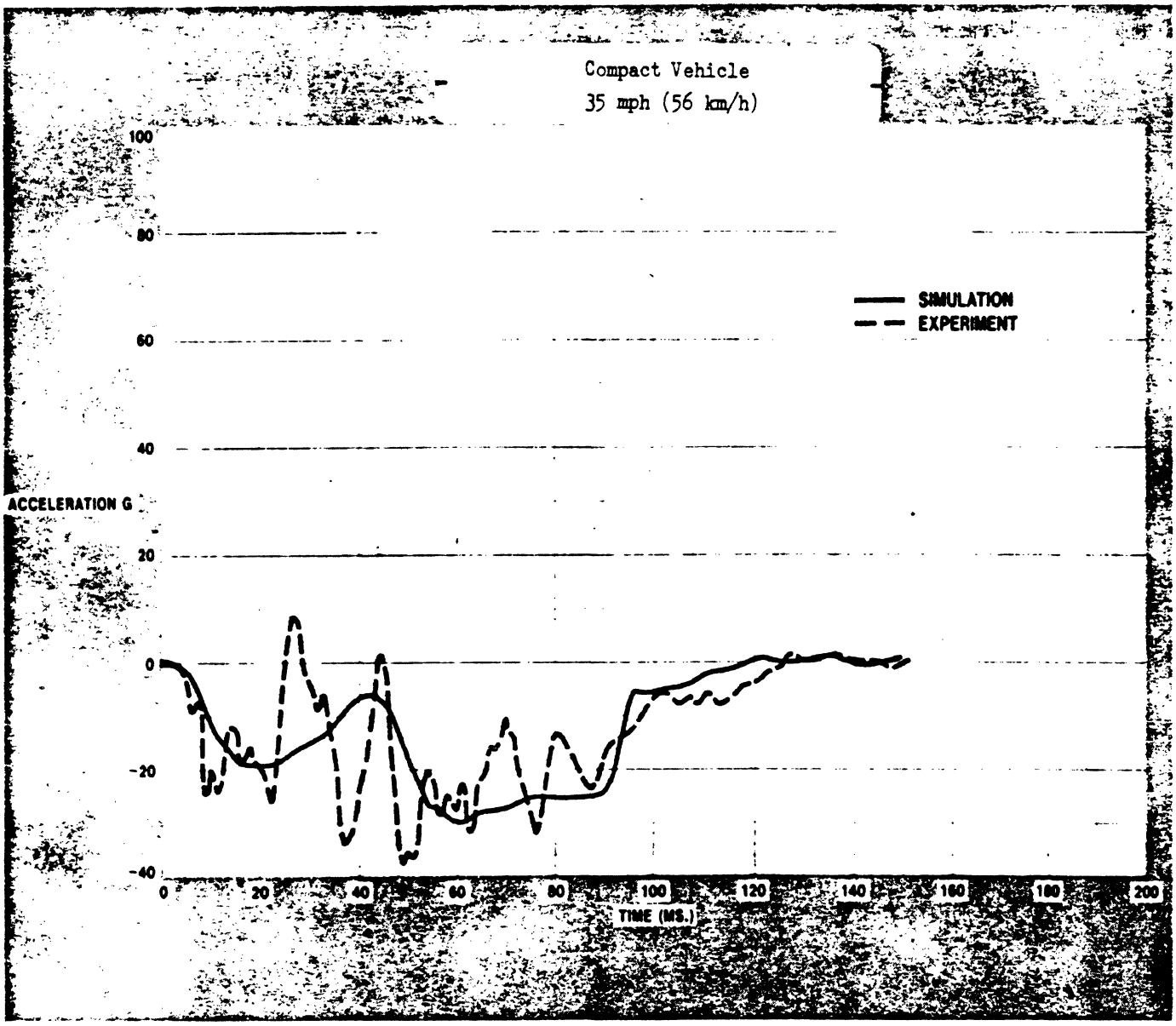


Fig. 10 - Comparison between the simulated and crash test results - passenger compartment deceleration

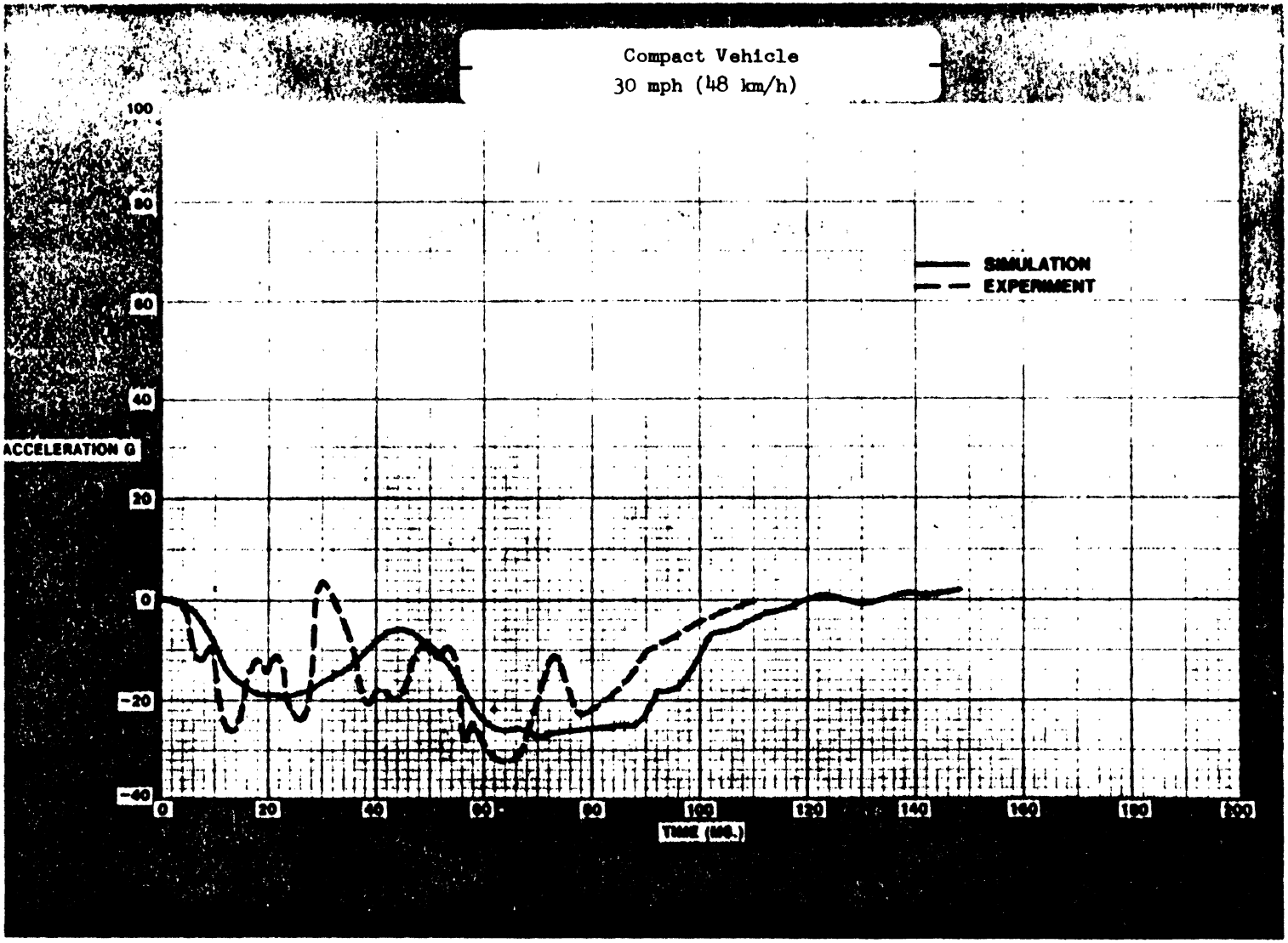


Fig. 11 - Comparison between the simulated and crash test results - passenger compartment deceleration

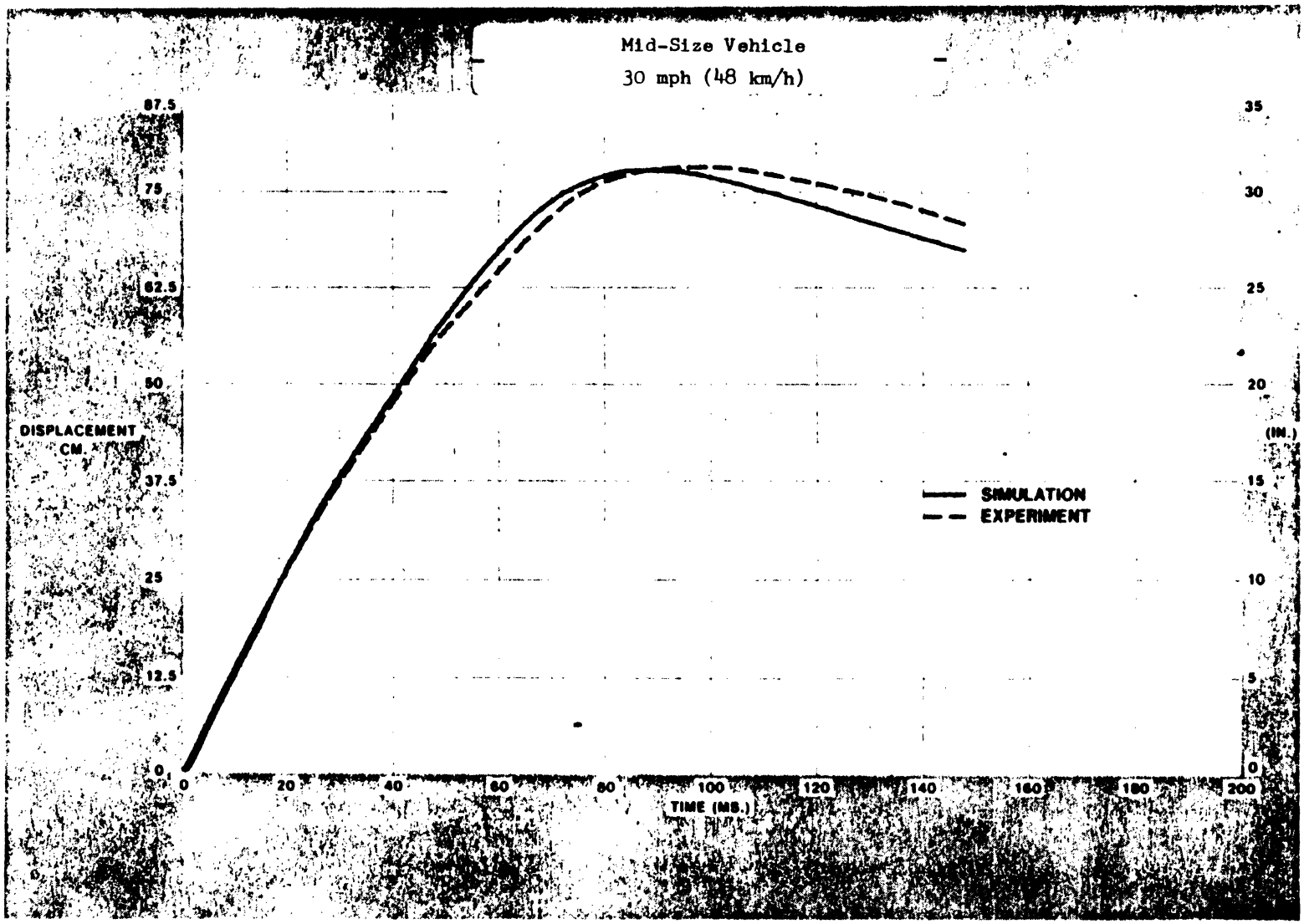


Fig. 12 - Comparison between the simulated and crash test results - passenger compartment travel

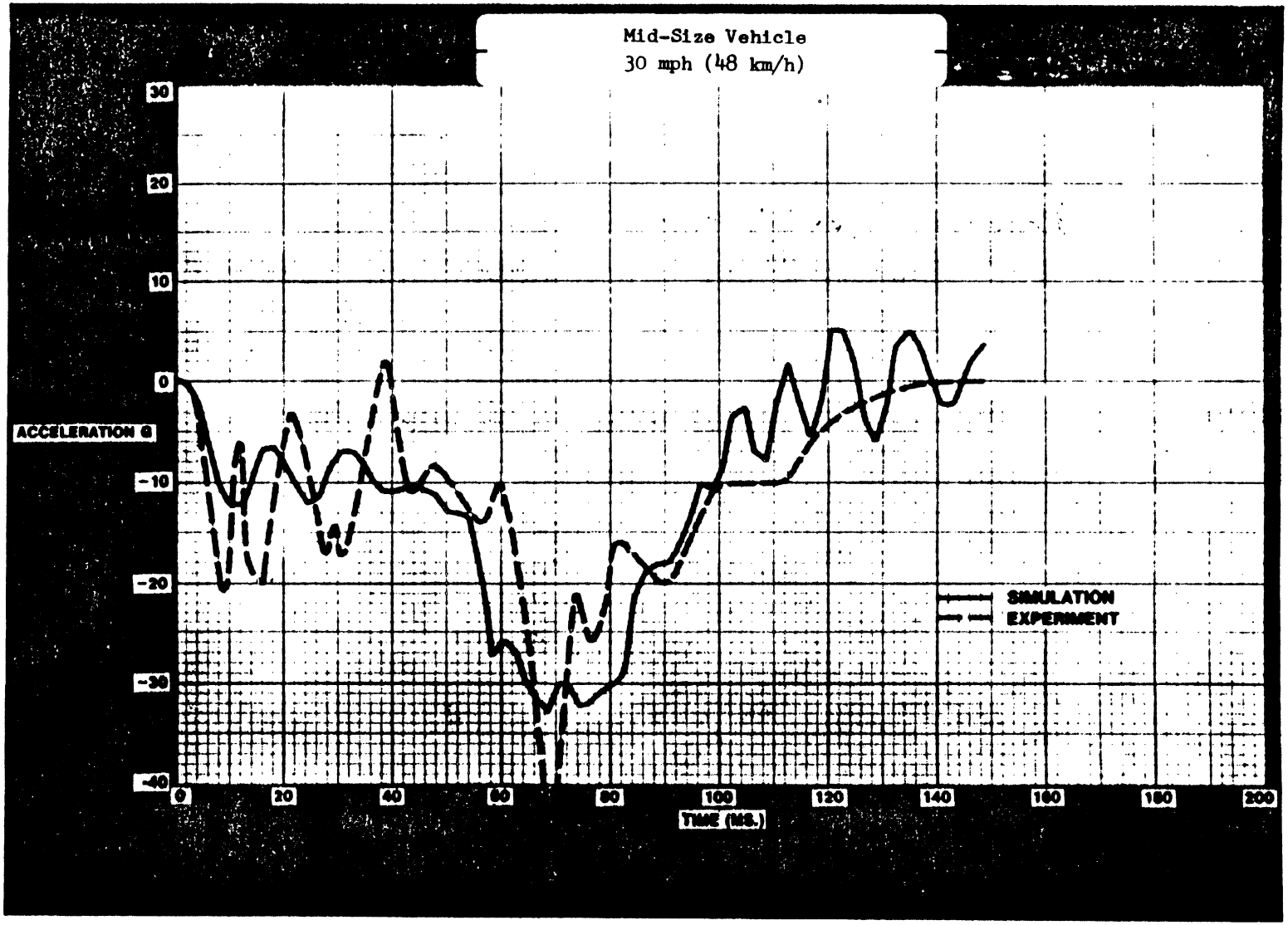


Fig. 13 - Comparison between the simulated and crash test results - passenger compartment deceleration

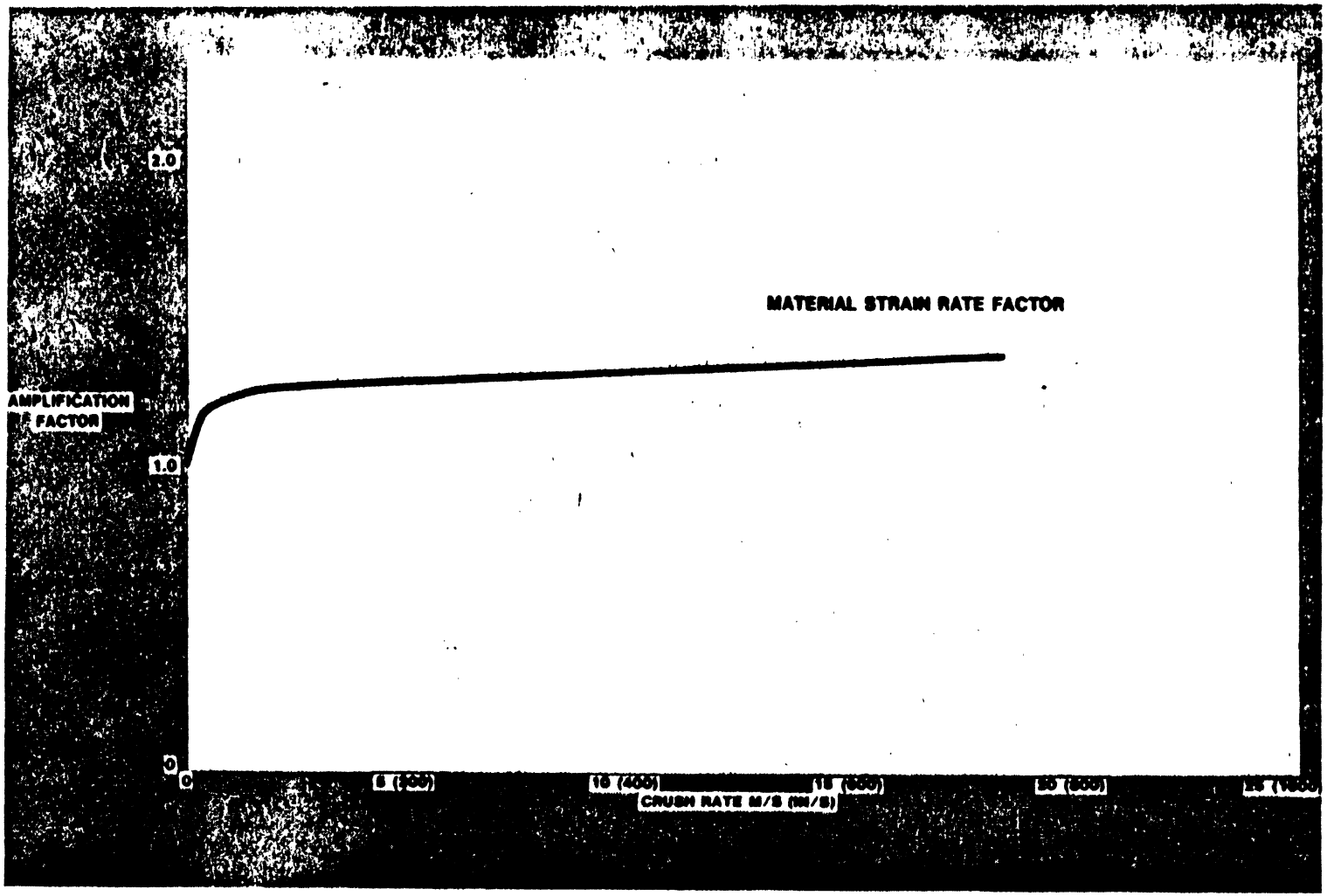


Fig. 14 - Material strain rate sensitive dynamic amplification factor

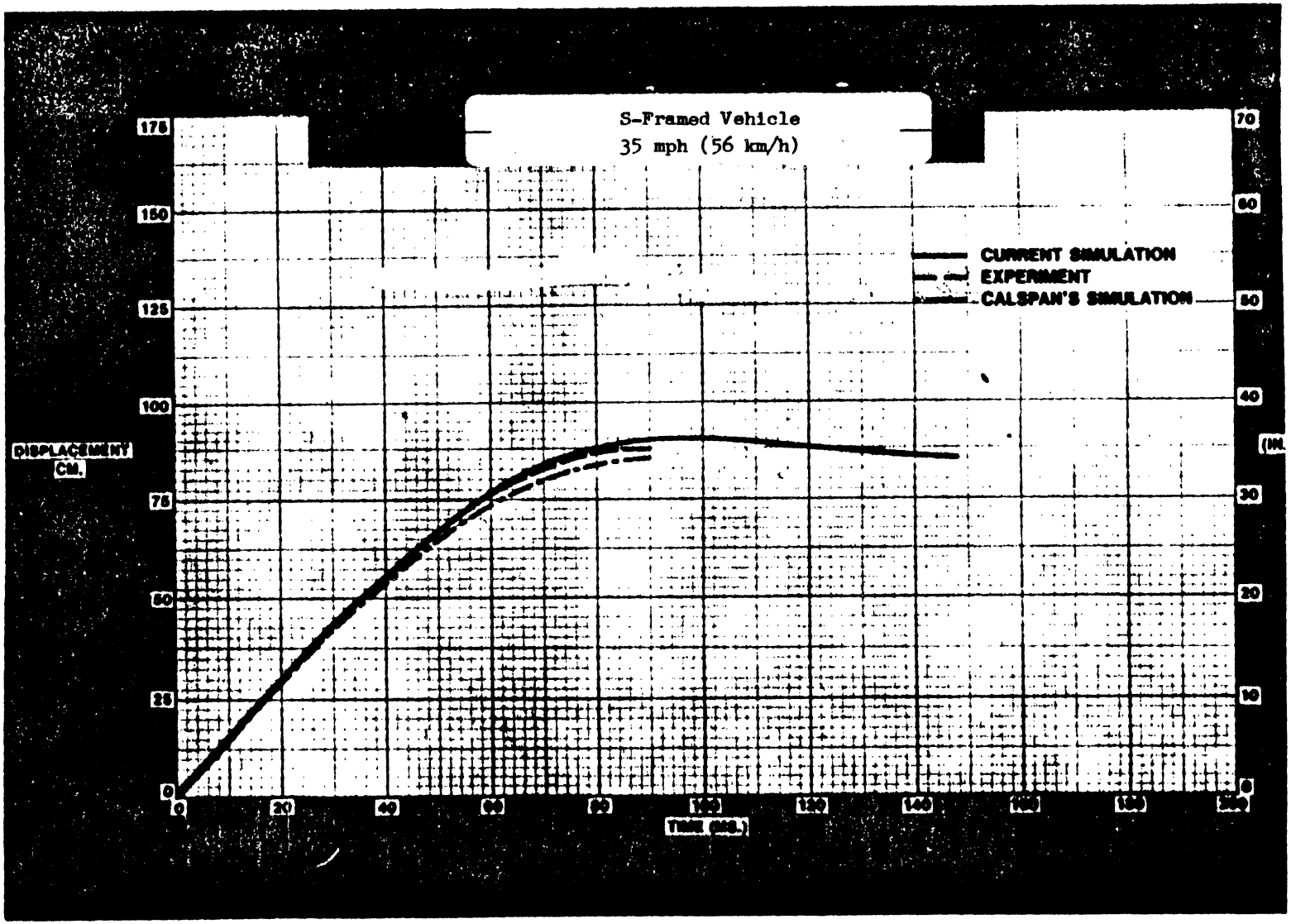


Fig. 15 - Comparison between the simulated and crash test results - passenger compartment travel

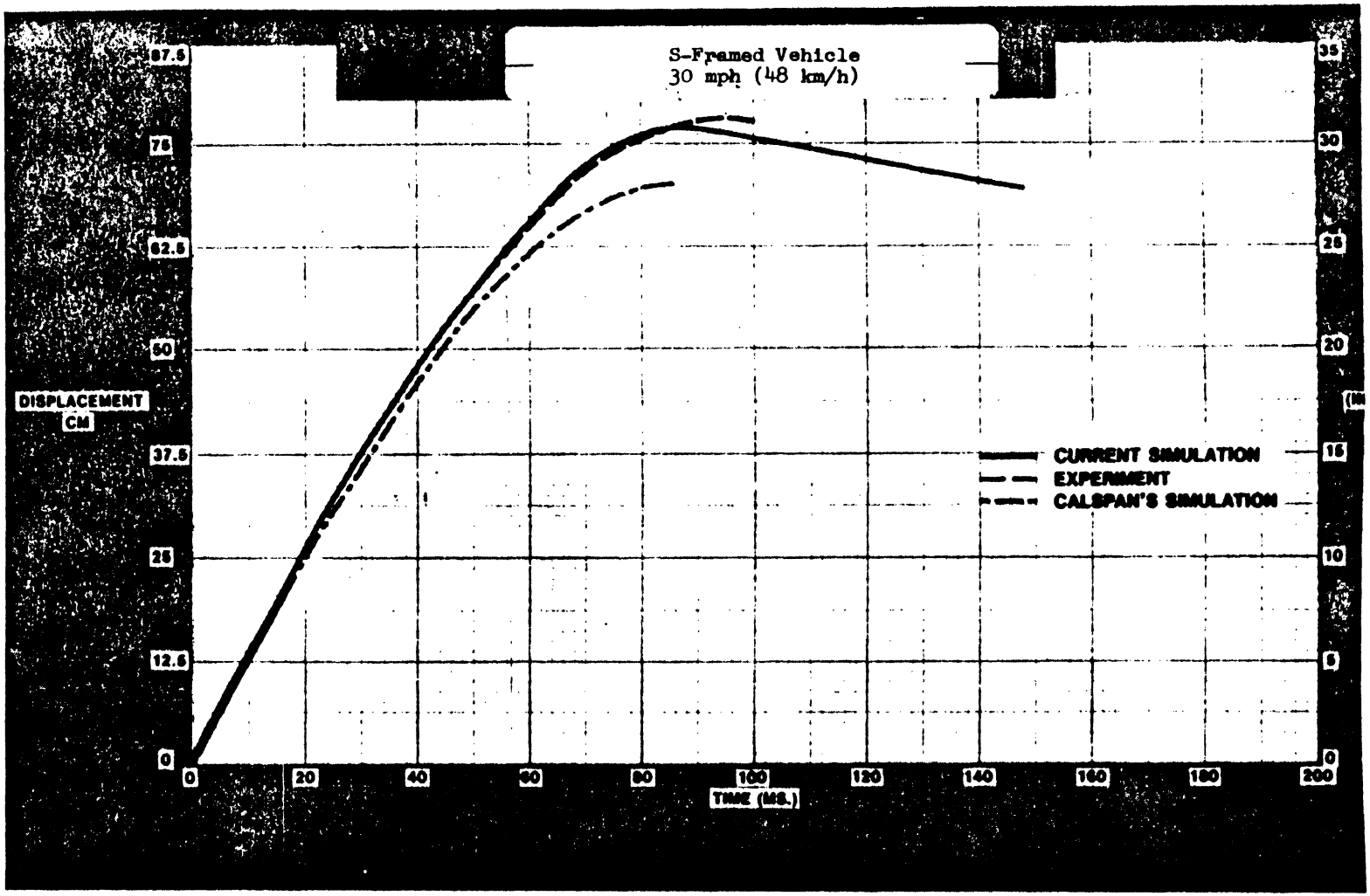


Fig. 16 - Comparison between the simulated and crash test results - passenger compartment travel

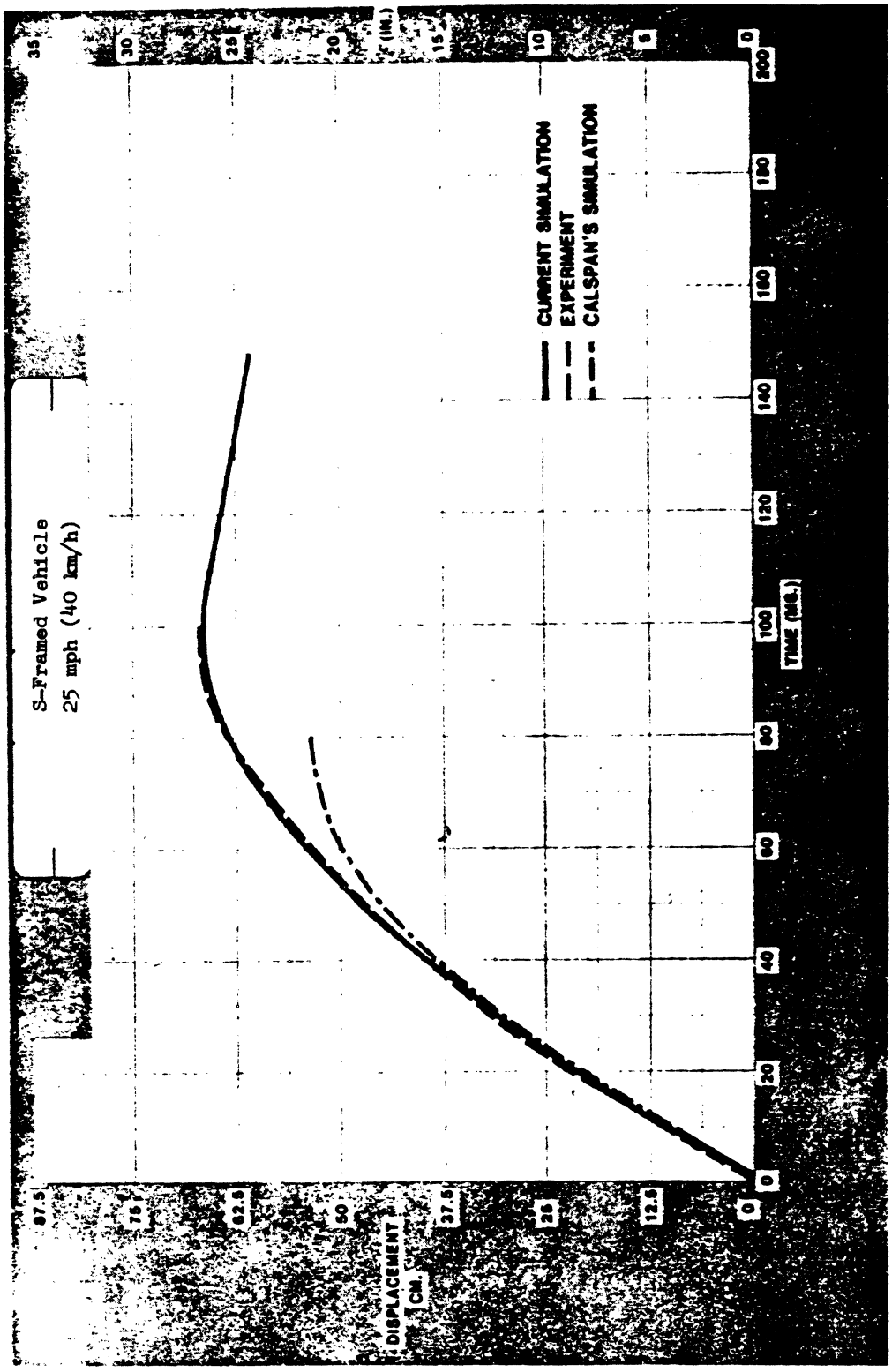


Fig. 17 - Comparison between the simulated and crash test results - passenger compartment travel

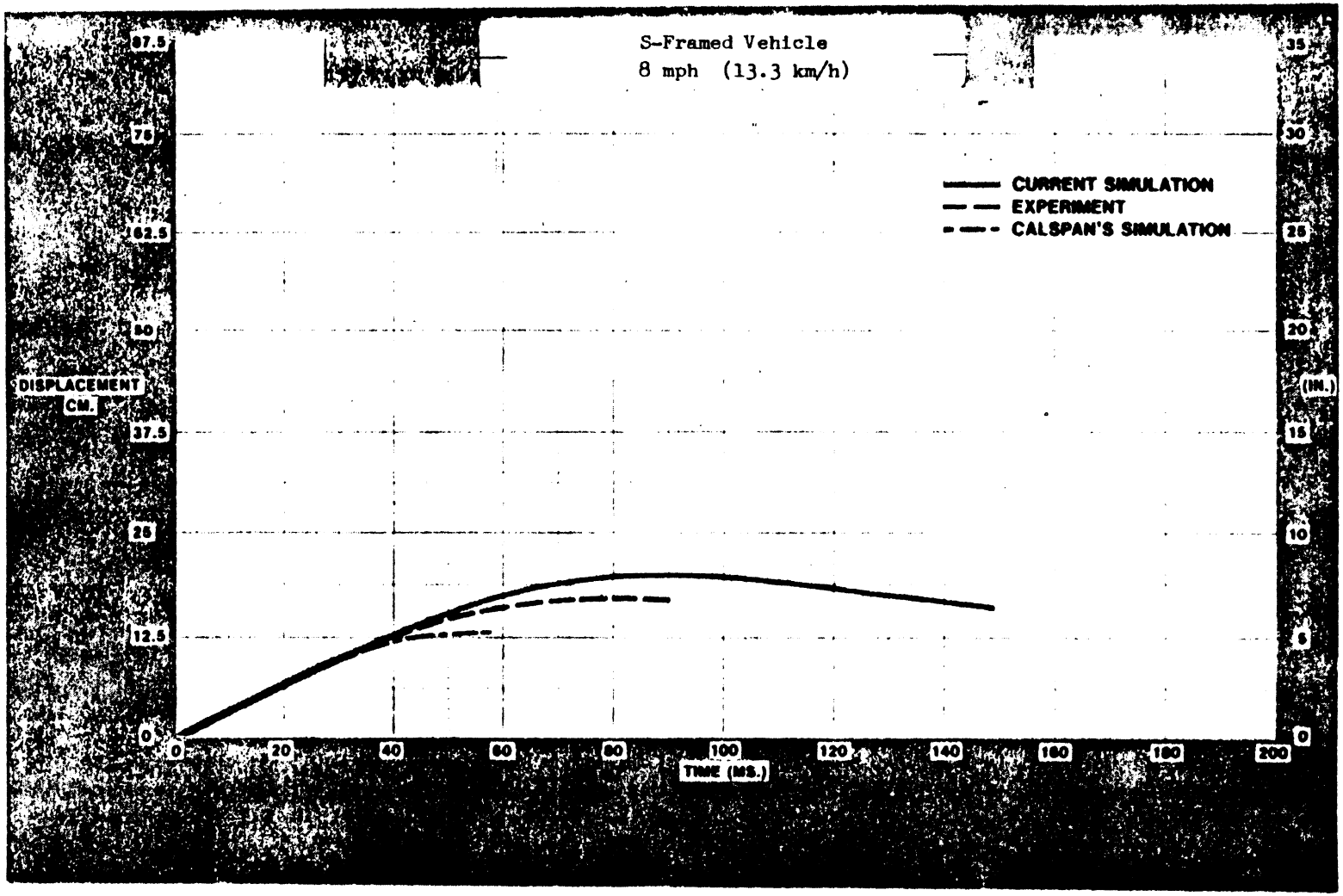


Fig. 18 - Comparison between the simulated and crash test results - passenger compartment travel

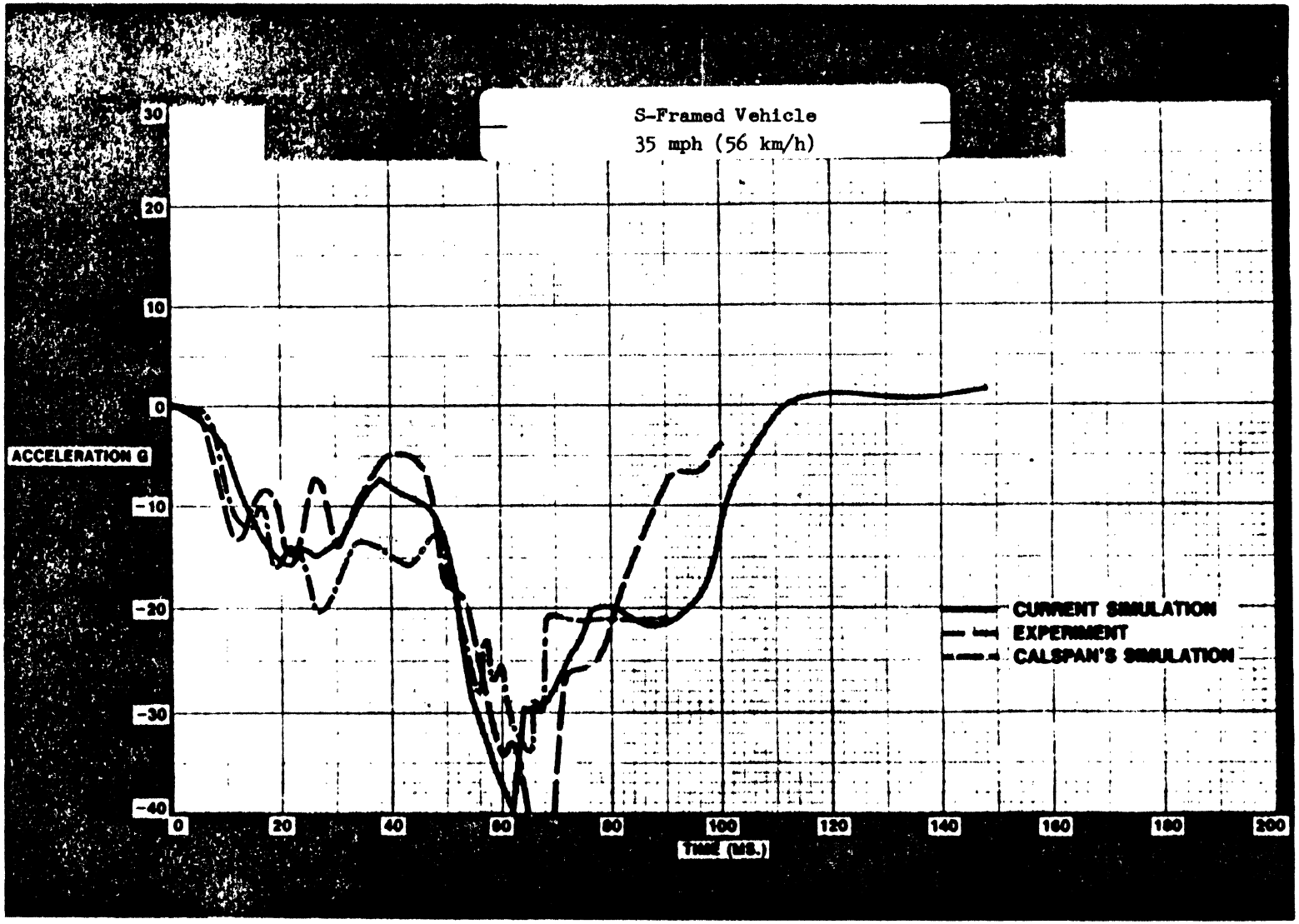


Fig. 19 - Comparison between the simulated and crash test results - passenger compartment deceleration

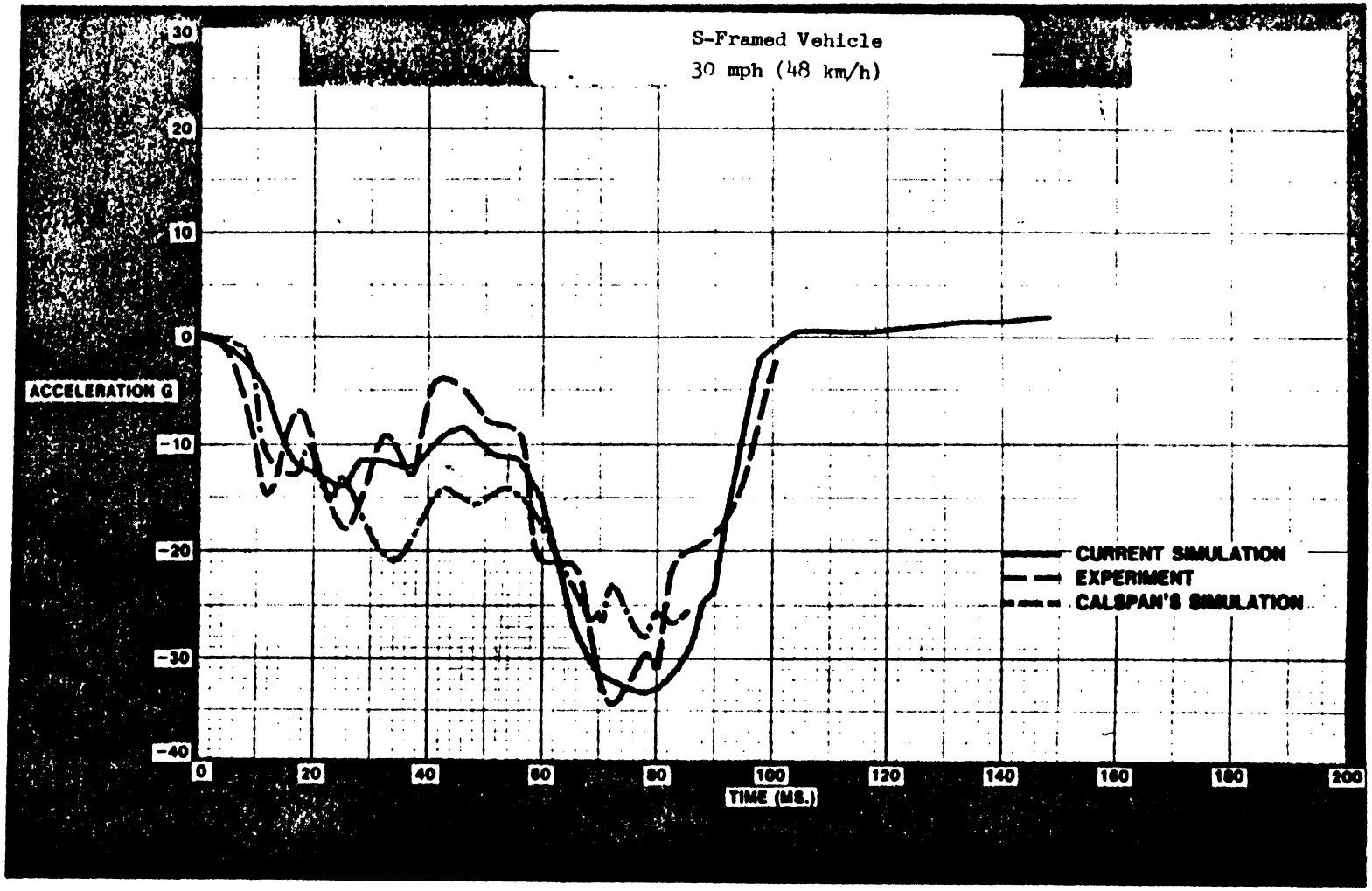


Fig. 20 - Comparison between the simulated and crash test results - passenger compartment deceleration

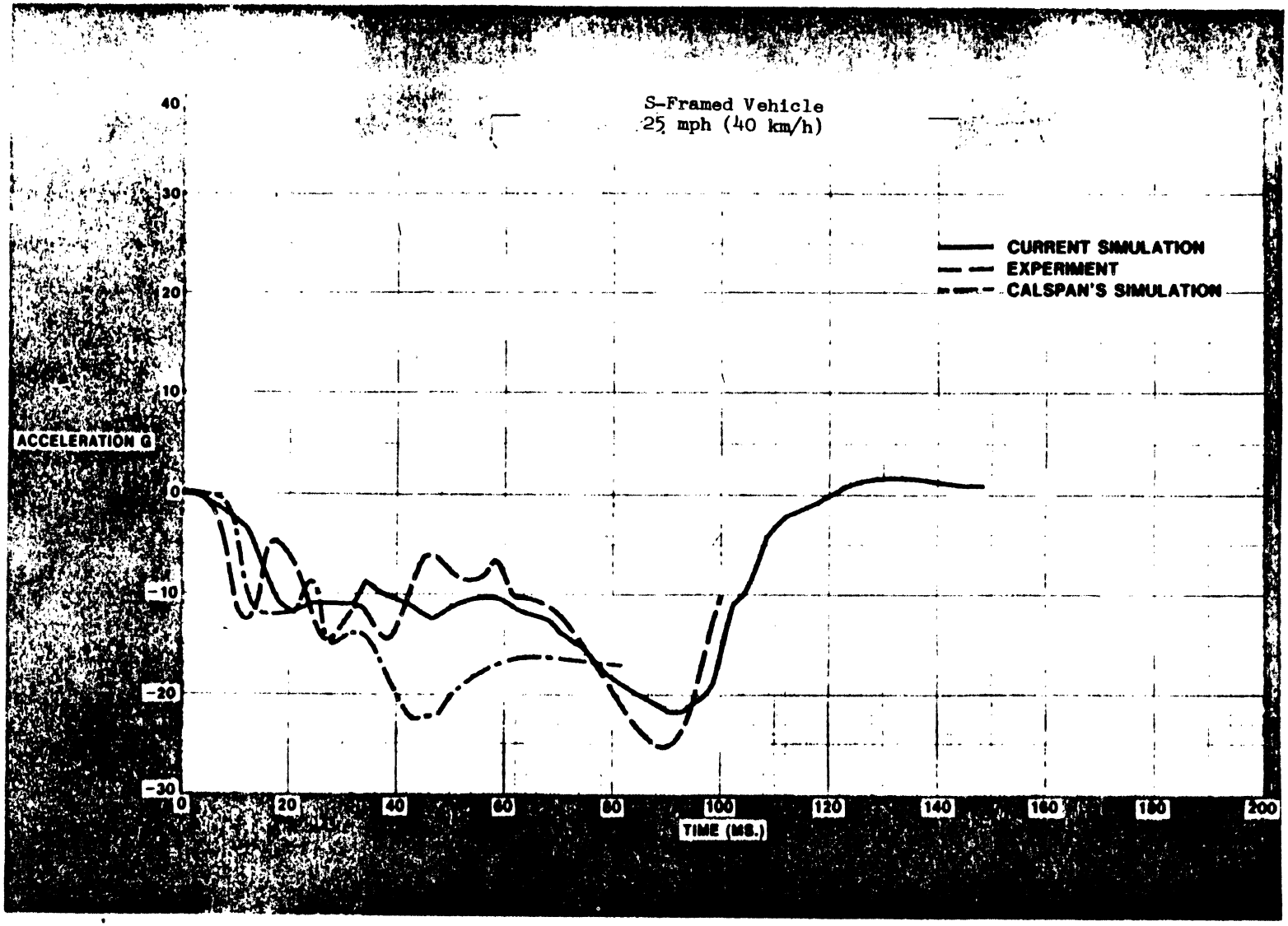


Fig. 21 - Comparison between the simulated and crash test results - passenger compartment deceleration

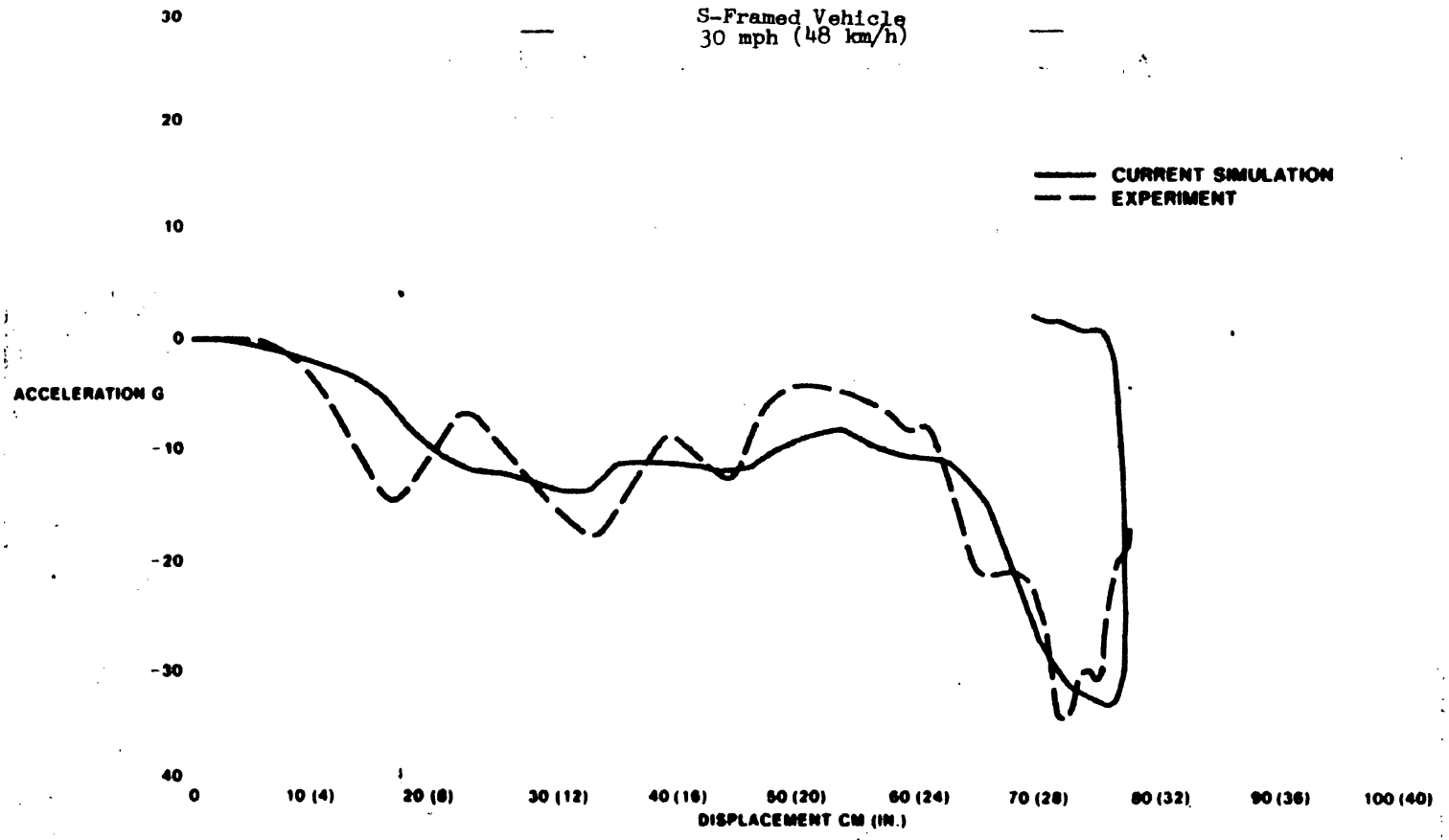


Fig. 22 - Comparison between the simulated and crash test results - passenger compartment deceleration versus front-end crush

TABLE 2 - OVERALL STATIC TO DYNAMIC AMPLIFICATION FACTOR FOR C SECTION FRAMED VEHICLES

| Vehicle | Maximum Dynamic Collapse cm. | (in.) | Static Energy kn-m | (in-klbs) | Kinetic Energy kn-m | (in-klbs) | Overall Dynamic Amplification Factor |
|---|---|---|---|---|---|---|---|
| 1 | 64.75 | (25.9) | 135.6 | (1200) | 222.6 | (1970) | 1.64 |
| 2 | 55.00 | (22.0) | 135.6 | (1200) | 271.2 | (2400) | 2.0 |
| 3 | 73.75 | (29.5) | 124.3 | (1100) | 210.2 | (1860) | 1.69 |
| 4 | 52.50 | (21.0) | 203.4 | (1800) | 345.8 | (3060) | 1.7 |

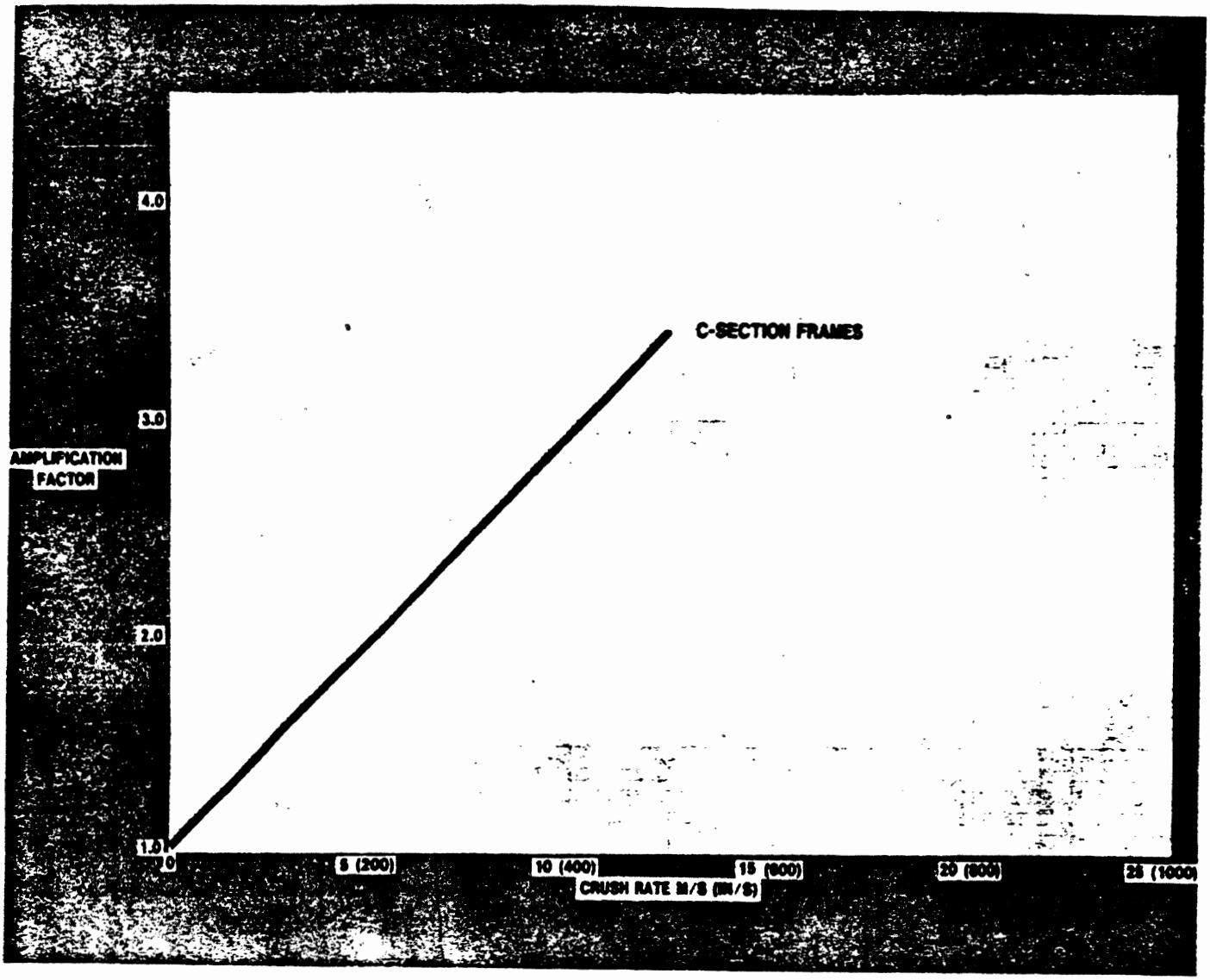


Fig. 23 - Dynamic amplification factor for C-section frame vehicles

Comparisons of the simulated results for the four tests are shown in Figs. 24 to 32. It can be seen from the figures that, subjectively, the deceleration responses of the passenger compartment predicted by the model compare well with those observed in the crash tests. The peak dynamic collapse predicted by the model is within 1.25% to 6.14% of the observed crash test results. The time to maximum crush predicted by the model ranges from 2 ms. to 10 ms. of that observed in crash tests.

A comparison of the time history of the kinetic energy of the occupant compartment between the simulation and a crash test is shown in Fig. 33. Some idea of the amount of dynamic amplification required in the foreframe can be had by examining Fig. 34 which shows the dynamic force-deflection properties of the foreframe predicted by the model and that obtained statically.

Considering the above, it is felt that the method of transforming the static data to the dynamic case is adequate for the class of vehicles considered in this study.

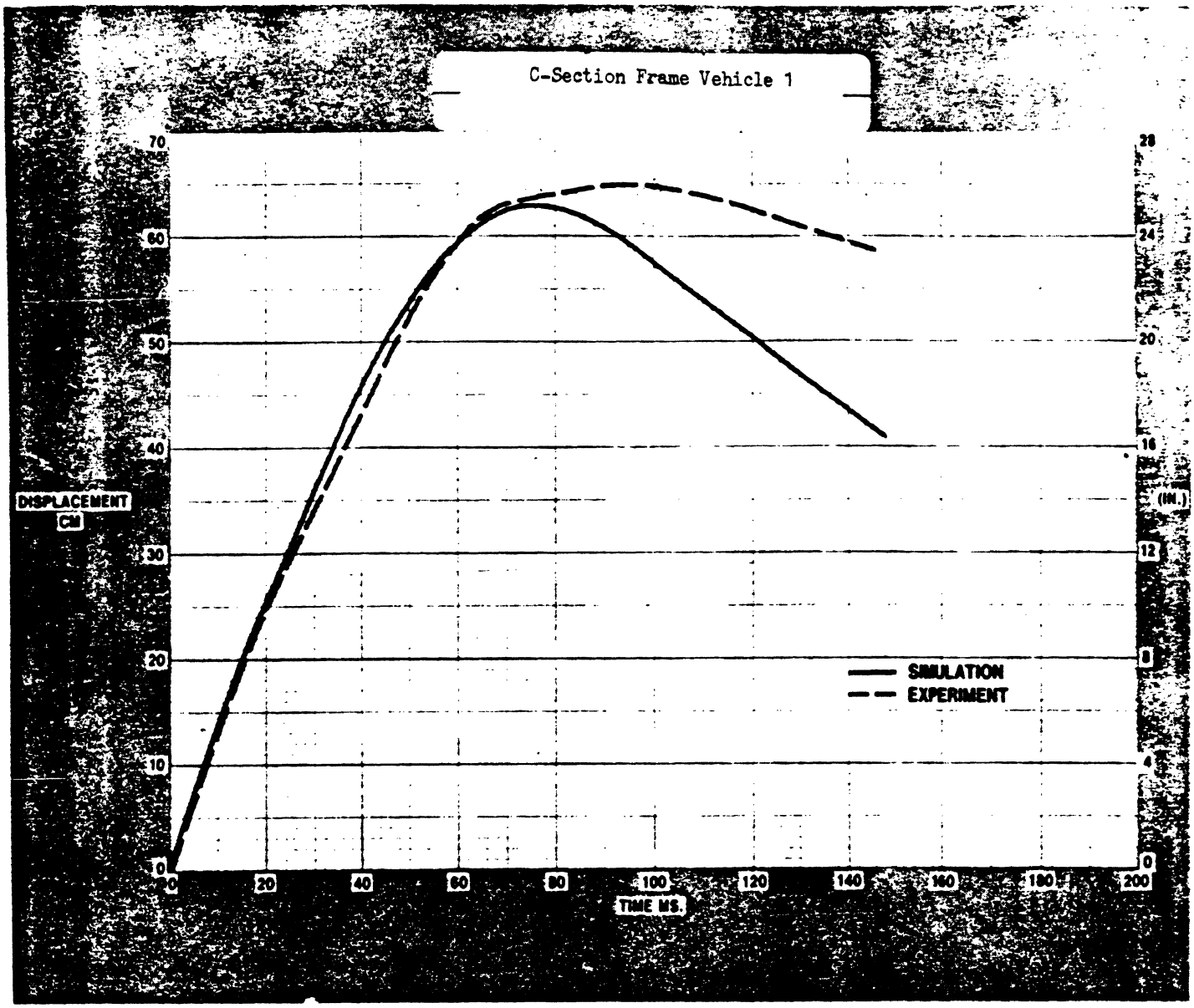


Fig. 24 - Comparison between the simulated and crash test results - passenger compartment travel

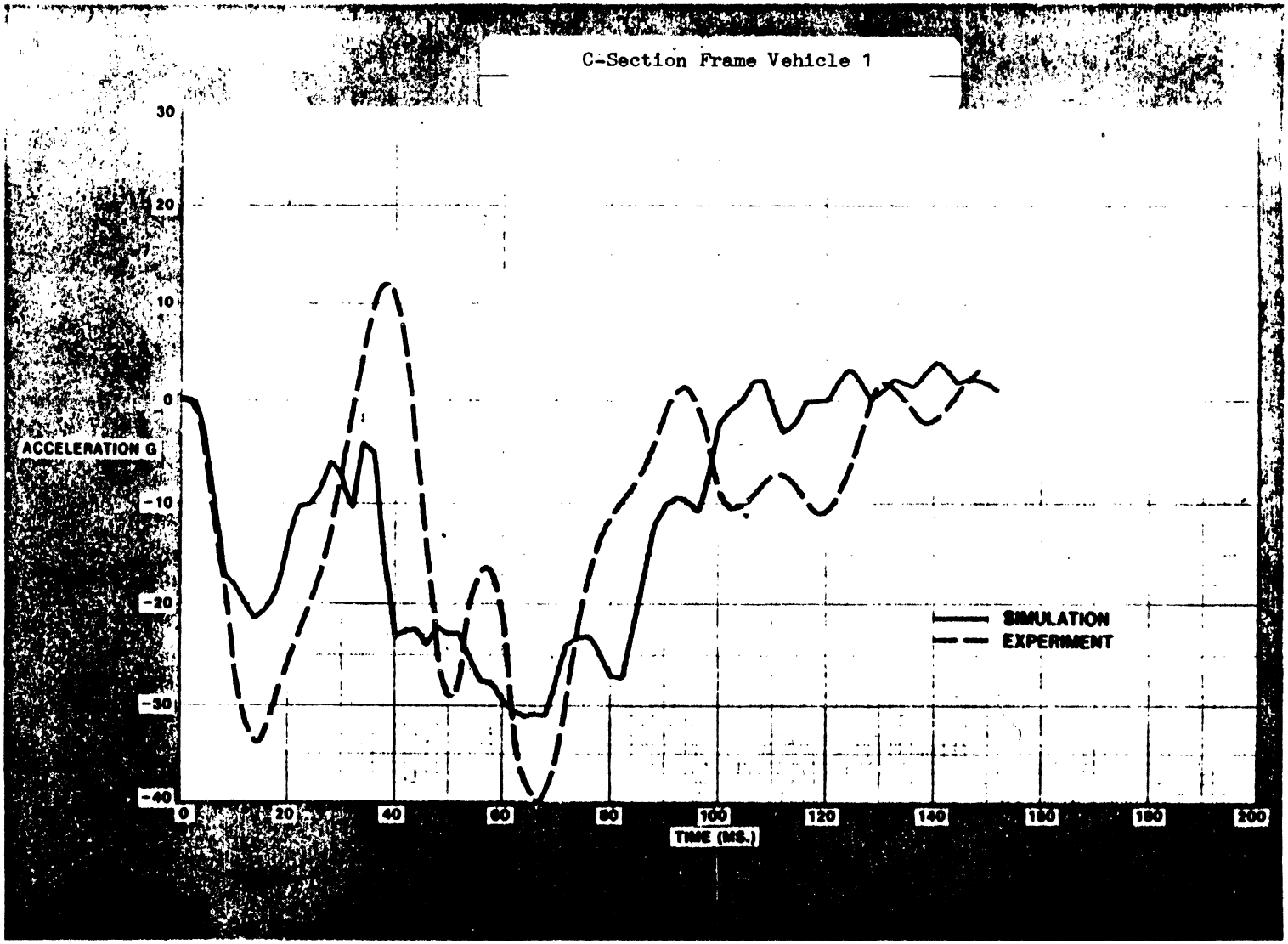


Fig. 25 - Comparison between the simulated and crash test results - passenger compartment deceleration

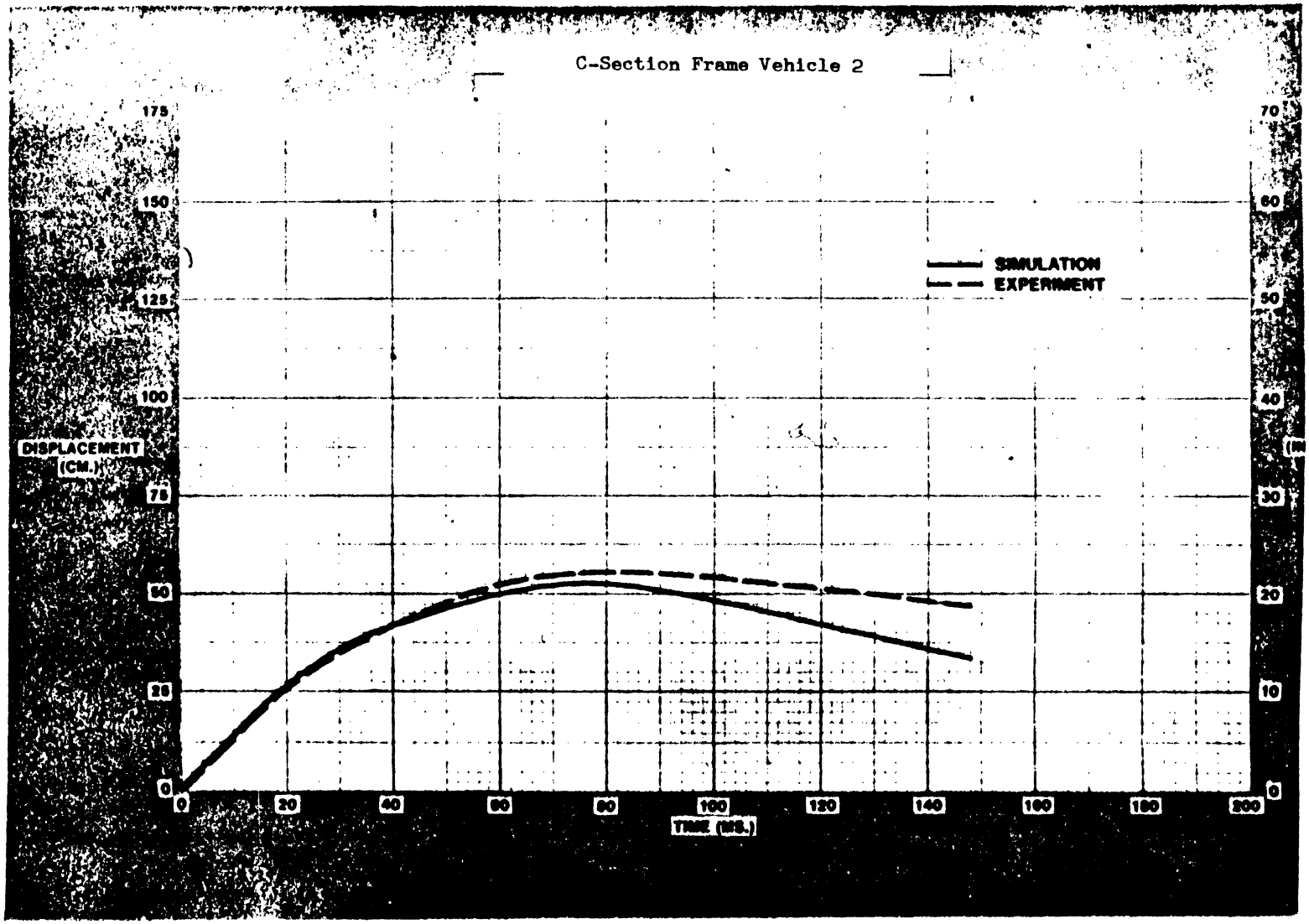


Fig. 26 - Comparison between the simulated and crash test results - passenger compartment travel

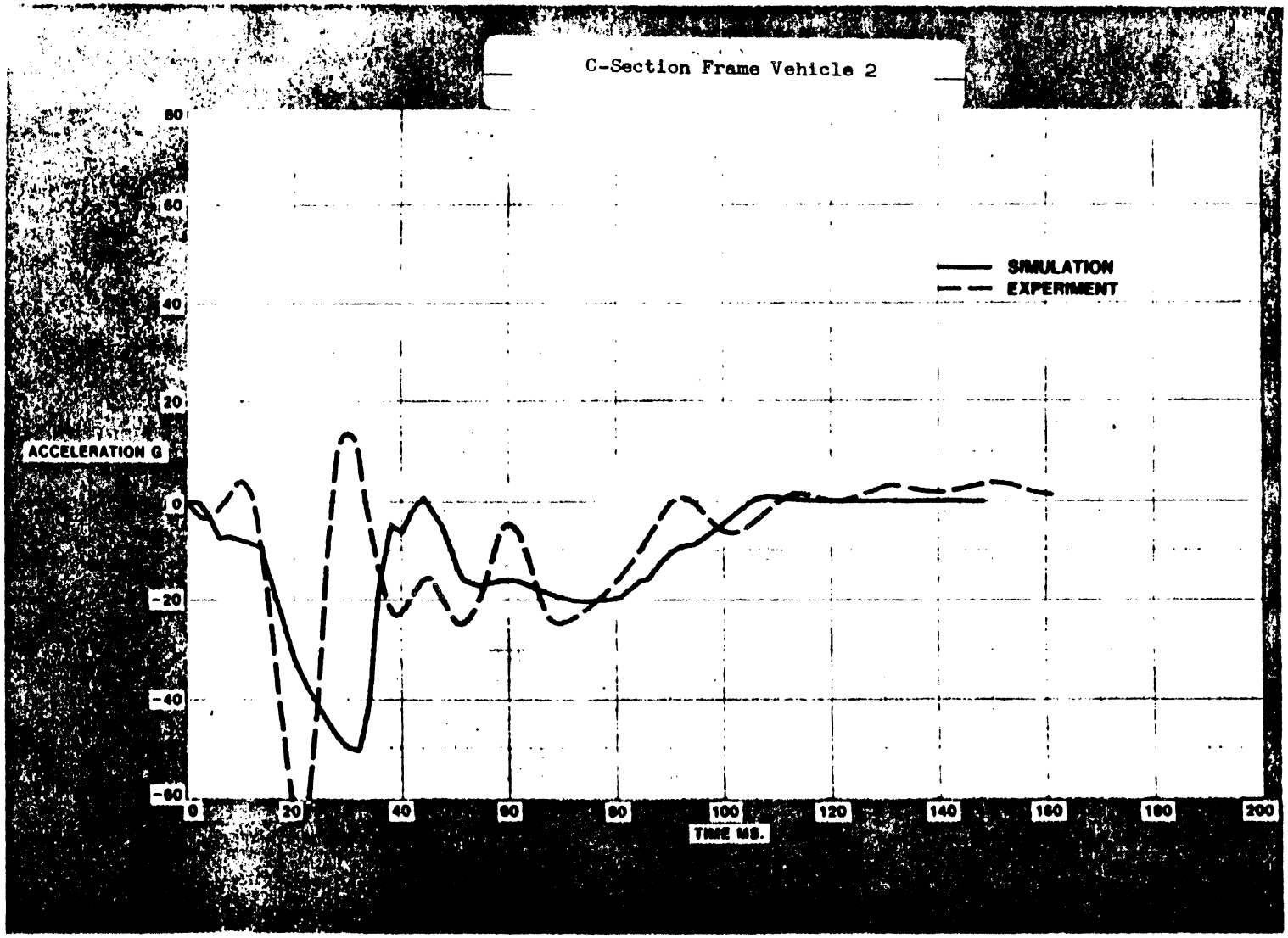


Fig. 27 - Comparison between the simulated and crash test results - passenger compartment deceleration

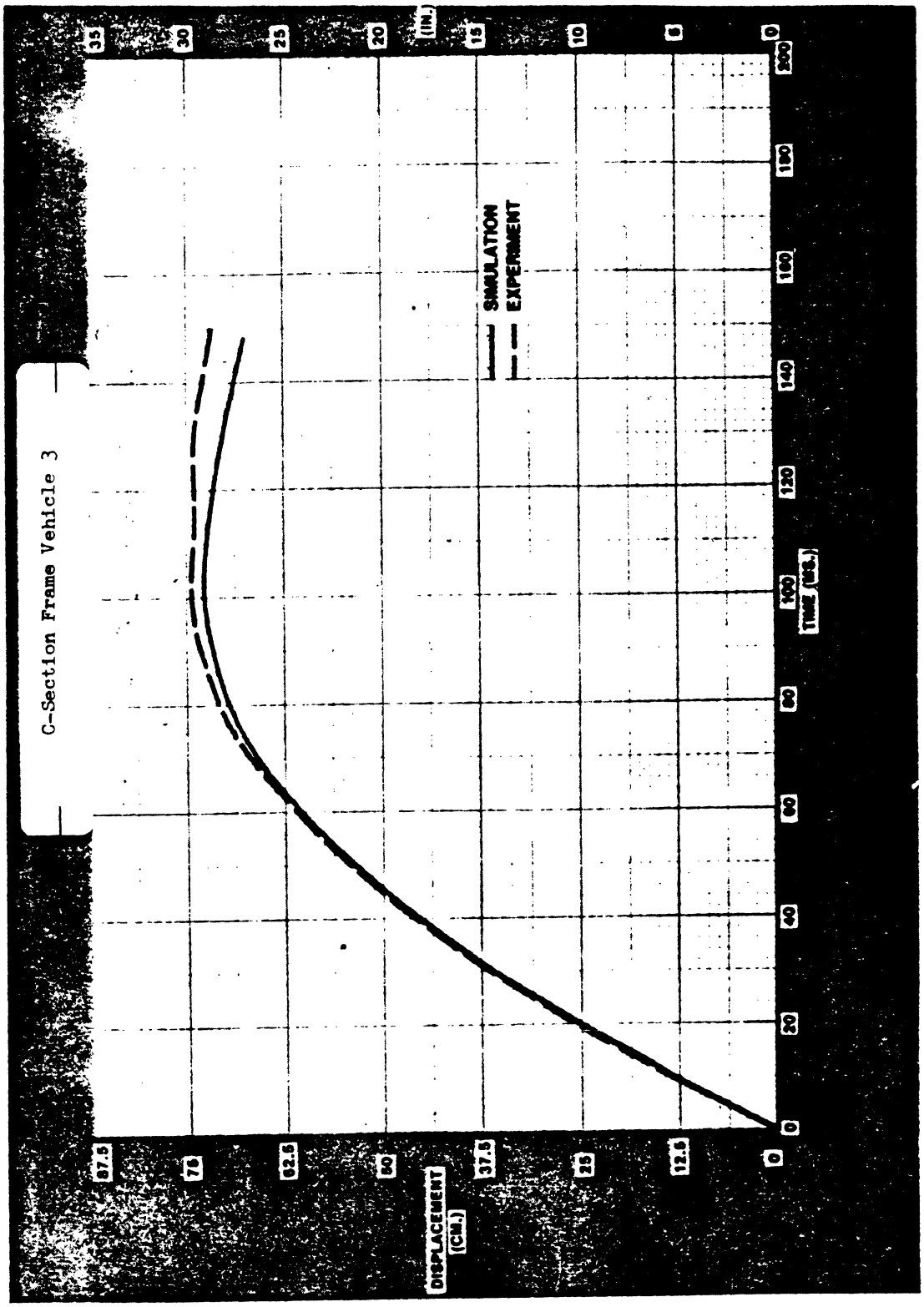


Fig. 28 - Comparison between the simulated and crash test results - passenger compartment travel

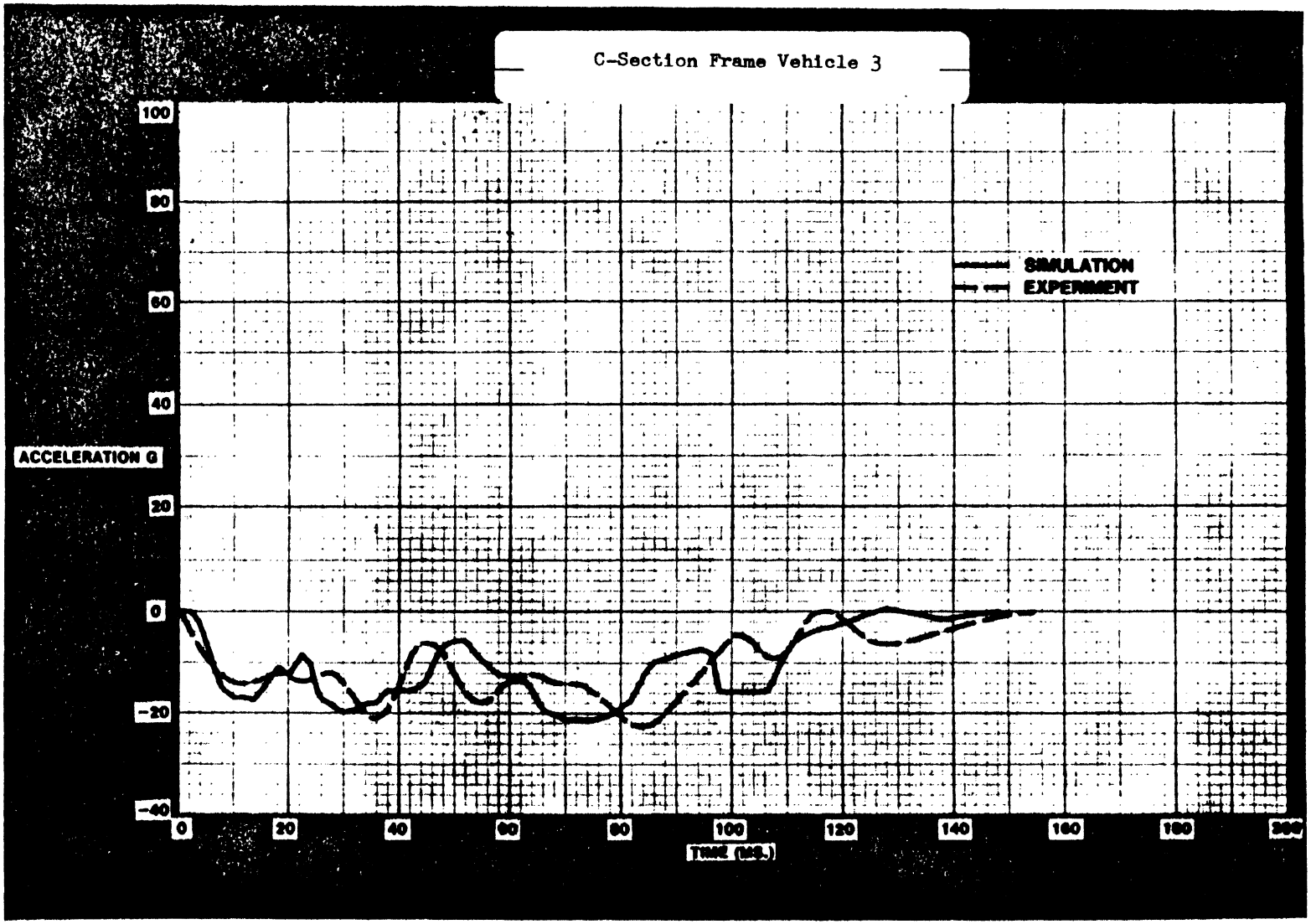


Fig. 29 - Comparison between the simulated and crash test results - passenger compartment deceleration

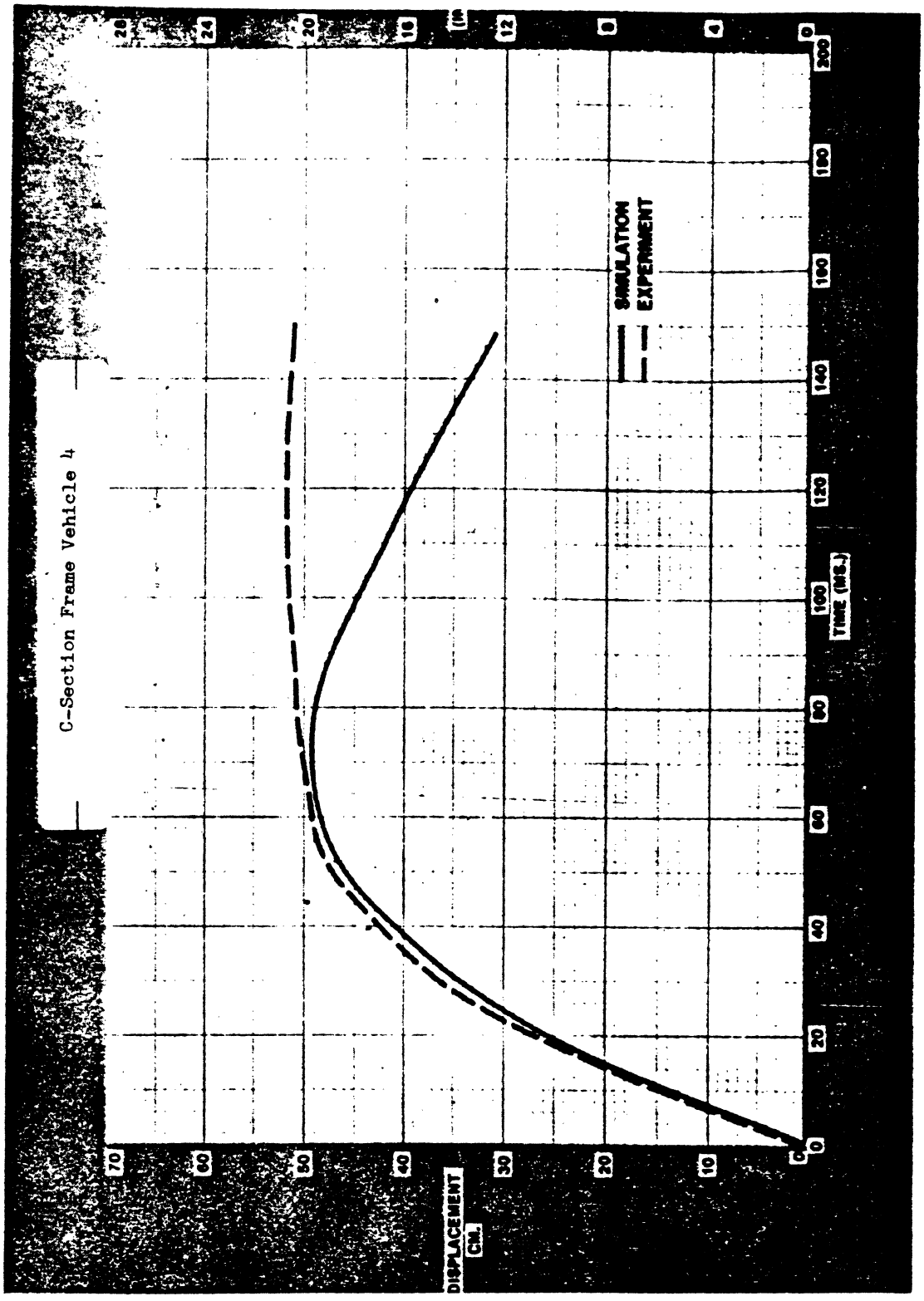


Fig. 30 - Comparison between the simulated and crash test results - passenger compartment travel

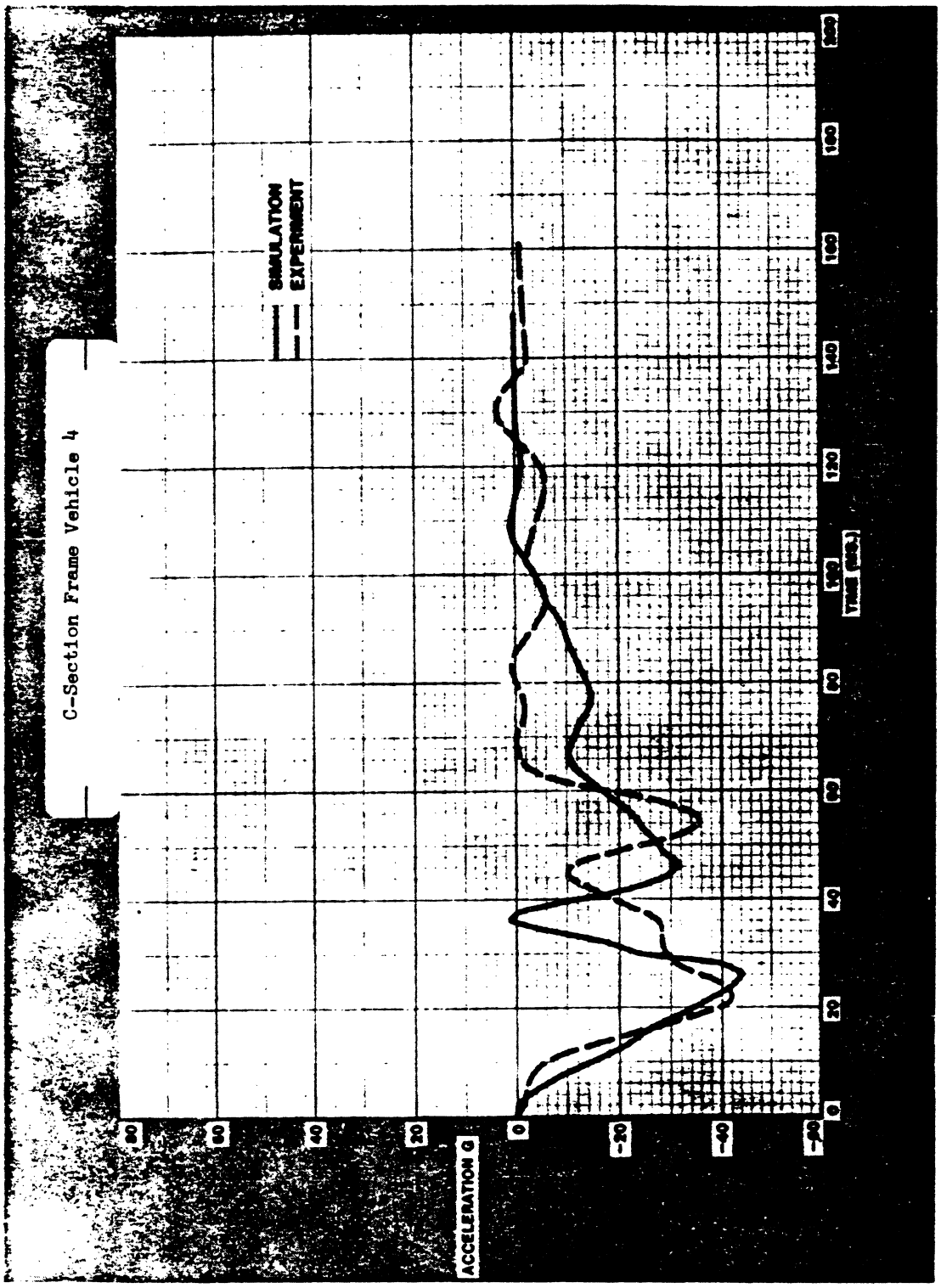


Fig. 31 - Comparison between the simulated and crash test results - passenger compartment deceleration

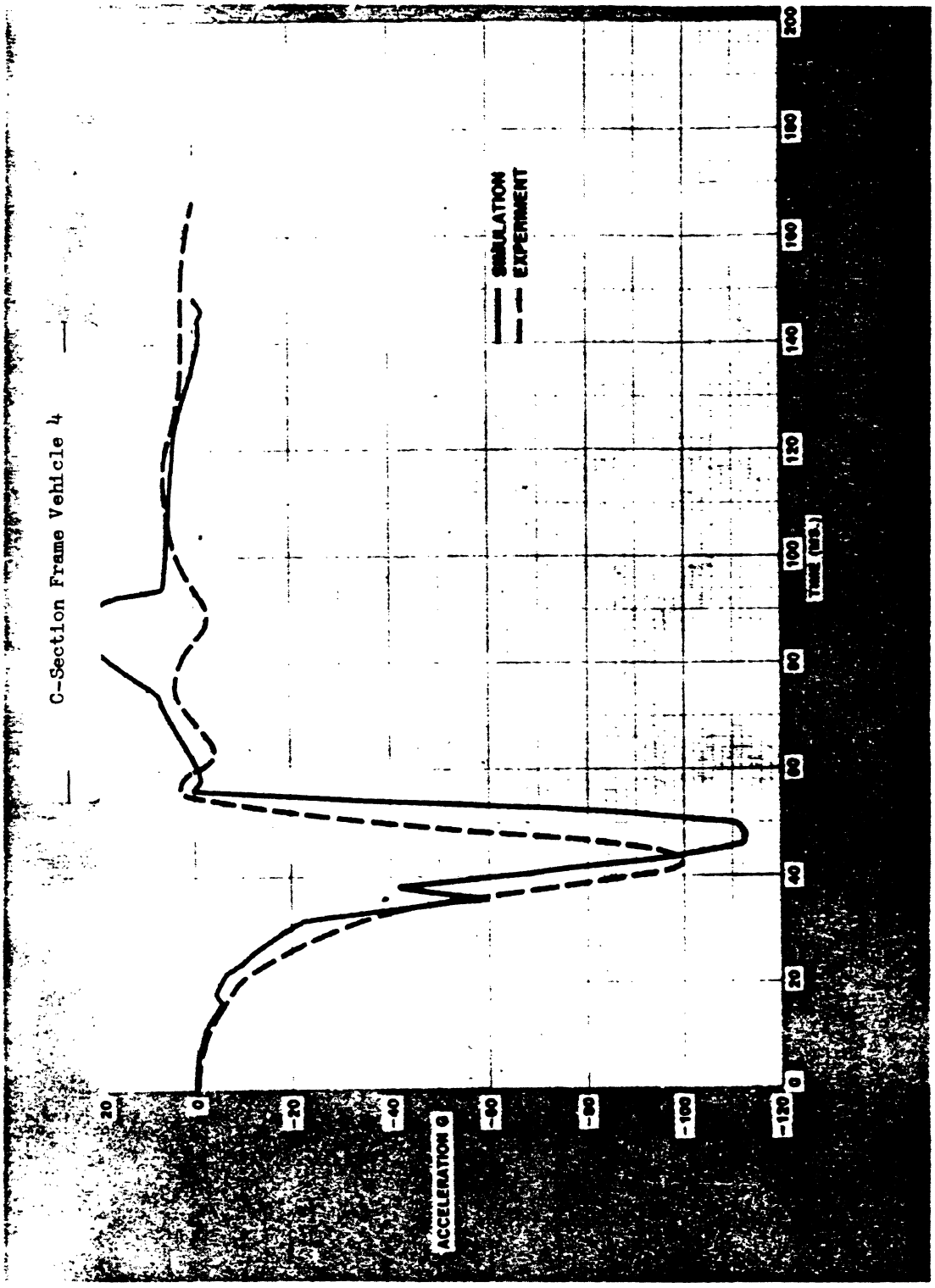


Fig. 32 - Comparison between the simulated and crash test results - engine deceleration

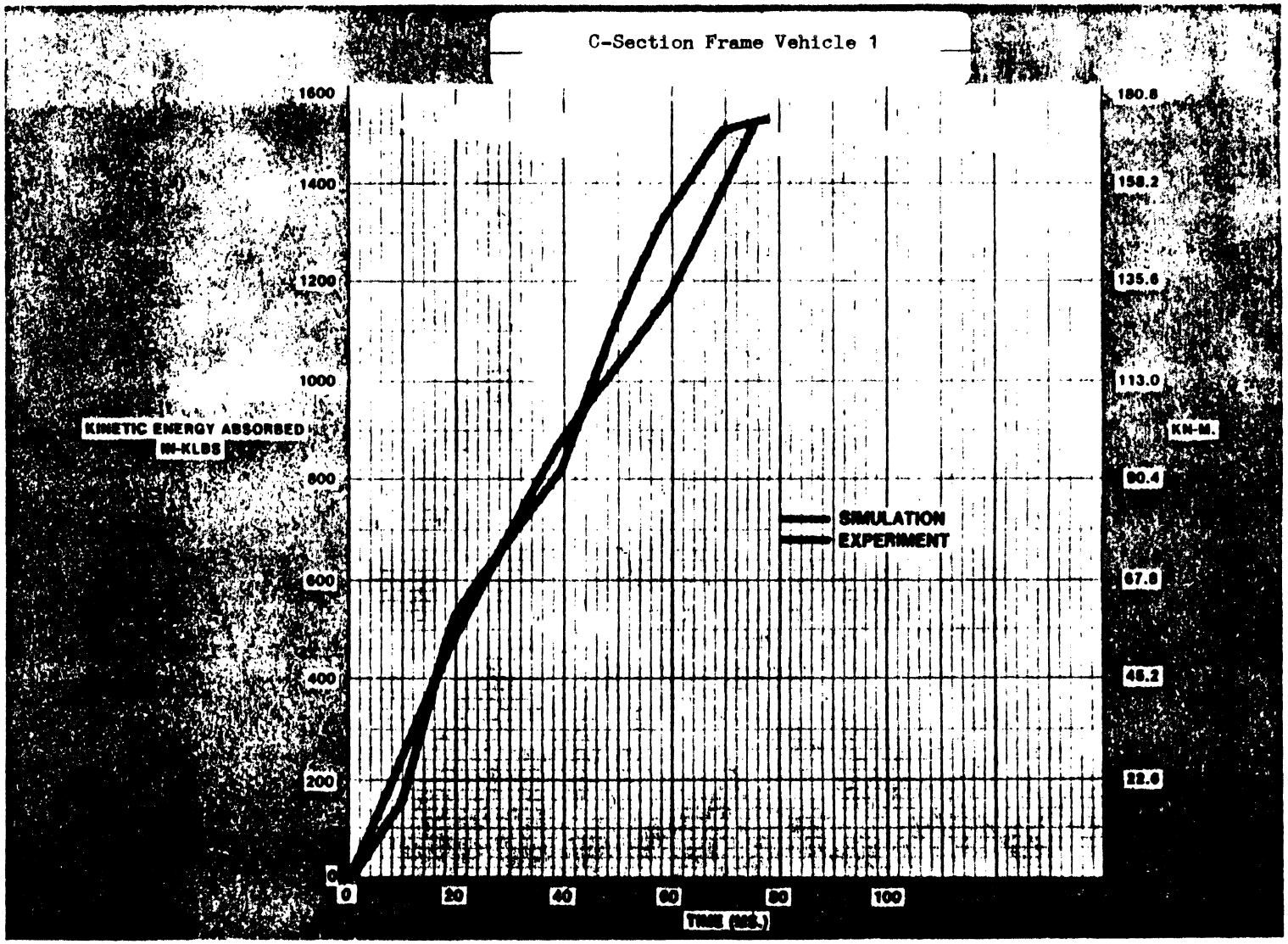


Fig. 33 - Comparison between the simulated and crash test results - kinetic energy absorbed

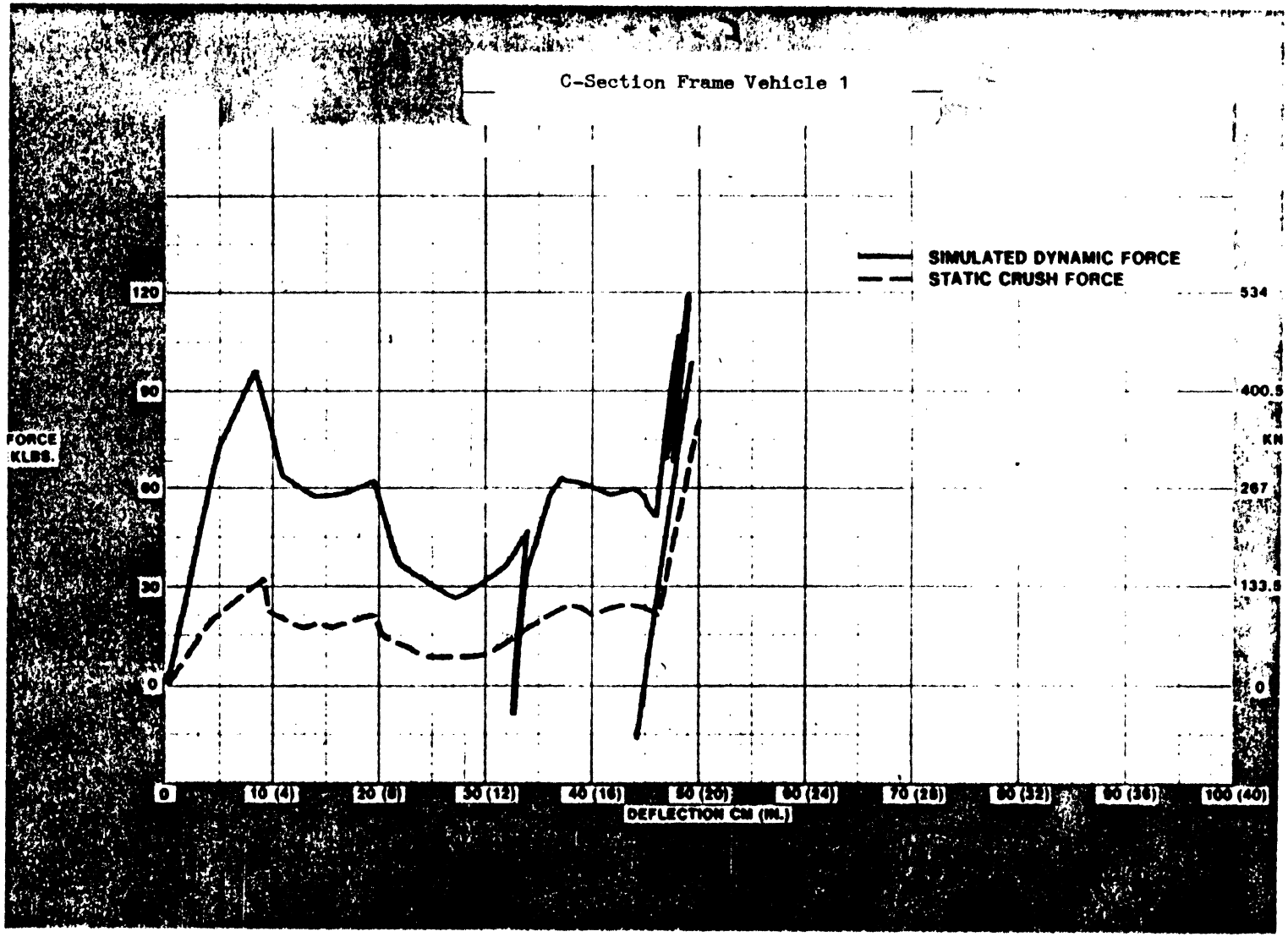


Fig. 34 - A representation of dynamic amplification factor - simulated dynamic force versus static crush force for C-section frame

## SUMMARY AND CONCLUSION

(i) A literature survey of structural response of dynamically deforming structures shows that material property changes as well as the inertia of the deforming structures have to be taken into account in using quasi-statically obtained data for dynamic simulation.

(ii) The empirically developed rate-dependent factor, shown in Fig. 2, when used in the mathematical model for the frames, in conjunction with a material rate sensitivity factor (Fig. 14) for the sheet metal, driveline, and firewall, predicts the inertial response of unitized and S-framed vehicles in frontal barrier crashes with reasonable accuracy.

(iii) For the three unitized construction vehicles and one S-framed vehicle, the model predictions are within 5% of test observations of the maximum dynamic collapse. The time to maximum dynamic collapse predicted by the model is within 2.0 to 12.3 ms. of the test results (see Table 3). Subjectively, the deceleration time histories of the occupant compartment

TABLE 3 - SUMMARY OF DYNAMIC COLLAPSE

| Vehicle | Impact Velocity mph (km/h) | Crash Result Peak cm(in) | Crash Result Time(ms) | Simulation Peak cm(in) | Simulation Time(ms) | Error* % Amplitude | Error* Phase (ms) |
|---|---|---|---|---|---|---|---|
| Sub-Compact 1 | 42 (67.2) | 79.50 (31.8) | 82.50 | 82.15 (32.86) | 79.0 | +3.33 | -3.5 |
| 2 | 42 (67.2) | 83.25 (33.3) | 89 | | | -1.41 | -10 |
| 3 | 37 (59.2) | 71.25 (28.5) | 74-82 | 72.35 (28.94) | 70.9 | +1.54 | -3.1 to -11.1 |
| 5 | 37 (59.2) | 73.75 (29.5) | 76-90 | | | -1.90 | -5.1 to -19.1 |
| 4 | 32 (51.2) | 61.25 (24.5) | 76-80 | 63.65 (25.46) | 74.2 | +3.92 | -1.8 to - 5.8 |
| 6 | 32 (51.2) | 61.25 (24.5) | 78 | | | +3.92 | -3.8 |
| Compact 1 | 35 (56) | 84.00 (33.6) | 90 | 82.50 (33.00) | 88.4 | -1.8 | -1.6 |
| 2 | 30 (48) | 70.50 (28.2) | 90 | 71.55 (28.62) | 86.4 | +1.49 | -3.6 |
| Mid-Size | 30 (48) | 78.75 (31.5) | 100 | 77.88 (31.15) | 88.10 | -1.11 | -11.9 |
| S-Framed 1 | 35 (56) | 86.75 (34.7) | 97 | 90.23 (36.09) | 95.25 | +4.01 | -1.75 |
| 2 | 30 (48) | 79.75 (31.9) | 100 | 77.10 (30.84) | 87.7 | -3.32 | -12.3 |
| 3 | 25 (40) | 66.75 (26.7) | 95 | 66.65 (26.66) | 96.85 | -0.15 | +1.85 |
| 4 | 8 (13.3) | 17.00 ( 6.8) | 80 | 20.03 ( 8.01) | 88.90 | +17.84 | +8.9 |
| C-Section Frame 1 | 30 (48) | 64.75 (25.9) | 86 | 62.88 (25.15) | 76.4 | -2.9 | -9.6 |
| 2 | 30 (48) | 55.00 (22.0) | 78 | 52.55 (21.02) | 76 | -4.45 | -2 |
| 3 | 30 (48) | 73.75 (29.5) | 106 | 72.83 (29.13) | 103 | -1.25 | -3 |
| 4 | 30 (48) | 52.50 (21.0) | 80 Onwards | 49.28 (19.71) | 72.6 | -6.4 | More than -7.4 |

*Negative sign indicates less amplitude or earlier timing in simulation than in the crash.

predicted by the model compare well with the observed test results.

(iv) The "dynamic amplification factor" of open, C-section frames appear to be higher than that of closed section, box frames.

(v) For the four different C-section framed vehicles tested and simulated, the dynamic crush predicted by the model was within 6.14% of the observed test results. The time to maximum crush predicted by the model was within 2.0 to 9.6 ms. of the observed test results. Subjectively, the deceleration-time histories of the passenger compartment predicted by the model compare well with the test results.

REFERENCES

1. M. M. Kamal, "Analysis and Simulation of Vehicle-to-Barrier Impact," SAE 700414, 1970 International Automobile Safety Conference Compendium, SAE, Inc., 1970

2. J. T. Herridge and R. K. Mitchell, "Development of a Computer Simulation Program for Collinear Car/Car and Car/Barrier Collisions", Report No. FH-11-7550-BCL G-0612-C. Prepared by Battelle's Columbus Laboratories for the Department of Transportation.

3. M.J. Manjoine, J. Appl. Mech, Vol 11, P. 211, 1944.

4. P. B. Lane and J. J. Grenawalt, "Properties and Applications of High Strength Cold-Rolled Steels; Plain Carbon and Killed Low Alloy", SAE Paper 740954.

5. A. Saxena and D. A. Chatfield, "High Strain Rate Behavior of Some Hot and Cold Rolled Low Carbon Steels," SAE Paper 760209, Automotive Engineering Congress and Exposition, February, 1976.

6. R. G. Davies and C. L. Magee, "The Effect of Strain Rate Upon the Tensile Deformation of Materials," Journal of Engineering Materials and Technology, April, 1975.

7. R. G. Davies and C. L. Magee, "The Effect of Strain Rate Upon the Bending Behavior of Materials," Journal of Engineering Materials and Technology, January, 1977.

8. P. H. Thornton, "Static and Dynamic Collapse Characteristics of Scale Model Corrugated Tubular Sections," Journal of Engineering Materials and Technology, ASME Paper No. 75-Mat-G.

9. M. A. Macaulay and R. G. Redwood, "Small Scale Model Railway Coaches under Impact", The Engineer, Dec. 25, 1964, pp 1041-1046.

10. R. C. VanKuren and J. E. Scott, "Energy Absorption of High-Strength Steel Tubes Under Impact Crush Conditions", SAE Paper 770213.

11. P. H. Thornton and C. K. Dharan, "The Dynamics of Structural Collapse", Materials Science and Engineering, Vol. 18, 1975, pp. 97-120.

12. C. M. Ni, "Impact Response of Curved Box Beam-Columns with Large Global and Local Deformations", AIAA/ASME/SAE 14th Structures, Structural Dynamics, and Materials Conference, AIAA Paper No. 73-401.

13. Y. Ohokubo, T. Akamatsu, and K. Shirasawa, "Mean Crushing Strength of Closed-Hat Section Members", SAE Paper 740040, SAE, Inc., 1974

14. T. Wierzbicki and T. Akerstrom, "Dynamic Crushing of Strain Rate Sensitive Box Columns", Proceedings of Second International Conference on Vehicle Structural Mechanics, April, 1977, SAE Paper No. 770592.

15. M. Tani and A. Funahashi, "Energy Absorption by the Plastic Deformation of Body Structural Members", SAE Paper No. 780368, SAE, Inc., 1978

16. N. E. Shoemaker, M. O. Ryder, and N. J. DeLeys, "Automobile Consumer Information Crash Test Program", DOT-HS-4-00910, Nov. 1976.

17. Ford Motor Company, "Safety Systems Optimization Model", DOT-HS-6-01446, Oct. 1976.

18. M. O. Ryder, Jr., "Classification of Automobile Frontal Stiffness/Crashworthiness by Impact Testing", DOT-HS-5-01099, Aug. 1976.

19. J. D. Campbell, "Dynamic Plasticity of Metals", Courses and Lectures No. 46, International Centre for Mechanical Sciences, July, 1970.